2003-04-10

The Rational Design and Synthesis of Ionophores and Fluoroionophores for the Selective Detection of Monovalent Cations

John S. Benco
Worcester Polytechnic Institute

The Rational Design and Synthesis of Ionophores and Fluoroionophores for the Selective Detection of Monovalent Cations

By

John S. Benco

A Dissertation

Submitted to the Faculty

of the

WORCESTER POLYTECHNIC INSTITUTE

in partial fulfillment of the requirements for the

Degree of Doctor of Philosophy

in

Chemistry

by

_____

April 7, 2003

APPROVED:

_____	_____
Dr. W. Grant McGimpsey, Major Advisor	Dr. James W. Pavlik, Committee Member
_____	_____
Dr. Robert E. Connors, Committee Member	Dr. Joseph S. Foos, Outside Reviewer

_____

Dr. James P. Dittami, Head of Department

Abstract

The rational design, synthesis and complexation characteristics of several monovalent cation-selective ligands are described. Molecular modeling employing a combination of dynamics, mechanics (AMBER94) and electrostatics was used to design ligands for the complexation of ammonium, potassium, sodium and lithium ions. A modular technique was used to synthesize an ammonium selective ionophore based on a cyclic depsipeptide structure (**8**). The ionophore was incorporated into a planar ion selective electrode (ISE) sensor format and the selectivity tested versus a range of metal cations. It was found that the membrane containing the polar plasticizer NPOE (nitrophenyloctylether) in the absence of ionic additive exhibited near-Nernstian behavior (slope = 60.1 mV/dec @ 37°C) and possessed high selectivity for ammonium ion over lithium and the divalent cations, calcium and magnesium (log $K^{POT}_{NH_4^+ j}$ = -7.3, -4.4, -7.1 for lithium, calcium and magnesium ions, respectively). The same membrane also exhibited sodium and potassium selectivity that was comparable to that reported for nonactin (log $K^{POT}_{NH_4^+ j}$ = -2.1, -0.6 for sodium and potassium, respectively, compared to -2.4, -0.9 in the case of nonactin).

N-(9-methylanthracene)-25,27-bis(1-propyloxy)calix[4]arene-azacrown-5 (**10**) was synthesized and tested as a fluoroionophore for the selective detection of potassium ions. Compound **10** acts as an "off-on" fluorescent indicator for ion complexation as a result of photoinduced intramolecular electron transfer (PET). Studies demonstrate that **10** is selective for potassium over other alkali metal cations, with excellent selectivity over sodium and lithium (log $K_{K,Na}$ ~ log $K_{K,Li} \leq$ -3.5) and moderate selectivity over rubidium and cesium (log $K_{K,Rb}$ ~ log $K_{K,Cs}$ ~ -1).

N-(9-methylanthracene)-25,27-bis(1-propyloxy)-4-*tert*-butylcalix[4]arene-azacrown-3 (**11**) was synthesized and tested as a fluoroionophore for the selective detection of lithium cations. When exposed to lithium ions in a 75:25 dichloromethane/THF solvent mixture, the molecule, which operates on PET, exhibited a >106-fold enhancement in

fluorescence emission intensity. Selectivity studies demonstrated that **11** effectively discriminates against sodium and potassium ions log $K_{Li,Na} \leq -3.8$ and log $K_{Li,K} \leq -2.3$.

A fluorescent sodium optode based on a fluoroionophore consisting of aminorhodamine B covalently-linked through an amide bond to a calix[4]arene has also been developed (**12**). The optode, fashioned by incorporation of the fluoroionophore into a single component polymer matrix, operates on the basis of PET. The fluorescence intensity increased linearly with increasing sodium ion concentration in the range 0.01 M to 2.0 M, exhibiting a three-fold enhancement over this range. The optode provides selectivity for sodium ions compared to potassium ions that is sufficient for clinical determinations of sodium ion concentration.

Acknowledgements

I would like to gratefully thank my Advisor, Dr. W. Grant McGimpsey, for his support and guidance throughout this research. During these past years he has been more than an Advisor to me, he has been a Mentor. This has been, and likely will be one of the best experiences in my life.

To my friends and colleagues in the lab's at WPI I'd like to say thank you. The ideas generated from all our discussions has made this work far richer than originally anticipated.

Thank you in particular to Dr. Hubert Nienaber for all his synthetic work on the fluoroionophores and his continued support and friendship over these three years. To Chris Cooper, Kathy Dennen, Cheryl Nowak, Ernesto Soto, Nui Wanichacheva and Selman Yavuz I would like to thank for all the good times.

I would also like to thank Bayer HealthCare for financial support and especially Kevin Sullivan and Chris Munkhlom for allowing me this unique opportunity.

Finally and most importantly I want to say thank you to my wife Kim and my two children, Kayla and Ryan for all of their support and understanding over these long years. This thesis is as much of them as it is me.

Table of Contents

List of Figures

Summary of Master Compounds

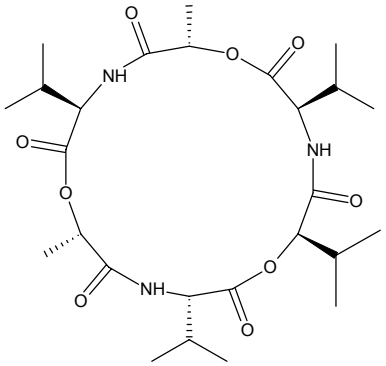

8

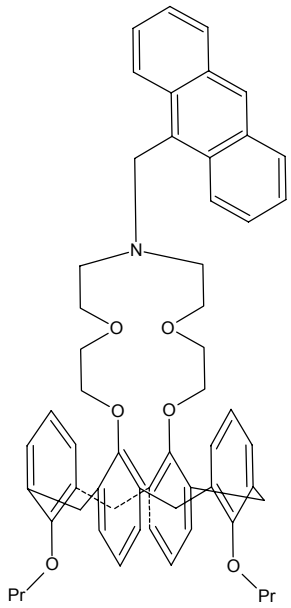

10

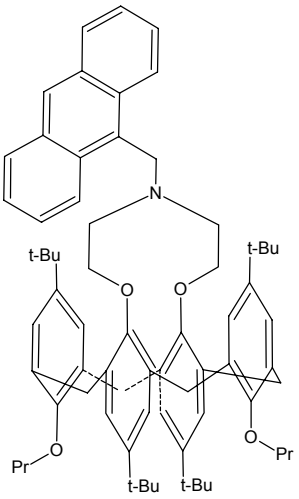

11

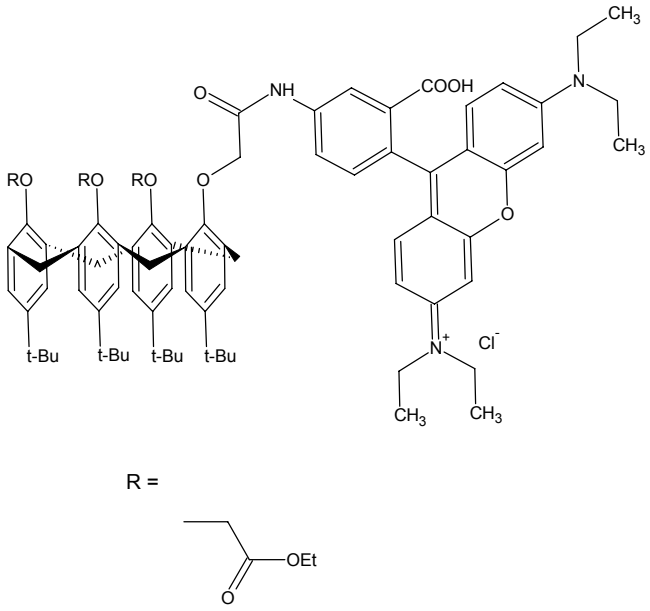

12

I: Introduction

The design of ligands for the complexation of ions has become a major research area in recent years as reflected in the numerous reviews that have been written on the subject.[1-11] This interest is due to the fact that ion-complexing ligands have applicability in a wide range of fields. For example, ion-complexing ligands have spurred the development of new catalysts, [1] antibiotics, [3] artificial sensory systems[4] and therapeutic agents in chelation therapy.[6,9] One of the major driving forces in the research of new ligands, or ionophores, is sensor development, particularly for clinical diagnostic purposes and attention has focused on attaining high selectivity and sensitivity to specific ions.[6,9,11] In particular, due to their significant importance in the clinical diagnosis of disease, research has centered on the complexation of alkali and alkali earth metal ions as well as metabolites such as ammonium ion. [11]

Typically, ionophores now in use for clinical purposes have been developed using empirical, trial and error techniques. Although many useful ionophores have been obtained this way an alternative, rational approach is called for in which the fundamental requirements of complexation are considered. Such an approach takes into account the specific guests and employs the modern techniques of molecular modeling. Rational ionophore design followed by systematic structural modifications in iterative steps is likely to yield not only more selective and sensitive ionophores but also a set of general rules that can be applied to the design of other systems.

To this end, it is the goal of this work to design novel ionophores for the complexation of monovalent cations such as potassium, sodium, lithium and ammonium based upon the fundamental requirements for stable and selective host-guest interactions. A further goal is to corroborate these requirements with modern molecular modeling techniques and thus provide a rational approach to the development of new ionophores. Using these approaches, our specific aim is the design and development of new ammonium ionophores that will be tested in potentiometric ion selective electrodes. An extension of this work is the design new of *fluoro*ionophores (fluorescent ionophores) for potassium, sodium and lithium, which could be used in optically-based sensors. This work will be presented in 7 major sections as follows; Basic Considerations in the Design of Ionophores, Basic Considerations in the Design of Fluoroionophores, Ionophore/Fluoroionophore Design Approach, General Experimental, Results and Discussion, Conclusions, and finally, Future Work. The Results and Discussion section will be subdivided for each particular ionophore/fluoroionophore and will contain an introduction, specific experimental details, a discussion of the results obtained and a concluding summary.

A: Basic Considerations in the Design of Ionophores

The first step in the process of developing selective and sensitive ionophores is to consider the thermodynamics of complexation. Ionophore selectivity can be discussed in terms of the thermodynamic stability of the metal ion–ionophore complex, where more stable complexes are indicative of more selective interactions.[10] Thermodynamic stability in these systems is a complex combination of enthalpic and entropic parameters that can be understood in part, by considering steric size-fit parameters and pre-organization of the ionophore. Table 1 gives a selection of thermodynamic values for alkali metal ion binding to a series of crown ethers (shown in Figure 1) as reported by Bradshaw and co-workers.[10] Examination of the table reveals that complexation is an enthalpically favorable process and an entroptically unfavorable process and that there may be a modest correlation between the free energy of complexation and the size match between the ion and ionophore. Thus when the size matches closely, the metal ion is centered within the cavity or pocket and experiences the most symmetrical electrostatic interactions. A smaller ion will experience a proportionally smaller electrostatic interaction and thus will not be as tightly bound. Conversely an ion that is larger cannot fit within the pocket symmetrically and as a consequence will not benefit from all of the electrostatic stabilizing interactions provided by the ionophore.

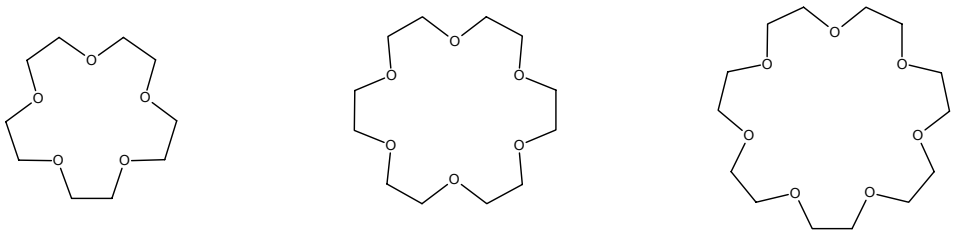

Figure 1: Left to right, 15-crown-5, 18-crown-6, 21-crown-7

Ligand	Cavity (Å)	Metal ion	Cation radius (Å)	−ΔG (kJ/mol)	−ΔH (kJ/mol)	TΔS (kJ/mol)
15-crown-5	0.86-0.92	Na	0.95	19.7	20.9	-1.30
		K	1.33	21.3	32.2	-10.9
		Cs	1.69	12.6	49.0	-36.4
18-crown-6	1.34-1.43	Na	0.95	25.1	31.4	-6.30
		K	1.33	34.7	56.1	-21.3
		Rb	1.48	30.6	50.7	-20.1
		Cs	1.69	27.2	47.3	-20.1
21-crown-7	~1.70	Na	0.95	10.0	43.5	-33.5
		K	1.33	24.3	36.0	-11.7
		Rb	1.48	27.6	40.2	-12.6
		Cs	1.69	28.5	46.9	-18.4

Table 1: Thermodynamic values for alkali metal ion binding to a series of crown ethers as reported by Bradshaw and co-workers.[10]

This correlation is particularly clear in the case of the 18-crown-6 and the 21-crown-7 where the average pocket sizes are on the order of 1.39 and 1.70 Å respectively. These values nicely match the ionic radius of potassium (1.33 Å) and that of cesium (1.69 Å) and as a result, the free energy of complexation for these two cations is the most favorable (-34.7 and -28.5 kJ/mol) in comparison to the other cations.

The differences in the free energy of complexation can give a measure of the ability of an ionophore to discriminate between various guests. This measure is the selectivity factor, logK, and is the ratio of the equilibrium constants for the binding of individual guests. This value can be calculated from the free energy of complexation, ΔG, as follows;

$$\ln K_i = -\Delta G_i/RT \qquad \textbf{(1)}$$

$$\ln K_j = -\Delta G_j/RT \qquad \textbf{(2)}$$

Where K is the equilibrium constant (this is also called a binding, stability, complexation or association constant), *i* is the ion of interest and *j* is the ion to be discriminated against, i.e. the interfering ion and R, T and G are the standard thermodynamic quantities.

Obtaining the ratios and converting to log;

$$\log K_{ij} = K_i/K_j \qquad \textbf{(3)}$$

gives $\log K_{ij}$, the selectivity factor (or coefficient).

For example, the 18-crown-6 ionophore has a ΔG of -25.1 and -34.7 kJ/mol for sodium and potassium respectively (Table 1), yielding $\log K_{K,Na} = 1.68$ or $K_{K,Na} = 48.1$ (at 25ºC). In other words the equilibrium constant for the binding of potassium is ca. 48 times larger than that of sodium and thus the 18-crown-6 is 48 times more selective for potassium than it is for sodium. It is this value, $\log K_{ij}$, which drives the development of new ionophores. The larger the difference in free energy of complexation between various guests, i.e. $\Delta\Delta G$, the larger the $\log K_{ij}$ and therefore the more selective and potentially useful is the ionophore.

It can also be concluded from the data in Table 1 that the overall thermodynamic stability of the complexes, as indicated by the free energy of complexation, is not solely dependent on enthalpic factors. Rather, in each case there are significant and multiple entropic costs of complexation that contribute to decreased stability. For the ion alone, there are both favorable and unfavorable entropy changes that occur. Upon binding the ion undergoes an entropically favorable loss of its solvation shell(s) but at the same time loses overall entropy, including a significant amount of translational entropy upon docking with the ionophore. Complexation also involves a decrease in entropy of the ionophore since it loses conformational freedom in the bound state. The reduction of conformational freedom is imposed upon the ionophore by the formation of ion-dipole interactions between the guest and the electron donors of the ionophore. These interactions reduce the degree to which bond rotation can occur and therefore imparts a more rigid structure upon the ionophore as compared to the unbound state. This overall entropic cost can be minimized however, and the resulting complex can be made more stable if the complexed and uncomplexed ionophore conformations are similar, i.e. if the ionophore conformation is pre-organized. A prime example of this effect is the natural antibiotic valinomycin in which six amide linkages force the cyclic depsipeptide structure into a pre-organized conformation through hydrogen bonding. This leaves the six-carboxyl carbonyls free to electrostatically complex K^+ in a three-dimensional octahedral arrangement (Figure 2). The rigidity imposed upon valinomycin not only reduces the overall entropic cost of complexation, it also prevents the structure from folding and wrapping around smaller cations, such as sodium, an effect that reduces selectivity. In

addition, the three-dimensional nature of the complexation pocket allows for enhanced stability of cations requiring octahedral (spherical) coordination geometries since the ion can be stabilized from above and below the plane of the ionophore, in contrast to crown ethers which essentially complex only along the single plane of the ligand. The pre-organized and rigid structure in combination with the three-dimensional binding site results in the improvement of the difference between the free energies of complexation for potassium and sodium ($\Delta\Delta G$ = -18.43 kJ/mol, $\log K_{K,Na}$ = 3.26)[14] in comparison to 18-crown-6 ($\Delta\Delta G$ = -9.6 kJ/mol, $\log K_{K,Na}$ = 1.68)[10] leading to a 38-fold improvement in the selective binding of potassium over that of sodium.

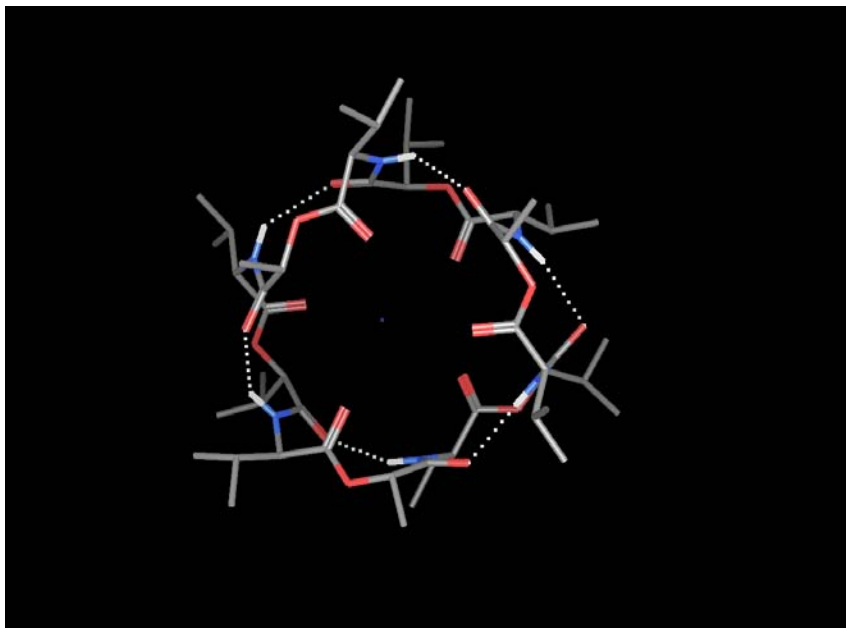

Figure 2: Valinomycin structure showing hydrogen bonds (dotted lines) (oxygen: red; nitrogen: blue).

Another general class of molecules that possesses attributes similar to those of valinomycin, i.e. pre-organization, rigid molecular structure and three-dimensional

complexation site, are container compounds such as calixarenes and calixarene-crown ethers (Figure 3).

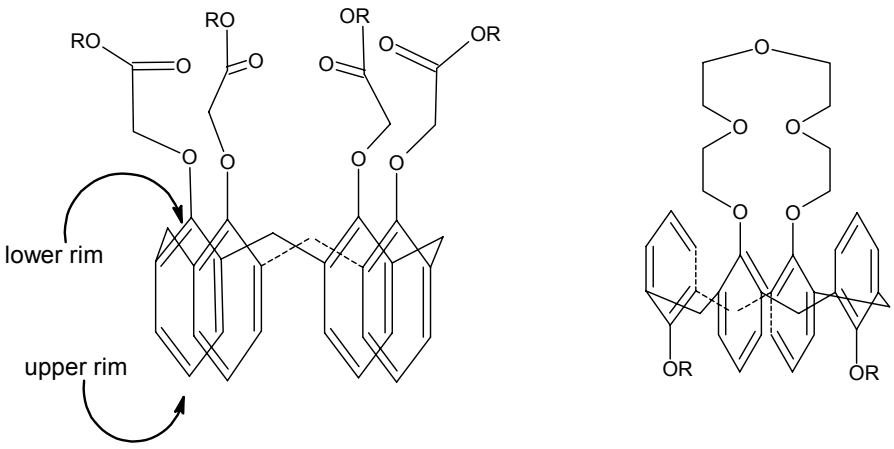

Figure 3: A tetraester calix[4]arene (left) and a 1,3-alternate calix[4]arene-crown-5 (right)

There are numerous reviews on these compounds and as a result, their structure and some of their complexation behaviors are fairly well understood.[11a] Calixarenes possess a pre-organized structure because the phenyl groups form a semi-rigid cone shape. In addition, various substituents may be placed along the lower rim to enhance complexation and thus increase selectivity. In addition, and like valinomycin, the binding site is three-dimensional and therefore can complex cations more efficiently than simple crown ethers which possess planar binding sites. In comparison to monensin esters, which are traditional sodium ionophores (see for example, Figure 4), some very simple calix[4]arenes (Figure 5) such as tetraethylester-*p*-octylcalix[4]arene[11c,12] and tetramethylester-*p*-*tert*-butylcalix[4]arene [13] exhibit higher selectivities (ca. one to two orders of magnitude increase over monensin esters).

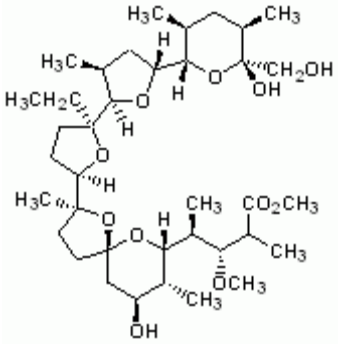

Figure 4: Methyl monensin

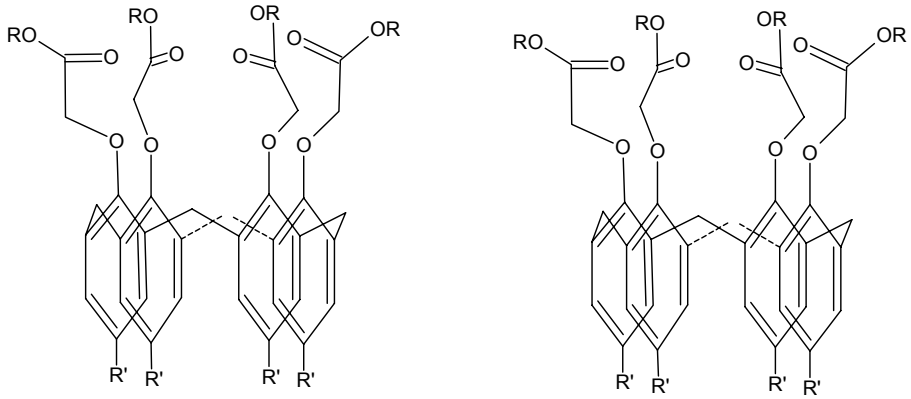

Figure 5: Tetraethylester-*p*-octylcalix[4]arene [12] (left) and tetramethylester-*p*-*tert*-butylcalix[4]arene [13] (right)

Calixarene-based counterparts for potassium are also well known, e.g., the 1,3-alternate calix[4]arene-crown-5 (Figure 3, right).[14] Although the molecule possesses the basic calix[4]arene structure, the addition of the crown-5 moiety further increases the rigidity of the molecule and thus the pre-organization. As a result, the pocket that is established is fixed and possesses little flexibility. Therefore the pocket can not deform to effectively stabilize cations that are smaller than potassium, such as sodium. In comparison to valinomycin, a marked enhancement in the $\Delta\Delta G$ of complexation between potassium and

sodium was found for this calix[4]arene-crown-5, -18.43 kJ/mol and -31.24 kJ/mol respectively. The increase of $\Delta\Delta G$ for the calix[4]arene-crown-5 in comparison to valinomycin leads to improved selectivity for potassium over sodium, $\log K_{K,Na} = 5.53$ and $\log K_{K,Na} = 3.26$, respectively.

In general, two design features must be incorporated into the ionophore to achieve high selectivity for a particular guest; the pocket of the ionophore must be an appropriate size to bind the guest and a pre-organized structure is needed to reduce the entropic and enthalpic costs of complexation. While these factors are primary drivers in the complexation of alkali metal ions additional features are required to obtain high selectivity for other cations, e.g. ammonium ion. In comparison to the alkali metal ions, which prefer octahedral (spherical) coordination shells, ammonium ions prefer a tetrahedral binding geometry. This is illustrated by the natural antibiotic nonactin, the most widely studied ammonium ionophore (Figure 6).

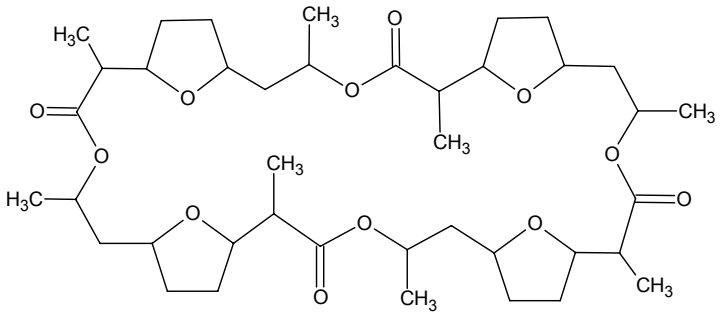

Figure 6: Nonactin

In the case of nonactin the ammonium cation is complexed through the four ethereal oxygen atoms in a tetrahedral geometry. However, due to the flexibility of the ionophore

various conformations can be adopted. As a result, nonactin can form "wrapping-type" complexes with alkali cations through the deformation of the pocket and thus is not very selective.[15] In particular, nonactin discriminates against potassium ion, which has a similar ionic radius (1.33 Å) to ammonium ion (1.43 Å), only by an order of magnitude ($\log K_{ij} \sim 1$) .[16,17]

To address the limitations of nonactin, research has focused on creating an ionophore that can supply a tetrahedral complexation geometry as well as a more rigid and potentially pre-organized structure. Attention has also been paid to the importance of hydrogen bonding. For example, Lehn et al. synthesized macrotricyclic cryptands (Figure 7) that exhibited a substantial enhancement (>100 fold) in the binding of ammonium over that of potassium, as determined by NMR studies.[18] This enhancement was attributed to the tetrahedral geometry provided by the ionophore and its ability to donate four hydrogen bonds to stabilize the cation. This result pointed out the particular importance of hydrogen bonding and symmetry considerations in the design of ammonium ion recognition sites.

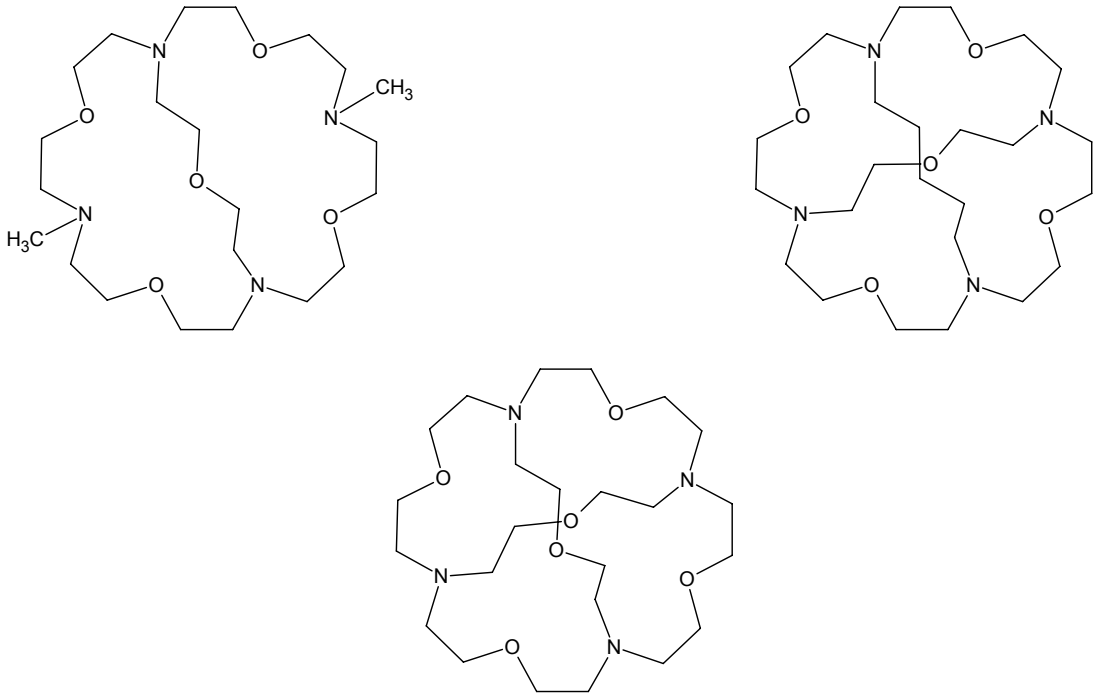

Figure 7: Lehn's cryptands

Initial complexation studies of ionophores are typically completed in solution giving association constants (also called binding or stability constants) of individual cations, from which the selectivities are calculated, (Equations **1**-**3**). However, one of the major goals of developing new and more highly selective ionophores is the attainment of *sensors*, which can be used in a variety of applications and in particular clinical diagnostic instrumentation. In a sensor format the individual association constants are not measured but rather the direct determination of the selectivity coefficient ($\log K_{ij}$) for the sensor over an interfering ion is made.

These sensors are based upon potentiometric ion selective electrodes (ISE's) in which an ionophore is doped into a plasticized-PVC membrane, which in some cases also contains a lipophilc salt. The constructed membrane is then placed into an electrode body,

typically called a Phillips body in which an internal electrolyte (usually .1M KCl) is added. The electrode is connected through a potentiostat and the cell is completed by using a reference electrode, (SCE or sat. Ag/AgCl). The two half cells can then be placed into testing solutions and the potential difference measured as a function of analyte activity, or concentration in dilute systems (Figure 8).

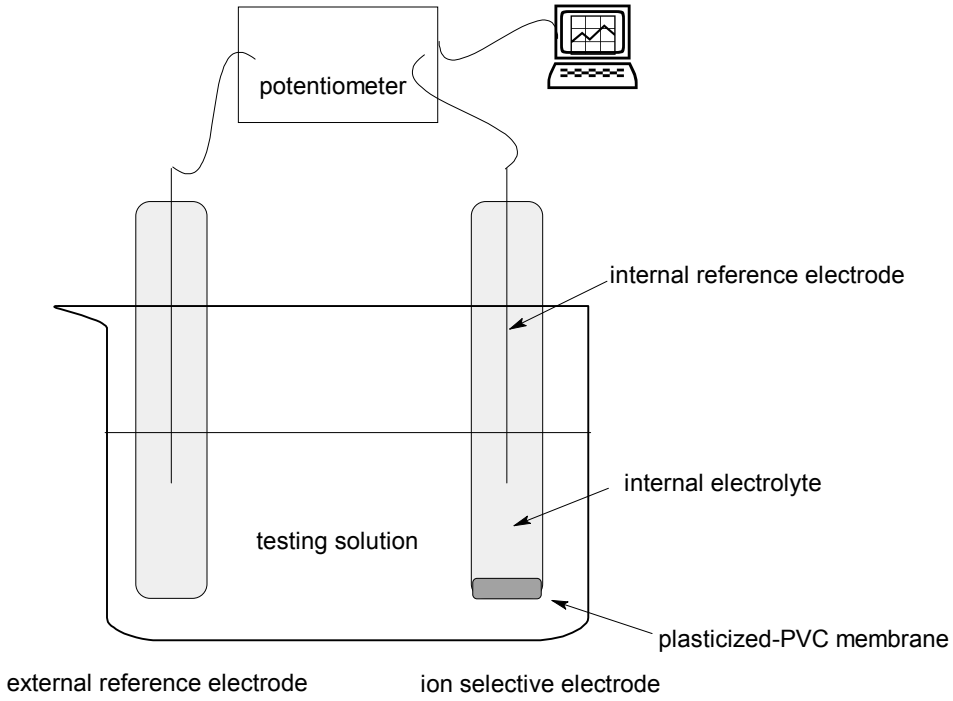

Figure 8: Basic construction of an ISE testing apparatus.

The operation of an ion selective electrode is dependent upon the establishment of a potential difference between the solution side and the internal electrolyte side of the electrode. This potential difference occurs at the solution-membrane interface. When the membrane is doped with an ionophore that is primarily selective for one ion this potential difference then becomes dependent upon the activity of this ion and is measured

against an external reference electrode. The function of the potential difference and the activity follow the well-known Nernst equation as shown;

$$E = E° - (2.303RT/nF)\log a \qquad \textbf{(4)}$$

Where E is the electromotive force (emf) of the cell in volts, E° is the emf cell constant, F is the Faraday constant, *a* is the activity of the analyte, n is the charge of the measured species and R and T are the usual thermodynamic quantities. This equation is in the form of y = mx + b and thus a plot of E verse log*a* will give a straight line with a slope of 2.303RT/nF. For the measurement of monovalent cations at 25°C, n = 1 and the slope becomes 59.16 mV/dec. Thus for any ISE that measures monovalent cations and is operating according to the Nernst equation a slope of 59.16 mV/dec would be expected.

For such systems, the selectivity of the ISE over other cations is one of the key parameters, primarily driven by the selectivity of the ionophore, and may be measured in one of several ways. The two typical methods are called the Fixed Interference Method (FIM) and the Separate Solution Method (SSM).[19] When these methods are used a selectivity coefficient for the sensor is determined and given as $\log K_{ij}^{POT}$. The "POT" refers to the fact that the selectivity value was determined potentiometrically and *i* = primary ion of interest, *j* = interfering ion. The reported selectivities are given as negative values and the more negative the better. For example, typical potassium ISE's possess selectivity values for potassium over sodium on the order of $\log K_{K,Na}^{POT} = -3.3$.

This is interpreted as the sensor being greater than three orders of magnitude more selective for potassium than for sodium.

Ion selective electrodes have been in wide use since the 1970's, particularly within the field of clinical diagnostics and therefore are well established as critical tools in the diagnosis of disease. The systems, employing the ISE technology, have changed little during this time and are still designed today using the same complex architecture that was developed over three decades ago and therefore has limited their applicability. To overcome these limitations, research has begun to focus on optical techniques of detection with a view to reduce overall complexity due to the fact that optically based systems do not require external reference electrodes and expensive electronic potentiostat equipment. In order to reach the goal of optically based clinical diagnostic systems new sensors are needed that owe their response to photonic energy rather than electrical differences. These sensors have been termed optodes and, in many cases, take advantage of ionophores that have been covalently linked to a fluorescent molecule (fluorophore) forming what is known as a fluoroionophore. Like their electrochemical counterparts, various considerations are required to be taken into account in order to develop new, highly selective and sensitive fluoroionophores.

B: Basic Considerations in the Design of Fluoroionophores

Over the past several years, there has been explosive growth in the development of fluoroionophores based on a variety of optical effects. A comprehensive review of such systems has been published by de Silva et. al.[20] One of the first considerations in the design of fluoroionophores is sensitivity and thus the preponderance of recent work has centered on the covalent linking of ionophores through an electron-donating group to electron transfer-sensitive fluorophores. The basic photophysical process of such molecules depends on an intramolecular electron transfer quenching mechanism in which the excited state of the fluorophore is quenched by electron transfer from an electron donating group in the fluoroionophore. This process is known as photoinduced electron transfer or PET. A thermodynamic prediction of the feasibility of electron transfer can be made by calculating the free energy of the process using the Rehm-Weller equation (Equation 5).

$$\Delta G_{PET} = E_{oxd/D} - E_{red/A} - \Delta E_{00} - e^2/4\pi\varepsilon r \qquad \textbf{(5)}$$

Where, $E_{oxd/D}$ is the oxidation potential of the electron donor, $E_{red/A}$ is the reduction potential of the electron acceptor, ΔE_{00} is the energy of the excited state that participates in the electron transfer process, usually a singlet state, and the final term is the Coulombic energy of the ion pair where e is the electron charge, ε is the dielectric

constant of the solvent and *r* is the distance between the two ions. The process is presented in terms of a frontier orbital energy diagram in Figure 9.

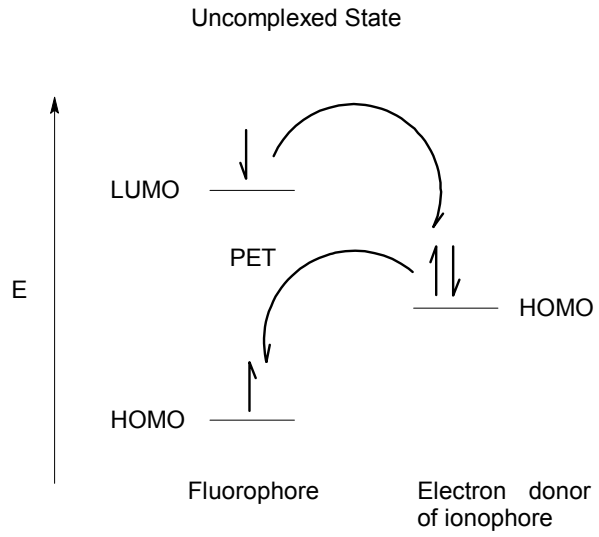

Figure 9: Frontier orbital energy diagram of fluorescence quenching in the PET mechanism.

Simplistically, Figure 9 shows that the reduction potential of the fluorophore is lowered in the excited state and is depicted in terms of the fluorophore HOMO being lower in energy than the HOMO of the electron donor in the ionophore. This being the case, an intramolecular electron transfer from the electron donor HOMO to the fluorophore HOMO occurs and simultaneously an electron transfer occurs from the LUMO of the fluorophore to the HOMO of the electron donor. As such, the radiative transition from $S_1 \rightarrow S_0$ is quenched and little or no fluorescence is observed.

Since these molecules incorporate a site for binding cations in which the electron-donating group participates, perturbation of the electron transfer process would be

expected upon complexation. Indeed, upon complexation the electrostatic field of the cation makes electron transfer to the fluorophore less efficient and leads to enhanced fluorescence emission, in effect turning the electron transfer off and turning the fluorescence on. This effect can be understood thermodynamically, i.e. the oxidation potential of the electron donor is increased relative to that of the acceptor in the complexed state. The process is presented in terms of frontier orbital energy diagram in Figure 10.

In Figure 10, the ionophore has bound a cation and is in the complexed state where the electron donor that participates in electron transfer is now involved in the complexation of the ion. Due to this ion-dipole interaction, the oxidation potential of the donor has increased and is shown in terms of the HOMO of the electron donor at a relatively lower energy with respect to the HOMO of the fluorophore. This therefore makes the intramolecular electron transfer thermodynamically less favorable and thus the radiative transition, $S_1 \rightarrow S_0$, occurs and fluorescence is observed.

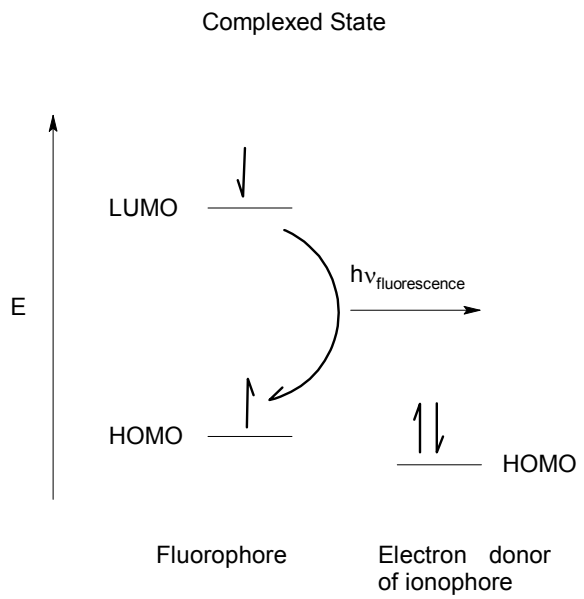

Figure 10: Frontier orbital energy diagram of fluorescence enhancement in the PET mechanism in the bound state.

In many cases, PET is highly efficient and the fluoroionophore is in an almost completely quenched state. Upon complexation the fluorescence is considerably enhanced and thus these systems have been given the term of "off-on" switches. This "off-on" PET mechanism has been reported in 9-anthryl-azacrown-5 in which 9-methylanthracene is covalently linked to the secondary amine of the azacrown moiety (Figure 11).[21a]

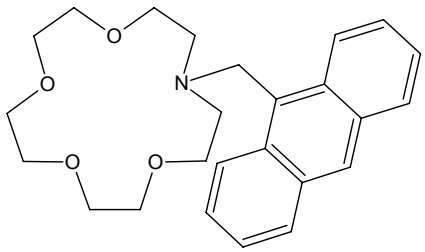

Figure 11: 9-Anthryl-azacrown-5

The free energy change for electron transfer in this molecule is estimated to be ΔG_{PET} = -0.41 eV (assuming the azacrown is the electron donor with an oxidation potential of 0.89 eV,[21b] 9-methyl-anthracene is the acceptor with a reduction potential of -1.97 eV and E_{00} = 3.17 eV,[21c] and the Coulombic term is 0.1 eV[21b]) . Upon complexation of sodium cations a >40 fold increase in the fluorescence quantum yield was observed.

Due to this high sensitivity, the majority of the early fluoroionophores have been developed with the PET mechanism in mind and for several reasons have typically been based upon crown ether structures. First, the synthetic flexibility offered by these structures allows the incorporation of a variety of fluorophores as well as electron donors. This allows for the tailoring of the fluoroionophore such that fluorophores and electron donors with the appropriate thermodynamic properties can be combined yielding potentially useful molecules. Also, these electron donor groups can be incorporated into the crown structure in positions that are potentially in close proximity to both the ion docking site and the fluorophore. For example the phenyl group in the crown structure of calix-benzocrown ethers is comparable to 1,2-dialkoxybenzenes in its electron donor behavior and in combination with a 9-cyanoanthracene (Figure 12) yields a fluoroionophore that is selective for potassium ions.[22]

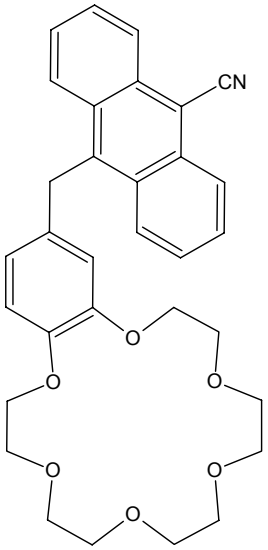

Figure 12: 9-Cyanoanthryl-benzocrown-6

A further consideration in the design of fluoroionophores is the linkage architecture between the fluorophore and the ionophore moieties. In particular, a systematic investigation of the effect of linker length on the "off-on" fluorescence mechanism was reported by Ji et al. for a series of potassium sensitive pyrenyl aza-18-crown-6 fluoroionophores.[23] In these molecules the pyrene group was tethered to the azacrown ionophore at the nitrogen atom by methylenic linkers with n = 1 - 4 methylene groups. The initial quantum yields, ϕ_0, increased in the order n = 1 < 2 ~ 3 < 4, 0.017, 0.024, 0.026, 0.072 respectively. As would be expected, the observed general trend is an increase in the ϕ_0 with increasing distance from the electron donor. The farther the fluorophore is from the electron donor, the less efficient the electron transfer there is and therefore the greater the ϕ_0. However, there is a discontinuity in the trend when n = 3. Here, the "n = 3 rule" was invoked to account for the fact that the ϕ_0 for n = 3 was approximately equal for n = 2. It was hypothesized that when n = 3, the alkyl chain can

fold onto itself, thereby decreasing the end-to-end distance between the pyrene moiety and the azacrown. Thus it was suggested that the pyrene moiety was folding over the crown, forming a sandwich complex, and thereby coming into closer proximity to the tertiary amine and consequently experiencing an enhancement of the electron transfer process, likely by way of a through space mechanism. As a result of this the ϕ_0 is lower than expected. This effect illustrates that indeed fluoroionophores are multi-component systems and that each piece needs to be considered in the design of new molecules.

C: Ionophore/Fluoroionophore Design Approach

New ionophores and fluoroionophores have been developed for ammonium, lithium, sodium and potassium ions, based upon the fundamental considerations for ionophore and fluoroionophore design as discussed above.

Proposed motifs for ammonium ion are based upon the cation's preference for tetrahedral binding which is expected to bias the ionophore's selectivity to ammonium ion over that of cations that prefer octahedral (spherical) complexation. In addition, a pre-organized and hence a rigid structure is designed into the target molecule. At the same time, the synthetic route must be reasonable and amenable to further tuning of the complexation properties of the ionophore. These criteria can potentially be met by using cyclic peptide and depsipeptide structures. The classic example of this type of structure, as noted above, is valinomycin, which possesses a pre-organized rigid structure and has been synthesized with a combination of solution and solid phase techniques. Using valinomycin as our inspiration, several target molecules have been designed and investigated using a combination of energy minimization, molecular dynamics, and docking energies to evaluate their potential as ammonium ionophores. One of these candidates, a cyclic hexadepsipeptide, has been synthesized and tested in ion selective electrodes and its potentiometric properties evaluated.

Lithium, sodium and potassium *fluoro*ionophores have been designed based upon calixarene and calixarene crown architectures, again due to their inherent pre-organized

structures as well as their facile synthetic pathways. Respective candidates were evaluated in the same manner as the ammonium ionophore targets with one additional computational parameter, i.e. electrostatics, to determine at least qualitatively, the extent of electron density redistribution upon complexation. This, in combination with ΔG_{PET} calculations will help predict the ability of these candidates to act as fluoroionophores.

II: General Experimental

Mass spectra were performed by SYNPEP Corporation, Dublin, CA or by Bayer Diagnostics, Medfield, MA. Melting points are measured in a Mel-Temp capillary melting point apparatus and are not corrected. ^{1}H- and ^{13}C- NMR spectra were recorded with a Bruker Avance 400 in $CDCl_3$ unless otherwise noted. Optodes were housed in a custom flow-through cell. IR spectra were obtained with a Perkin Elmer Spectrum One FT-IR Spectrometer. All solvents and reagents were analytical reagent grade and used as supplied from Aldrich Chemical Co. Poly(vinyl chloride) (PVC), nitrophenyloctylether (NPOE), dioctyl phthalate (DOP), potassium tetrakis(4-chlorophenyl)borate (KtpClPB) and D-Hydroxyisovaleric acid were purchased form Fluka AG (Buch, Switzerland). Amino acids L and D-valine-N-fmoc were purchased from Calbiochem-Novabiochem Corp. Calix[4]arene was purchased from Acros. 4-*p-tert*-Butylcalix[4]arene-tetraaceticacid-tetraethylester and 4-*p-tert*-butylcalix[4]arene was obtained from Fluka. Buffers were prepared with deionized water (18 MΩ·cm).

Fluorescence Measurements

Fluorescence emission and excitation spectra were obtained with a Perkin Elmer LS-50B Fluorimeter. In the case of *in situ* studies, fluorescence was measured as a function of metal ion concentrations where the metal ions were added as the acetate or hexafluorophosphate salts. For sensor studies, aqueous solutions of the chloride salts

were used. Fluorescence areas were determined by integrating the spectrum over a fixed wavelength range.

Molecular Modeling Calculations

Molecular modeling was preformed on an SGI 320 running Windows NT. Calculations were carried out using the Molecular Operating Environment (MOE) ver. 2000.02 computing package (Chemical Computing Group Inc., Montreal, Quebec, Canada.). Structures were minimized first using the AMBER94 potential control under a solvent dielectric of 5. PEF95SAC was used to calculate partial charges. Minimized structures were then subjected to a 30 ps molecular dynamics simulation. The structures were heated to 400 K, equilibrated at 310 K and cooled to 290 K in the dynamics thermal cycle at a rate of 10 K/ps. The lowest energy structures obtained from these dynamics calculations were then minimized again. Using the minimized structures, docking energies of the cation complexes were calculated by employing the default parameters supplied with the program. Electrostatic calculations were then preformed on the molecules using the default parameters.

III: Results and Discussion

A: Ammonium Ionophore (8)

Metabolites such as urea and creatinine are important disease indicators[25] and for this reason considerable effort has been expended in developing diagnostic tools for their detection. Concentrations of urea and creatinine in biological media can be detected indirectly by measuring the amount of ammonium ion generated upon enzyme-catalyzed hydrolysis.[25,26] The measurement of the ion has traditionally been accomplished by the use of ion selective electrodes (ISE) doped with the natural antibiotic nonactin.[25-34] A serious drawback to the use of nonactin is that it is only about ten times more selective for the ammonium ion than it is for the potassium ion.[25,26] This lack of selectivity is particularly problematic when the concentration of ammonium ion generated from creatinine is less than the background potassium concentration. This has led a number of groups to develop new ammonium ionophores. For example, Chin and co-workers synthesized 1,3,5-tri(3,5-dimethylpyrazol-1-ylmethyl)-2,4,6-triethylbenzene in which the three pyrazole groups provide hydrogen bonding sites.[35] An ISE incorporating this molecule showed improvement in ammonium ion selectivity over potassium ion as compared to nonactin ($\log K^{POT}_{NH_4^+,K^+} = -2.6$), illustrating the importance of hydrogen bonding and symmetry. However, the limit of detection for this ionophore is two orders of magnitude higher than for nonactin and therefore it is not sufficiently sensitive for some applications. Kim et al. investigated the use of thiazole-containing benzocrown ethers as ammonium ionophores and reported potassium selectivity comparable to nonactin and enhanced selectivity for ammonium over sodium ion

($\log K^{POT}_{NH_4^+,Na^+} = -3.9$).[36] Similarly, others have used 19-crown-6 structures with decalino blocking groups to control selectivity, reporting increased selectivity for ammonium over both smaller and larger cations.[37]

The approach taken here to the design and synthesis of ammonium ionophores has, like Lehn[18] and others,[35-37] focused on the incorporation of hydrogen bond donors in tetrahedrally-symmetric complexation sites. Given the structural complexity of some of the synthetic ionophores reported, we have used a molecular motif that both lends itself to straightforward synthesis and allows structural modifications to be incorporated without substantial changes in synthetic strategy. Our experience to date, as well as that of others,[39-42] has shown that ionophores based on cyclic peptide and depsipeptide structures, i.e., those that are similar to natural ionophores, can be readily synthesized in high yield by either solution or solid phase methods.

In the work reported here we have taken valinomycin as our inspiration for the design of a new ammonium ion specific ionophore. Valinomycin is a naturally occurring antibiotic having high selectivity for potassium ions. It has a cyclic depsipeptide structure consisting of alternating amide and ester units (six of each, twelve in total) and has been synthesized on a solid phase support.[42] Valinomycin pre-organizes through hydrogen bonding of its amide carbonyl groups to form a pocket which presents its six ester carbonyl groups as sources of electrostatic stabilization for potassium ions.[43] Thus, the pocket provides an octahedral type complexation site with a size that is a close match to the estimated ionic radius of potassium (1.33 Å). We report here the synthesis of an

ammonium ion-specific ionophore, **8**, which has some of the same structural elements as valinomycin. Compound **8** is a cyclic depsipeptide consisting of alternating amide and ester groups (three of each, six in all) which is, in effect, one half of the valinomycin structure. Compound **8** does not fold onto itself and therefore it provides a complexation site that is approximately the same size as valinomycin, a necessary feature because the ammonium ionic radius (1.43Å) is comparable to that of potassium.[18] An important difference though, is that **8** is not capable of providing an octahedral binding site. However, it has hydrogen bond donors arranged tetrahedrally (necessary for ammonium complexation) and it is this distinction that we expected to allow the ionophore to discriminate efficiently between potassium and ammonium ions.

Below we describe the synthesis of **8**; the incorporation of this ionophore into a planar ISE sensor format; testing of the potentiometric response of the electrode in a commercial clinical diagnostic 'Point-of-Care' instrument; and the results of selectivity studies for ammonium versus other metal cations.

Ammonium Ionophore Experimental

Synthesis of 3. (Scheme 1, see text p. 53**)**

Note: All NMR and Mass Spectroscopy data in Appendix A1.

L-Lactic acid benzyl ester (BzlO-L-lac, 1) (based on a modified procedure).[42] 10 g (111 mmol) of L-lactic acid was dissolved in 150 mL of anhydrous benzyl alcohol. The solution was saturated with HCl gas and stirred for 18 hr where upon the solution was diluted with 200 mL CH_2Cl_2. The organic layer was washed 3 times with 100 mL 1 N KOH, and then with 100 mL 10% citric acid and dried over Na_2SO_4. The CH_2Cl_2 was removed under vacuum at 40 °C. The benzyl alcohol was removed by vacuum distillation (2.5 mmHg) and the product recovered as a colorless oil at 120°C, 10.3 g, yield 51.3%. The NMR spectra conforms to the literature.[44] ^{1}H-NMR (400 MHz, $CDCl_3$), δ 1.47 (s, 3H), 3.05 (s, 1H), 4.33-4.59 (m, 1H), 5.24 (s, 2H), 7.39 (m, 5H); ^{13}C-NMR (100 MHz, $CDCl_3$), δ 20.3 (CH_3), 66.8 (CH), 67.2 (CH_2), 128.2, 128.5, 128.6, 135.2 (Ar), 175.5 (C=O).

BzlO-L-lac-D-val-N-fmoc (2). 19.4 g (57.2 mmol) of D-valine-N-fmoc was dissolved in 175 mL of CH_2Cl_2 to which 8.92 mL (1 eq.) of diisopropylcarbodiimide (DIPCDI) was added. The solution was stirred for 25 min. where upon 10.3 g (1 eq.) of the formed L-lactic acid benzyl ester (**1**) and .696 g (.1 eq) of 4-dimethylaminopyridine (DMAP) was added. This mixture was then stirred for an additional 18 hr. The insoluble urea thus formed was removed by filtration and the solution was washed once with 100 mL of

water, thrice with 100 mL saturated $NaHCO_3$, thrice with 100 mL 10% citric acid and then dried over Na_2SO_4. The CH_2Cl_2 was then removed under vacuum at 40 °C to yield a yellow gum. The product was obtained by recrystallization using cold ether to yield 22.6 g of a white solid, yield 79%. mp. 104-106 °C; R_f .43 (CH_2Cl_2); ^{1}H-NMR (400 MHz, $CDCl_3$), δ .84 (d, *J* = 6.9 Hz, 3H), .91 (d, *J* = 6.9 Hz, 3H), 1.44 (s, 3H), 2.14-2.18 (m, 1H), 4.14-4.18 (m, 1H), 4.30-4.36 (m, 3H), 5.11-5.14 (m, 3H), 5.22 (d, *J* = 9.1 Hz, 1H), 7.24-7.34 (Ar, 9H), 7.53 (d, *J* = 7.4 Hz, 2H), 7.69 (d, *J* = 7.5 Hz, 2H); ^{13}C-NMR (100 MHz, $CDCl_3$), δ 15.9 (CH_3), 16.4 (CH_3), 17.9 (CH_3), 30.3 (CH), 46.1 (CH), 57.9 (CH_2), 66.0 (CH), 66.1 (CH_2), 68.3 (CH), 119.0, 124.1, 126.0, 126.7, 127.2, 127.4, 127.6, 134.1, 140.3, 142.7, 142.9 (Ar), 155.1, 169.0, 170.2 (C=O). ESI MS *m/z* (%) calcd. for $C_{30}H_{32}NO_6$ ($M+H^+$) 502.2, found 502.2 (15), $M+Na^+$ calcd. 524.2, found 524.4 (100), $M+K^+$ calcd. 540.2, found 540.2(11)

L-Lac-D-val-N-fmoc (3). 22.6 g (45 mmol) of the formed BzlO-L-lac-D-val-N-fmoc (**2**) was dissolved in 150 mL CH_2Cl_2. The benzyl ester group was removed by using 2 g of Pd activated carbon, 10 wt%, and H_2 at atmospheric pressure over 3 hr. The spent catalyst was removed by filtration and the solution was washed thrice with 100 mL saturated $NaHCO_3$. The aqueous phase was acidified with 3N HCl and extracted with CH_2Cl_2. The organic layer was washed with 100 mL brine, dried over Na_2SO_4 and concentrated totally under vacuum at 40°C, to afford in quantitative yield the title compound as a white crystalline solid, 18.5 g. mp 62-64 °C; R_f .45 (9:1 CH_2Cl_2/MeOH); ^{1}H-NMR (400 MHz, $CDCl_3$), δ 0.93 (d, *J* = 6.8 Hz, 3H), 0.99 (d, *J* = 6.8 Hz, 3H), 1.53 (d, *J* = 6.8 Hz, 3H), 2.25 (m, 1H), 4.22 (m, 1H), 4.37-4.42 (m, 3H), 5.17 (m, 2H), 5.33 (d,

J = 9.0 Hz, 1H), 7.29-7.41 (Ar, 4H), 7.59 (d, *J* = 7.4 Hz, Ar, 2H), 7.76 (d, *J* = 7.5, Ar, 2H); ^{13}C-NMR (100 MHz, $CDCl_3$), δ 16.9 (CH_3), 17.5 (CH_3), 19.0 (CH_3), 47.0 (CH), 59.0 (CH_2). 67.1 (CH), 69.0 (CH), 120.0, 124.9, 125.1, 127.1, 127.7, 141.3, 143.7, 143.8 (Ar), 156.4, 171.3, 174.4 (C=O). EIS MS *m/z* (%) calcd for $C_{23}H_{25}NO_6Na$ ($M+Na^+$) 434.2 found 434.2(100)

Synthesis of 6. (Scheme 2, see text p. 53**)**

D-Hydroxisovaleric acid benzyl ester (BzlO-D-hyval, 4). The title compound was prepared in same the manner as L-lactic acid benzyl ester using 19.5 g (139 mmol) of D-hydroxyisovaleric acid to yield 29.0 g, yield 84.4%. The NMR spectra conforms to the literature.[45,46] ^{1}H-NMR (400 MHz, $CDCl_3$), δ 0.83 (d, J = 6.8 Hz, 3H), 1.00 (d, J = 6.8 Hz, 3H), 2.06-2.11 (m, 1H), 2.92 (d, J = 6.2 Hz, 1H), 4.08 (dd, J = 6.2, 3.5 Hz, 1H), 5.17 (d, J = 12.1 Hz, 1H), 5.23 (d, J = 12.1 Hz, 1H), 7.31-7.38 (m, 5H); ^{13}C-NMR (100 MHz, $CDCl_3$), δ 15.9 (CH_3), 18.8 (CH_3), 32.2 (CH), 67.2 (CH_2), 75.0 (CH), 128.4, 128.5, 128.6, 135.2 (Ar), 174.8 (C=O).

BzlO-D-hyval-L-val-N-fmoc (5). 24.0 g (70.7 mmol) of L-valine-N-fmoc, 14.5 g (1 eq.) of the formed D-Hydroxisovaleric acid benzyl ester (**4**), 36.2 g (1 eq.) PyBop, 9.5 g (1 eq.) HOBT and 25 mL (2 eq.) of diisopropylethylamine (DIPEA) were added to 200 mL CH_2Cl_2. This mixture was then stirred for 4 hr. The resulting solution was washed thrice with 100 mL saturated $NaHCO_3$, thrice with 100 mL 1N HCl and dried over Na_2SO_4. The CH_2Cl_2 was then removed under vacuum at 40 °C. The product was obtained by flash chromatography (Biotage Flash40 column 15 cm x 7 cm, hexane/ CH_2Cl_2/EtOAc

60/35/5) to yield 19.0 g of a colorless oil, yield 51.5%. R_f .43 (CH_2Cl_2); ^{1}H-NMR (400 MHz, $CDCl_3$), δ 0.92-1.01 (m, 12H), 2.25-2.28 (m, 2H), 4.24 (d, *J* = 7.0 Hz, 1H), 4.38-4.46 (m, 3H), 4.92 (d, *J* = 4.2 Hz, 1H), 5.13-5.19 (m, 2H), 5.27-5.29 (m, 1H), 7.29-7.42 (Ar, 9H), 7.60 (d, *J* = 7.3 Hz, Ar, 2H), 7.77 (d, *J* = 7.5 Hz, Ar, 2H); ^{13}C-NMR (100 MHz, $CDCl_3$), δ 17.1, 17.3, 18.8, 19.1 (CH_3), 30.1, 31.3 (CH), 47.1 (CH), 59.1 (CH), 67.2 ($2CH_2$), 77.9 (CH), 120.0, 125.1, 125.1, 127.1, 127.7, 128.4, 128.4, 128.6, 135.1, 141.3, 143.8 (Ar), 156.1, 169.0, 171.6 (C=O); EIS MS *m/z* (%) calcd. for $C_{32}H_{35}NO_6Na$ ($M+Na^+$) 552.2 found 552.2(100), calcd. $M+K^+$ 568.2 found 568.2(48).

D-hyval-L-val-N-fmoc (6). 14.5 g (27 mmol) of **5** was dissolved in 100 mL CH_2Cl_2. The benzyl ester group was removed by using 2 g of Pd activated carbon, 10 wt%, and H_2 at atmospheric pressure over 2 hr. The spent catalyst was removed by filtration and the solution was washed thrice with 100 mL saturated $NaHCO_3$. The aqueous phase was acidified with 3N HCl and extracted with CH_2Cl_2. The organic layer was dried over Na_2SO_4 and concentrated totally under vacuum at 40°C, to afford the title compound as a colorless gum, 9.6 g, yield 80%. R_f .59 (9:1 CH_2Cl_2/MeOH); ^{1}H-NMR (400 MHz, $CDCl_3$), δ 0.92-1.04 (m, 12H), 2.27-2.30 (m, 2H), 4.23 (d, *J* = 6.9 Hz, 1H), 4.38-4.45 (m, 3H), 4.93 (d, *J* = 4.0 Hz, 1H), 5.35 (d, *J* = 9.0 Hz, 1H), 7.29-7.41 (Ar, 4H), 7.59 (d, *J* = 7.4 Hz, Ar, 2H), 7.76 (d, *J* = 7.5 Hz, Ar, 2H); ^{13}C-NMR (100 MHz, $CDCl_3$), δ 17.0, 17.4, 18.9, 19.1 (CH_3), 30.0, 31.1 (CH), 47.1 (CH), 59.2 (CH), 67.2 (CH_2), 120.0, 124.0, 125.1, 127.0, 127.7, 141.7, 143.7 (Ar), 156.4, 171.7, 173.8 (C=O). EIS MS *m/z* (%) calcd. for $C_{25}H_{29}NO_6Na$ ($M+Na^+$) 462.2 found 462.4(100), calcd. $M+K^+$ 478.2 found 478.2(48).

Synthesis of the acyclic depsipeptide, 7. (Scheme 3, see text p. 54**)**

Solid phase synthesis was carried out on 2.9 g of Wang resin (1.1 mmol/g loading). The resin was prepared by adding 20 mL of DMF and mixing for 30 min. under N_2 at which point the DMF was removed by aspiration. During which time, 3.28 g (2.5 eq. to resin loading) of **3** was dissolved in 50 mL of CH_2Cl_2 to which 1.25 mL diisopropylcarbodiimide was added. This was stirred for 25 min. at which point the CH_2Cl_2 was removed under vacuum at 40°C giving a white residue. 10 mL of DMF was added to the white residue and this solution was then added to the swelled resin. 40 mg (0.1 eq) of 4-dimethylaminopyridine was also added and the mixture was mixed under N_2 for 1 hr. The reaction solution was removed by aspiration and the resin was washed thrice with 20 mL DMF, thrice with 20 mL MeOH and dried under vacuum. Loading was tested by cleaving the fmoc protection group from a known mass of resin (20 mg) with 20% piperidine in DMF and monitoring the UV absorption at 290 nm. Using a molar extinction coefficient value of 4950 a loading of 50% was obtained. The process was repeated in full to obtain 70% loading. The remaining resin was deprotected with 20% piperidine in DMF (30 mL, 10 min.). The solution was removed by aspiration and the resin was washed thrice with 20 mL DMF, thrice with 20 mL MeOH, thrice with 20 mL DMF. 3.50 g. (2.5 eq) of **6** was added to 30 mL of DMF and 4.15 g (2.5 eq.) of PyBOP, 1.08 g (2.5 eq.) HOBT, and .278mL (5 eq.) of diisopropylethylamine. This mixture was then added to the resin and mixed under N_2 for 4 hr. The solution was removed by aspiration and the resin was washed thrice with 20 mL DMF, thrice with 20 mL MeOH, once with EtOH and dried under vacuum. Complete coupling was confirmed

by the Kaiser test for free amine. The general procedure was repeated again for the addition of the final block, **3**. The linear depsipeptide, **7**, was cleaved from the dried resin with TFA/H_2O/TIS 95/2.5/2.5 over 2 hr. by mixing under N_2. The cleavage mixture was removed by aspiration and was concentrated to give a brown residue. The brown residue was dissolved and concentrated twice more with toluene. The crude product was purified by flash chromatography (Biotage Flash40 column 15cm x 7cm, CH_2Cl_2/MeOH 95/5) to obtain 380 mg of an off white powder, yield 88% based on 70% resin loading. mp 144-146 °C; R_f .49 (9:1 CH_2Cl_2/MeOH); ^{1}H-NMR (400 MHz, DMSO-d_6), δ 0.72-0.84 (m, 24H), 1.21-1.26 (m, 6H), 1.96-2.00 (m, 4H), 4.12-4.14 (m, 2H), 4.68 (d, *J* = 5.4 Hz, 1H), 4.74 (d, *J* = 7.0 Hz, 1H), 5.04 (d, 6.8 Hz, 1H), 8.12 (d, *J* = 8.4 Hz, 1N<u>H</u>), 8.37 (d, *J* = 8.5 Hz, 1N<u>H</u>); ^{13}C-NMR (100 MHz, DMSO-d_6), δ 17.3, 17.5, 17.8, 18.2, 18.2, 18.3, 18.3, 18.9, 19.2, 19.3 (CH_3), 30.3, (2CH), 30.4 (2CH), 57.4, 57.6, 57.7, 69.8, 70.9, 78.1 (CH), 158.2, 158.6, 169.0, 169.7, 170.0, 170.8 (C=O); EIS MS *m/z* (%) calcd. for $C_{26}H_{46}N_3O_{10}$ ($M+H^+$) 560.3 found 560.4(100).

Synthesis of 8. (Scheme 3)

150mg (.276 mmol) of the acyclic depsipeptide, **7**, was dissolved into 20 mL thionyl chloride and mixed for 1.5 hr. at which point the solution was concentrated to give a white solid. The residue was immediately taken up in 150 mL anhydrous benzene and .144 mL (1.05 mmol) triethylamine and mixed for 18 hr. The solvent was removed under vacuum, 40°C. The residue was taken up in 100 mL CH_2Cl_2 and washed with 100 mL 10% citric acid, 100 mL saturated $NaHCO_3$, dried over Na_2SO_4 and the organic layer concentrated totally to afford 75 mg of an off white powder, yield 50%. mp 96-98 °C; R_f

.58 (CH_2Cl_2); ^{1}H-NMR (400 MHz, CD_3CN), δ .85-.88 (m, 24H), 1.26-1.40 (m, 6H), 2.14 (m, 4H), 4.19-4.26 (m, 3H), 4.82 (d, *J* = 4.3 Hz, 1H), 5.00 (m, 1H), 5.12 (m, 2H), 6.77 (d, *J* = 7.8 Hz, 1NH), 6.95 (d, *J* = 6.4 Hz, 1NH), 7.02 (d, *J* = 7.08 Hz, 1NH); ^{13}C-NMR (100 MHz, $CDCl_3$) δ 14.7, 16.1, 16.5, 16.9, 17.0, 17.6, 17.7, 17.9, 18.2, 18.5 (CH_3) 29.0, 29.1, 29.4, 29.7 (CH), 56.0, 57.4, 57.6, 69.1, 70.8, 78.7 (CH), 168.0, 169.1, 169.6, 169.6, 170.6, 171.2 (C=O). EIS MS *m/z* (%) calcd. for $C_{26}H_{44}N_3O_9Na$ ($M+Na^+$) 564.2 found 563.7(100), calcd. $M+K^+$ 580.2 found 579.7(40).

ISE Membrane and Electrode Preparation.

Four membrane cocktails were prepared to test **8**. The specific formulations are as follows: M1: 69/30/1 wt% of NPOE/PVC/**8**, M2: same as M1 with 50 mole % of KtpClPB to **8**, M3: 69/30/1 wt% of DOP/PVC/**8**, M4: same as M3 with 50 mole % KtpClPB to **8**. Membrane cocktails were prepared as 10 wt% solutions in THF. The base electrodes were constructed in a thick film planar format[47] using a polymeric internal electrolyte layer.[48,49] A single wafer which is composed of 100 individual electrode elements was used for the sensor construction. The polymer for the internal electrolyte was prepared as a 10 wt% solution in EtOH and spun on to the planar wafer at 750 rpm for 30 seconds and allowed to dry for 1 hour before membrane deposition. Internal electrolyte thickness was ca. 3.5 μm. The wafer was then quartered giving 4 wafers of 25 sensors each. Membrane cocktails were deposited (.9 mL) onto the wafers and allowed to cure for 24 hours before use giving a membrane thickness of ca. 105 μm. The planar wafers were singulated by hand giving 25 sensors for each formulation.

ISE Testing.

The sensors were housed in the proprietary flow through cell used with the Bayer Diagnostics Rapidpoint 400 critical care system. This system uses a saturated Ag/AgCl reference cell. Two flow cells were constructed which contained 3 sensors of each formulation for a total of 12 tested sensors. Each cell was tested individually on the Rapidpoint system, which maintains a 37 °C temperature for the cell. The sensors were tested using solutions containing NH_4Cl (0.1 – 100 mM), 100 mM Tris buffer (pH 7.2) and .05g/l Brij 700. Selectivity testing was based on the separate solution method (SSM),[50,51] where $i = j = 0.1$M.

Ammonium Ionophore Results and Discussion

Ionophore Modeling and Synthesis

As we have noted, **8** possesses some structural similarities to valinomycin in that it provides an appropriately-sized binding pocket for complexation of ammonium or potassium cations (ionic radii: 1.43 Å and 1.33 Å, respectively).[18] However, instead of providing an octahedral complexation geometry like valinomycin, **8** is only able to stabilize ions with tetrahedral binding requirements such as ammonium ion. It is on this basis that we predicted enhanced ammonium ion/potassium ion selectivity for **8** over that of valinomycin. This is supported by Figure 13 showing the results of modeling the binding of ammonium and potassium ions with **8**.

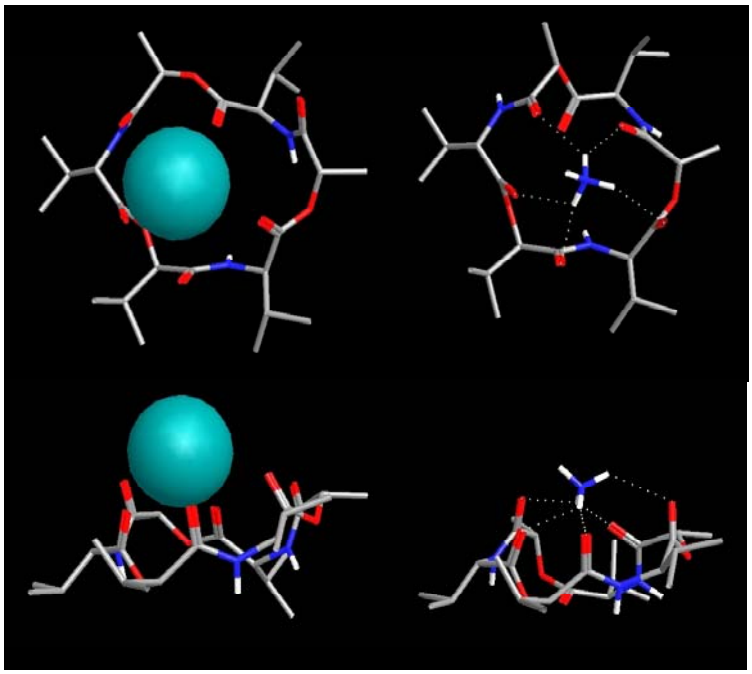

Figure 13: Minimized structures of **8** complexed with potassium ion (left) and with ammonium ion (right).

These minimized structures (obtained as described above) show the ammonium cation centrally located within the pocket and able to hydrogen bond with at least five of the carbonyl groups in **8**. In contrast, the potassium cation adopts a position that is shifted to one side and therefore provides an unfavorable binding site for potassium.

Modeling of **8** also indicates that it may offer enhanced ammonium/potassium selectivity over nonactin, the ammonium ionophore commonly used in ISE applications. Minimized structures of nonactin with ammonium and potassium ions are shown in Figure 14.

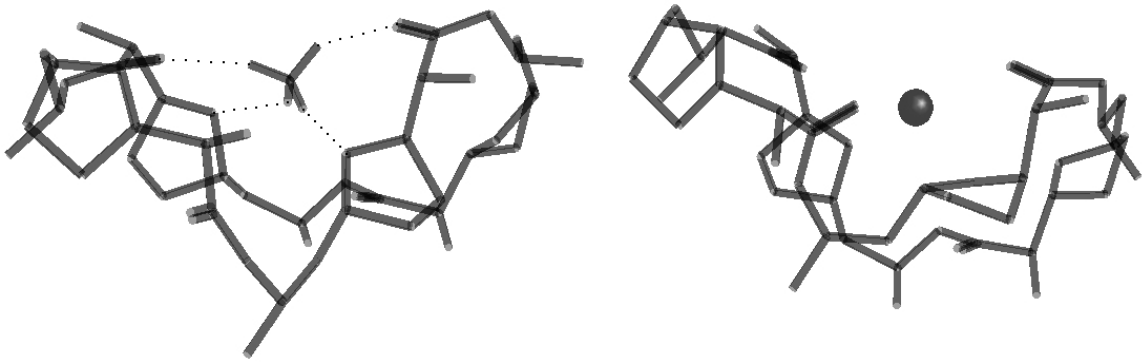

Figure 14: Minimized structures of nonactin complexed with ammonium ion (left) and with potassium ion (right).

The crown ether backbone of nonactin is quite flexible and allows for the formation of wrapping-type complexes with both ions. In such complexes the ions are enveloped by the nonactin structure and have multiple binding opportunities with the ethereal and/or carbonyl oxygen atoms present. It is important to note that formation of this envelope is essential for binding potassium ions because it is only in this conformation that an octahedral binding geometry is provided. On the other hand the cyclodepsipeptide **8**

possesses a more rigid backbone structure that cannot easily form a "wrapping-type" structure. As a result, an octahedral binding site is not provided and potassium ion binding will not be favorable. However, since a tetrahedral complexation geometry is available, ammonium ion binding can occur.

To estimate the efficiency of ammonium binding in **8** compared with that in nonactin, docking energies were obtained for the ion/ionophore complexes in each case. In the case of **8**, the difference in docking energies between ammonium ion and potassium ion was calculated to be 6 kcal/mol more negative than that calculated for nonactin. While these calculations give relative values only, they indicate qualitatively that **8** should be at least comparable to nonactin in terms of its ammonium/potassium ion selectivity.

Schemes 1-3 show the strategy used for the synthesis of **8**. The same solution and solid phase techniques reported previously for the synthesis of valinomycin[42] have been used here with the exception that a Fmoc protection strategy was employed. This strategy allows the synthesis to be carried out on a commercially available solid phase support (Wang resin). Also, cleavage can be carried out under mild conditions. Thus, block components **3** and **6** were synthesized in solution, **3** was loaded on a Wang resin coupled with **6** and then again with **3** to yield **7** which was subsequently cleaved from the resin and cyclized to form **8**. Although **8** was synthesized from the same component groups found in valinomycin (L-lactic acid, D-hydroxisovaleric acid, L- and D-valine), it is clear that a variety of hydroxylated amino acid derivatives and natural amino acids can be used in order to produce an ionophore with the appropriate binding site size and symmetry.

(We note that the stereochemistry of the individual groups in valinomycin has been preserved in the design of **8**.) This approach, then, represents a flexible strategy that will allow future systematic investigations of the effects of structure on the efficiency and selectivity of ammonium ion complexation.

Scheme 1

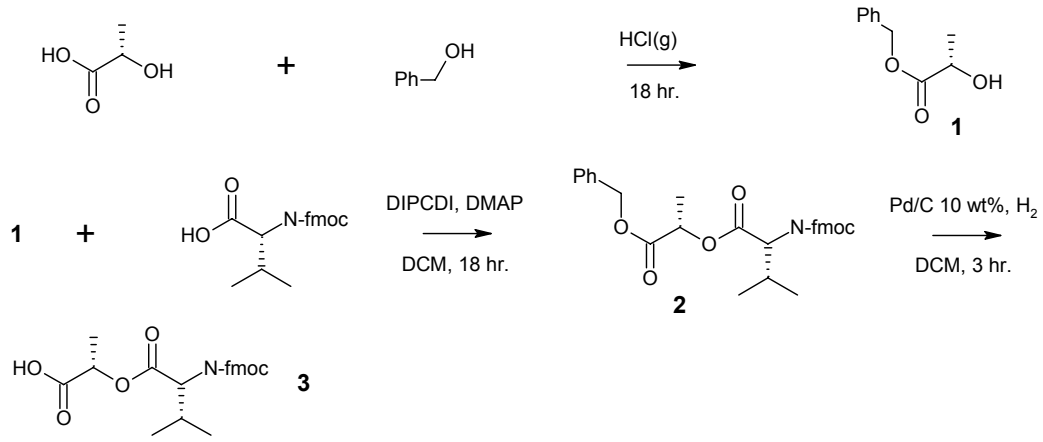

Scheme 2

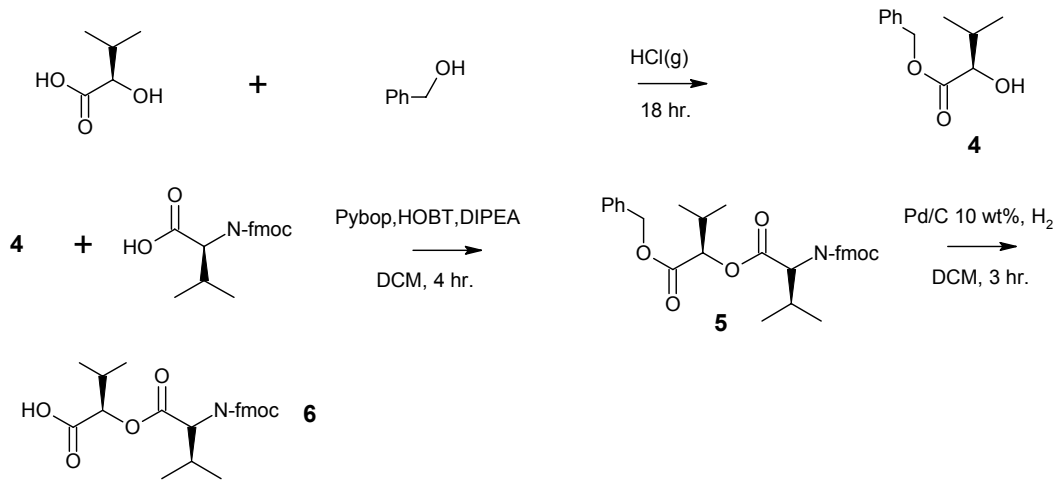

Scheme 3

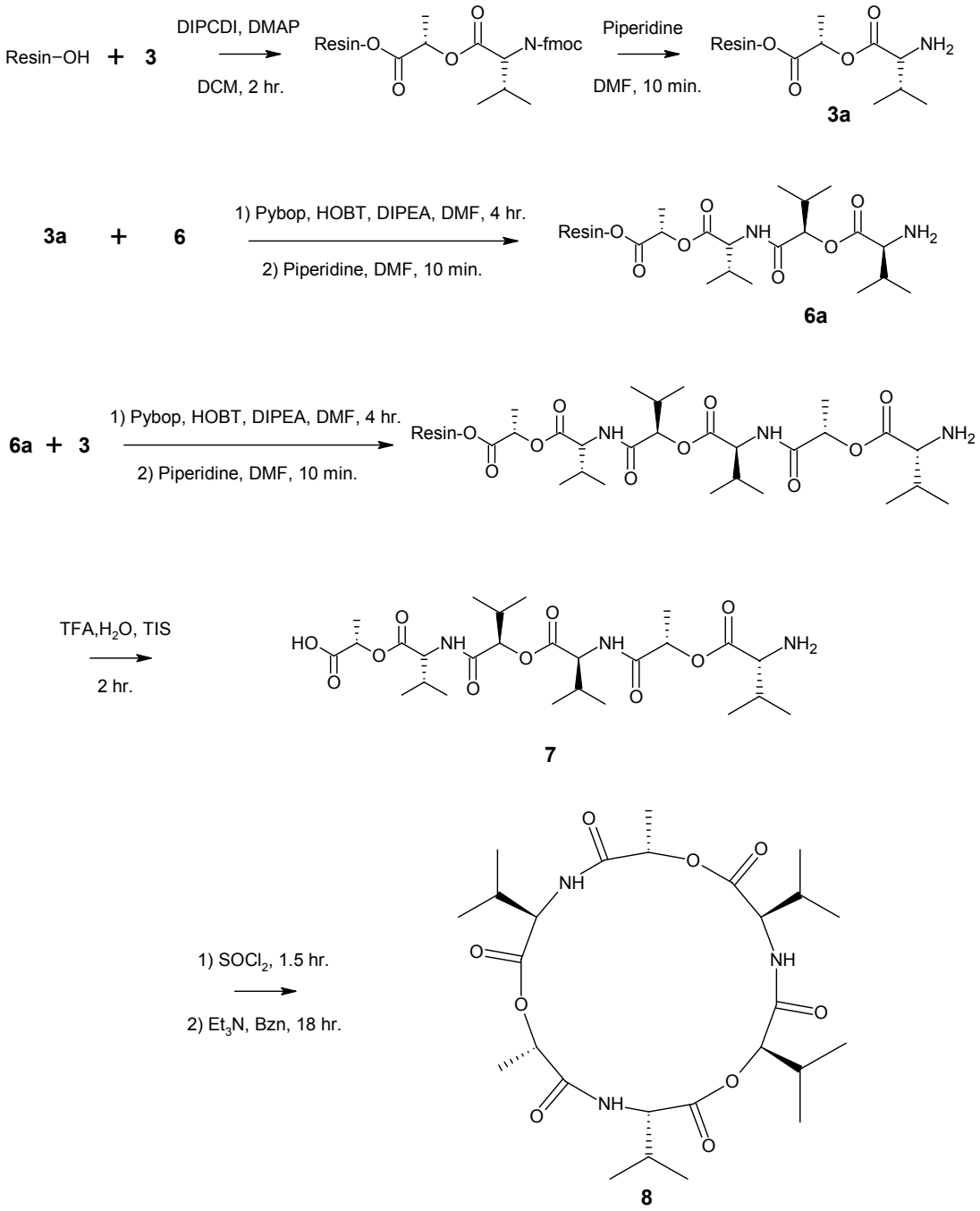
Resin−OH + 3
DIPCDI, DMAP
DCM, 2 hr.
Resin-O
N-fmoc
Piperidine
DMF, 10 min.
NH2
3a
3a + 6
1) Pybop, HOBT, DIPEA, DMF, 4 hr.
2) Piperidine, DMF, 10 min.
NH
6a
6a + 3
TFA,H2O, TIS
2 hr.
HO
7
1) SOCl2, 1.5 hr.
2) Et3N, Bzn, 18 hr.
8

Sensor Fabrication and Testing

With the advent of micro-fabrication techniques, planar type electrodes have become an attractive alternative to traditional Phillips body ISE's due to the ability to construct and test many sensors at once. In addition, planar type electrodes make use of polymeric solid internal contacts, which allow for the construction of an all-solid state ISE. The all-solid state format has advantages over traditional Phillips body ISE's such as ease of construction, cost effectiveness and ability for miniaturization. Systems such as these have been shown to be quite stable and have been shown to give potentiometric selectivities that are comparable to traditional ISE's.[52] In particular, ammonium sensors have been constructed using the all-solid contact concept and have been shown to possess selectivities that are typical of nonactin based Phillips body ISE's.[53]

These advances have led to a substantial increase in the use of the planar format and has prompted manufacturers to offer clinical diagnostic instrumentation that utilizes planar ISE's.[54,55] Following this trend, **8** was incorporated into a planar ISE structure employing a polymeric solid contact material[47-49] and tested in a commercially available Point-of-Care clinical diagnostic system. Figures 15 and 16 show an edge on and top view of the planar electrode substrate and Figure 17 shows an actual sensor.

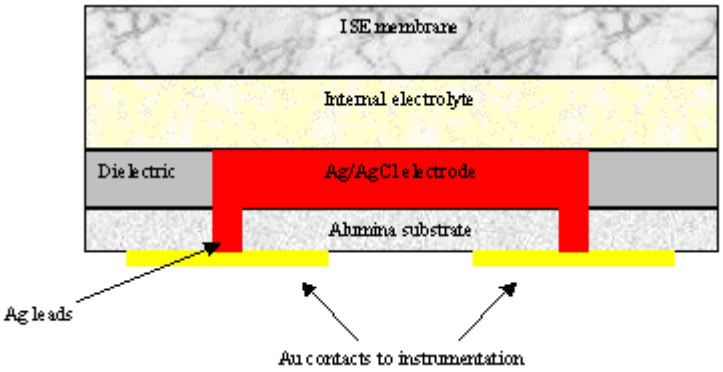

Figure 15: Edge on view of planar ISE

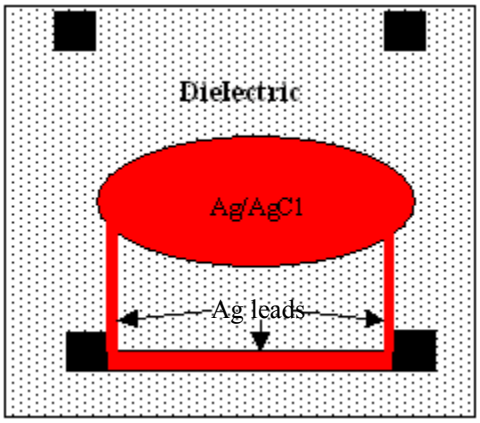

Figure 16: Top view of planar ISE

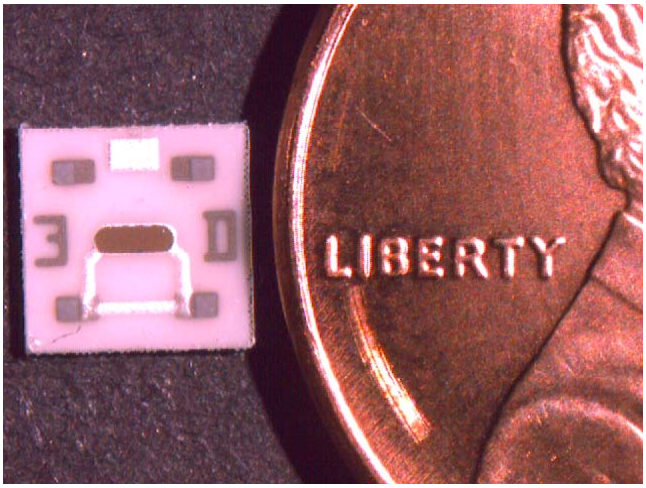

Figure 17: Actual ISE

Figure 15 presents a side cut-away view of a single ISE chip measuring ca. 5mm X 5 mm. On the back side of the chip are printed gold electrical contacts (yellow) that connect to the front side electrode (red) via holes in the substrate. A Ag/AgCl internal electrode is electrically isolated with dielectric. Over this lies the internal polymeric electrolyte and then the plasticized PVC membrane. Figure 16 shows the top view of this configuration with additional dielectric (black squares) covering the holes. As a comparison, figure 17 presents an actual ISE chip side by side with a penny to provide scale. The alphanumeric designation on the chip is used for tracking purposes only.

Four membrane formulations were tested in order to determine which environment would yield the best potentiometric properties of sensors constructed with **8**. Each sensor membrane consisted of plasticized PVC. Formulations differed as to the type of plasticizer used and whether an ionic additive was present. NPOE (nitrophenyloctylether) and DOP (dioctyl phthalate) were used as plasticizers since they have been used in other ammonium sensitive electrodes and yielded good results.[11c] We also investigated the effect of a lipophilic ionic additive, i.e. KtpClPB (potassium tetrakis(4-chlorophenyl)borate), in combination with the two plasticizers.

Figure 18 shows the potentiometric responses of the four membrane formulations to increasing concentrations of aqueous NH_4Cl.

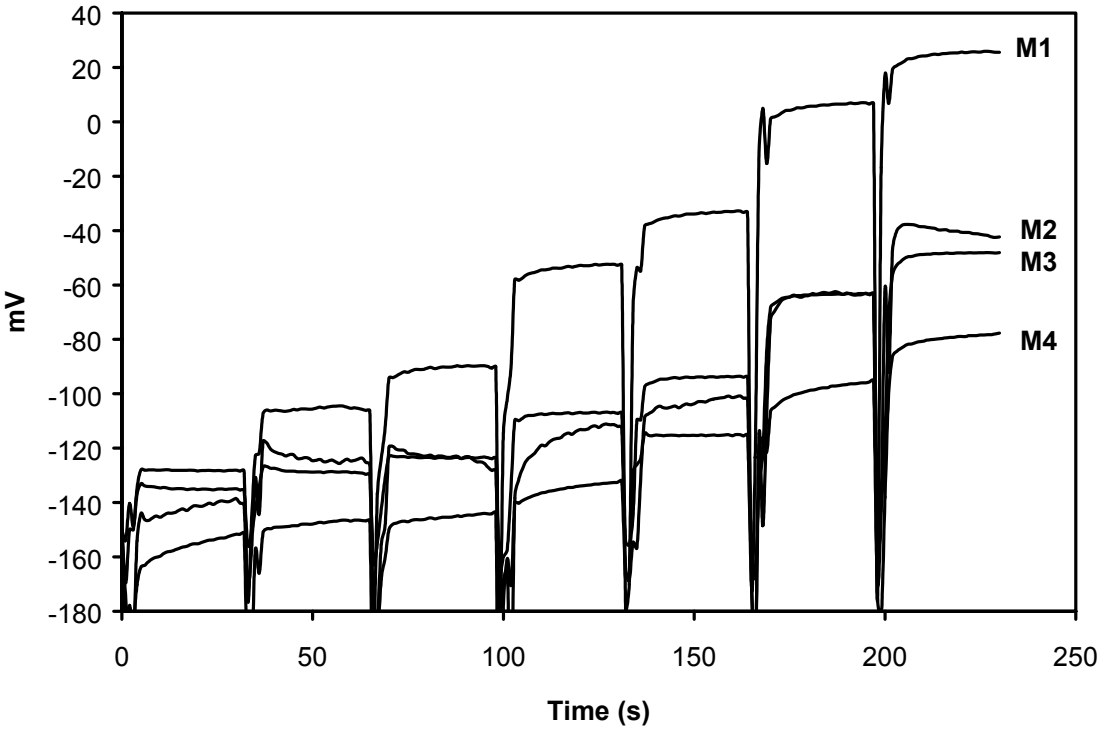

Figure 18: Potentiometric responses of planar ISE's to ammonium ion (10^{-4} M to 10^{-1}M) for membranes 1-4 based on **8**.

Two effects can be observed in the data, one that we attribute to the plasticizer and a second due to the ionic additive. It can be seen from Table 2, membranes containing the plasticizer NPOE, both in the presence and absence of KtpClPB, consistently produced sensors with the highest slopes, i.e., the closest to the ideal Nernstian condition of 61.5 mV/dec at 37 °C. We attribute this effect to the higher polarity that NPOE ($\varepsilon = 24$) imparts to the membrane compared to DOP ($\varepsilon = 3.88$).[56] It is known that depsipeptide structures such as valinomycin (and likely **8**) experience intramolecular hydrogen bonding (H-bonding) interactions.[43] In the case of **8** these interactions would be expected to interfere with the complexation of ammonium ions (since this complexation also requires H-bonding). In a polar environment such as that provided by NPOE, the

intramolecular H-bonding will probably be decreased thus allowing for more efficient ammonium ion complexation.[44,57] Such would not be the case in lower polarity environments such as those produced by the presence of DOP. In fact, our NMR dilution studies support this suggestion. In this study NMR spectra of **8** were obtained over a concentration range of 2 – 20 mM in non-polar ($CDCl_3$) and polar (MeCN-d_3) solvents. This concentration range brackets the concentration of **8** in the membranes tested. In the non-polar environment, spectra of **8** at each concentration exhibited broad and structureless NH resonances symptomatic of intramolecular H-bonding, while in the polar medium, NH resonances were sharp, suggesting the disruption of H-bonding.

In addition to this apparent polarity effect, it was observed that a 50 mol% loading of the ionic additive, KtpClPB (in combination with either the NPOE or DOP), results in significant deviations from Nernstian behavior and substantially reduces the selectivity, particularly over the divalent cations (See selectivity data in Table 2). Although it has been shown previously that modest numbers of anionic sites within liquid polymeric membranes can improve the potentiometric properties of ISE's, a low molar ratio of ionophore to ionic sites can substantially degrade selectivity and decrease the slope.[50,57-59] This behavior is confirmed in the present study. It is likely that the deleterious effect on selectivity by the ionic additive, which is present in the membrane in a 1:2 ratio relative to **8**, is due to non-specific ion exchange, likely through the formation of ion-pairs.[60,61]

Table 2 shows the results of selectivity studies that were carried out using the separate solution method[50,51] on four membrane preparations.

Selectivity coefficients, log $K^{POT}_{NH_4^+ j}$						
Membrane[a]	Li^+	Na^+	K^+	Ca^{2+}	Mg^{2+}	Slope[b]
M1	-7.3	-2.1	-0.6	-4.4	-7.1	60.1
M2	-1.9	-1.5	-1.0	-1.3	-1.5	55.8
M3	-5.0	-1.9	-0.6	-3.9	-7.3	45.8
M4	-3.2	-1.5	-0.4	-3.4	-3.9	39.4
Nonactin[d]	-4.4[28]	-2.4[25]	-0.9[25]	-2.5[28]	-4.2[28]	59.3[c]

[a] M1: 69/30/1 wt% of NPOE/PVC/**8**, M2: same as M1 with 50 mole % of KtpClPB to **8**, M3: 69/30/1 wt% of DOP/PVC/**8**, M4: same as M3 with 50 mole % KtpClPB to **8**.[b] Determined between10^{-3} M to 10^{-1} M cation, at 37°C. [c] At 25 °C. [d] Data for nonactin taken from references indicated.

Table 2. Selectivity of **8** versus other Cations

It is clear from this data that the optimum potentiometric characteristics are obtained using the NPOE plasticizer in the absence of added ionic sites. Membranes produced with this formulation gave near Nernstian responses, i.e. near 61.5 mV/dec at 37°C, of 60.1 mV/dec. Taking membrane M1 as the best example, this formulation exhibited excellent selectivity for ammonium ion over the divalent cations calcium and magnesium as well as lithium, and good selectivity over sodium and potassium ($\log K^{POT}_{NH_4^+ j}$ = -2.1, -0.6 respectively) that is comparable to nonactin ($\log K^{POT}_{NH_4^+ j}$ -2.4, -0.9 for sodium and potassium respectively).[25,28] This selectivity dropped considerably for most ions with the

addition of ionic additive and is reflected in the non-Nernstian slopes as previously noted. Membranes that were formulated using DOP as the plasticizer exhibited substantial sub-Nernstian behavior, making comparisons of selectivity less meaningful. As indicated above this effect is likely induced by the low polarity of the polymeric solvent inducing intramolecular hydrogen bonding and thus reducing the ability of the ionophore to complex the cations. However, again, potassium selectivity was comparable to that of nonactin.

The ionic selectivity pattern for M1, $NH_4^+ > K^+ > Na^+ >> Ca^{++}$, $>> Mg^{++} \sim Li^+$, indicates a substantial improvement over that of nonactin with respect to the divalent cations as well as lithium ion. The high ammonium/lithium selectivity can be attributed to a size fit effect. As noted, the pocket of **8** is designed to accommodate the larger cations and this, coupled to the fact that **8** cannot form wrapping type complexes, precludes the possibility of favorable binding to lithium ion whose ionic radius (0.68 Å) is much smaller than that of ammonium ion.

High selectivity of **8** for ammonium ion over the divalent cations is likely due to two effects, a size fit effect for both calcium and magnesium ions and in the case of calcium ion, a low coordination geometry. The size-fit effect is straightforward since calcium and magnesium ions have radii of 0.99 and 0.82 Å respectively, and thus are too small to be effectively complexed. The second effect specific to calcium ion can be attributed to the fact that this ion has been shown to favor ligands with six coordinating groups such as

ETH 1001.[11c] Compound **8** cannot present all six carbonyl groups at one face due to dipole-dipole repulsion and therefore would not be able to stabilize the calcium ion.

The data presented shows that new ammonium ionophores based upon cyclodepsipeptide motifs are an attractive alternative to others presented in the literature. While the potentiometric data is comparable to nonactin, modifications to the ionophore backbone are expected to enhance its selectivity. In particular, it has been shown that the addition of bulky substituents to other ionophores has improved selectivities through steric effects.[37] This approach also has the added advantage of increasing the lipophilicity of the compounds, thereby making them more compatible with non-polar membrane environments. Due to the facile nature of depsipeptide synthesis, the introduction of bulky groups such as phenyl or long alkyl chains will allow for additional tuning of the ionophore's potentiometric properties.

Summary of Ammonium Ionophore work

We have reported here the modular synthesis of a new ammonium selective ionophore based upon a cyclic depsipeptide motif. Like Lehn and others,[18,35-37] this ionophore was rationally designed to take advantage of the tetrahedral symmetry of the ammonium cation in order to discriminate against cations requiring octahedral binding geometries. This is particularly important where a size fit effect can not improve discrimination over cations of similar size, notably potassium. In addition, the structure was designed with the view of incorporating a rigid pre-organized backbone which has been shown to enhance selectivity by reducing the enthalpic costs of complexation, a prime example of which is the pre-organized structure of valinomycin.[43] This approach yielded an ionophore which, when incorporated into an ISE format, provides selectivity for ammonium ion over potassium and sodium that is comparable to nonactin. We believe that the flexible modular approach used here will enable us to tune the structure of similar molecules so as to achieve higher selectivity and sensitivity characteristics.

B: Potassium Fluoroionophore (10)

The use of crown ethers that are covalently-bound to calix[4]arenes to selectively complex with specific ions has been studied extensively.[14,62-72] Reinhoudt et al. reported selective binding of potassium ions (relative to sodium or lithium) with calix[4]arene-crown-5 structures, noting that the K^+/Na^+ selectivity was dependent on the calix[4]arene-crown conformation (i.e., cone, partial cone or 1,3-alternate).[14,62]

Since these early reports, studies have expanded to include benzocrown and azacrown structures and their selectivity and sensitivity for binding a wide variety of metal cations and their practical application as sensors, particularly optical sensors. For example, Dabestani et al. reported the synthesis and characterization of an calix[4]arene-benzocrown-6 structure consisting of a 9-cyanoanthryl fluorophore covalently-linked through a methylenic bridge to the benzo group.[24,63,64] This fluoroionophore acts as an "off-on" fluorescence switch that is triggered by ion complexation. In the absence of cation, the benzocrown group quenches the cyanoanthryl excited singlet state by photoinduced electron transfer (PET), while in the presence of complexed cation, the electrostatic field of the ion disrupts this PET process. This particular system exhibited high sensitivity for cesium ions (important in the detection of radioactive contamination) and relatively good selectivity for cesium over other alkali metal ions. Similar structures make use of azacrown rings instead of benzocrowns,[21a,65-72] presumably because the lower oxidation potential of the amine (1.15 V)[73] relative to the benzo group (1.45 V)[73] allows greater flexibility in the selection of the fluorophore used in the system, i.e., the

amine provides greater driving force for the electron transfer process. Kim et al. have synthesized calix[4]arene-azacrown-5 compounds where the nitrogen of the azacrown is substituted with benzyl or picolyl groups.[69] In the picolyl systems, selectivity for silver ions was found to be an order of magnitude higher than for other cations measured. The presence of the pyridinyl ring apparently contributes to the metal ion binding.

More recently, Dabestani and co-workers suggested that a structure consisting of separate binding sites for cesium and potassium cations could function as a proton-activated logic device.[66] This structure consists of a calix[4]arene-benzocrown-6 covalently-linked through the benzo group to an anthryl azacrown-6. The anthryl azacrown structures (crown-5, crown-6) have been shown previously to be sensitive to sodium and potassium cations among others, although the selectivity for these ions over other alkali metal ions is only modest.[21a,22]

Our focus in this work is the construction of fluoroionophores specific for potassium cations that can be incorporated into solid-state optical sensors for clinical diagnostic measurements. It is clear from the previous discussions that pre-organization, size fit and a rigid backbone are key elements in the design of selective ionophores and fluoroionophores. In contrast to other molecular architectures, calix[n]crown's are ideal motifs which embody these characteristics and offer the potential for developing novel fluoroionophores for potassium. For example, 18-crown-6 structures possess a pocket size that is 1.34-1.43 Å and is appropriate for binding potassium (ionic radius, 1.33 Å).[10] However, due to the high flexibility of the structure the ionophore discriminates against

sodium by only about two orders of magnitude ($\log K_{K,Na} = 1.7$).[10] There are several factors for this low specificity that are induced by the presence of the flexible backbone. One such factor is the ability of the crown to form wrapping type complexes around smaller cations, such as sodium. Due to this, there is a small difference in the enthalpy of complexation between potassium and sodium (-56.1 and -31.4 kJ/mol respectively) which is typically the main driver in the differences in specificity (see Table 1). In contrast to this, calix[4]arene-crown-5 is able to discriminate against sodium with over five orders of magnitude specificity.[14] This dramatic increase is typically due to a large difference in the enthalpy of complexation which is brought on by a rigid and hence pre-organized state. With this in mind we have synthesized **10** (and its model compound **9**), which combines the known optical response of anthryl azacrown-6 to potassium ions with expected enhanced selectivity provided by coupling the azacrown to a 1,3-alternate calix[4]arene. Described here are the results of these initial studies, potentially promising increased selectivity for potassium over sodium and other alkali metal.

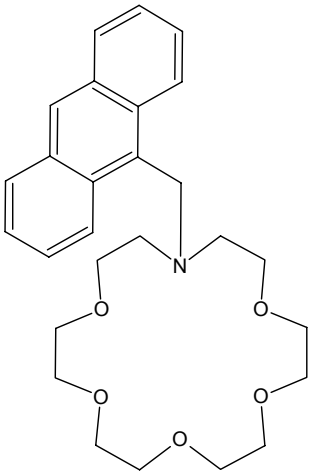

9

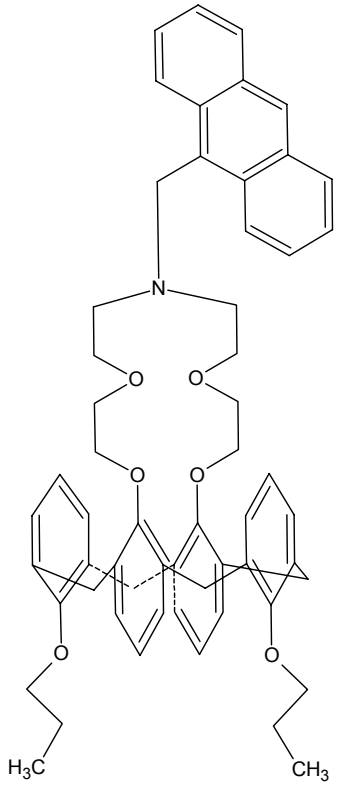

10

Potassium Fluoroionophore Experimental

Synthesis of 9 (by Kathy Dennen)

N-(9-anthrylmethyl)-monoaza-18-crown-6 (9). The synthesis of **9** was based on a modified literature procedure.[21a] 1-aza-18-crown-6 (0.515g, 1.95 mmol), 9-chloroanthracene (0.400g, 1.76 mmol), and triethylamine (0.526g, 0.74 mL) were refluxed in 1,4-dioxane (200 mL) for 24 hours. The solvent was evaporated, and the product extracted with a 2:3 CH_2Cl_2/H_2O mixture. The organic phase was rinsed three times with water and then dried over anhydrous magnesium sulfate. Further purification was done using thin layer chromatography preparatory plates in the dark (17:1 CH_2Cl_2/EtOH), to yield N-(9-anthrylmethyl) monoaza-18-crown-6 (0.176g, 0.388 mmol). The product was then recrystallized with CH_2Cl_2/ether to yield a yellow solid (22%). ^{1}H NMR (400 MHz, $CDCl_3$). δ 2.9 (t, 4H, J = 5.24 Hz), 3.7-3.5 (m, 20H), 4.6 (s, 2H), 8.6-7.4 (m, 9H). ^{13}C NMR (100 MHz, $CDCl_3$). δ 52.4, 54.3, 70.6, 71.1, 71.2, 71.3 (CH_2), 124.8, 125.2, 125.7, 127.9, 131.8 (Ar).

Synthesis of 10 (by Dr. Hubert Nienaber)

25,27-Bis(1-propyloxy)calix[4]arene. The preparation of dipropyl-calix[4]arene followed a literature method.[72] In a 250 mL round bottom flask 5.08 g (11.9 mmol) calix[4]arene, 4.87 g (28.6 mmol) 1-iodopropane and 3.95 g (28.6 mmol) K_2CO_3 were suspended in 150 mL dry acetonitrile and heated under reflux for 24 hours. The solvent was removed *in vacuo* and 50 mL 2N HCl and 50 mL CH_2Cl_2 were added and the phases

were separated. The aqueous phase was extracted two times with 30 mL CH_2Cl_2, the organic phases were combined, dried with Na_2SO_4 and the solvent removed *in vacuo*. The crude product was recrystallized from methanol/CH_2Cl_2 (5:1) and gave 4.37 g (72%) of 25,27-bis(1-propyloxy)calix[4]arene as white crystals. The ^{1}H NMR spectrum corresponds to the published data.[62] ^{1}H NMR (400 MHz, $CDCl_3$) δ 1.32 (t, *J* = 7.3 Hz, 6H), 2.08 (m, 4H), 3.40 (d, *J* = 12.9 Hz, 4H), 3.98 (t, *J* = 6.2 Hz, 4H), 4.35 (d, *J* = 12.9 Hz, 4H), 6.65 (t, *J* = 7.5 Hz, 2H, Ar), 6.74 (t, *J* = 7.5 Hz, 2H, Ar), 6.92 (d, *J* = 7.5 Hz, 4H, Ar), 7.06 (d, *J* = 7.5 Hz, 4H, Ar), 8.30 (s, 2H).

2-(2-Chloroethoxy)ethyl-p-toluenesulfonate. Preparation was done according to a standard procedure for the preparation of p-toluenesulfonic esters.[74] In a round bottom flask 9.53 g (50 mmol) of p-toluenesulfonylchloride were mixed with 7.47 g (60 mmol) 2-(2-chloroethoxy)ethanol in 50 mL $CHCl_3$. The mixture was stirred and cooled below 5°C and 10.1 g (100 mmol) triethylamine were added drop-wise at this temperature. After the addition was completed, the mixture was stirred for another 3h at room temperature. At which point, a mixture of 50 g ice and 20 mL conc. HCl was added carefully and stirred for 30 min. The chloroform phase was separated, washed three times with 30 mL water, dried with Na_2SO_4 and the solvent removed *in vacuo* upon which 12.5 g (90%) of a yellowish oil was obtained. The product was used without further purification. ^{1}H NMR (400 MHz,$CDCl_3$) δ 2.45 (s, 3H), 3.55 (t, *J* = 7.4 Hz, 2H), 3.65 – 3.77 (m, 4H), 4.17 (t, *J* = 7.2 Hz, 2H), 7.42 (d, *J* = 7.5 Hz, 2H, Ar) , 7.84 (d, *J* = 7.5 Hz, 2H, Ar),

25,27-Bis(1-propyloxy)-26,28-bis(5-chloro-3-oxapentyloxy)calix[4]arene. A solution of 2.54 g (5 mmol) 25,27-bis(1-propyloxy)calix[4]arene, 5.57 g (20 mmol) 2-(2-chloroethoxy)ethyl p-toluenesulfonate and 3.36 g (10 mmol) Cs_2CO_3 in 150 mL dry acetonitrile was heated at reflux under nitrogen for 24 h. The solvent was removed *in vacuo* and 50 mL 2N HCl and 50 mL CH_2Cl_2 were added and the phases were separated. The aqueous phase was extracted two times with 30 mL CH_2Cl_2, the organic phases were combined, dried with Na_2SO_4 and the solvent removed in vacuo. The crude product was recrystallized twice from methanol/CH_2Cl_2 (5:1) and gave 3.07 g (85%) of 25,27-bis(1-propyloxy)-26,28-bis(5-chloro-3-oxapentyloxy)calix[4]arene as white crystals. The ^{1}H NMR spectrum corresponds to the published data.[68] ^{1}H NMR (400 MHz,$CDCl_3$) δ 0.93 (t, J = 7.2 Hz, 6H), 1.65 (m, 4H), 3.50 – 3.80 (m, 28H), δ 6.67 - 6.72 (m, 4H, Ar), 6.97 (d, J = 7.6 Hz, 4H, Ar) and 7.05 (d, J = 7.6 Hz, 4H, Ar).

N-tosyl 25,27-bis(1-propyloxy)calix[4]arene-azacrown-5. A solution of 1.45g (2 mmol) 25,27-bis(1-propyloxy)-26,28-bis(5-chloro-3 oxapentyloxy)- calix[4]arene, 0.343 g (2 mmol) p-toluenesulfonamide and 1.38 g (10 mmol) K_2CO_3 in 70 mL dry DMF was heated at reflux under nitrogen for 24 h. The solvent was removed *in vacuo* and 50 mL 2N HCl and 50 mL CH_2Cl_2 were added and the phases were separated. The aqueous phase was extracted two times with 30 mL CH_2Cl_2, the organic phases were combined, dried with Na_2SO_4 and the solvent removed *in vacuo*. The crude product was purified by column chromatography using ethyl acetate:hexane 1:4 (R_f = 0.4) to provide 1.15 g (70%) N-tosyl 25, 27-bis(1-propyloxy)calix[4]arene-azacrown-5. The ^{1}H NMR spectrum corresponds to the published data.[68] ^{1}H NMR (400 MHz, $CDCl_3$) δ 0.72 (t, J = 7.3 Hz,

6H), 1.28 (m, 4H), 2.45 (s, 3H), 3.20 – 3.80 (m, 28H), 6.74 - 6.82 (m, 4H, Ar), 7.01 – 7.06 (m, 8H, Ar), 7.34 (d, 2H, *J* = 7.4 Hz, Ar), 7.74 (d, 2H, *J* = 7.4 Hz, Ar).

25,27-Bis(1-propyloxy)calix[4]arene-azacrown-5. The reductive detosylation of N-tosyl 25,27-Bis(1-propyloxy)calix[4]arene-azacrown-5 followed the procedure described by Quici et al.[73] Under nitrogen, 380 mg (10 mmol) $LiAlH_4$ was added carefully to a solution of 410 mg (0.5 mmol) N-tosyl 25,27-bis(1-propyloxy)calix[4]arene-azacrown-5 in 80 mL dry THF. The suspension was heated to reflux for 24h and then allowed to cool to rt., and the excess $LiAlH_4$ was decomposed with a stoichiometric amount of water. The aluminum oxide was removed by filtration and carefully washed with 80 mL THF and the solvent evaporated. The crude product was purified on prep. TLC using ethyl acetate:hexane 1:1 (R_f = 0.2) to afford 203 mg (61%) 25,27-bis(1-propyloxy)calix[4]arene azacrown-5 as a pale yellow solid. The ^{1}H NMR spectrum corresponds to the published data.[68] ^{1}H NMR (400 MHz,$CDCl_3$) δ 0.82 (t, *J* = 7.3 Hz, 6H), 1.52 (m, 4H), 2.77 (s, 4H), 3.43 – 3.60 (m, 16H), 3.77 (s, 8H), 6.78 (t, *J* = 7.5 Hz, 2H, Ar), 6.83 (t, *J* = 7.5 Hz, 2H , Ar), 7.03 (d, *J* = 7.5 Hz, 4H, Ar) and 7.13 (d, *J* = 7.5 Hz, 4H, Ar).

N-(9-methyl-anthracene)-25,27-bis(1-propyloxy)calix[4]arene-azacrown-5(10). Note: NMR and Mass Spectroscopy data in Appendix A2. A solution of 100 mg (0.15 mmol) 25,27-bis(1-propyloxy)calix[4]arene-azacrown-5, 35 mg (0.15 mmol) 9-(chloromethyl)anthracene and 46 mg (0.45 mmol) triethylamine in 50 mL of dry dioxane was refluxed for 24h. The solvent was removed *in vacuo* and 50 mL 2N HCl and 50 mL

CH_2Cl_2 were added and the phases were separated. The aqueous phase was extracted two times with 30 mL CH_2Cl_2, the organic phases were washed once with 30 mL of 2N NaOH, separated, dried with Na_2SO_4 and the solvent was evaporated *in vacuo*. The crude product was purified on prep. TLC using CH_2Cl_2 (R_f = 0.3) to afford 23 mg (18%) N-(9-methyl-anthracene)-25,27-bis(1-propyloxy)calix[4]arene-azacrown-5, the title compound, as white crystals. mp 188-190; ^{1}H NMR (400 MHz,$CDCl_3$) δ 0.69 (t, *J* = 7.4 Hz, 6H), 1.21 (m, 4H), 2.75 (d, *J* = 4.5 Hz, 4H), 3.27 (s, 8H), 3.38 (t, *J* = 7.3 Hz, 4H), 3.46 (s, 4H), 3.80 (s, 8H), 4.58 (s, 2H), 6.79 (m, 4H, Ar), 7.05 (dd, *J* = 7.4, 11.2 Hz, 8H, Ar), 7.48 (t, *J* = 7.1 Hz, 2H, Ar), 7.57 (t, *J* = 7.1 Hz, 2H, Ar), 8.01 (d, *J* = 8.3 Hz, 2H, Ar), 8.43 (s, 1H, Ar), 8.59 (d, *J* = 8.8 Hz, 2H, Ar). ^{13}C NMR (100 MHz,$CDCl_3$) δ 10.4 (CH_3), 22.8, 38.6, 54.2, 70.2, 71.2, 72.4, (CH_2), 122.5, 122.7, 125.2, 125.7, 125.9, 129.4, 130.1, 130.2, 131.8, 134.2, 134.5, 157.2, 157.5 (Ar). MS *m/z* (%) calcd. for $C_{57}H_{62}NO_6$ ($M+H^+$) 856.4 found 856.4(100).

Potassium Fluoroionophore Results and Discussion

Emission spectra of 9 and 10

Figure 19 shows the fluorescence spectra obtained for N-(9-anthrylmethyl)-monoaza-18-crown-6, **9**, in the absence and presence of added concentrations of potassium acetate in dichloromethane. We consider **9** as a model for **10** since it contains the same fluorophore/amine electron transfer system as **10** and the size and electrostatic characteristics of the complexation sites are qualitatively similar in both compounds as determined by molecular modeling. This model compound was synthesized in order to serve as a baseline in the determination of whether the selectivity and sensitivity of the azacrown moiety is increased by the incorporation of the calix[4]arene group.

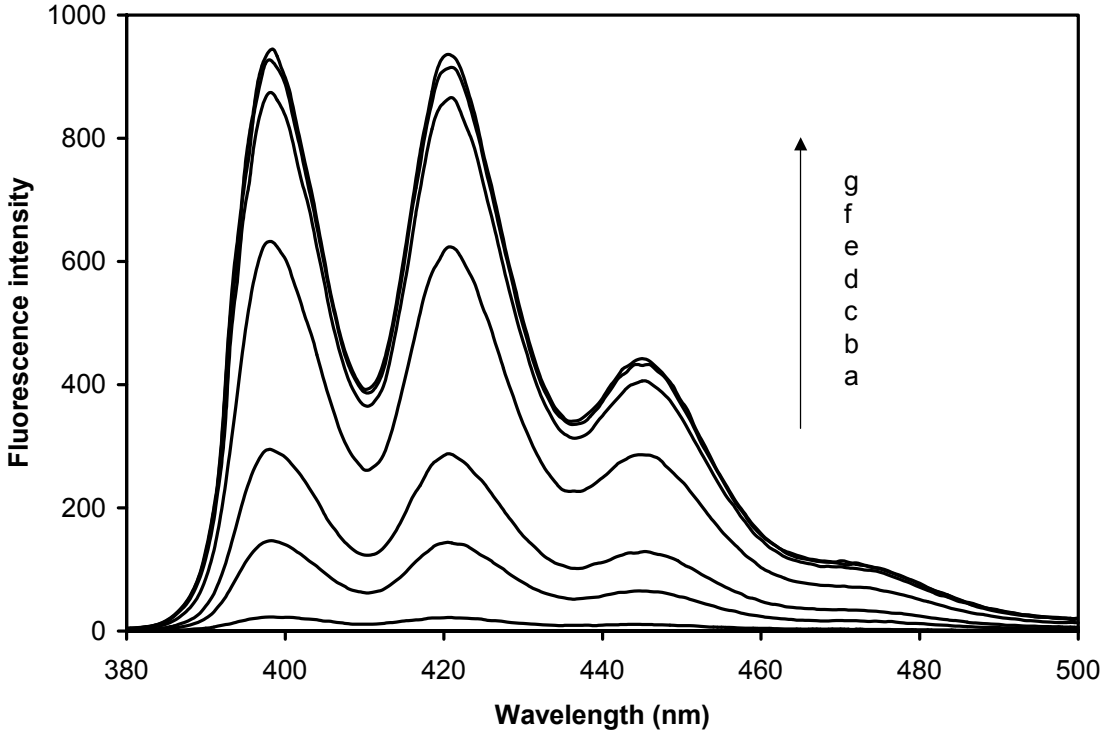

Figure 19: Fluorescence emission spectra (λ_{ex} 355 nm) of **9** (5.5×10^{-6} M) in dichloromethane with added BTMAH (9.0×10^{-7} M) as a function of $[K^+]$. a: 0 μM, b: 1.25 μM, c: 2.5 μM, d: 5 μM, e: 7.5 μM, f: 10 μM, g: 11.3 μM.

The fluorescence behavior of **9** clearly demonstrates that the PET "off-on" switching mechanism that occurs in response to ion complexation is operative. In the absence of ions the anthryl fluorescence is at a minimum and increases linearly with addition of potassium acetate up to a concentration marginally higher than the concentration of **9**, after which it begins to plateau. This indicates that the ion and ionophore are likely forming a 1:1 complex in solution as expected given the reported behavior of similar azacrowns.[21a] The results obtained show a ca. 50–fold enhancement of the fluorescence intensity upon addition of potassium ions. This is consistent with previously published

data[21a] and certainly indicates sufficient sensitivity and dynamic range for further study following incorporation of the calix[4]arene group.

Protonation of the nitrogen atom in the azacrown can potentially block the electron transfer process and for this reason, the organic base, benzyltrimethylammonium hydroxide (BTMAH), was added to minimize protonation. In fact, the addition of base to solutions of **9** in the absence of potassium ions causes a 4-fold decrease in the fluorescence intensity, consistent with this protonation effect. Nevertheless, some fluorescence is still observed. It is difficult to unambiguously determine the origin of this fluorescence, i.e. whether it reflects the intrinsic rate constants for fluorescence and electron transfer in this molecule or whether there is a low background concentration of potassium, sodium or other cations present as impurities. Indeed, the intensity of the fluorescence emission in the presence of base and in the absence of added potassium is somewhat variable and it is possible to reduce this intensity by using rigorously cleaned glassware during sample preparation, suggesting that at least some of the effect is due to impurity ions.

Figure 20 shows the fluorescence spectra obtained for **10** in the absence and presence of added potassium acetate in dichloromethane solution. In order to compare directly the behavior of **9** and **10**, the spectrum for **10** in the absence of potassium ions was normalized to that of **9** to account for differences in sample absorbance at the excitation wavelength. As with **9**, the fluorescence intensity of **10** in the presence of added base,

increases dramatically with addition of potassium ions, although the dynamic range for **10** is considerably less than for **9**, (8.5-fold and 50-fold increases respectively).

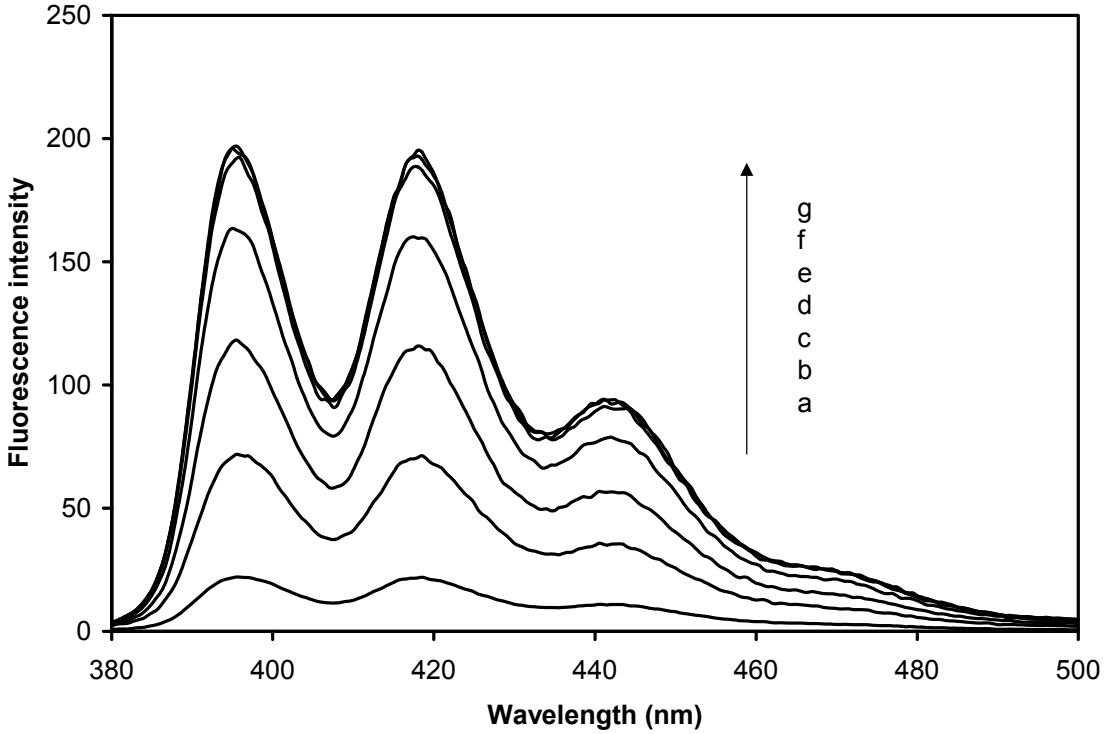

Figure 20: Fluorescence emission spectra (λ_{ex} 355 nm) of **10** (1.1×10^{-6} M) in dichloromethane with added BTMAH (1.0×10^{-7} M) as a function of [K^+]. a: 0 μM, b: .5 μM, c: 1 μM, d: 1.5 μM, e: 2 μM, f: 2.5 μM, g: 3 μM.

The reason for this reduced response is unclear. One potential explanation is that the ion occupies a site in **10** relative to the electron lone pair on the azacrown nitrogen atom as well as to the anthryl fluorophore that is different than in **9**. For example, if the most stable position of the ion in the complex is at a greater distance from the nitrogen lone pair in **10**, this could lead to a weaker electrostatic interaction and result in less effective interference with the electron transfer quenching process. Such an effect could

conceivably be caused by an interaction between the ion and the π-systems of the phenyl rings of the calixarene group. The binding of cations through π-interactions has been observed for other host-guest molecules as well as the 1,3 alternate calix[4]arene-crown-5 used in the present study.[14,75-77] In fact, electrostatics calculations on the potassium ion-**10** complex point out significant changes in charge density in the calixarene phenyl rings upon complexation. Figures 21 and 22 present the results of the electrostatic calculations where the electron density decreases in the order: red, green, blue. As shown, in the uncomplexed state (Figure 21) there is a high electron density localized around the calix[4]arene aromatic moieties as indicated by the substantial red coloration. In contrast, Figure 22 shows that complexation causes the electron density in the aromatic rings to be reduced significantly, as evidenced by the shift to a substantial blue coloration. Additionally, it was found that when the structure of **9** complexed with potassium ion was minimized, a $K^{+\cdots}N$ distance = 3.00 Å was optimal whereas a $K^{+\cdots}N$ distance of 3.48 Å was observed for **10.** Therefore, a weaker interaction with the amine electron donor and consequently a reduction in the fluorescence response would be expected for **10** compared to **9**. Figure 23 shows the minimized potassium-**10** complex with the calculated distances of the cation to the oxygen and nitrogen atoms.

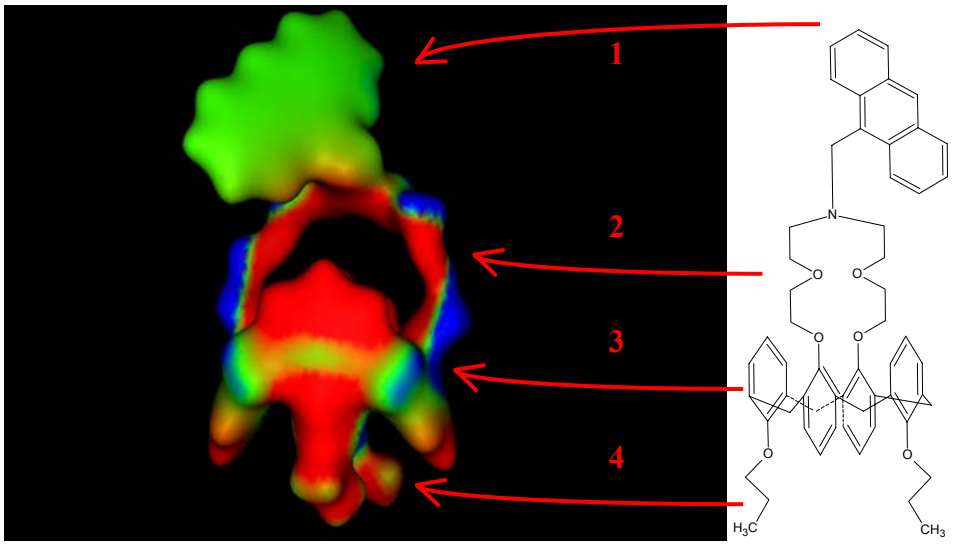

Figure 21: Electrostatic computational results for **10** in the uncomplexed state. The magnitude of electron density decreases in the order: red>green>blue. **1**, anthracene fluorophore; **2**, binding site; **3**, calix[4]arene; **4**, propyl substituents.

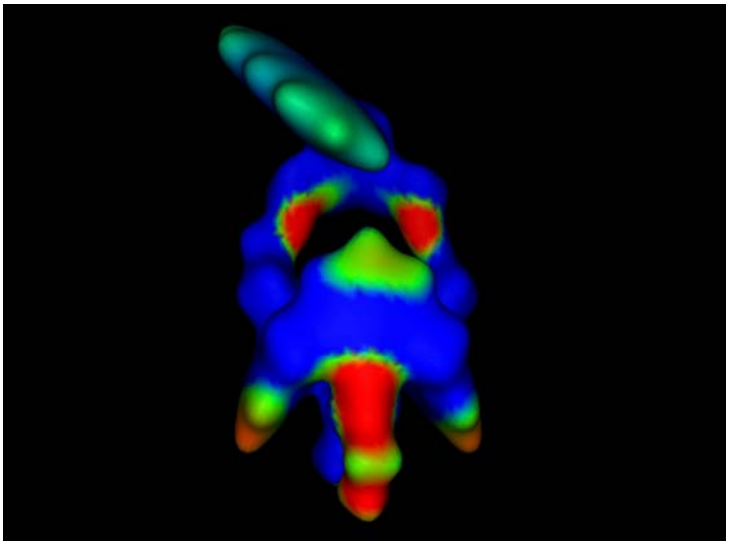

Figure 22: Electrostatic computational results for **10** in the complexed state. The magnitude of electron density decreases in the order: red>green>blue.

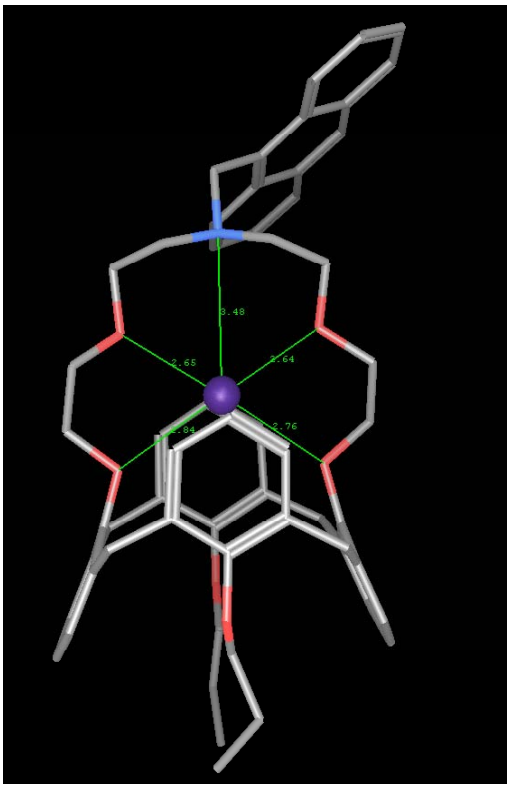

Figure 23: Minimized structure of **10** in the complexed state with potassium showing the distances, in Å, to the heteroatoms.

Selectivity

Since it is our eventual intention to use molecules similar to **10** in sensors for the detection of potassium ions in blood samples, the selectivity of **10** for potassium over other analytes is an important consideration. Given the structural similarities between **10** and 1,3-alternate calix[4]arenes it is reasonable to expect similar binding properties.[14] Therefore, we expect that metal ion complexation in **10** is governed by electrostatic interactions, particularly with the azacrown oxygen atoms, and through cation-π

interactions, but selectivity is controlled enthalpically from the pre-organized structure, size fit effects and steric effects from the propyl substituents appended to the two rotated aryl rings of the calix[4]arene.[14] Figure 24 shows the dependence of the emission intensity of **10** on cation concentration. (The values in the plot are normalized to the fluorescence intensity in the absence of ion.) These results suggest high selectivity of **10** for potassium ion in comparison with the other alkali metal cations studied, including sodium. This is an important property for blood analysis applications since sodium is present in relatively high concentrations in whole blood.

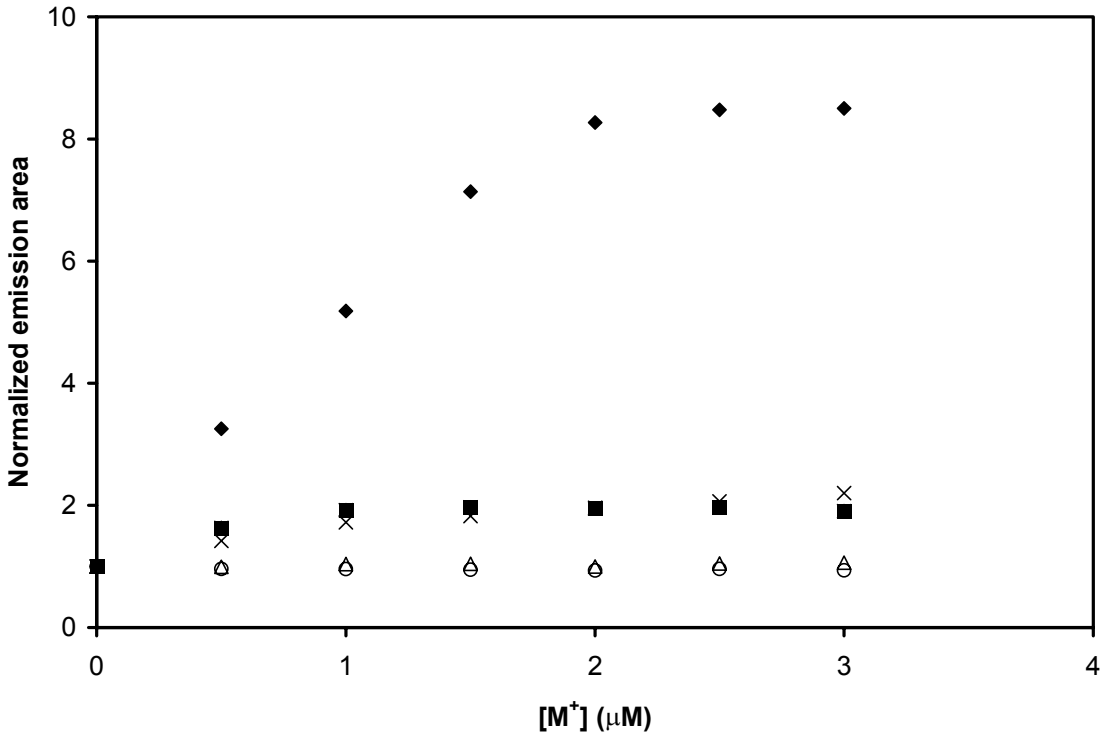

Figure 24: Emission area of **10** versus the concentration of various alkali metal ions: Li (o), Na (Δ), K (♦), Rb (■), Cs (×).

Selectivity was calculated by a method (illustrated in Figure 25) that is qualitatively similar to the fixed interference method (FIM) and separate solution methods (SSM) used

in ion selective electrode applications.[50] Figure 25 shows a hypothetical plot of fluorescence emission intensity as a function of ion concentration for primary and 'interfering' ions. Selectivity is calculated from Equation 6 and is represented as a logarithmic value.

$$\log K_{i,j} = \log\left(\frac{[i]}{[j]}\right) \qquad \textbf{(6)}$$

Here, [j] is the concentration of the interfering ion in the plateau region of the plot and for sensor applications is normally chosen to fall within a physiological concentration range for that ion. This is the concentration of interfering ion that provides the maximum fluorescence response; [i] is the concentration of the primary ion that produces the same fluorescence response as the maximum fluorescence produced by the interfering ion and as such represents a minimum unambiguous detection limit for the primary ion. From Figure 24 it is clear that sodium and lithium ions produce virtually no response. These results allow only a lower limit of the selectivity to be calculated using Equation 6. Thus log $K_{K,Na}$ ~ log $K_{K,Li}$ $\leq$-3.5, a value similar to that obtained for valinomycin and considerably larger than obtained for **9**. For cesium and rubidium, log $K_{K,Cs}$ = log $K_{K,Rb}$ = -1.0, a value that is comparable to that obtained for the related 1,3 alternate calix[4]arene-crown-5.[14] These results are summarized in Table 3. For comparison, Table 3 also shows selectivity results obtained previously for the related calix[4]arene-crown-5 and valinomycin.

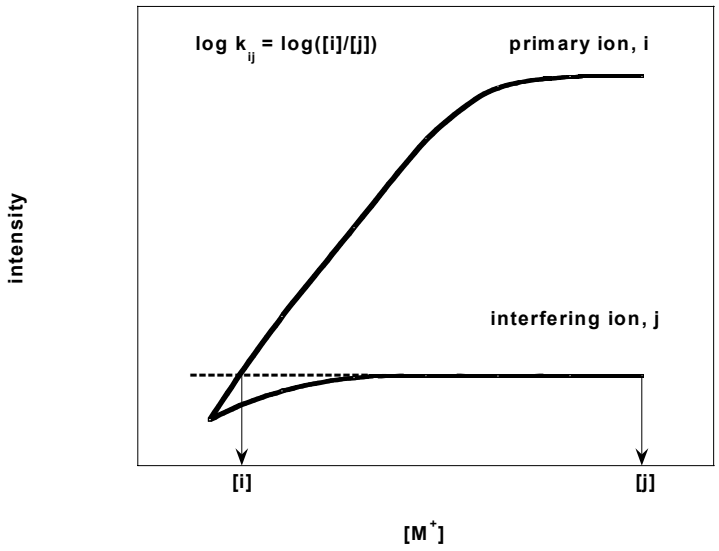

Figure 25: Hypothetical plot of fluorescence emission intensity as a function of ion concentrations for primary (i) and interfering (j) ions.

	Selectivity coefficients, log $K_{K,j}$			
Compound	Li^+	Na^+	Rb^+	Cs^+
9	-	-1.3	-	-
10	≤-3.5	≤ -3.5	-1.0	-1.0
Ref 14[a]	-4.84	-5.39	-0.48	-2.25
Ref 14[b]	-3.52	-3.26	-0.48	-0.38

a: 1,3 alternate calix[4]arene-crown-5 in $CHCl_3$. b: valinomycin in $CHCl_3$.

Table 3. Selectivity data (log K_{ij}) for **10** and related compounds.

Since the complexes apparently have a 1:1 ion/ionophore stoichiometry as suggested by similar calix[4]arene-crowns and molecular modeling, ion concentrations much higher

than the concentration of **10** do not result in further increases in fluorescence intensity.[14,78-82] The concentration of **10** in turn is limited by the requirement that absorbances at the excitation wavelength in our fluorescence experiments must be less than 0.04 in order to obtain a linear fluorescence response. Therefore, the concentration of **10** used in these measurements is limited and by necessity the ion concentrations are well below physiological norms. However, in the eventual sensor configuration, considerably shorter path lengths will make much higher ionophore concentrations possible, possibly giving sensitivity in the physiological range.

Solvent effects

Previous studies of analogous anthryl-calix[4]arene-benzocrowns indicated a considerable and complex solvent effect on the intensity of fluorescence in such compounds.[64] Specifically, addition of methanol to dichloromethane was observed initially to cause an increase in the fluorescence presumably due to complexation of the methanol with the oxygen atoms of the benzocrown ether, i.e., electron transfer was less efficient. With continued addition of methanol, the increase in polarity in turn increased the efficiency of electron transfer and led to a decrease in the fluorescence. Given this reported medium effect and its potential importance in the operation of a sensor based on this molecular structure, we have investigated the effect of solvent on **10**, both in the absence and presence of added potassium ions. In the absence of ions, the addition of methanol to the dichloromethane solutions caused an increase in the fluorescence intensity at small mole ratios of methanol to dichloromethane (ca. 0.17, 10% v/v, ca. 3M)

and then a decrease as the methanol was increased further. This behavior is similar to that reported for the benzocrown systems.[64] It is likely here that at low methanol concentrations, the increase in fluorescence intensity is due to a hydrogen bond interaction between methanol and the azacrown nitrogen. However, at higher methanol concentrations the drop in fluorescence intensity observed can be ascribed to an increase in the efficiency of electron transfer due to an increase in solvent polarity. This polarity effect presumably overshadows the hydrogen bonding effect. Alternatively, hydrogen bonding to the azacrown could be reduced due to self-association of the added methanol, particularly since the concentration of methanol is quite high, ca. 3M.

In the presence of added potassium ions, an additional effect of solvent is observed. Figure 26 shows the delta response of **10** as a function of the mole fraction of dichloromethane in methanol. The delta response is determined from the slope of the fluorescence intensity versus ion concentration curve at a specific solvent composition. It is clear that as the mole fraction of methanol decreases, the delta response increases dramatically. We ascribe this behavior to a solvation effect in that, as the solvent polarity decreases with increased dichloromethane concentration, the potassium ions seek out a more energetically favorable solvation environment, namely the complexation site in **10**. Solvation effects on complexation such as observed here have been noted in other calix[4]arene systems.[82] This response to solvation is expected to have an important impact on the composition of the membrane that is eventually chosen to host **10** in sensor applications.

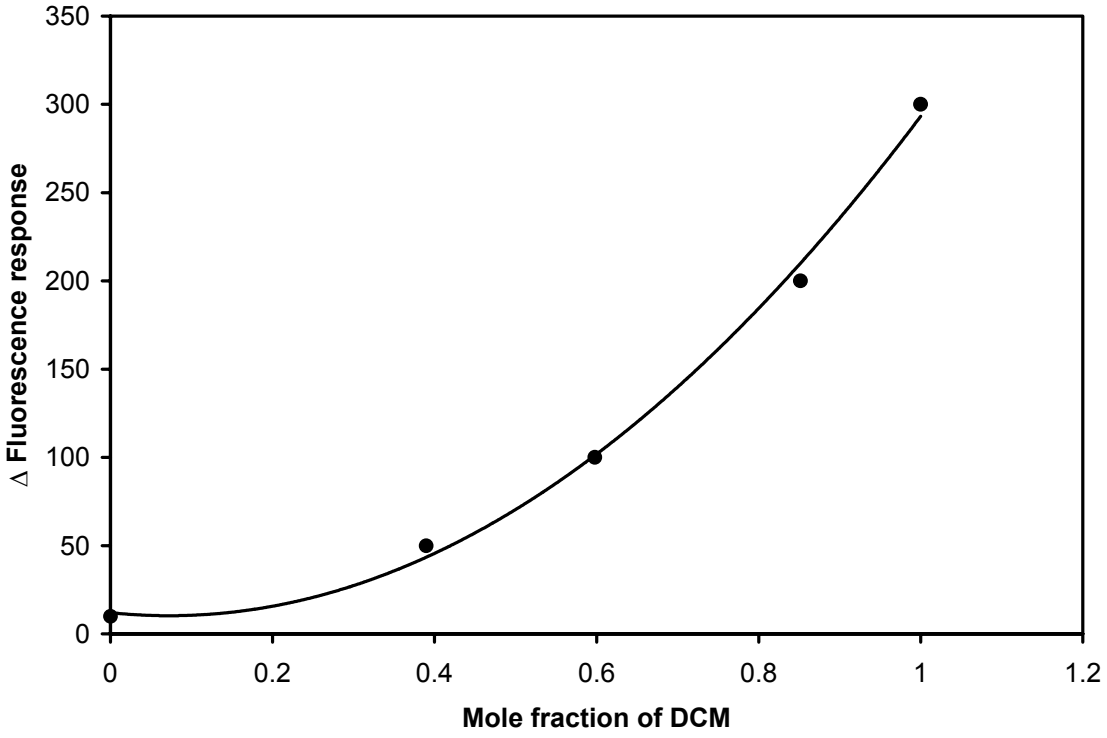

Figure 26: Delta fluorescence response to K^+ of **10** as a function of the mole fraction of dichloromethane in methanol.

Summary of Potassium Fluoroionophore work

The, N-(9-methyl-anthracene)-25,27-bis(1-propyloxy)calix[4]arene-azacrown-5 (**10**), complexes with potassium ions in organic solution triggering a substantial increase in anthryl fluorescence emission through the disruption of the PET quenching process. Preliminary measurements indicate that the selectivity for potassium ions over other alkali metal cations, particularly sodium and lithium, for **10** is increased dramatically over that of the anthryl azacrown model compound, **9**. This large increase in the selectivity for potassium over sodium and lithium can be attributed to the rigid and pre-organized structure of **10** such that the motif can not wrap around these smaller cations without a large thermodynamic cost to complexation. This again is in contrast to the flexible architecture of **9** where a small difference in enthalpies exists for the respective potassium and sodium complexes. In addition, these preliminary solution phase studies indicate a 1:1 complexation between **10** and the ion, suggesting that **10** could be sensitive to potassium in the normal physiological concentration range once incorporated into a sensor. Furthermore, the observed fluorescence response to changes in solvent polarity suggests that the sensor substrate composition will have an important impact on the efficiency of **10** as an ionophore and could allow further optimization of sensitivity and selectivity.

C: Lithium Fluoroionophore (11)

We have shown through our previous work, as well as that of others, that the calix[4]arene-crown architecture provides an ideal framework for the development of highly selective hosts.[14,24,62-72] For example, the calix[4]arene-crown-5 structures (see for example Figure 3, right) are able to achieve higher selectivities than that of valinomycin, the natural antibiotic that is used extensively as a highly selective potassium ionophore.[14,62]

As we have noted, in the calix[4]arene-crown structures the ion binding event occurs in a relatively rigid, pre-organized pocket with electrostatic stabilization provided by the oxygen groups in the crown as well as by cation-π interactions between the ion and the phenolic aromatic rings of the calixarene. The rigidity of the binding pocket combined with the possibility of varying the size of the pocket by changing the size of the crown through straightforward synthetic methods suggested to us the possibility of developing a systematic series of highly selective alkali metal ionophores and fluoroionophores that are based on a simple size-fit criterion. To this end, we synthesized and tested **10**, which showed, as described above, excellent selectivity for potassium. These results led us to our conception of a lithium fluoroionophore (**11**) based on a similar structure.

High selectivity in ionophores and fluoroionophores is particularly important for the accurate detection of lithium ions in physiological media since ions that may interfere

with lithium ion complexation, including sodium ion, are present at significantly higher concentrations. It is generally accepted that for an ionophore to accurately measure lithium ion concentration, it must have a selectivity ratio of lithium over sodium that is greater than 10^4.[83] Earlier studies of lithium ionophores involved a variety of crown ethers, including dibenzo-14-crown-4.[84] When incorporated into an ion selective electrode (ISE) this system was found to be ~10 times more selective for lithium than sodium ions. In another study, a ten-fold improvement in lithium/sodium selectivity was attained by the incorporation of bulky substituents on a series of lipophilic derivatives of 13- through 16-crown-4 ethers.[85] It was suggested that these substituents sterically hinder the complexation of larger cations while at the same time reducing the tendency of crown ethers to form 2:1 sandwich-type complexes with larger cations. A similar improvement, $\log K_{Li,Na} = -2.15$, was observed with the covalent linkage of benzyloxymethyl groups to 13- and 14-crown-4 rings.[86] More recently, a marked enhancement in lithium/sodium selectivity was achieved with the addition of a decalino subunit to a 14-crown-4, $\log K_{Li,Na} = -3.0$.[87] A similar system exhibited an estimated selectivity $\log K_{Li,Na} < -4$ when incorporated into an optode.[88] However, when employed in an ISE, the same ionophore attained a significantly lower selectivity, $\log K_{Li,Na} = -2.5$.[87]

Here we describe the synthesis and testing of N-(9-methyl-anthracene)-25,27-bis(1-propyloxy)-4-*p*-*tert*-butylcalix[4]arene-azacrown-3 (**11**). Compound **11** consists of a *p*-tert-butylcalix[4]arene group combined with an azacrown-3 moiety to create a considerably smaller binding pocket than in **10**, the potassium-selective fluoroionophore we discussed earlier. Our results show that **11** is highly selective for lithium ions over

sodium and potassium ions. Described here are the synthetic details, fluorescence results and the results of selectivity studies.

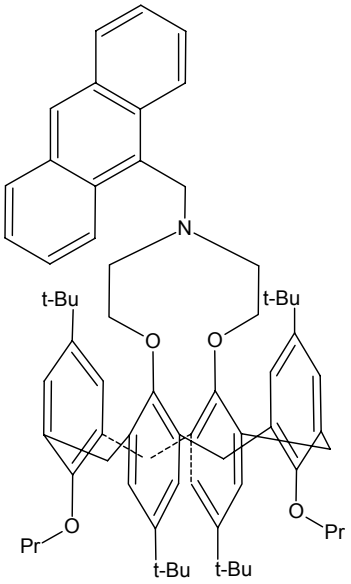

11

Lithium Fluoroionophore Experimental

(Synthesis by Dr. Hubert Neinaber)

Note: All NMR and Mass Spectroscopy data in Appendix A3.

Dipropyl-4-*p-tert*-butylcalix[4]arene: CAS [137693-26-6]

In a 500 mL round bottom flask 6.489g 4-*p-tert*-butylcalix[4]arene (10 mmol), 4.10g 1-iodopropane (24.1 mmol) and 4.14g (30 mmol) K_2CO_3 were suspended in 300mL dry acetonitrile and boiled under reflux for 24 hours. The solvent was removed *in vacuo* and 50 mL 2N HCl and 50 mL CH_2Cl_2 were added and the phases were separated. The aqueous phase was extracted two times with 30mL CH_2Cl_2, the organic phases were combined, dried with Na_2SO_4 and the solvent removed *in vacuo*. The crude product was recrystallized from methanol/CH_2Cl_2 (5:1) and gave 5.57 g (76%) of dipropyl-4-*p-tert*-butylcalix[4]arene as white crystals. ^{1}H NMR (400 MHz, $CDCl_3$); δ 1.03 (s, 18 H,), δ 1.26 (s, 24 H), 2.03 (m, 4H), 3.31 (d, 4H, J = 12.9 Hz), 3.95 (t, 4H, J = 6.4 Hz), 4.30 (d, 4H, J = 12.8 Hz), 6.88 (s, 4H, Ar), 6.93 (s, 4H, Ar), 8.00 (s, 2H). ^{13}C NMR (100 MHz, $CDCl_3$) ; δ 11.3 (CH_3), 23.9 (CH_2), 31.5, 32.1 (CH_3), 32.3, 34.2, 34.4 (CH_2), 78.5 (C), 125.5, 125.9, 128.1, 133.3, 141.6, 147.1, 150.4, 151.3 (Ar).

25,27-Bis(1-propyloxy)-26,28-bis(2-chloroethoxy)-4-*p-tert*-butylcalix[4]arene

To a solution of 7.329g (10 mmol) dipropyl-4-*p-tert*-butylcalix[4]arene in 300 mL dry acetonitrile, 9.39g (40 mmol) 2-chloroethyl-p-toluenesulfonate and 9.77g (30mmol) Cs_2CO_3 were added and the mixture was refluxed under nitrogen for 24 h. The solvent

was removed *in vacuo* and 50 mL 2N HCl and 50 mL CH_2Cl_2 were added and the phases were separated. The aqueous phase was extracted two times with 30mL CH_2Cl_2, the organic phases were combined, dried with Na_2SO_4 and the solvent removed *in vacuo*. The crude product was recrystallized from methanol/CH_2Cl_2 (3:1) and gave 4.89g (57%) of 25,27-bis(1-propyloxy)-26,28-bis(2-chloroethoxy)-4-*p-tert*-butylcalix[4]arene as white crystals. ^{1}H NMR (400 MHz, $CDCl_3$); δ 0.55 (t, 6H, *J* = 7.5 Hz), 0.93 (m, 4H), 1.26 (s, 18 H), 1.31 (s, 18 H), 2.60 (m, 4H), 3.30 (t, 4H, *J* = 7.5 Hz), 3.52 (m, 4H), 3.83 (m, 8H), 6.95 (s, 4H), 6.97 (s, 4H). ^{13}C NMR (100 MHz, $CDCl_3$); δ 10.1 (CH_3), 22.4 (CH_2), 31.5, 31.7 (CH_3), 34.9, 34.0, 39.1, 40.1, 68.8, 71.3 (CH_2), 125.2, 125.6, 132.7, 133.0, 144.5, 144.6, 153.3, 155.0 (Ar). ESI MS *m/z* (%) calcd. for $C_{54}H_{75}Cl_2O_4$ [M+H$^+$] 857.48 found 857.40(100), calcd. for [M+Na$^+$] 879.48 found 879.43(95), calcd. for [M+K$^+$] 895.45 found 895.29(43).

N-Tosyl-25,27-bis(1-propyloxy)-4-*p-tert*-butylcalix[4]arene-azacrown-3

A solution of 2.58g (3 mmol) 25,27-bis(1-propyloxy)-26,28-bis(2-chloroethoxy)-4-*p-tert*-butylcalix[4]arene, 0.513g (3mmol) p-toluenesulfonamide, 4.89g (15mmol) Cs_2CO_3 and 0.17g (1mmol) KI in 150mL dry DMF was heated at reflux under nitrogen for 24 h. The solvent was removed *in vacuo* and 50 mL 2N HCl and 50 mL CH_2Cl_2 were added and the phases were separated. The aqueous phase was extracted two times with 30mL CH_2Cl_2, the organic phases were combined, dried with Na_2SO_4 and the solvent removed *in vacuo*. The crude compound was recrystallized from methanol/CH_2Cl_2 (4:1) and gave 1.45g (51%) of N-tosyl-25,27-bis(1-propyloxy)-4-*p-tert*-butylcalix[4]arene-azacrown-3

as white crystals. ^{1}H NMR (400 MHz, $CDCl_3$); δ 0.56 (t, 6H, *J* = 7.5 Hz), 0.68 (m, 4H), 1.11 (s, 18 H), 1.26 (s, 18 H), 2.20 (m, 4H), 2.39 (s, 3H), 3.14 (m, 4H), 3.36 (m, 4H), 3.94 (m, 8H), 7.04 (s, 8H), 7.19 (d, 2H, *J* = 8.0 Hz), 7.48 (d, 2H, *J* = 8.2), ^{13}C NMR (100 MHz, $CDCl_3$); δ 10.1 (CH_3), 21.9 (CH_2), 31.7, 31.9 (CH_3), 34.2, 40.1 (CH_2), 50.7 (CH_3), 72.5, 74.2 (CH_2), 126.5, 126.8, 127.2, 130.0, 132.5, 134.2, 137.0, 143.0, 144.0, 145.7, 155.0, 155.6 (Ar). ESI MS *m/z* (%) calcd. for $C_{61}H_{81}NO_6SNa$ [M+Na^+] 978.57 found 978.73(94).

25,27-Bis(1-propyloxy)-4-*p-tert*-butylcalix[4]arene-azacrown-3

To a solution of 1.2g (1.25 mmol) N-tosyl-25,27-bis(1-propyloxy)-4-tert-butylcalix[4]arene-azacrown-3 in 80 mL dry THF was carefully added 1g of potassium metal under nitrogen. The mixture was heated to reflux for 24 h, at which temperature the potassium was molten, and then allowed to cool to rt. The main excess of potassium was removed and the rest was carefully hydrolyzed with water. The solvent was removed *in vacuo* and 50 mL 1N KOH and 50 mL CH_2Cl_2 were added and the phases were separated. The aqueous phase was extracted two times with 30mL CH_2Cl_2, the organic phases were combined, dried with Na_2SO_4 and the solvent removed *in vacuo*. The crude compound was recrystallized from methanol/CH_2Cl_2 (4:1) and gave 0.82g (82%) of 25,27-bis(1-propyloxy)-4-*p-tert*-butylcalix[4]arene-azacrown-3 as white crystals. ^{1}H NMR (400 MHz, $CDCl_3$); δ 0.55 (t, 6H, *J* = 7.5 Hz), 0.81 (m, 4H), 1.23 (s, 18 H), 1.27 (s, 18 H), 1.89 (m, 4H), 3.10 (m, 4H), 3.26 (m, 4H), 3.95 (m, 8H), 5.30 (s, 1H), 6.95 (s, 4H), 6.99 (s, 4H). ^{13}C NMR (100 MHz, $CDCl_3$); δ 10.0 (CH_3), 22.0 (CH_2), 31.5, 31.6 (CH_3), 33.9,

34.0, 39.8, 47.8, 68.1, 72.7 (CH_2), 125.9, 126.0, 132.4, 133.1, 143.9, 144.9, 154.0, 155.7 (Ar). ESI MS *m/z* (%) calcd. for $C_{54}H_{76}NO_4$ [M+H$^+$] 802.56 found 802.52(100).

N-(9-methylanthracene)-25,27-bis(1-propyloxy)-4-*p-tert*-butylcalix[4]arene-azacrown-3 (11)

A mixture of 200 mg (0.25 mmol) 25,27-bis(1-propyloxy)-4-*p-tert*-butylcalix[4]arene-azacrown-3, 85 mg (0.37 mmol) 9-(chloromethyl)anthracene, 75 mg (0.75 mmol) triethylamine and 17 mg (0.1 mmol) KI in 80 mL of dry dioxane was refluxed for 48h under nitrogen and protected from light. The solvent was removed *in vacuo* and 50 mL 2N KOH and 50 mL CH_2Cl_2 were added and the phases were separated. The aqueous phase was extracted two times with 30mL CH_2Cl_2, the organic phases were combined, dried with Na_2SO_4 and the solvent removed *in vacuo*. The crude product (80 mg) of was purified on prep. TLC using CH_2Cl_2/Et_3N (50:1) (R_f = 0.25). This fraction was almost pure and yielded after recrystallization from methanol/CH_2Cl_2 (4:1) 26 mg (31%) of the pure N-(9-methylanthracene)-25,27-bis(1-propyloxy)-4-*p-tert*-butylcalix[4]arene-azacrown-3 as slightly yellow crystals.^{1}H NMR (400 MHz, $CDCl_3$) ; δ 0.55 (t, 6H, *J* = 7.4), 0.70 (m, 4H), 1.10 (s, 18H), 1.27 (s, 18H), 1.70 (m, 4H), 3.15 (m, 4H), 3.52 (m, 4H), 4.01 (m, 8H), 4.06 (s, 2H), 7.00 (s, 4H), 7.05 (s, 4H), 7.40 (m, 4H), 7.92 (m, 2H), 8.20 (m, 2H), 8.31 (s, 1H). ^{13}C NMR (100 MHz, $CDCl_3$); δ 10.2 (CH_3), 21.9 (CH_2), 31.8, 31.9 (CH_3), 34.2, 34.3, 40.2, 49.7, 51.4, 70.2, 74.5 (CH_2), 125.1, 125.6, 125.7, 126.6, 126.8, 127.3, 129.1, 131.5, 131.7, 131.8, 132.2, 134.3 143.6, 145.3, 155.5, 155.9 (Ar). ESI MS *m/z* (%) calcd. for $C_{69}H_{86}NO_4$ [M+H$^+$] 992.63 found 992.69(82).

Fluorescence Measurements

Fluorescence emission and excitation spectra were obtained with a Perkin Elmer LS-50B Fluorimeter in 75:25 dichloromethane:THF. 6μM Benzyltrimethylammonium hydroxide was added as a proton scavenger. Fluorescence was measured as a function of metal ion concentrations where the metal ions were added as the hexafluorophosphate salts. Fluorescence areas were determined by integrating the spectrum over a fixed wavelength range.

Lithium Fluoroionophore Results and Discussion

Solvent effects

Previous studies of anthryl-benzocrown ether calixarenes indicated a considerable and complex solvent effect on the intensity of fluorescence[24] and a similar effect was observed in our study of the N-(9-methylanthracene)-25,27-bis(1-propyloxy)calix[4]arene-azacrown-5 (**10**) (see Figure 26). In both systems, in the absence of ions, the addition of methanol to dichloromethane solutions of the fluoroionophore caused an increase in the fluorescence intensity at small mole ratios of methanol to dichloromethane (ca. 0.17, 10% v/v) and then a decrease as the methanol concentration was increased further. It is likely that at low methanol concentrations, a hydrogen bonding interaction occurs between methanol and the azacrown nitrogen atom, disrupting the electron transfer quenching process and leading to the increase in fluorescence emission intensity observed. Conversely, the polar environment provided by higher methanol concentrations can increase the efficiency of electron transfer and cause a decrease in emission intensity. Furthermore, it can be reasonably expected that the polarity effect will dominate at high methanol concentration while a specific solute-solvent interaction will be more important at low methanol concentration.

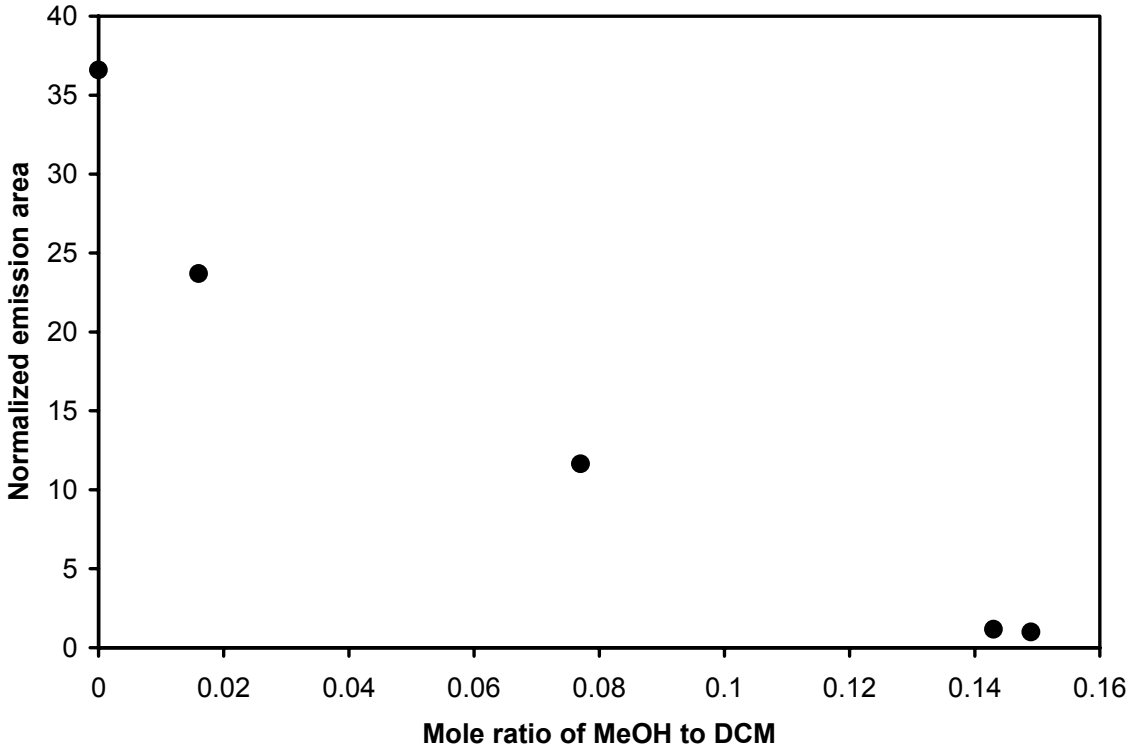

Figure 27: Normalized emission area of **11** (λ_{ex} 355 nm,1 × 10^{-6} M) as a function of the mole ratio of MeOH in dichloromethane.

The effect of methanol on the emission of **11** is different. Figure 27 shows the fluorescence emission of **11** as a function of the mole fraction of methanol in dichloromethane solution. With only small additions of methanol there is a dramatic decrease in the fluorescence quantum yield, i.e. there is no intensity increase at low methanol concentration. The fluorescence is completely quenched by the addition of methanol at a mole fraction of 0.15. This effect can be attributed to a more pronounced stabilization of charge separation in **11** than in other anthryl-benzocrown- and anthryl-azacrown-calixarenes. This is supported by the results of previously reported solution thermodynamics studies of calix[4]arene crown-3 systems.[82,89] In these studies, it was

observed that molecules with the crown-3 structure can complex small neutral molecules, such as nitromethane and malonitrile (and likely methanol) with relatively high stability constants ($\log K_s$ = 1-2 in $CDCl_3$). ^1H NMR data from this work show that an interaction occurs between the guest molecule and the π-systems of the calix[4]arene aromatic rings.[89] At the same time it was suggested that larger systems (e.g., crown-5) have weaker binding with neutral molecules due to the higher flexibility of the crown. This, in combination with the previously reported NMR data, suggests that **11** is likely to be more highly solvated in methanol than the larger crown-5 structures. Since higher solvation by methanol can be expected to enhance the electron transfer efficiency, the observed quenching effect of methanol on the emission intensity is understandable.

This solvent effect causes a practical problem in experiments on ion complexation since it masks the effect of ion binding on the emission intensity. As a result, all subsequent experiments on ion complexation were carried out in 75:25 (v/v) dichloromethane/THF using the hexafluorophosphate salts of the alkali metals, which are reasonably soluble in this solvent system.

Fluorescence Emission of 11

Figure 28 shows the fluorescence spectra obtained for **11** in the absence and presence of added concentrations of lithium hexafluorophosphate in 75:25 dichloromethane/THF. The fluorescence behavior of **11** clearly demonstrates that the PET "off-on" switching mechanism occurs in response to ion complexation. In the absence of ions the anthryl

fluorescence is at a minimum and increases with addition of lithium hexafluorophosphate yielding a maximum 106-fold enhancement.

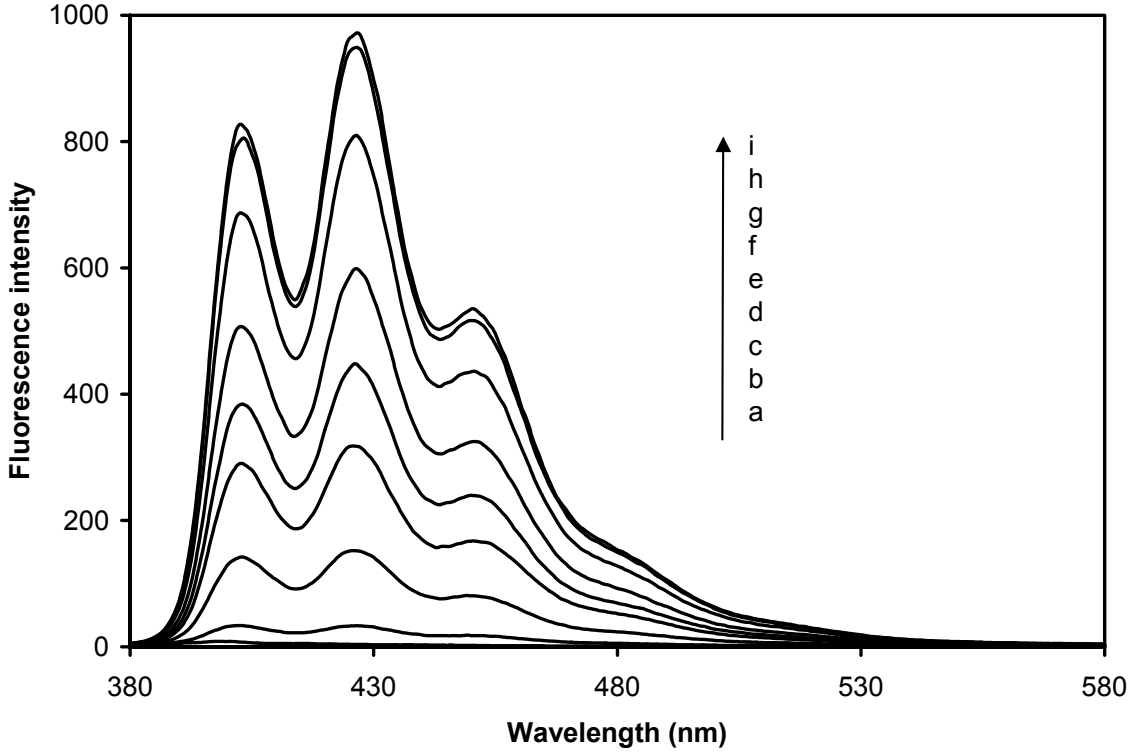

Figure 28: Fluorescence emission spectra (λ_{ex} 355 nm) of **11** (2×10^{-6} M) in 75:25 dichloromethane/THF with added BTMAH (6.0×10^{-6} M) as a function of [Li^+]. a: 0 μM, b: 2 μM, c: 3 μM, d: 4 μM, e: 4.5 μM, f: 5.5 μM, g: 6.5 μM, h: 8 μM, i: 15 μM.

Other PET based systems exhibit dramatic increases in fluorescence intensity but few have shown enhancements of this magnitude. The size of the fluorescence enhancement is directly related to the magnitude of the charge density of the bound ion that is experienced by the lone pair of the azacrown nitrogen atom, i.e., the electrons involved in the PET process. This is best illustrated by a comparison of the results for **11** with those

for **9** and **10,** both of which are fluoroionophores that signal the binding of potassium ions by the PET process (as we previously discussed above).

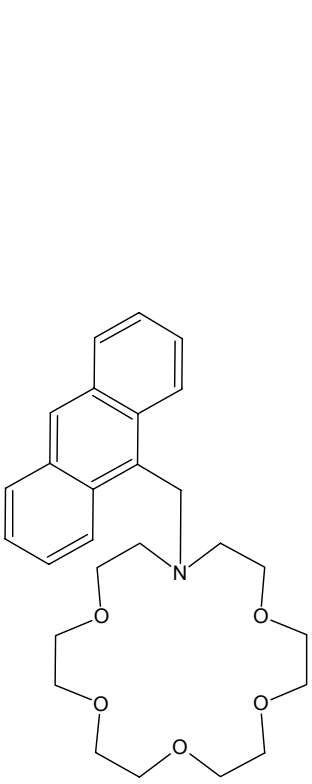

9

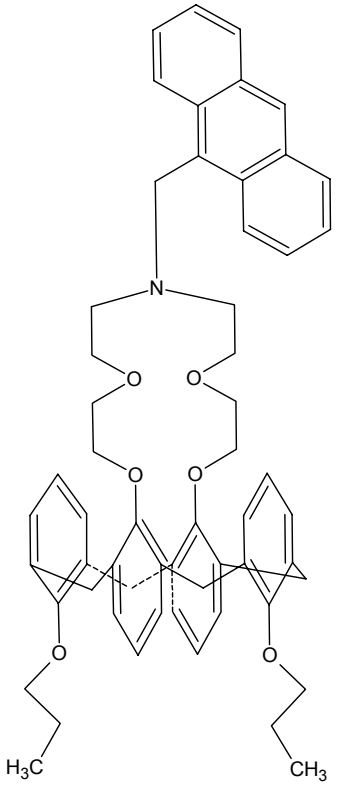

10

For **9** and **10**, the fluorescence enhancements observed were 50-fold and 8-fold, respectively. Modeling studies of **9** indicate that the most stable ion-fluoroionophore complex possesses a $K^{+}\cdots N$ distance = 3.0 Å while for **10** this distance is 3.5 Å. This difference could be expected to result in significantly smaller charge density at the azacrown nitrogen lone pair in complexes of **10** than in complexes of **9**, producing fluorescence enhancements consistent with those observed. The increased distance of the cation from the amine in **10** can be attributed to interactions between the cation and the

calixarene π-systems in **10**, an effect that has been observed for other host-guest molecules.[75-77] Modeling of **9**, however yields a minimized structure with a $Li^{+\cdots}N$ distance = 3.8 Å, considerably greater than either **9** or **10** and if taken on its own, counter to the observed fluorescence behavior. However, the lithium ion possesses a much larger intrinsic charge density, 1.47 versus 0.74 $qÅ^{-1}$ for lithium and potassium ions, respectively, and this difference is sufficient to explain the observed enhancement.

Selectivity

While the strength of the metal ion-fluoroionophore complex in **11** is governed by electrostatic interactions, particularly with the azacrown oxygen atoms, and through cation-π interactions, selectivity is controlled primarily by a size fit effect and steric effects from the t-butyl substituents appended to the two rotated aryl rings of the calix[4]arene.[14] Compound **11** was designed with the goal of excluding on a size-fit basis all ions larger than lithium (ionic radius = 0.68 Å). The structure of **11** was based in part on 14-crown-4 derivatives which are an appropriate size match for lithium. This crown was incorporated into **11** as an azacrown-3. In addition to providing an appropriately sized pocket, we expected that the bulky nature of the calix[4]arene structure would reduce the possibility of 2:1 sandwich-type complexes forming with larger cations. As part of our design process, molecular dynamics calculations were performed to determine the suitability of **11** for selectively binding lithium ion. Figure 29 shows the results of molecular dynamics calculations for **11** in the complexed state with lithium ion (left) and

sodium ion (right) (ionic radius = 0.95 Å). The minimized structure shows the lithium cation centered within the cavity with $Li^{+}\cdots O$ distances of 1.90, 2.02, 1.94, 1.95 Å. This is in contrast to sodium, which is positioned asymmetrically in the binding site ($Na^{+}\cdots O$ distances of 2.85, 2.44, 2.12, 2.13 Å) and is a considerably greater distance from the azacrown nitrogen atom. ($Na^{+}\cdots N$ distance = 4.84 Å versus $Li^{+}\cdots N$ distance = 3.80 Å). The calculations also indicate that the sodium complex is ca. 25 Kcal/mol less thermodynamically stable than the lithium complex. As expected, calculations for potassium ion (ionic radius = 1.33 Å) complexes with **11** (not shown) yielded structures in which the cation was pushed out of the binding pocket entirely ($K^{+}\cdots N$ distance of 5.98 Å). Although these calculations are qualitative, they suggested that **11** should have a high degree of discrimination over sodium and potassium cations.

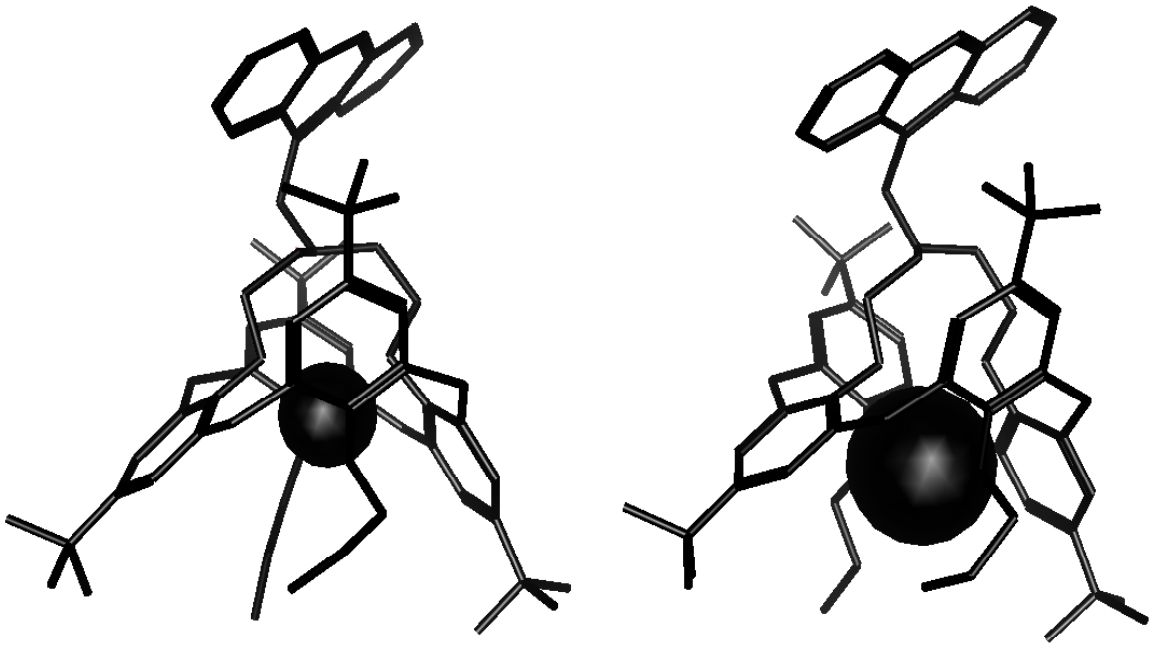

Figure 29: Minimized structures of **11** with Li^{+} (left) and Na^{+} (right).

Figure 30 shows the dependence of the emission intensity of **11** on cation concentration for lithium, sodium and potassium. (The values in the plot are normalized to the

fluorescence intensity in the absence of ion.) These results suggest high selectivity of **11** to lithium in comparison with the other alkali metal cations studied.

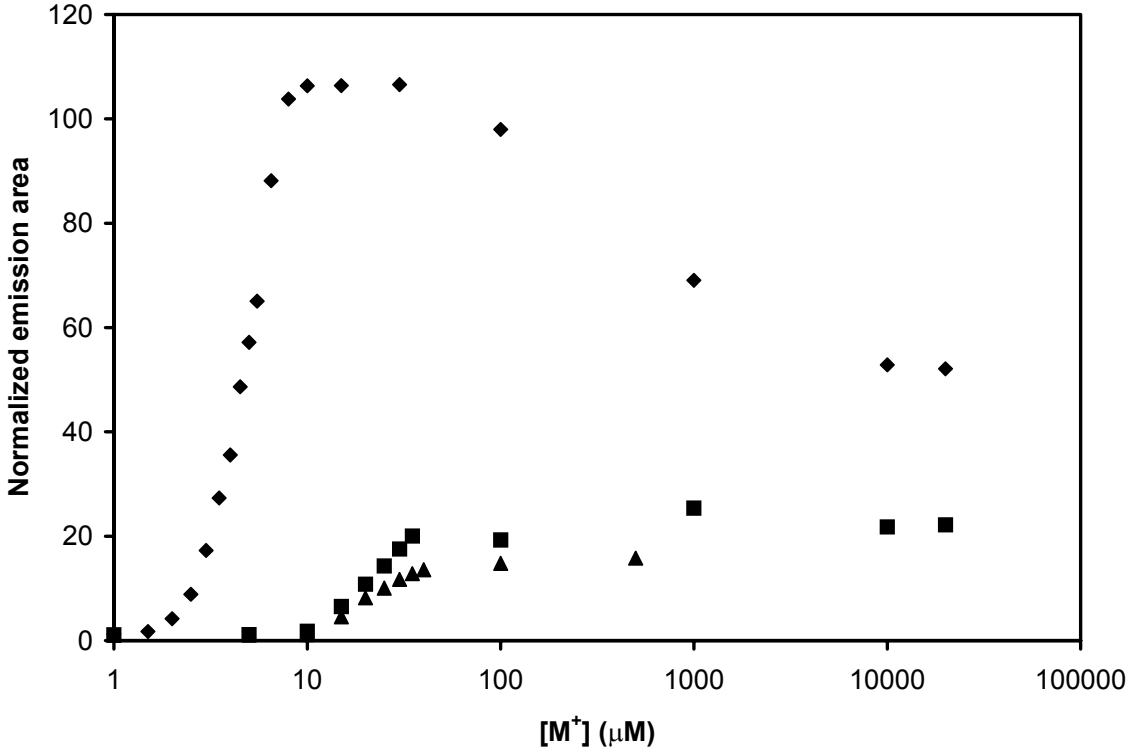

Figure 30: Emission area of **11** versus the concentration of various alkali metal ions: Li (♦), Na (■), K(▲).

From Figure 30 it is clear that for potassium and sodium ions, the integrated fluorescence intensity as a function of added ion initially increases until it reaches a plateau, beyond which it is constant up to the maximum concentration tested. In the case of lithium ions, the fluorescence intensity increases, plateaus at ca. 10 μM and then begins to decrease beyond 50 μM. This fluorescence quenching behavior is similar to other PET based systems and has been attributed to a "medium effect" due to the increase of ionic

strength.[22,24,63-66] It is also clear that the enhancement in fluorescence emission in the presence of lithium ions is significantly larger than for sodium or potassium. The selectivity was calculated from equation **8**, where *i* = primary ion, *j* = interfering ion (as above, see equation **6**).

$$\log K_{i,j} = \log\left(\frac{[i]}{[j]}\right) \qquad \textbf{(8)}$$

Here, [j] is the highest tested concentration of the interfering ion in the plateau region of the plot, 20 mM and .5 mM for sodium and potassium ions, respectively. The primary ion concentration, [i], is the concentration that produces the same fluorescence response as the maximum fluorescence produced by the interfering ion and as such represents a minimum unambiguous detection limit for the primary ion, (3.2 μM lithium and 2.8 μM lithium for sodium and potassium, respectively). In the case of sodium, the calculation yields a selectivity value for lithium versus sodium, log $K_{Li,Na}$ = -3.8. However, this concentration represents the solubility limit of the sodium salt used and therefore, this selectivity should be regarded as a lower limit only. Similar results were obtained for lithium versus potassium, log $K_{Li,K}$ = -2.3. We note that again this is a lower limit. The value quoted is less than that for lithium/sodium selectivity because the potassium salt used was less soluble and we were limited to a maximum concentration of 0.5 mM. However, as with sodium the actual selectivity is likely much higher. In fact, given that the ionic radius of potassium is larger than that of sodium, and that from the molecular

dynamics calculations the potassium complex is less stable than that of sodium, the lithium/potassium selectivity is expected to be at least two orders of magnitude greater than the lower limit quoted.

Summary of Lithium Fluoroionophore Work

The N-(9-methylanthracene)-25,27-bis(1-propyloxy)-4-*p*-*tert*-butylcalix[4]arene-azacrown-3 (**11**) acts as a fluoroionophore in the presence of the alkali metal ions (lithium, sodium, potassium). In the absence of ion, fluorescence of the anthryl group is substantially quenched by intramolecular electron transfer (PET) from the nitrogen atom in the azacrown moiety. In the presence of complexed ion, the electric field of the ion disrupts the PET process, thereby switching on the anthryl fluorescence emission. For lithium, the enhancement in fluorescence is dramatic (>106-fold).

Molecular dynamics calculations predicted high selectivity of **11** for lithium ion over sodium and potassium ions on the basis of a size-fit effect. This is confirmed by smaller fluorescence enhancements for the latter two ions. Selectivity was calculated based on the observed fluorescence behavior, yielding $\log K_{Li,Na} = -3.8$. and $\log K_{Li,K} = -2.3$. These values are regarded as lower limits due to limited solubilities of the sodium and potassium salts used in the experiments. Nevertheless, the observed selectivities indicate that **11** is one of the most selective lithium ligands reported.

D: Sodium Fluoroionophore (12) and Optode Fabrication

In the preceding work with our potassium fluoroionophore **10** and our lithium fluoroionophore **11**, we reported on the photoinduced electron transfer (PET) mechanism by which these molecules operate and on the solution phase complexation of cations. It was shown that complexation of potassium and lithium ions in an organic solution triggered a substantial increase in anthryl fluorescence emission through the disruption of the PET quenching process for **10** and **11**, respectively. It was also shown that the molecules possess high selectivity for their primary ions over that of interfering ions, (e.g. $\log K_{K,Na} \leq -3.5$, $\log K_{Li,Na} = -3.8$ for **10** and **11**, respectively)

In solution, we were limited to testing at fluoroionophore concentrations that do not absorb beyond .04 in a 1 cm cell, i.e. < 10 μM. Since complexation follows a 1:1 stoichiometry, only micromolar cation concentrations could be tested. This value is far below the physiological concentration range of important cations, i.e. mM range. However, the ultimate intended use of fluoroionophores is in the construction of optically based sensors where the fluoroionophore will be contained within a thin polymeric film. Since these films will have a thickness on the order of microns, larger fluoroionophore concentrations will be possible, potentially promising sensitivity with the physiological range. A logical extension of the work described up to this point then, is the incorporation of a fluoroionophore into an optically based format that is suitable for the eventual application of a sensor in the clinical diagnosis of disease.

The development of optical sensors, optodes, based on polymeric membranes has been extensively studied.[11c,50] For example, tetraethylester-*p*-*tert*-butyl-calix[4]arene (Figure 31) as well as the tetramethylester-*p*-*tert*-butyl-calix[4]arene (Figure 5, right) have been incorporated as one of several components into an organic polymer membrane consisting of PVC, various plasticizers, a pH sensitive fluorophore and in some cases a lipophilic salt (e.g., KtpClPB).[90,91] The operation of such an optode usually involves the partitioning of the ion from the aqueous phase into the membrane organic phase followed by binding of the ion to the calix[4]arene and then a release of a proton from the fluorophore, which in the process alters the fluorescence intensity. This process is depicted in Figure 32 where *aq* and *org* denote the aqueous and organic phases respectively, I is the ion, L is the ligand or ionophore, IL^+ is the ion-ionophore complex, C^- is the anionic fluorophore, CH is the neutral fluorophore. The signaling mechanism has been referred to as cation exchange and operates as follows: the cation, I^+, enters the membrane organic phase and is bound by the ionophore, L_{org}, creating a positive charge site, IL^+_{org}; a proton is then released from the fluorophore, CH_{org}, creating a negative charge site C^-_{org} , thereby maintaining electrical neutrality within the membrane organic phase. The charged and uncharged versions of the fluorophore have different spectroscopic properties enabling the optical detection of ion binding.

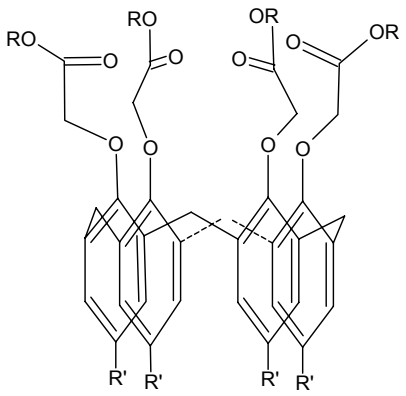

R = ethyl, R' = t-butyl

Figure 31: Tetraethylester-*p*-*tert*-butyl-calix[4]arene

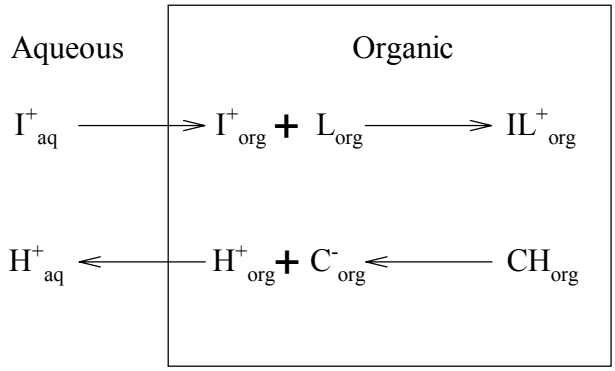

Figure 32: Cation exchange process of bulk optodes

Despite exhibiting high selectivity, these multi-component systems are complex and difficult to optimize. In addition to these drawbacks, since the signaling mechanism is pH dependent, samples that are exposed to the optode must be buffered in order to reliably measure the cation concentration independent from pH changes. This significantly limits the utility and applicability of such optodes.

These multi-component devices have been simplified by eliminating the two-component ionophore/fluorophore couple and replacing it with the single fluoroionophore concept as discussed above. For example, Waldner et al. synthesized a sodium selective fluoroionophore consisting of acridine and the 26,27,28-tri-*tert*-butylester-*p*-*tert*-butyl-calix[4]arene structure (Figure 33).[92] This new fluoroionophore was doped into a commercial acrylate polymer (poly(hydroxybutyl acrylate)) and exhibited an increase in fluorescence intensity of 3 fold over a sodium concentration range of 0 to 2 M range. Despite the fact that no selectivity data was given and the fluorophore of choice is known to be pH sensitive, thus limiting its use as a sensor in important applications such as clinical diagnosis, the system employed a one component polymer matrix thereby promising simplified sensor construction.

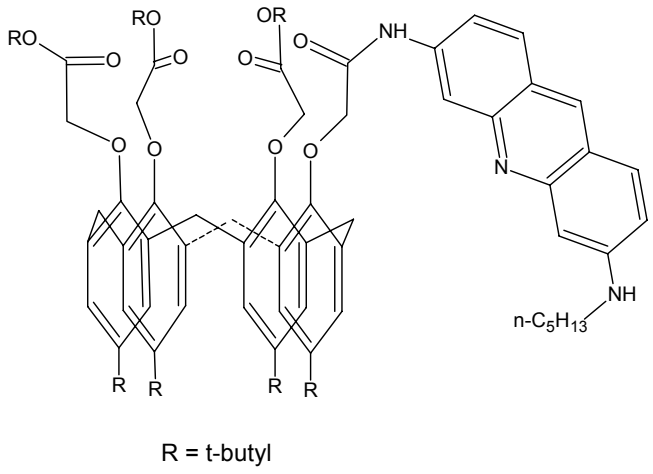

Figure 33: Acridine-tri-*tert*-butylester-*p*-*tert*-butyl-calix[4]arene fluoroionophore

Here we describe the development of a simple one-component sodium bulk optode using fluoroionophore **12** which is based upon a tetraethylester-*p*-*tert*-butyl-calix[4]arene covalently linked through an amide bond to a rhodamine-B fluorophore. As mentioned

above, the calix[4]arene structure is an established sodium ion selective ionophore with good selectivity over potassium ion in the physiological range and therefore makes this an appropriate candidate for the ionophoric moiety.

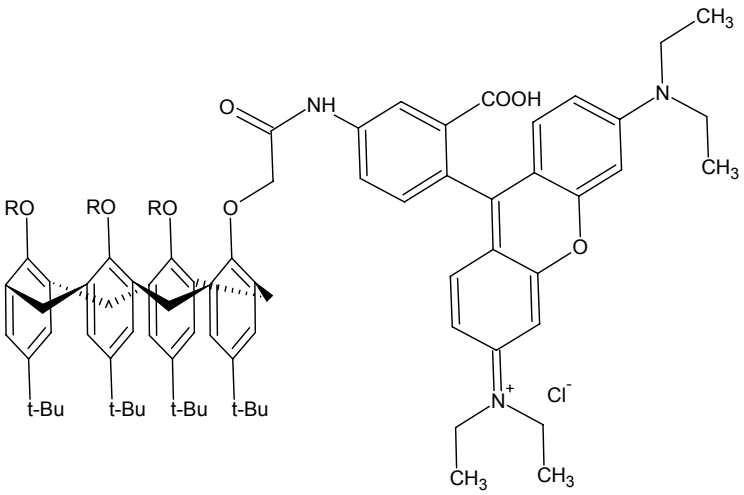

12

Our choice of rhodamine-B as the fluorophore was based on several considerations. First, in order to make operative the "off-on" PET process in the fluoroionophore, it is necessary to incorporate both the fluorophore and an electron donating group into the molecule. Furthermore, the free energy of the PET process must be negative following photoexcitation of the fluorophore. The free energy requirement is satisfied by linking the rhodamine to the calix[4]arene by an amide bond. The redox potentials of the rhodamine and amide and the excited state energy of the rhodamine combine to make PET a thermodynamically accessible process. Another consideration in our choice of

rhodamine is its insensitivity to pH in the human physiological range.[93] This obviates the need for a complex multicomponent optode. Finally, the rhodamine excited state is accessible to visible light, making the use of inexpensive light sources and detectors possible. The result as described below is an optode with a wide dynamic response range and sodium/potassium ion selectivity suitable for clinical measurements.

Sodium Fluoroionophore Experimental

Synthesis of 12 (by Dr. Hubert Neinaber)

4-*p*-*tert*-Butylcalix[4]arene-tetraaceticacid tetraethyl ester and 4-*p*-*tert*-butylcalix[4]arene-tetraaceticacid triethyl ester were prepared as previously described.[94,95] Rhodamine B amine was purchased from Sigma and purified by dissolving 500 mg in 200 mL dichloromethane and extracting the solution three times with 100 mL 2N HCl. The aqueous phases were brought to pH 12 with 20% KOH and extracted three times with 100 mL dichloromethane. The organic phase was dried over $MgSO_4$ and the solvent removed *in vacuo*.

In a nitrogen atmosphere 650 mg (0.67 mmol) 4-*p*-*tert*-butylcalix[4]arene-tetraaceticacid triethyl ester was dissolved in 5 mL $SOCl_2$ and refluxed for 15 min. After this the excess $SOCl_2$ was evaporated, the residue was dissolved in 3 mL dry CH_2Cl_2 and the solution again evaporated to remove all $SOCl_2$. The white crystalline residue (acid chloride) was dissolved in 50mL dry CH_2Cl_2 and at 0°C a mixture of 310 mg (0.68 mmol) Rhodamine B amine and 202 mg (2 mmol) triethylamine in 5 mL dry CH_2Cl_2 were added during a period of 10 min. The mixture was stirred for another 16 h at room temperature, diluted with 200 mL CH_2Cl_2 and washed three times with 100 mL 2N HCl. The organic phase was dried over $MgSO_4$, evaporated, and the resulting residue was purified by column chromatography on silica with dichloromethane/methanol-mixtures of increasing polarity (dichloromethane/methanol gradient: 10% to 25% methanol). The product was isolated as 530 mg (56% yield) of a pink solid. mp 230-233°C (decomp.). MS *m/z* (%) calcd. for

$C_{86}H_{106}N_3O_{14}$ (M^+) 1404.7, found 1404.8(100). IR (KBr pellet, cm^{-1}): 3387cm^{-1} (O-H), 2963 cm^{-1} (C-H), 1753cm^{-1} (C=O), 1698 cm^{-1} (C=O), 1614 cm^{-1} (C=O), 1590 cm^{-1} (C=O).

Optode 1 Preparation and testing

2 mL of MeOH was added to 6 mg of fluoroionophore **12** and 350 mg of a custom copolymer of 40% hydroxybutylacrylate and 60% isopropylacrylamide (donated by Dr. Robert Hatch, Bayer Diagnostics, Elkhart, IN). This composition was mixed for 18 hr before use. 150 μL of the membrane solution was deposited onto 18 mm diameter glass microscope slides. Using a P-6000 Spin Coater (Integrated Technologies, Inc.) the slides were spun at 3000 rpm for 60 seconds. This produced sensors with membrane thickness of ca. 10 μm. Membranes were dried under ambient conditions for 2 hours and stored in the dark. The prepared optodes were housed in a custom flow-through cell and positioned at ca. 45º relative to the excitation beam. Fluorescence emission spectra were taken with λ_{ex} = 540 nm. Time drives were obtained with $\lambda_{ex/em}$ 540/585 nm. NaCl and KCl were analytical grade and obtained from Aldrich. Aqueous test samples were prepared in 18 MΩ·cm deionized water.

Sodium Fluoroionophore Results and Discussion

Principle of Operation

The fluoroionophore, **12**, contains the three components that are typically employed in PET-based systems, namely a fluorophore, a host-guest site and a spacer group. The rhodamine fluorophore is particularly appropriate for this system since it is insensitive to pH in the physiological range, thereby eliminating the need to correct for pH.[93] In addition, its visible absorption (540 nm) and emission properties (585 nm) will allow the use of readily available and relatively inexpensive commercial light sources, e.g., LED's, and detection systems in the final sensor instrumentation. To be operative the PET mechanism must have a negative free energy change, ΔG_{PET}, and in this the rhodamine group is again an appropriate selection. The amide linkage between the rhodamine and the calixarene ionophore also serves as a source of electrons that can reduce the rhodamine group following photoexcitation. The oxidation potential of the amide group,[96] the reduction potential of the rhodamine ground state[97] and the energy available in the rhodamine excited singlet state (as determined from fluorescence excitation and emission spectra) combine in the Rehm-Weller equation to yield an estimated value of ΔG_{PET} = -0.13 V, indicating that electron transfer is a spontaneous process following photoexcitation.

Indeed, electrostatic calculations on **12** show a substantial shift in the electron density within the amide linkage upon complexation of sodium ion. Figure 34 presents the

results of the calculations and as before, the magnitude of electron density decreases in the order of red > green > blue. These results suggest that upon binding of sodium ion the amide linkage will be involved in the complexation and thus increases the electron donor's oxidation potential relative to that of the rhodamine acceptor. This result, in combination with the ΔG_{PET} calculations indicates that an enhancement in the fluorescence would be expected upon complexation.

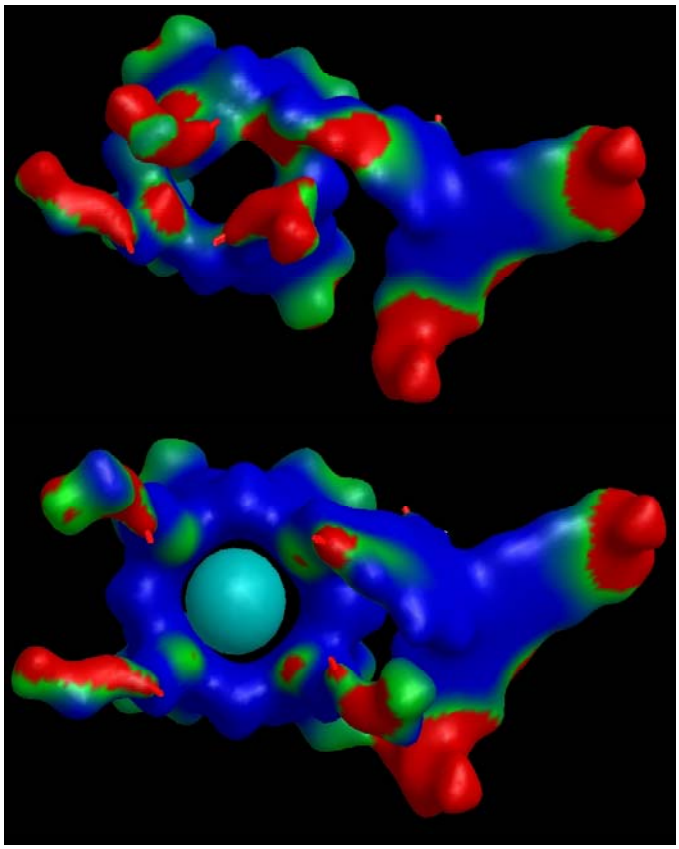

Figure 34: Electrostatic calculation results for **12** in the uncomplexed state (top) and complexed state with sodium (bottom). The magnitude of electron density decreases in the order of Red, Green, Blue.

The polymer membrane is also crucial to the functioning of the optode. In particular it is desirable to use a matrix that is sufficiently hydrophobic so as to insure the long-term

mechanical stability of the membrane in aqueous environments. However, it must also be sufficiently hydrophilic to allow for water uptake and ion transport from the aqueous phase into the organic phase of the membrane. In addition, the membrane must be optically transparent at the excitation and emission wavelengths of the fluorophore. Copolymers of acrylamides and alkyl acrylates have been applied in similar applications,[98] and in this work we have chosen a copolymer of 40% hydroxybutylacrylate and 60% isopropylacrylamide (Figure 35).

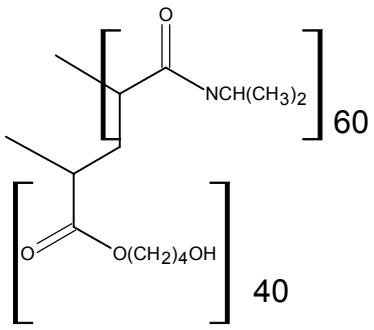

Figure 35: Sodium optode membrane copolymer

Sensor Response

The new sodium optode was exposed to various concentrations of pure aqueous NaCl spanning the range 0.025 to 2 M. Figure 36 shows the fluorescence emission spectra obtained for these various concentrations. The fluorescence intensity was a linear (R^2 = 0.9996) function of the sodium ion concentration (Inset, Figure 36). Within this range, a 2.7 fold enhancement in the fluorescence was observed, comparable to the acridine-tri-*tert*-butylester-*p*-*tert*-butyl-calix[4]arene fluoroionophore constructed by Waldner et al

(3.1 fold).[92] Figure 37 shows the dynamic response of the optode to sodium within the range of 0.01 - 0.2 M. The data indicate that response times of the optode are on the order of 2 minutes with a maximum 30% increase in the fluorescence intensity.

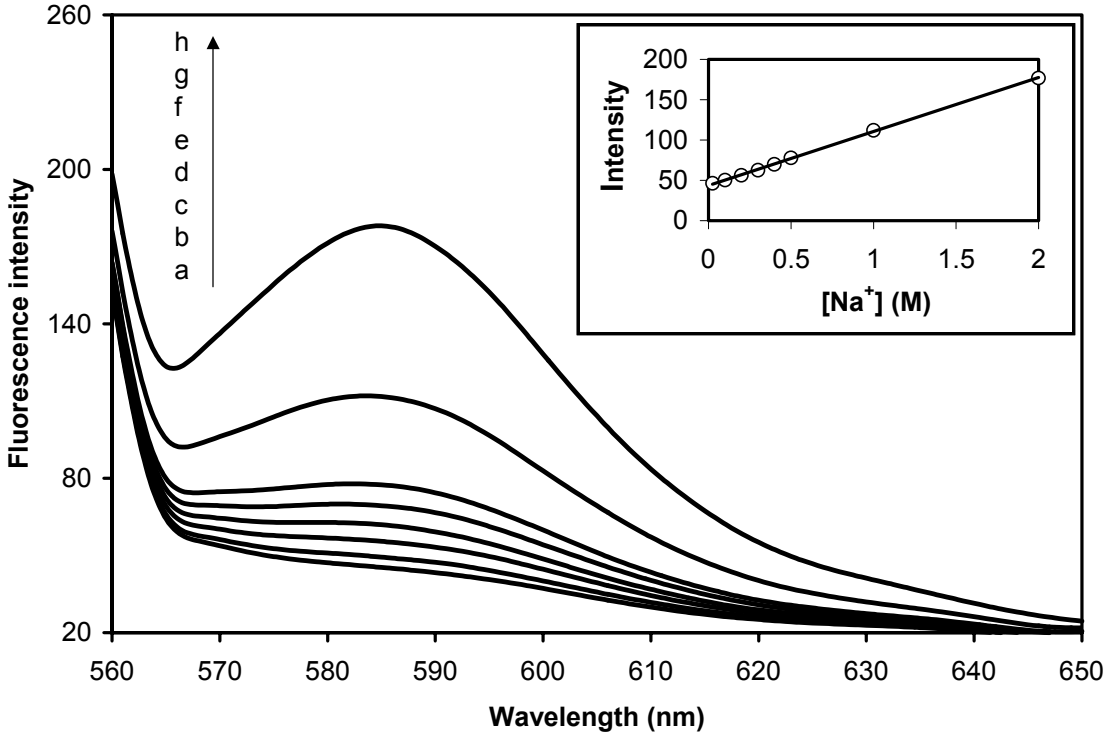

Figure 36: Emission spectrum of Optode with incorporated **12** (λ_{ex} 540 nm) as a function of sodium concentration; a (.025M), b (.1M), c (.2M), d (.3M), e (.4M), f (.5M), g (1M), h (2M). Inset showing linear correlation of λmax (585 nm) to sodium cation concentration.

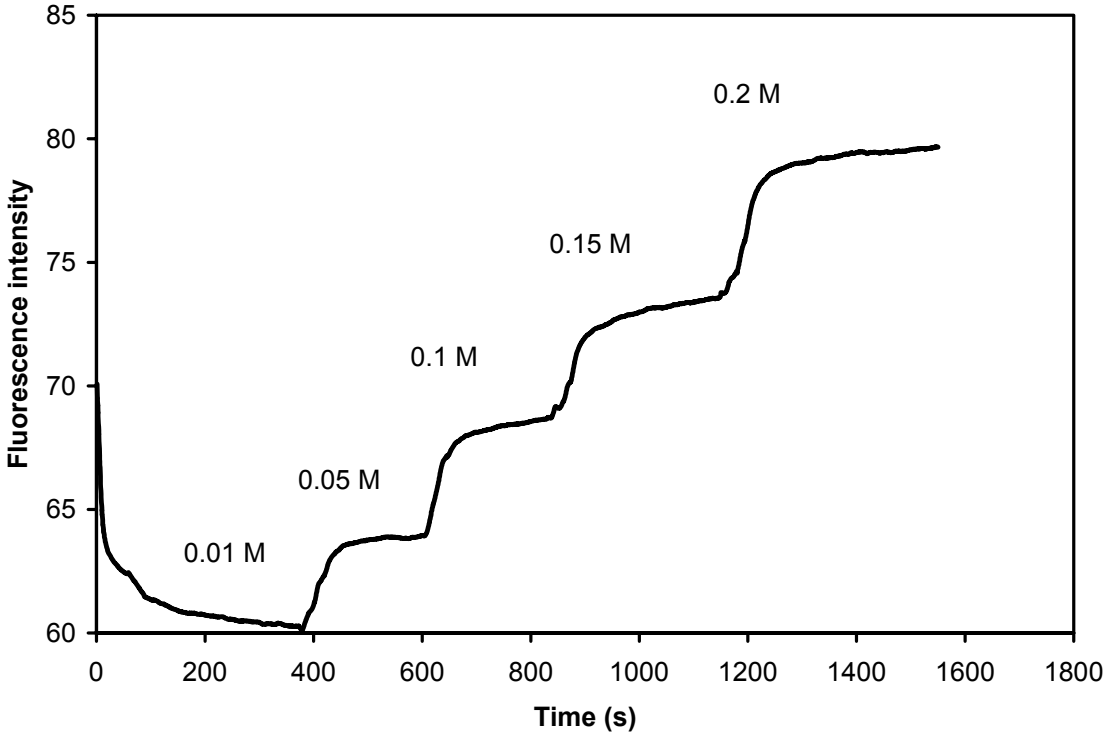

Figure 37: Dynamic response of Optode to increasing concentrations of aqueous solutions of sodium chloride ($\lambda_{ex/em}$ 540/585 nm).

Selectivity

The tetraethylester-*p*-*tert*-butylcalix[4]arene ionophore has been shown previously in ion selective electrodes (ISE's) as well as in optically-based systems to be highly selective for sodium ions compared to potassium ions.[34,90,91] For example, when incorporated into ISE membranes composed of plasticized PVC, the sensors discriminate against potassium by more than two orders of magnitude, logK = -2.5.[34] This relatively high selectivity is attributed to the rigid calixarene skeleton providing a framework for the creation of a pocket size that closely matches that of sodium (ionic radius, 0.95 Å) and thus excludes

larger sized cations such as potassium (ionic radius, 1.33 Å). This size selection is also reflected in the free energy of complexation, ΔG, where the sodium complex has been shown to be 21.3 kJ/mol more favorable (negative) than that of potassium.[82] These factors again point to the notion that preorganization and size fit are key components in the design of selective ligands.

Although calix[4]arenes are known to have good selectivity for sodium over potassium ions, selectivity data for the previously reported acridine-calix[4]arene (Figure 33) based sensor were not measured.[92] In this research we have measured the sodium/potassium ion selectivity using the Separate Solution Method for optodes (log $K^{opt}_{Na,K}$ SSM), based on the recommended procedure of Bakker et al.[50]

The SSM method is superficially different from the method employed to calculate the selectivity for compounds **10** and **11**. Specifically, the sensor is exposed to a specified level of just the primary ion of interest [i], in this case sodium, and the fluorescence output determined. The sensor is then exposed to a level of interfering ion, [j], that is as high as required to achieve the same measured fluorescence emission as determined in the presence of [i] alone. The selectivity is then calculated exactly as it is in equation **6** by taking the ratio of [i] to [j]. In this fashion the selectivity for sodium over potassium was determined and compared to previous results of an optode[90] and ISE[34] system based on the tetraethylester-*p*-*tert*-butyl-calix[4]arene ionophore as well as to the required selectivity in extracellular media[83] (Table 4).

	$\log K^{opt}_{Na,K}$
Required[83]	-0.6
optode 1	-0.6
optode 2[90]	-2.3
ISE[34]	-2.5

Table 4: Selectivity data of optode 1, comparative optode 2, ISE and required selectivity.

Optode 2 operates on the cation-exchange mechanism and is composed of a plasticized/PVC membrane incorporating tetraethylester-*p*-*tert*-butyl-calix[4]arene (Figure 31), and a tetraphenylporphine (TTP) fluorescent dye[90] (Figure 38).

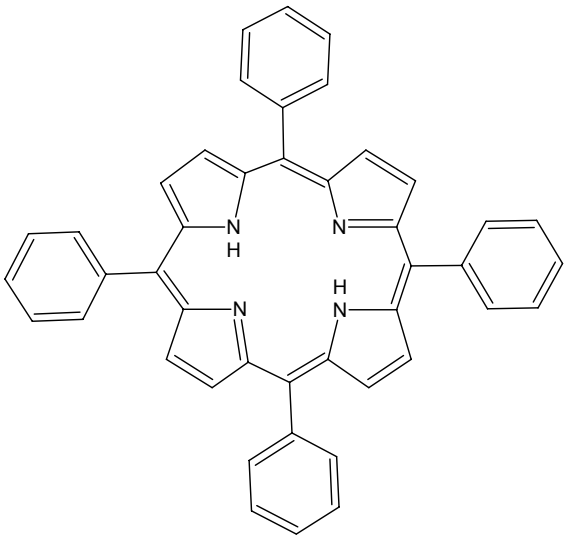

Figure 38: Tetraphenylporphine (TPP) used in optode 2

While the TPP and ISE systems operate by a different mechanisms their selectivity is quite comparable, i.e. discriminating against potassium by ca. 2 orders of magnitude, indicating that the ability of calix[4]arene to discriminate between sodium and potassium

is relatively unaffected by their environments. Based on these precedents it could be expected that optode 1 would show comparable selectivity. Our preliminary results for optode 1 show good selectivity, although somewhat lower than for the optode or ISE, -0.6, -2.3, -2.5, respectively.

This reduction of selectivity may not be unexpected in light of other work conducted with similar calix[4]arenes that have been substituted with bulky groups at the lower rim. Indeed, Cadogan et al investigated the effect on the selectivity of a number *p*-*tert*-butyl-calix[4]arenes showing that as the substituents became more bulky a corresponding reduction in the selectivity was observed.[99] In particular *tert*-butyl and adamantyl substituted calix[4]arenes provided ISE's with $\log K_{Na,K}$ = -1.1 and -0.1 showing the significant dependence on steric factors. In addition to this effect, it was observed that the response times of these ISE's also increased (up to ca. 60 seconds with adamantyl substitution) with increased steric hindrance, indicating that the bulky substituents reduced the rate of complexation. This fact may inpart explain the lengthy response time noted for our optode. However, we note that optode 1 meets the selectivity requirement for testing in extracellular media, e.g. whole blood, plasma and serum therefore making this system of practical utility.

Summary of Sodium Fluoroionophore work

In this work we have reported on the development of a new and simplified sodium optode based on aminorhodamine B and calix[4]arene. This new fluoroionophore responded to increasing concentrations of sodium (.025M – 2 M) with an increase in fluorescence intensity, ca. 2.7 fold. Although the total change across this range is good, the delta response in the physiological range (0.1-0.2 M) is limited (0.12 units/mM). This becomes particularly relevant when millimolar changes are required to be resolved for clinical diagnosis. Therefore further development is needed to enhance the signal-to-noise ratio of this optode.

From an evaluation of the optode response, the sensor was able to reach equilibrium in ca. 2 minutes. In most circumstances this would be an adequate response time, however most modern day diagnostic instrumentation are able to provide an analytical result within ca. one minute. Consequently additional effort is needed to improve this response characteristic.

The response of the sensor is governed by two aspects; complexation of the cation and diffusion of the cation into the polymeric membrane. The former is fixed for this system, however the latter can be tuned. Specially, the response time of a sensor, dependent upon diffusion into the bulk, is proportional to the square of the distance or thickness of the membrane layer divided by the diffusion coefficient of the polymer (Equation 7).[19]

$$t_{95} = 1.13d^2/D \qquad \textbf{(7)}$$

Here t_{95} is the time to 95% of the total response in seconds, d is the thickness of the polymer layer in cm, and D is the diffusion coefficient in cm^2/s. Thus, increasing the diffusion coefficient of the polymer can potentially reduce the response time of the sensor. The diffusion coefficient in turn is controlled by the hydrophilicity/hydrophobicity of the polymer. Hence higher hydrophilicity means more water uptake and therefore faster diffusion of cations into the membrane. The polymer chosen for this work is a copolymer of hydrophilic (40%, hydroxybutyl) and hydrophobic (60%, isopropyl) monomers and therefore it could reasonably be expected that an increase in the ratio of the hydroxybutyl/isopropyl moieties would lead to a reduction of the sensor response time.

Since sodium concentrations within extracellular media, such as whole blood and plasma, are relatively high (clinical range ca. 135-150 mM) compared to other potential interfering cations such as potassium (clinical range ca. 3.5-5 mM), the selectivity burden for sodium ionophores is small and is required to be $\log K_{Na,K} = -0.6$.[83] In the selectivity studies completed in this work it was found that the optode has the required sodium/potassium ion selectivity for sodium ion determinations in extracellular media.

IV: Conclusions

In this work we have taken a rational approach to the design of new ionophores and fluoroionophores in which the fundamental requirements of complexation were considered while employing the modern techniques of molecular modeling. This has resulted in the synthesis and complexation studies of novel ionophores for the monovalent: ammonium, potassium, sodium and lithium ions. The results of these complexation studies were corroborated with molecular modeling predictions for selectivity and thus provide a framework for the development of future ionophores and fluoroionophores.

Specifically, we have reported here on the modular synthesis of a new ammonium selective ionophore based upon a cyclic depsipeptide motif (**8**). This ionophore was designed to take advantage of the tetrahedral symmetry of the ammonium cation in order to discriminate against cations with requirements for a spherical coordination geometry. Moreover, through molecular modeling, **8** was predicted to be more selective for ammonium than potassium ions. In addition, the structure was designed with the view of incorporating a rigid pre-organized backbone which has been shown to enhance selectivity by reducing the enthalpic costs of complexation. This approach yielded an ionophore which, when incorporated into an ISE format, provides selectivity for ammonium ion over potassium (logK = -0.6) and sodium (logK = -2.1) ions that is comparable to nonactin. We believe that the flexible modular approach used here will

enable us to tune the structure of similar molecules so as to achieve higher selectivity and sensitivity characteristics.

In addition to the ionophore **8,** we have also designed, synthesized and tested fluoroionophores for metal ion detection and in one case we have created an optical sodium ion sensor from a fluoroionophore. Specifically, a potassium fluoroionophore was designed, modeled and synthesized and shown to have high selectivity. N-(9-methyl-anthracene)-25,27-bis(1-propyloxy)calix[4]arene-azacrown-5, **10**, was shown by modeling and dynamics calculations to exhibit appropriate size-fit behavior and to possess a pre-organized structure conducive to binding potassium ions. In addition, electrostatic calculations were shown to give good evidence for the redistribution of electron density in **10** following binding. This evidence is particularly important for predicting whether the photoinduced electron transfer (PET) mechanism, upon which the function of **10** as a fluoroionophore is based, is operative. In fact, **10** was shown to complex with potassium ions in organic solution triggering a substantial increase in anthryl fluorescence emission through the disruption of the PET quenching process (8.5-fold enhancement). Preliminary measurements indicate that the selectivity for potassium ions over other alkali metal cations particularly sodium and lithium ($\log K_{K,Na} = \log K_{K,Li} \leq -3.5$) for **10** is increased dramatically over that of the anthryl azacrown model compound, **9,** ($\log K_{K,Na} = -1.3$) . This large increase in the selectivity for potassium over sodium and lithium can be attributed to the rigid and pre-organized structure of **10** such that the molecule can not wrap around these smaller cations without a large thermodynamic cost of complexation. In addition, these preliminary solution phase studies indicate a 1:1

complexation between **10** and the ion, suggesting that **10** could be sensitive to potassium in the normal physiological concentration range once incorporated into a sensor. Furthermore, the observed fluorescence response to changes in solvent polarity suggests that the sensor substrate composition will have an important impact on the efficiency of **10** as an ionophore and could allow further optimization of sensitivity and selectivity.

The N-(9-methyl-anthracene)-25,27-bis(1-propyloxy)-4-*p*-*tert*-butylcalix[4]arene-azacrown-3, **11**, further illustrates the significant role that size-fit as well as pre-organization criteria play in the selectivity of ionophores. By a reduction in the size of the azacrown moiety we have created a binding site appropriate for the stable complexation of lithium ions which excludes larger cations such as sodium and potassium. We have shown that **11** acts as a fluoroionophore in the presence of the lithium ions and that the enhancement in fluorescence is dramatic (>106-fold). Molecular dynamics calculations predicted high selectivity of **11** for lithium ion over sodium and potassium ions on the basis of a size-fit effect. This is confirmed by smaller fluorescence enhancements for the latter two ions. Selectivity calculations yielded $\log K_{Li,Na}$ = -3.8. and $\log K_{Li,K}$ = -2.3. These values are regarded as lower limits due to limited solubilities of the sodium and potassium salts used in the experiments. Nevertheless, the observed selectivities indicate that **11** is one of the most selective lithium ligands reported.

A logical extension of the work described up to this point then, is the incorporation of a fluoroionophore into an optically based format that is suitable for the eventual application of a sensor in the clinical diagnosis of disease. In this work we have reported on the

development of a new and simplified sodium optode based on a molecule that incorporates aminorhodamine B as a fluorophore and *p-tert*-butylcalix[4]arene as the ionophore (**12**). The *p-tert*-butylcalix[4]arene was chosen due to its relatively high sodium ion selectivity which is attributed to the rigid calixarene skeleton providing a framework for the creation of a pocket size that closely matches that of sodium (ionic radius, 0.95 Å) and thus excludes larger sized cations such as potassium (ionic radius, 1.33 Å). These factors again point to the notion that pre-organization and size fit are key components in the design of selective ligands.

This new fluoroionophore, when incorporated into an optode, responded to increasing concentrations of sodium (0.025 – 2 M) with an increase in fluorescence intensity of ca. 2.7 fold. Although the total change across this range is good, the delta response in the physiological range (0.1-0.2 M) is limited (0.12 units/mM). This becomes particularly relevant when millimolar changes are required to be resolved for clinical diagnostics. Therefore further development is needed to enhance the signal-to-noise ratio of this optode. From an evaluation of the optode response, the sensor was able to reach equilibrium in ca. 2 minutes. Since sodium concentrations within extracellular media, such as whole blood and plasma are relatively high (clinical range ca. 135-150 mm) compared to other potential interfering cations such as potassium (clinical range ca. 3.5-5 mM), the selectivity burden for sodium ionophores is small and is required to be $\log K_{Na,K} = -0.6$.[90] In the selectivity studies completed in this work it was found that the optode has the required sodium/potassium ion selectivity ($\log K_{Na,K} = -0.6$) for sodium determinations in extracellular media.

V: Future Work

A: Ammonium Ionophore

The ammonium ionophore, **8**, when tested in an ion selective electrode (ISE) proved to be selective for ammonium ions over alkali and alkali earth metal ions. This observed behavior demonstrates that cyclic depsipeptides can be used as the basis for new ionophores. This is also illustrated by the cyclic depsipeptide valinomycin which is highly selective for potassium ions.

In designing **8** and in going forward with future ammonium ionophores based on depsipeptide structures it is important to recognize that the depsipeptide backbone structure will play an important role in the ionophore's selectivity.[100-102] For example, analogs of valinomycin, in which changes in the chirality of the valine residues were made, have been synthesized and they typically show drastic reductions in the ability to bind potassium.[100,101] Presumably, these chirality changes disrupt the hydrogen bonding network typically present in the parent valinomycin (see figure 2) resulting in molecules which contain only five N-H···O=C hydrogen bonds as compared to six for valinomycin. As a result the structures became asymmetric, poorly pre-organized and exhibit two orders of magnitude reduction in the binding constant for potassium ions in comparison to valinomycin.

In light of the above discussion, it is clear that systematic investigation into the effect of chiral substitution within **8** is warranted. Since **8** is modular in terms of its synthesis, simple replacement of the various residues will lead to a series of new compounds. In addition, the sequence of the alkyl substituents can be modified, leading to further understanding of the mechanism of complexation within **8**. For example, the L-lactic acid residue used to form compound **1** (see Scheme **1**) can be changed to either L or D Hydroxyisovaleric acid leading to two variations of **8** (see Figure 39 for compound **13** as an example using L-Hydroxyisovaleric acid). These compounds will be tested within ISE's and the selectivity for ammonium over other ions determined. The results of these selectivity studies will be compared to theoretical molecular modeling predictions of the various compounds.

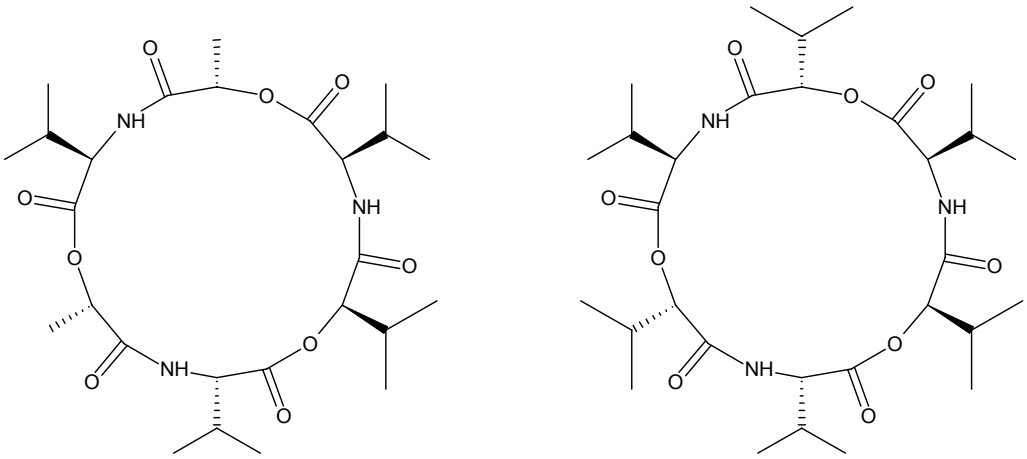

8 **13**

Figure 39: Compound **8** (left) and proposed derivative **13** (right)

B: Bicyclic Ammonium Ionophore

The selectivity displayed by **8** was achieved by designing the ionophore such that tetrahedral cations (ammonium ion) would be stabilized whereas cations requiring a spherical coordination geometry would not, e.g. sodium and potassium ions. However, it is desirable to have ammonium ionophores that can achieve far greater discrimination over potassium and sodium ions, than exhibited by **8**, for use in new measurement technologies. This is particularly important in the measurement of creatinine (Figure 40) in biological media where the normal physiological levels, 0.7 – 1.3 mM, are far below the concentration of potassium (3 – 5 mM) and sodium (135 – 150 mM).

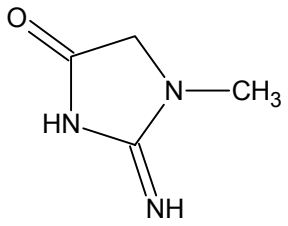

Figure 40: Creatinine

To date, the most commonly used ammonium ionophore is nonactin. Nonactin based ISE's have been modified to contain an enzyme layer over the polymeric membrane. These layers encapsulate enzymes which can convert metabolites, such as urea and creatinine, into ammonium and thus give a measure of the urea or creatinine concentration (1 mole of urea is converted to 2 moles of ammonium ion whereas 1 mole of creatinine is converted to 1 mole of ammonium cation). However, since nonactin

based ISE's are only ten times more selective for ammonium over potassium ion, a correction, which contributes error to the measurement, must be made to adjust for the interference by potassium. Thus more selective ammonium ionophores would eliminate the need for this correction and therefore enable a more precise measurement of the urea or creatinine concentration.

In order to accomplish the desired goal of more selective ammonium ionophores we first have had to develop a metric by which to judge if the resulting molecule would potentially be more selective or not. This work involved modeling several known ammonium ionophores in the complexed state with ammonium and potassium ion. These complexes were examined computationally and their docking energies (E_D) calculated. The energy of the ammonium complex minus the energy of the potassium complex (to give ΔE_D) was then compared to the experimentally derived selectivity coefficients for ammonium over potassium ions ($\log K_{NH_4^+,K^+}$). Specifically, we chose nonactin and the Lehn cryptands (Figures 6 and 7 and shown below in Table 5) since data for all these compounds were presented in one manuscript and their selectivity coefficients were determined under the same conditions.[18] This data is shown in Table 5.

Compound	$\log K_{NH_4^+,K^+}$	ΔE_D (Kcal/mole)
nonactin	0.20	-4.0
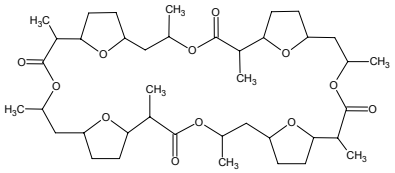		
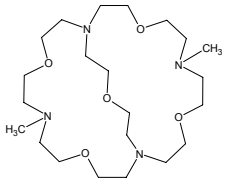	0.40	-12
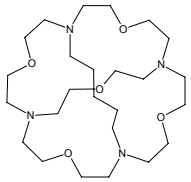	1.8	-18
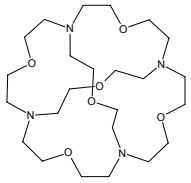	2.7	-20

Table 5: Selectivity data for various ammonium ionophores and ΔE_D of the ammonium/potassium ion complexes.

Table 5 shows the results of the modeling calculations for the various ammonium ionophores. The data suggests that a trend exists where larger (and more negative) differences between the energies of ammonium and potassium ion complexes are indicative of higher selectivity coefficients for ammonium over potassium ions. Indeed, molecular modeling has proved successful in reproducing experimental results for other ionophores such as valinomycin, nonactin and crown ethers, although it has been cautioned that such calculations should be taken as qualitative due to the approximations

involved.[19] However, it is proposed that these qualitative calculations can be prospectively used as a guide in the development of new ionophores.

Here we propose the design of new ammonium ionophores with a view to obtaining improved selectivity over potassium and sodium ions based on a bicyclic depsipeptide structure. Using the above modeling results as a guide, we have designed several ionophores which are predicted to be superior to **8** and potentially better than nonactin in terms of their ammonium/potassium ion selectivity. These compounds are based on the backbone of **8** and the bi- and tri-cyclic structures of Lehn's cryptands. Our previous work indicated that **8** discriminated against potassium but it was clear that it could be improved. We reasoned that if we could introduce an additional site for hydrogen bonding to an ammonium ion and yet make the site inaccessible to cations requiring octahedral or spherical binding geometry we would see an improvement in the selectivity. Ideally, if this site could also be introduced through a bridge, thus forming a bicyclic structure, we would obtain additional rigidity in the molecule and perhaps increase pre-organization thus potentially improving selectivity further. Keeping **8** as our base molecule we introduced a bridge that can be synthesized from readily available amino acids, i.e. lysine and glutamic acid giving compound **14** (Figure 41). In Figure 41, it is shown that the same sterochemistry is retained as in **8** and that a bridge has been added using a derivative of glutamic acid.

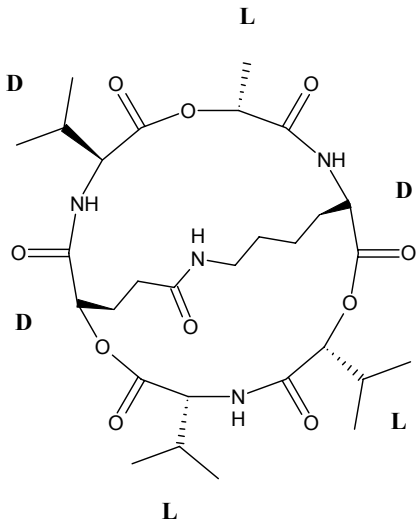

Figure 41: Proposed bicyclic depsipeptide **14**

Molecular modeling calculations were carried out on the ammonium and potassium complexes of **14** resulting in ΔE_D = -19 Kcal/mol and therefore is 15 Kcal/mol more negative than ammonium/potassium ion complexes of nonactin (see Table 5). If the data in Table 5 is predictive, we would expect that **14** would be one to two orders of magnitude more selective than nonactin for ammonium ion over potassium ion.

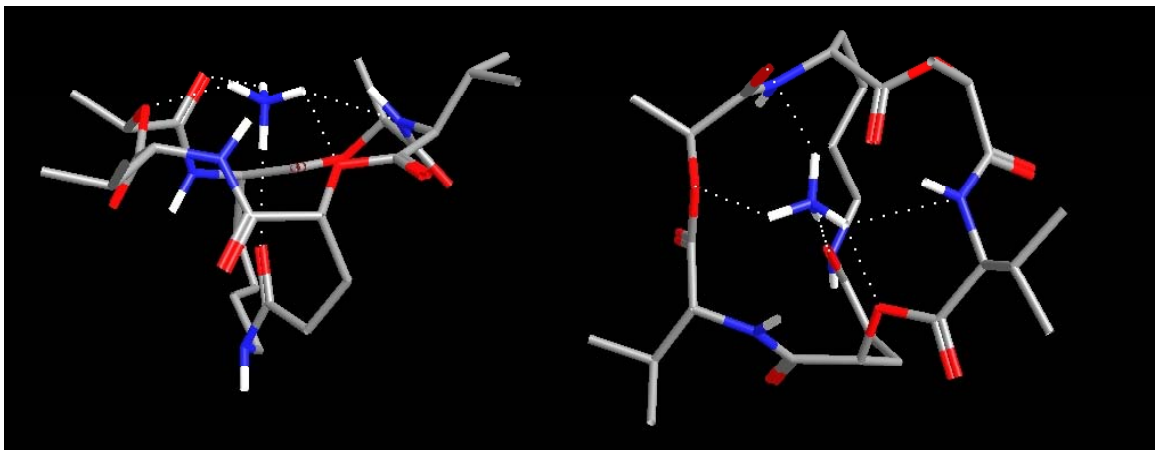

Figure 42: Modeling results for compound **14**

The synthesis of this molecule has begun in our laboratory but is long (20+ steps). The length of this synthesis is partly due to the many protection and de-protection steps that are required to build the structure. In light of this we have also investigated an all-amide version of **14**. This compound, **15** (Figure 43), can be synthesized directly by solid phase techniques and only 3 solution phase steps will be required.

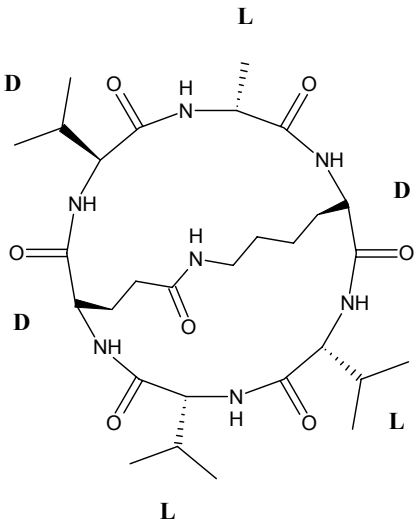

Figure 43: Proposed all amide bicyclic ammonium ionophore, **15**

Molecular modeling calculations on **15** indicated that this compound can potentially have better selectivity than nonactin (ca. one order of magnitude) but less so than **14**. Calculations show ΔE_D = -16 Kcal/mol making **15** an intermediate structure in our series. The synthesis of this molecule has also begun in our laboratory.

Upon completion of these molecules, they will be incorporated into ion selective electrodes in the same manner as **8** and the potentiometric properties investigated. The results of these tests will then be compared to the modeling data. These results will then

be used to fine-tune the molecular modeling calculations to improve upon any inconsistencies. This new model will then be verified on additional molecular structures eventually providing a platform with which the rational design of new ionophores can be accomplished.

C: Alternative Fluorophores

In this work we have presented the design, synthesis and testing of two fluoroionophores based on calix[4]arene-azacrown structures covalently linked to an anthracene fluorophore, **10** and **11**. These compounds employ the same fluorophore and therefore excitation of each can be accomplished with λ_{ex} = 355 nm. However, there are two limitations to using fluorophores that are excited at 355 nm. First, the instrumentation for which these molecules have been created uses LED's as excitation sources (for cost considerations) and at the present time there are no commercially available inexpensive LED's that emit below ca. 390 nm. Second, the samples measured with this instrument are whole blood, constituents of which absorb and emit in the 350 – 400 nm region. This will introduce interfering signals and reduce signal-to-noise. In order to overcome these issues a new fluorophore in place of anthracene will need to be used, preferably one which absorbs >450 nm light and yet still would provide for a negative ΔG_{PET}.

Here we propose the modification of our fluoroionophores, **10** and **11** with an alternative fluorophore that will satisfy the above requirements of long wavelength excitation (>400 nm) and negative $\Delta G_{PET.}$ Two fluorophores have been identified that will yield fluoroionophores with the desired characteristics that can overcome the limitations noted above. One of these compounds, **16** (Figure 44), is a chloromethyl derivative of 4,4-difluoro-4-bora-3a,4a-diaza-*s*-indacene and can be purchased from Molecular Probes.

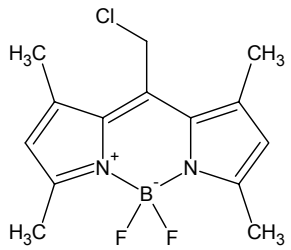

Figure 44: Proposed replacement fluorophore, **16**, for anthracene

This compound has $\lambda_{ex/em}$ ~503/513 nm,[93,103] and therefore can be excited by commercially available LED's. Also, excitation in the 500 nm region would substantially reduce any background fluorescence from whole blood samples and therefore will improve the reliability of analyte measurements. In addition to the longer wavelength excitation, the molecule has been coupled to a simple azacrown forming a fluoroionophore and shown to operate through the PET mechanism.[104] Compound **16**, is also an appropriate choice since it is available as a chloromethyl derivative and thus can directly replace the 9-chloromethyl-anthracene in the synthetic strategies of **10** and **11**.

The other potential chromophore is tetramethylrosamine, **17** (Figure 45), which has $\lambda_{ex/em}$ = 550/574 nm[93] and again can be excited by commercially available LED's, beyond the region where whole blood absorbs. In addition, it is reasonable to expect that the reduction potential will be within the same range (ca. –0.54 eV) as the rhodamine fluorophore that we described in our sodium optode work , and therefore will also be expected to participate in a PET type mechanism.

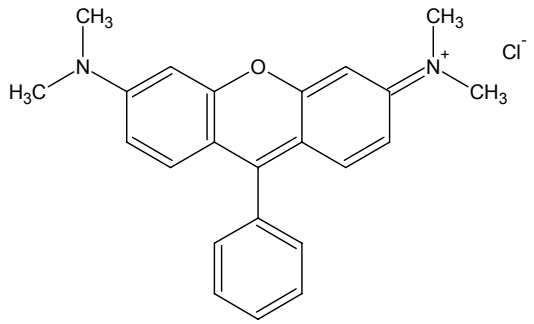

Figure 45: Proposed replacement fluorophore, **17**, for anthracene

One literature reference presents a synthetic route to a haloalkyl derivative (i.e. chloromethyl) that will allow a direct replacement of the 9-chloromethyl-anthracene in the synthetic strategies of **10** and **11**.[105] This method was modified to give a bromomethyl version, **22**, and is shown in Figure 46. The synthetic strategy is shown in Scheme 4 and the synthesis of this compound has been briefly explored (see Appendix A4 for details).

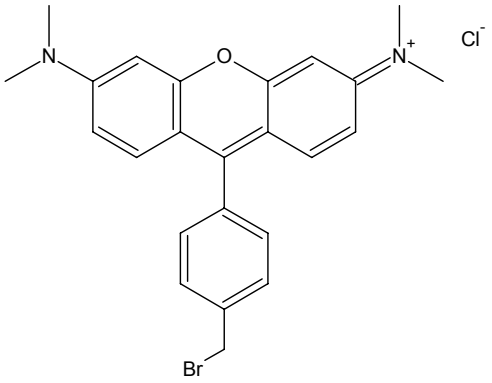

Figure 46: Bromomethyl derivative, **22**, of **17**

Scheme 4:

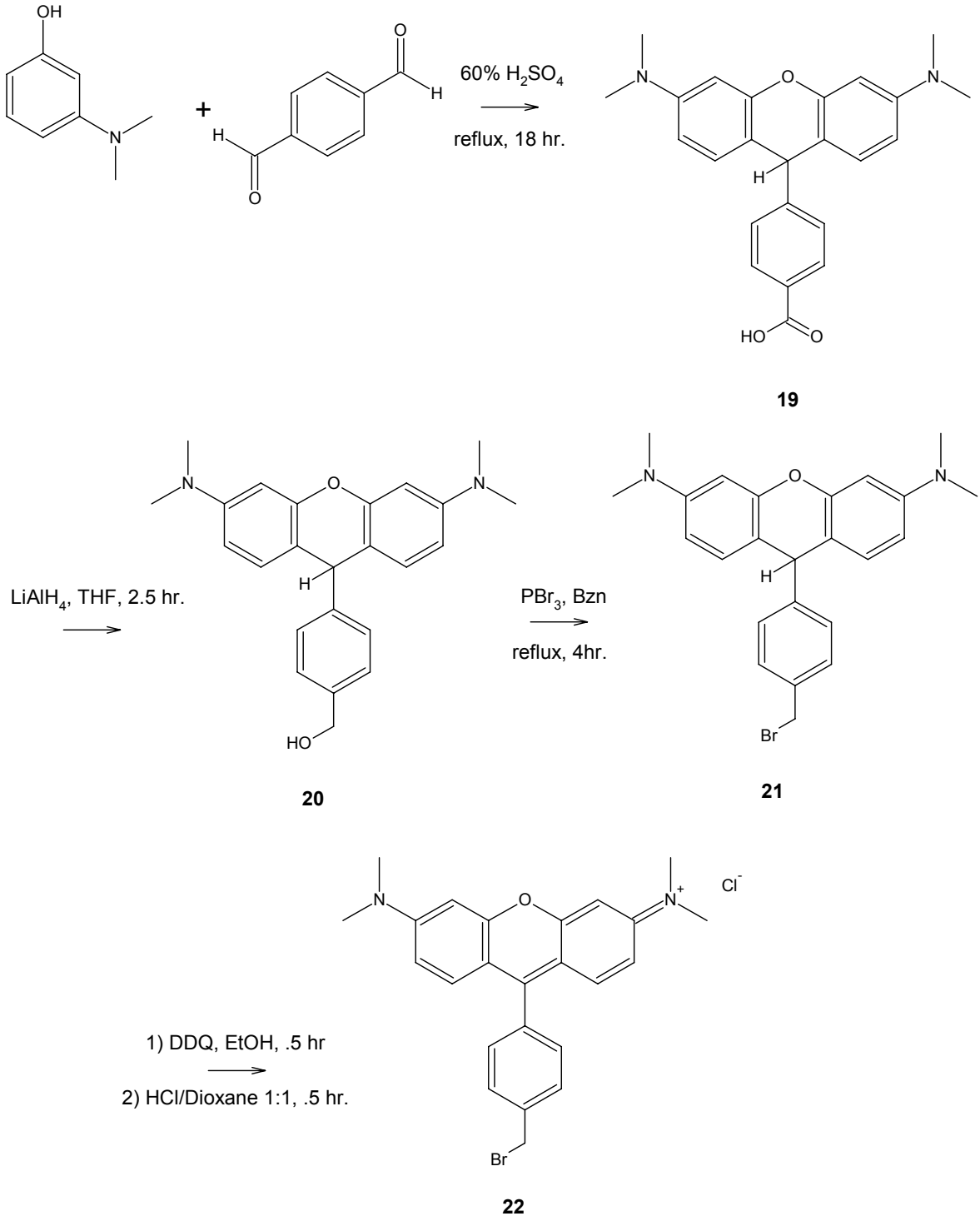

In general, the synthesis of these compounds was not straightforward. In particular it was found that each intermediate was not stable under ambient light conditions since it was

observed that the products, beginning as slightly pink to white in color, turned to deep red and purple while exposed to ambient light. In addition it was found that on TLC plates this reaction appeared to proceed at an even more rapid rate, turning bright pink immediately after exposure to the UV light source. The intermediate products, **19-21**, are not fully conjugated while the final product, **22**, is and has been reported to be bright red in color compared to the slight pink/white color of **19-21**. Given this color difference and the observations noted above, it was speculated that **19-21** were photo-oxidizing to a fully conjugated system. Thus, after initial attempts all reactions were carried out in the dark. It was also found that the intermediates photo-oxidized on silica gel during column chromatography and adhered to the silica causing the products to bleed off the column. However, even with these problems reasonable amounts (gram quantities) of the intermediates could be obtained except for **21** for which a 16% yield was achieved after chromatography on silica gel. This low yield was due to the fact that the product adhered to the silica gel. However by TLC, the reaction appeared to be nearly quantitative. Modification of the purification procedures is likely to improve on these initial attempts.

D: Ammonium Fluoroionophore

The analysis of ammonium cations in aqueous or biological media has traditionally been accomplished through the use of ISE's. In contrast, sensors that operate on optical detection schemes are few and rely on indirect methods of signal transduction. Essentially all schemes are tied to a pH sensitive chromophore that is either protonated or deprotonated by the presence of ammonium cations through the cation exchange mechanism. Thus, in all cases the response of the sensors are also dependent upon the sample pH which in turn necessitates the control of this parameter. This limits the utility and practicality of the proposed optodes. More recently, optical sensors based upon neutral ionophores, i.e. nonactin coupled with pH sensitive fluorophores have been developed.[106-108] Upon exposure to ammonium cations the nonactin ion selective membrane binds the cations while the pH sensitive fluorophore deprotonates, thus maintaining electrical neutrality (Figure 32). Deprotonation of the dye induces a change in the spectroscopic properties of the fluorophore which is proportional to the ammonium cation concentration and is typical of cation exchange mechanisms.

Based on our above work, we propose to design, synthesize and test an ammonium fluoroionophore that directly binds ammonium ions and that is pH independent. In our previous work, we reported on the design and synthesis of a new ammonium ionophore and its application in a planar ion selective electrode (ISE). This ionophore was based upon a cyclo-depsipeptide structure, a structure that lends itself to facile synthetic

modification and seemed an appropriate starting point for developing a new ammonium fluoroionophore. Based upon our success with this ionophore and our previously reported work with fluoroionophores it was reasonable to conclude that with an appropriate modification to the parent cyclo depsipeptide backbone, covalent linkage of a fluorophore will yield the desired target. In particular, the backbone can be modified such that a carboxylic acid moiety will be available as an attachment site. Given the work with our calix[4]arene aminorhodamine fluoroionophore, **12**, where the fluorophore linkage was through an amide, we concluded that aminorhodamine B will be a good choice for attachment to the modified depsipeptide, particularly since thermodynamic calculations indicate that the rhodamine fluorophore attached through an amide linkage will operate via the PET mechanism ($\Delta G_{pet} = 0.13V$). The rhodamine fluorophore is also appropriate since it is known to be pH insensitive and thus will yield, when coupled to the depsipeptide, the first pH independent fluoroionophore that directly responds to the ammonium cation. To this end, we have investigated the feasibility of our proposal beginning with the synthesis (Schemes 5-7) of the modified cyclo depsipeptide structure (**28**). We have also attempted covalent attachment of aminorhodamine B (see Appendix A5 for details).

Scheme 5

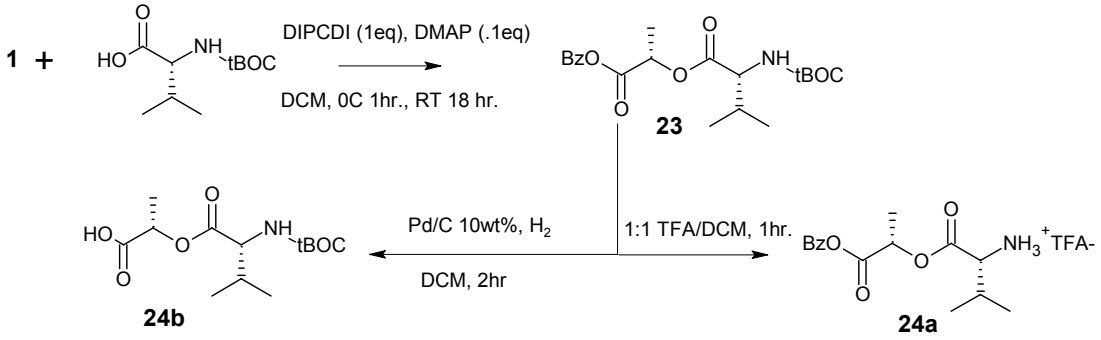

Scheme 6

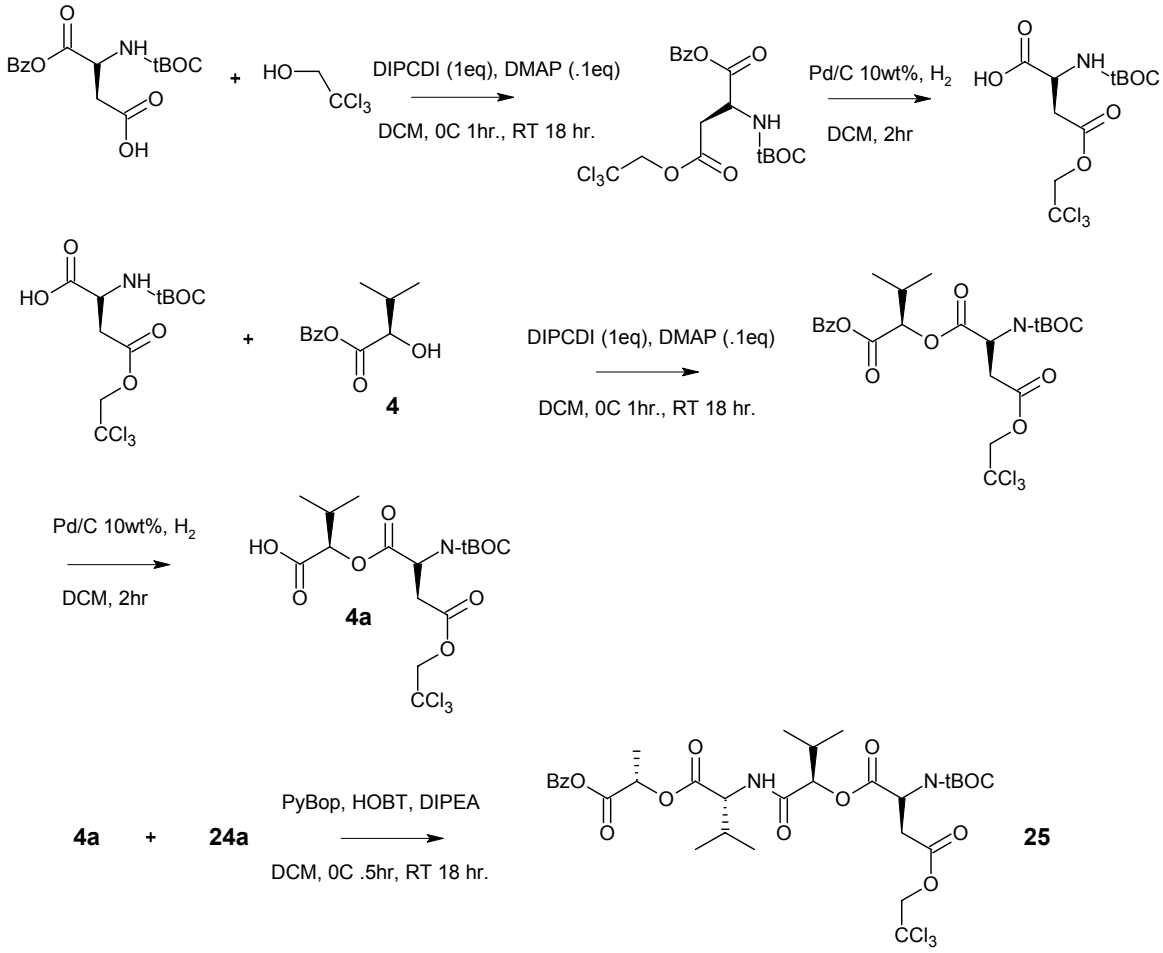

Scheme 7

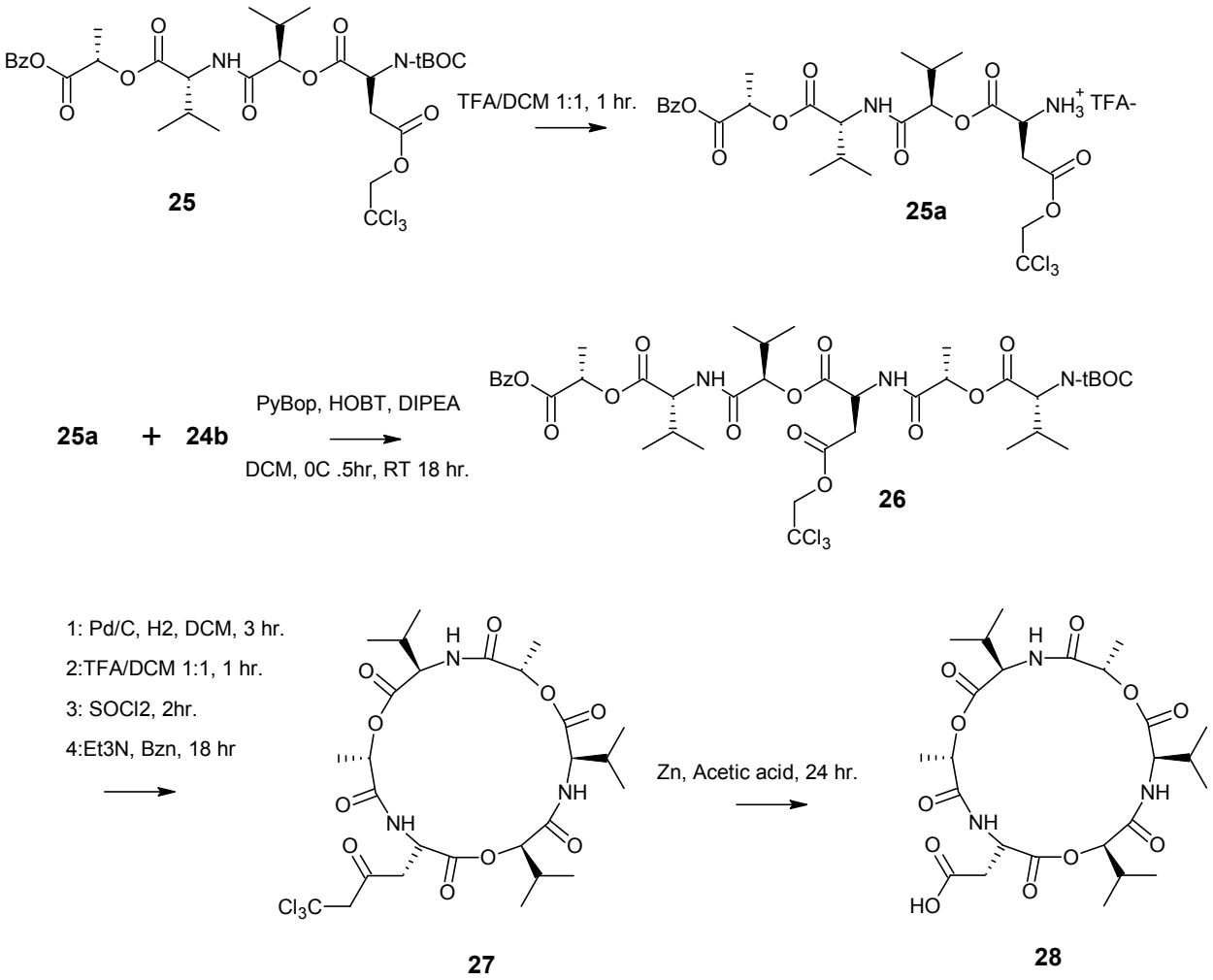

The synthesis of compound **28** was reasonably straightforward, yielding 445 mg of product. The final step was the attachment of a fluorophore to give the fluoroionophore. The first attempts at coupling a fluorophore were with aminorhodamine B, the same fluorophore used for compound **12**. Three standard coupling strategies were used; conversion of **28** to an acid chloride and coupling under basic conditions (Et_3N); the

carbodiimide method as used for **23**, and standard peptide coupling strategy as used for **25**. However, TLC and Mass Spectral analysis showed that no product was formed.

One assumption is that steric interference was to blame for the lack of product formation. Therefore, we synthesized a derivative (**29,** Figure 47) of **28** that involved replacement of the aspartic acid residue in the formation of **25** with a glutamic acid residue yielding a monocyclic depsipeptide with a $-R(CH)_2COOH$ attachment site as compared to a $-RCH_2COOH$ site in **28**.

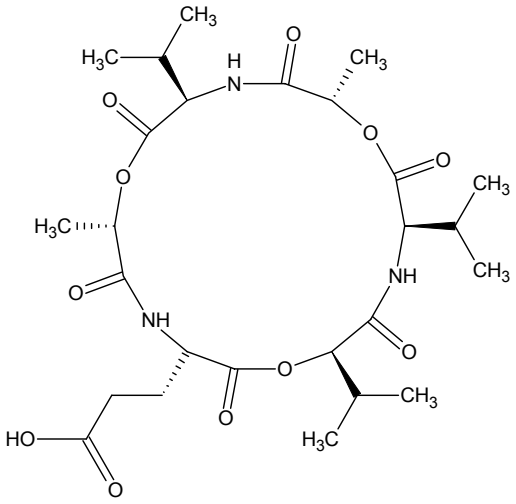

Figure 47: Glutamic acid derivative **(29)** of **28**

This change was made assuming that the additional methylenic linkage would reduce any steric interference. However attempts to couple the fluorophore using the same procedures for **28** again yielded no product. This, in combination with the above result, suggested that the fluorophore, aminorhodamine B, was the reason for the lack of product formation.

To confirm if the aminorhodamine B fluorophore was the issue we chose to investigate a different fluorophore, a 7-nitrobenzofurazan which is commercially available as an N-methyl-4-hydrazino-7-nitrobenzofurazan (Figure 48). This fluorophore has also been shown to operate on a PET mechanism.[109-112]

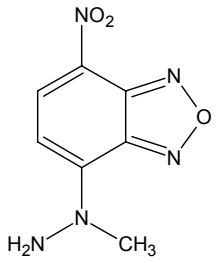

Figure 48: N-methyl-4-hydrazino-7-nitrobenzofurazan

Covalent linkage through the primary amine and the free carboxylic acid group on the cyclic depsipeptide would yield the desired product. Again, attempts to couple this fluorophore to both **28** and **29** using either the carbodiimide or peptide coupling strategy failed. However, using an acid chloride intermediate and coupling under basic conditions (Et_3N) we obtained some detectable product (via Mass Spectral analysis) from both cyclic depsipeptides **28** and **29**, although the recovered amounts were small and impure, ca. 2 mg each (5% yield) and ca. 50% pure. This result is inconclusive, due to the low yield of product, and does not provide any significant insight into the reasons for the lack of product formation.

It is clear from these results that additional investigation into the coupling of a fluorophore to either **28** or **29** is warranted. Specifically, coupling of fluorophores to

model compounds, such as fully protected aspartic and glutamic acid residues may prove beneficial in the elucidation of these reaction mechanisms.

E: Sodium Fluoroionophore II

We, as well as others, have shown that the modification of the ring size in azacrown calixarenes is effective in controlling the selectivity of these ligands. In particular, Dabestani et al. has shown that calix[4]arene-azacrown-6 structures are selective for cesium[63-66] while here we have shown that calix[4]arene-azacrown-5 and -azacrown-3 systems are selective for potassium and lithium ions, respectively.

By extrapolation, we propose that an calix[4]arene-azacrown-4 covalently linked to a anthracene fluorophore will possess high sodium selectivity over other alkali metal ions and offer a new and highly selective fluoroionophore for sodium. Indeed, calix[4]arene-crown-4 structures are known and have been shown to possess some of the highest sodium/potassium selectivities known, ($\log K^{POT}_{Na,K} = -5.0$).[11c,113,114]

This new fluoroionophore should have both higher selectivity and sensitivity for sodium than compound **12** (see above). Specifically, as already noted, selectivity will be improved due to a rigid binding site of appropriate size as well as sensitivity because the PET mechanism is more favorable thermodynamically (ΔG_{PET} -0.41V based on **10** vs. -0.13V for **12**). Thus, have we proposed the synthesis and testing of **34** (Figure 49 and Scheme 8).

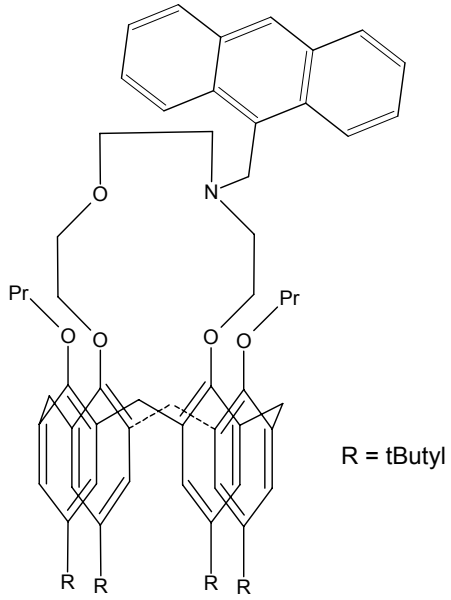

Figure 49: Proposed sodium fluoroionophore **34**

Scheme 8

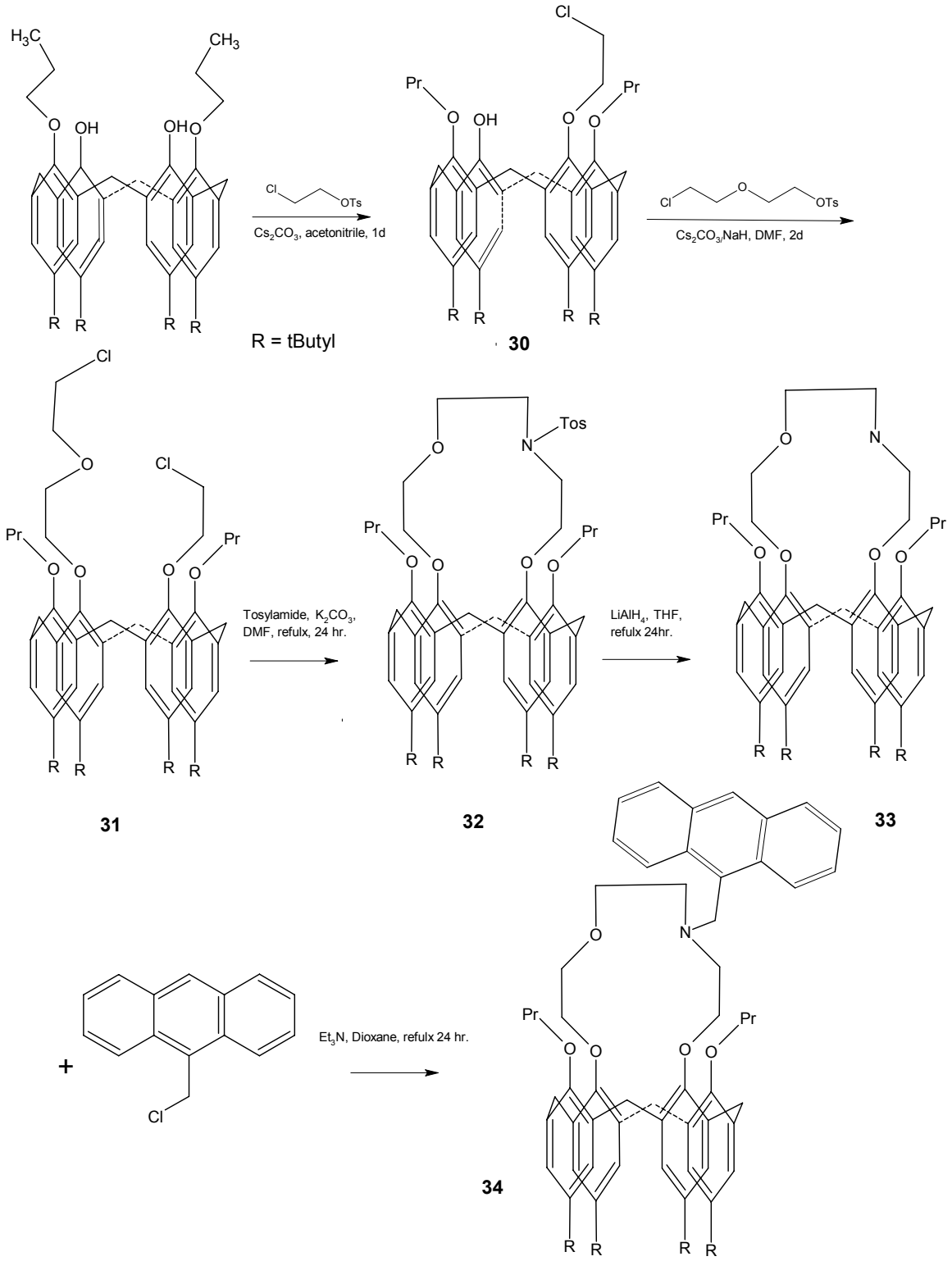
H3C
CH3
O
OH
OH
O
R
R
R
R
Cl
OTs
Cs2CO3, acetonitrile, 1d
R = tButyl
Pr
Cl
Cl
OTs
Cs2CO3/NaH, DMF, 2d
30
Tosylamide, K2CO3, DMF, refulx, 24 hr.
Tos
N
LiAlH4, THF, refulx 24hr.
31
32
33
+
Et3N, Dioxane, refulx 24 hr.
34

The synthesis of this compound has been explored in our lab, but with mixed results. We expected that the structure of the calix[4]arene system would yield the 1,3-alternate conformer after the initial alkylation to **30** and **31** based on our previous results with **12**, the lithium fluoroionophore discussed above. However, we found that we obtained a mixture, presumably of 1,3 alternate and partial cone conformers which were not separable. Since it is known that the different conformers of calix[4]arene crowns give a range of selectivities we speculate that the same will be true for our fluoroionophore as well. This introduces significant uncertainty in experimental results that will be obtained from a mixture of conformers. In addition, quantification of the relative ratio of conformers is likely to be problematic since the NMR signals overlap to a great extent.

To overcome these issues we propose a new sodium fluoroionophore (**40**) that would be based on a diisopropyl-4-*p*-*tert*-butylcalix[4]arene (or di-tert-butyl-) rather than the dipropyl-*p*-*tert*-butyl-calix[4]arene of **34**. It has been found that rotation about the aryl rings is suppressed by bulky substituents leading to the cone conformation in high yields.[115] Thus, we suggest that diisopropyl-4-*p*-*tert*-butylcalix[4]arene, **35**, will ensure that alkylation to **36** and **37** will result in the cone conformer rather than a mixture of partial-cone and 1,3-alternate as obtained with **34**. The proposed synthetic pathway is shown in Scheme 9.

Scheme 9

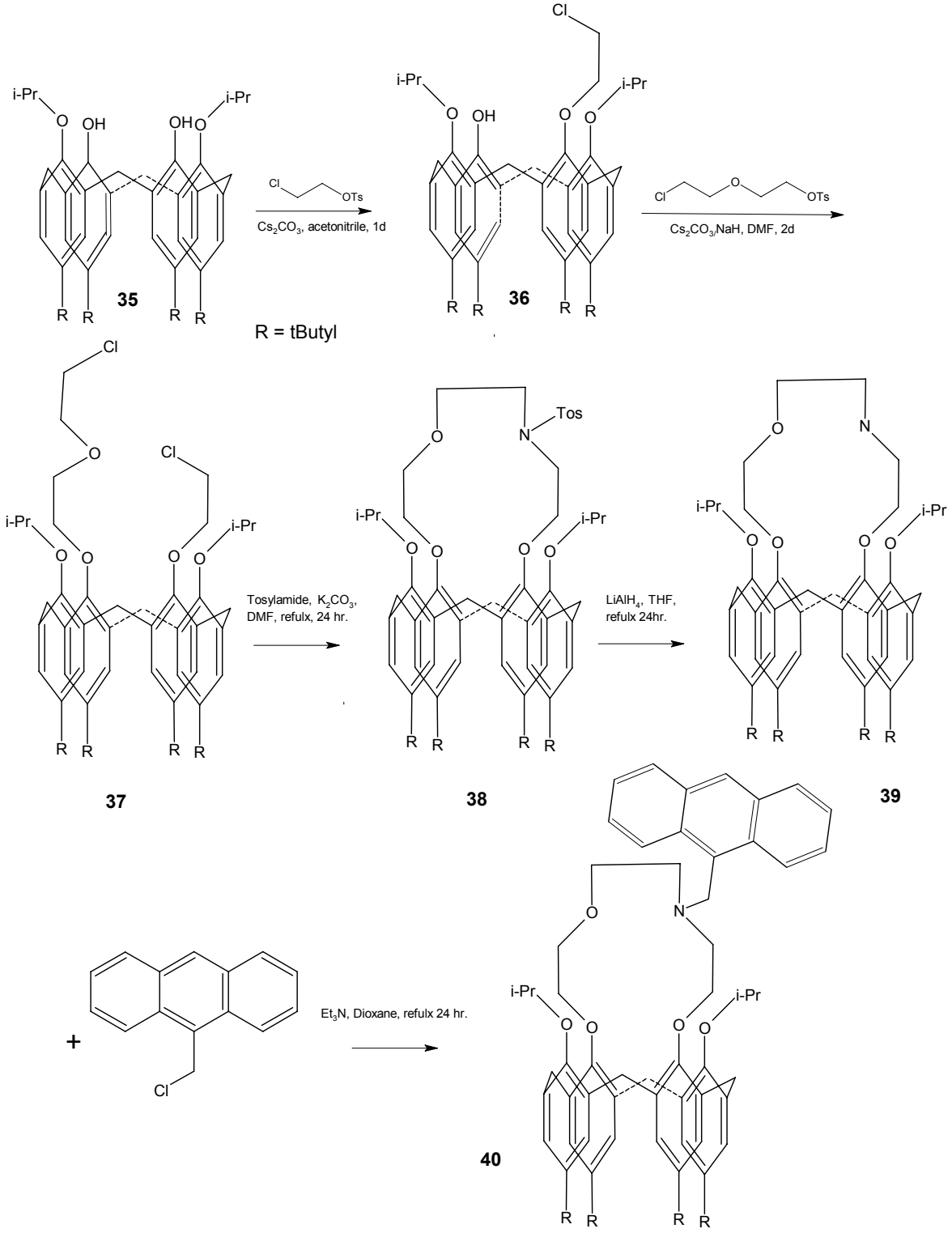
i-Pr
O
OH
OH
O
i-Pr
R R R R
35
Cl
OTs
Cs_2CO_3, acetonitrile, 1d
Cl
i-Pr
O
OH
O
O
i-Pr
R R R R
36
Cl
O
OTs
Cs_2CO_3/NaH, DMF, 2d
R = tButyl
Cl
O
Cl
i-Pr
O
O
O
O
i-Pr
R R R R
37
Tosylamide, K_2CO_3, DMF, refulx, 24 hr.
Tos
N
O
i-Pr
O
O
O
O
i-Pr
R R R R
38
$LiAlH_4$, THF, refulx 24hr.
O
N
i-Pr
O
O
O
O
i-Pr
R R R R
39
+
Cl
Et_3N, Dioxane, refulx 24 hr.
O
N
i-Pr
O
O
O
O
i-Pr
R R R R
40

References

1) Leadbeater, N. E., Marco, M. *Chem. Rev.* **2002,** *102,* 3217-3274.

2) Haupt, K., Mosbach, K. *Chem. Rev.* **2000,** *100,* 2495-2504.

3) Faul, M. M., Huff, B. R. *Chem. Rev.* **2000,** *100,* 2407-2473.

4) McQuade, D. T., Pullen, A. E., Swager, T. M. *Chem. Rev.* **2000,** *100,* 2537-2574.

5) Valeur, B., Leray, I. *Coord. Chem. Rev.* **2000,** *205, 3-40.*

6) Alexander, V. *Chem. Rev.* **1995,** *95,* 273-342.

7) Danil de Namor, A.F., Cleverley, R.M., Zapata-Ormachea, M. L. *Chem. Rev.* **1998,** *98,* 2495-2525.

8) Babine, R.E., Bender, S. L. *Chem. Rev.* **1997,** *97,* 1359-1472.

9) Hancock, R. D., Martell, A. E. *Chem. Rev.* **1989**, *89,* 1875-1914.

10) Bradshaw, J. S., Izatt, R. M., Bordunov, A. V., Zhu, C. Y., Hathaway, J. K. *Comprehensive Supramolecular Chemistry*; Lehn, J. M. et al. Ed.; Pergammon: New York, 1996, Vol. 1, 35-95.

11) (a) Calixarenes, C. D. Gutsche, The Royal Society of Chemistry; Cambridge, 1989; (b) de Namor, A.F.D., Cleverley, R.M., Zapata-Ormachea, M.L. *Chem. Rev.* **1998,** *98,* 2495-2525.; (c) Bühlmann, P., Pretsch, E. Bakker, E. *Chem. Rev.* **1998**, *98,* 1593-1687.

12) Sakai, T., Harada, T., Deng, G., Kawabata, H., Kawahara, Y., Shinka, S. *J. Inclusion Phenom. Mol. Recognit. Chem.* **1992**, *14,* 285.

13) Diamond, D., Svehla, G., Seward, E.M., McKervey, M.A. *Anal. Chim. Acta* **1988,** *204* 223-231.

14) Casnati, A., Pochini, A., Ungaro, R., Bocchi, C., Ugozzoli, F., Egberink, R.J.M., Struijk, H., Lugtenberg, R., de Jong, F., Reinhoudt, D.N. *Chem. Eur. J.* **1996,** *2,* 436-445.

15) Pullman, A. *Chem. Rev.* **1991,** *91,* 793-812.

16) Brown, S.S, Mitchell, F.L., Young, D.S., Eds.; *Chemical Diagnosis of Disease*; Elsevier/North-Holland Biomedical Press: 1979.

17) Pranitis, D.M.; Meyerhoff, M.E. *Anal. Chem.* **1987,** *59,* 2345-2350.

18) Graf, E.; Kintzinger, J.P.; Lehn, J.M.; LeMoigne, J. *J. Am. Chem. Soc.* **1982,** *104,* 1672-1678.

19) Bakker, E.; Buhlmann, P.; Pretsch, E. *Chem. Rev.* **1997,** *97,* 3083-3132.

20) De Silva, A. P., Gunaratne, H.Q.N., Gunnlaugsson, T., Huxley, A.J.M., McCoy, C.P., Rademacher, J.T., Rice, T.E. *Chem. Rev.* **1997,** *97*, 1515-1566.

21) (a)A. P. de Silva and S. A de Silva, *J. Chem. Soc. Chem. Commun*. **1986**, 1709-1710. (b) Kawai,H., Nagamura, T., Mori, T., Yoshida, K. *J. Phys. Chem.* **1999,** *103,* 660-664. (c) Murov, S. L., Carmichael, I., Hug, G.L. *Handbook of Photochemistry 2nd ed*.; Marcel Dekker Inc. New York, 1991.

22) de Silva, A.P., Sandanayake, K.R.A.S. *J. Chem. Soc., Chem. Commun.* **1989,** 1183-1184.

23) Ji, H., Dabestani, R., Brown, G. M., Hettich, R. L. *Photochem. Photobiol*. **1999,** *69,* 513-516.

24) Ji, H., Dabestani, R., Brown, G. M., Hettich, R. L. *J. Chem. Soc., Perkin Trans. 2,* **2001,** 585-591.

25) Brown, S.S, Mitchell, F.L., Young, D.S., Eds. *Chemical Diagnosis of Disease;* Elsevier/North-Holland Biomedical Press: 1979.

26) Hall, E.A.H. *Biosensors;* Open University Press: Buckingham, U.K., 1990: Chapter 9.

27) Alegret, S.; Bartoli, J.; Jimenez, C.; Martinez-Fabregas, E.; Martorell, D.; Valdes-Perezgasga, F. *Sens. Actuators B* **1993,***16*, 453-457.

28) Pranitis, D.M.; Meyerhoff, M.E. *Anal. Chem.* **1987,** *59,* 2345-2350.

29) Liu, D.; Meyerhoff, M.E.; Goldberg, H.D.; Brown, R.B. *Anal. Chim. Acta* **1993,** *274,* 37-46.

30) Borchardt, M.; Dumschat, C.; Cammann, K. *Sens. Actuators B* **1995,** *25,* 721-723.

31) Yasuda, K.; Miyagi, H.; Hamada, Y.; Takata, Y. *Analyst* **1984,** *109,* 61-64.

32) Shin, J. H.; Yoon, S.Y.; Yoon, I.J.; Choi, S.H.,; Lee, S.D.; Nam, H.; Cha, G.S. *Sens. Actuators B* **1998,** *50,* 19-26.

33) Stamm, C.; Seiler, K.; Simon, W. *Anal. Chim. Acta* **1993,** *282,* 229-237.

34) Buhlmann, P.; Pretsch, E.; Bakker, E. *Chem. Rev.* **1998,** *98,* 1593-1687.

35) Chin, J.; Walsdorff, C.; Stranix, B.; Oh, J.; Chung, H.J.; Park, S.M.; Kim, K. *Angew. Chem. Int. Ed.* **1999,** *38,* 2756-2759.

36) Kim, H.S.; Park, H.J.; Oh, H.J.; Koh, Y.K.; Choi, J.H.; Lee, D.H.; Cha, G.S.; Nam, H. *Anal. Chem.* **2000,** *72*, 4683-4688.

37) Suzuki, K.; Siswanta, D.; Otsuka, T.; Amano, T.; Ikeda, T.; Hisamoto, H.; Yoshihara, R.; Ohba, S. *Anal. Chem.* **2000,** *72,* 2200-2205.

38) Kubik, S.; Goddard, R. *J. Org. Chem.* **1999,** *64,* 9475-9486.

39) Ghadiri, M.R.; Granja, J.R.; Milligan, R.A.; McRee, D.E.; Khazanovich, N. *Nature* **1993,** *366,* 324-327.

40) Granja, J.R.; Ghadiri, M.R. *J. Am. Chem. Soc.* **1994,** *116,* 10785-10786.

41) Hartgerink, J. D.; Granja, J.R.; Milligan, R.A.; Ghadiri, M.R. *J. Am. Chem. Soc.* **1996,** *118,* 43-50.

42) Isin, B.F.; Merrifield, R.B.; Tosteson, D.C. *J. Am. Chem. Soc.* **1969,** *91,* 2691-2695.

43) Pullman, A. *Chem. Rev.* **1991,** *91,* 793-812.

44) Gallo, E.A.; Gellman, S.H. *J. Am. Soc.* **1993,** *115,* 9774-9788.

45) Kogan, T.P.; Somers, T.C.; Venuti, M.C. *Tetrahedro,* **1990,** *46,* 6622-6632.

46) Dinh, T.Q.; Du, X.; Armstrong, R.W. *J. Org. Chem.* **1996,** *61,* 6606-6616.

47) Benco, J.S.; Foos, J. US Patent No. 5554272, **1996**.

48) Chan, A.D.C. US Patent No. 5804049, **1998**.

49) Chan, A.D.C. US Patent No. 5911862, **1999**.

50) Bakker, E.; Buhlmann, P.; Pretsch, E. *Chem. Rev.* **1997,** *97,* 3083-3132.

51) Buck, R.P.; Lindner, E. *Pure & Appl. Chem.* **1994,** *66,* 2527-2536.

52) Cadogan, A.; Gao, Z,; Lewenstam, A.; Ivaska, A. *Anal. Chem.* **1992,** *64,* 2496-2501.

53) Tinkilie, N.; Cubuk, O.; Isildak, I. *Anal. Chim. Acta* **2002,** *452,* 29-34.

54) Zaloga, G.P.; Hill, T.R.; Strickland, R.A.; Kennedy, D.; Visser, M.; Ford, K.; Whitley, J.; Holt, G.; Booker, C. *Crit. Care Med.* **1989,** *17,* 920-925.

55) D,Orazio, P.A.; Maley, T.C.; McCaffrey, R.R.; Chan, A.D.C; Orvedahl, D.; Foos, J.; Degnan, S.; Benco, J.; Boden, M.; Murphy, C.; Edelman, P.G.; Ludi, H. *Clin. Chem.* **1997,** *43,* 1804-1805.

56) Berrocal, M.J., Cruz, A., Badr, I.H.A., Bachas, L. *Anal. Chem.* **2000,** *72,* 5295-5299.

57) Dobler, M. *Ionophores and their Structures;* Wiley-Interscince: New York, 1981.

58) Schaller, U.; Bakker, E.; Spichiger, U.E.; Pretsch, E. *Anal. Chem.* **1994,** *66,* 391-398.

59) Rosatzin, T.; Bakker, E.; Suzuki, K.; Simon, W. *Anal. Chim. Acta* **1993,** *280,* 197-208.

60) Armstrong, R.D.; Todd, M. *J. Electroanal. Chem.* **1987,** *237,* 181-185.

61) Armstrong, R.D.; Todd, M. *J. Electroanal. Chem.* **1988,** *257,* 161-166.

62) Casnati, A., Pochini, A., Ungaro, R., Ugozzoli, F., Arnaud, F., Fanni, S., Schwing, M.-J., Egberink, R. J. M., de Jong, F., Reinhoudt, D. N. *J. Am. Chem. Soc.* **1995,** *117,* 2767-2777.

63) Ji, H.-F., Brown, G. M., Dabestani, R. *Chem. Commun.* **1999**, 609-610.

64) Ji, H.-F., Dabestani, R., Brown, G. M., Sachleben, R. A. *Chem. Commun.* **2000**, 833-834.

65) Ji, H.-F., Dabestani, R., Hettich, R. L., Brown, G. M. *Photochem. Photobiol.* **1999**, *70,* 882-886.

66) Ji, H.-F., Dabestani, R., Brown, G. M. *J. Am. Chem. Soc.* **2000**, *122*, 9306-9307.

67) Kim, J. S., Lee, W. K., No, K., Asfari, Z. Vicens, J. *Tet. Lett.* **2000**, *41*, 3345-3348.

68) Kim, J. S., Shon, O. J., J. Ko, W., Cho, M. H., Yu, I. Y., Vicens, J. *J. Org. Chem.* **2000**, *65,* 2386-2392.

69) Kim, J. S., Shon, O. J., Sim, W., Kim, S. K., Cho, M. H., Kim, J.-G., Suh, I.H., Kim, D. W. *J. Chem. Soc. Perkin Trans 1* **2001**, 31-36.

70) Kubo, K., Ishige, R., Kato, N., Yamamoto, E., Sakurai, T. *Heterocycles* **1997**, *45,* 2365-2379.

71) Yoshida, K., Mori, T., Watanabe, S., Kawai, H., Nagamura, T. *J. Chem. Soc. Perkin Trans. 2* **1999**, 393-398.

72) Kim, J.S., Yu, I. Y., Pang, J. H., Kim, J. K., Lee, K. W., Oh, W. Z. *Microchem. J.* **1998**, *58,* 225-235.

73) S. L. Murov, I. Carmichael, G.L. Hug; *Handbook of Photochemistry 2nd ed.*; Marcel Dekker Inc. New York, 1991.

74) *Organikum,(Autorencollectiv)*; 16. Auflage; VEB Deutscher Verlag der Wissenschaften Berlin, 1986, 559.

75) Quici, S., Manfredi, A. Buttafava, M. *J. Org. Chem.* **1996**, *61,* 3870-3873.

76) Kubik, S., Goddard, R. *J. Org. Chem.* **1999,** *64,* 9475-9486.

77) Ma, J.C., Dougherty, D.A. *Chem. Rev.* **1997**, *97,* 1303-1324.

78) Dijkstra, P.J., Brunink, J.A., , Bugge, K.E., Reinhoudt, D.N., Harkema, S., Ungaro, R., Ugozzoli, F., Ghidini, E. *J. Am. Chem. Soc.* **1989,** *111,* 7567-7575.

79) Ghidini, E., Ugozzoli, F., Ungaro, R., Harkema, S., El-Fadl, A.A., Reinhoudt, D.N. *J. Am. Chem. Soc.* **1990,** *112,* 6979-6985.

80) Nijenhuis, W.F., Buitenhuis, E.G., de Jong, F., Sudholter, E.J.R., Reinhoudt, D.N. *J. Am. Chem. Soc.* **1991,** *113,* 7963-7968.

81) Brzozka, Z., Lammerink, B., Reinhoudt, D.N., Ghidini, E., Ungaro, R. *J. Chem. Soc. Perkin Trnas. 2* **1993,** *2,* 1037.

82) Danil de Namor, A.F., Cleverley, R.M., Zapata-Ormachea, M. L. *Chem. Rev.* **1998,** *98,* 2495-2525.

83) Oesch, U. Ammann, D, Simon, W. *Clin. Chem.* **1986,** *32,* 1448-1459.

84) Olsher, U. *J. Am. Chem. Soc.* **1982,** *104,* 4006-4007.

85) Kitazawa, S., Kimura, K, Yano, H., Shono, T. *J. Am. Chem. Soc.* **1984,** *106,* 6978-6983.

86) Christian, G.D., Xie, R.Y., Wen, X. *Anal. Chem.* **1988,** *60,* 2561-2564.

87) Suzuki, K., Yamada, H., Sato, K., Watanabe, K., Hisamoto, H., Tobe, Y., Kobrio, K. *Anal. Chem.* **1993,** *65,* 3404-3410.

88) Watanabe, K., Nakagawa, E., Yamada, Hisamoto, H., Suzuki, K. *Anal. Chem.* **1993,** *65,* 2704-2710.

89) Arduini, A., Fabbi, M., Mantovani, M., Mirone, L., Pochini, A., Secchi, A., Ungaro, R. *J. Org. Chem.* **1995,** *60,* 1454-1457.

90) Yang, X., Wang, K., Xiao, D., Guo, C., Xu, Y. *Talanta* **2000,** *52,* 1033-1039.

91) Shortreed, M., Bakker, E., Kopelman, R. *Anal. Chem.* **1996,** *68,* 2656-2662.

92) Waldner, A., Barnard, S. M., Beckelmann, D., Reinhoudt, D., Berger, J. PCT WO9740014.

93) Haugland, R. P. *Handbook of Fluorescent Probes and Research Products,* 9th ed ; Molecular Probes: Eugene, OR, USA, p.53.

94) Arnaud-Neu, F., Collins, E.M., Deasy, M., Ferguson, G., Harris, S.J., Kaitner, B., Lough, A.J., McKervey, M.A., Marques, E., Ruhl, B.L., Schwing-Weill, M.J., Seward, E.M. *J.Am.Chem.Soc.* **1989,** *111,* 8681-8691.

95) Barrett, G., Bohmer, V., Ferguson, G., Gallagher, J.F., Harris, S.J., Leonard, R.G., McKervey, M.A., Owens, M., Tabatabai, M., Vierengel, A., Vogt, W. *J. Chem. Soc. Perkin Trans. 2* **1992,** 1595-1601.

96) O'Donnell, J. F., Mann, C. K. *J. Electroanal. Chem.* **1967,** *13,* 157-162.

97) Kotlyar, A. B., Borovok, N., Hazani, M. *Biochemistry* **1997,** *36,* 15823-15827.

98) Waldner, A., Beerli, R., Barnard, S. M. U.S. Patent 6,245,574.

99) Cadogan, A. M., Diamond, D., Smyth, M. R., Deasy, M., McKervey, A., Harris, S. J. *Analyst,* **1989,** *114,* 1551-1554.

100) Langs, D.A., Grochulski, P., Duax, W.L., Pletnev, V.Z., Ivanov, T. *Biopolmers* **1991,** *31,* 417-423.

101) Pletnev, V.Z., Mikhailova, I.Y., Ivanova, V.T., Langs, D.A., Grochulski, P., Duax, W.L. *Biopolymers* **1991,** *31,* 409-415.

102) Forester, T.R., Smith, W., Clarke, J.H.R. *J. Phys. Chem.* **1994,** *98,* 9422-9430.

103) Karolin, J., Johansson, L.B.A., Strandberg, L., Ny, T. *J. Am. Chem. Soc.* **1994,** *116,* 7801-7806.

104) Wolfbeis, O. S., Daub, J., Gareis, T., Kollmannsberger, M. U.S. patent 5,981,746; **1999.**

105) Haugland, R.P., Malekzadeh, M.N., Zhang, Y. U.S. patent 5,459,268; **1995.**

106) Seiler, K. Morf, W. E., Rusterholz, B., Simon, W. *Anal. Sci.* **1989,** *5,* 557-561.

107) Stamm, C., Seiler, K, Simon, W. *Anal. Chim. Acta.* **1993,** *282,* 229-237.

108) Wang, E., Zhu, L., Ma, L., Patel, H. *Anal. Chim. Acta.* **1997,** *357,* 85-90.

109) Street, K.W., Krause, S.A. *Anal. Lett.* **1986,** *19,* 735-745.

110) Resch, U., Rurack, K., Bricks, J.L., Slominski, J.L. *J. Fluor.* **1997,** *7,* 231s-233s.

111) Ramachandram, B., Samanta, A. *J. Phys. Chem. A* **1998,** *102,* 10579-10587.

112) Ramachandram, B., Samanta, A. *Chem. Phys. Lett.* **1998,** *290,* 9-16.

113) Yamamoto, H., Shinkai, S. *Chem. Lett.* **1994,** 1115-1118.

114) Yamamoto, H., Ueda, K., Sandanayake, K.R.A.S., Shinkai, S. *Chem. Lett.* **1995,** 497-498.

115) Iwamoto, K. Araki, K. Shinkai, S. *J. Org. Chem.* **1991,** *56,* 4955-4962.

Appendix

Appendix A1:
NMR and Mass Spectroscopy data for compound **8**

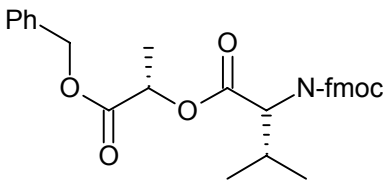

BzlO-L-lac-D-val-N-fmoc (2)

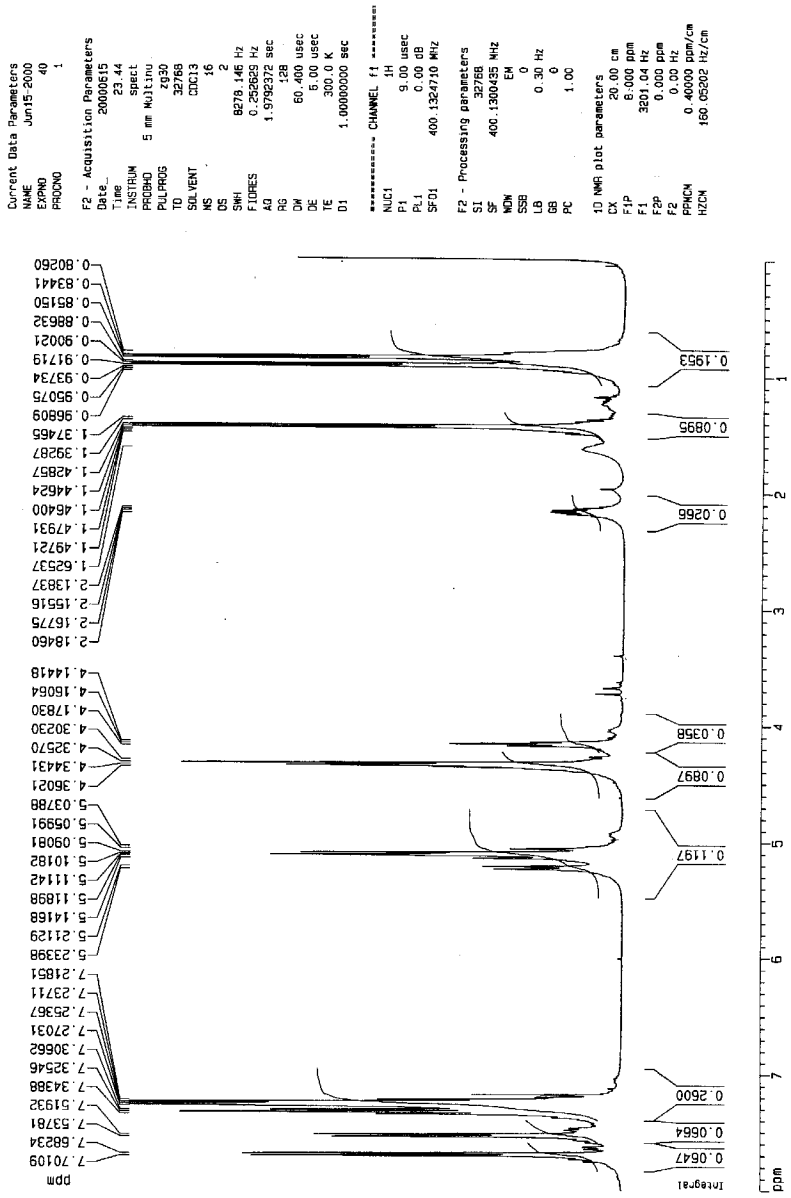

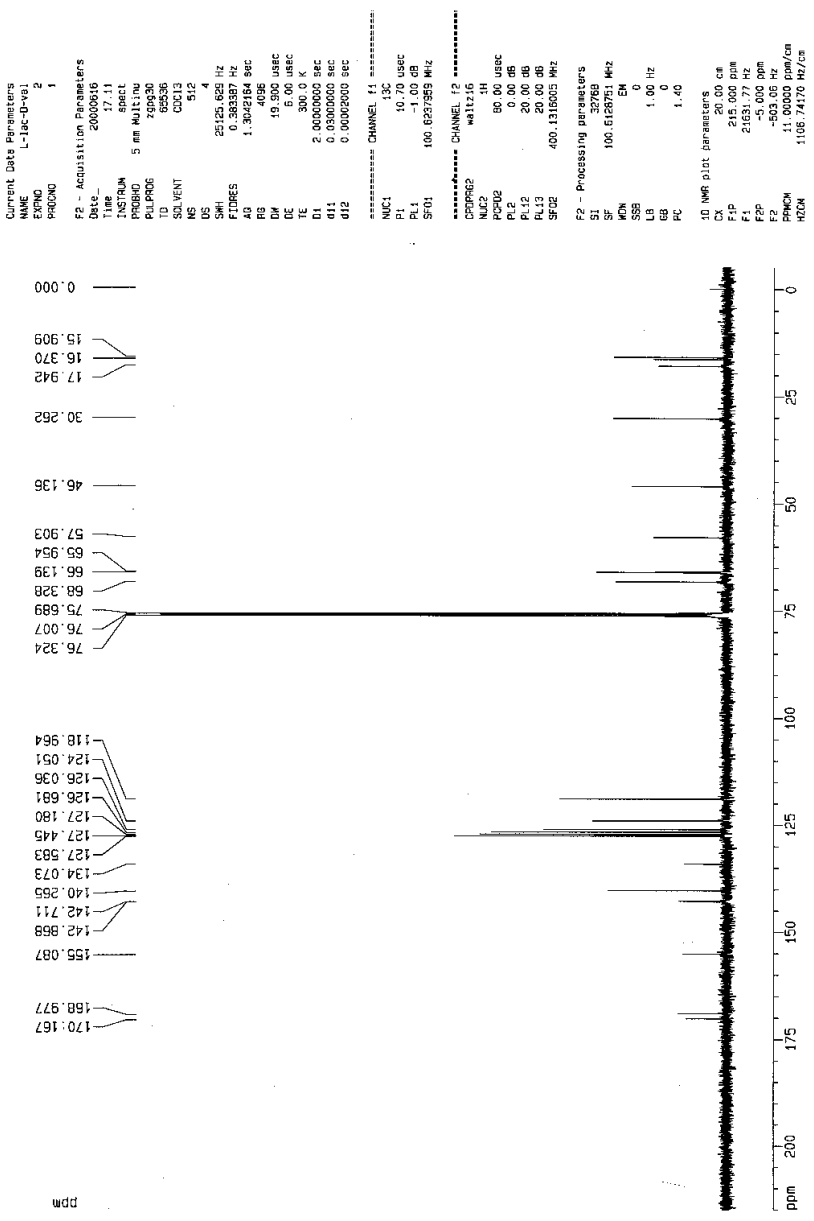
Current Data Parameters
NAME L-lac-D-val
EXPNO 2
PROCNO 1
F2 - Acquisition Parameters
Date_ 20000616
Time 17.11
INSTRUM spect
PROBHD 5 mm Multinu
PULPROG zgpg30
TD 65536
SOLVENT CDCl3
NS 512
DS 4
SWH 25125.628 Hz
FIDRES 0.383387 Hz
AQ 1.3042164 sec
RG 4096
DW 19.900 usec
DE 6.00 usec
TE 300.0 K
D1 2.00000000 sec
d11 0.03000000 sec
d12 0.00002000 sec
NUC1 13C
P1 10.70 usec
PL1 -1.00 dB
SFO1 100.6237959 MHz
CHANNEL f2
CPDPRG2 waltz16
NUC2 1H
PCPD2 80.00 usec
PL2 0.00 dB
PL12 20.00 dB
PL13 20.00 dB
SFO2 400.1316005 MHz
F2 - Processing parameters
SI 32768
SF 100.6128751 MHz
WDW EM
SSB 0
LB 1.00 Hz
GB 0
PC 1.40
1D NMR plot parameters
CX 20.00 cm
F1P 215.000 ppm
F1 21631.77 Hz
F2P -5.000 ppm
F2 -503.26 Hz
PPMCM 11.00000 ppm/cm
HZCM 1106.74170 Hz/cm
0.000
15.909
16.370
17.942
30.262
46.136
57.903
65.954
66.139
68.328
75.689
76.007
76.324
118.964
124.051
126.036
126.681
127.180
127.445
127.583
134.073
140.265
142.711
142.868
155.087
168.977
170.167
wdd
ppm

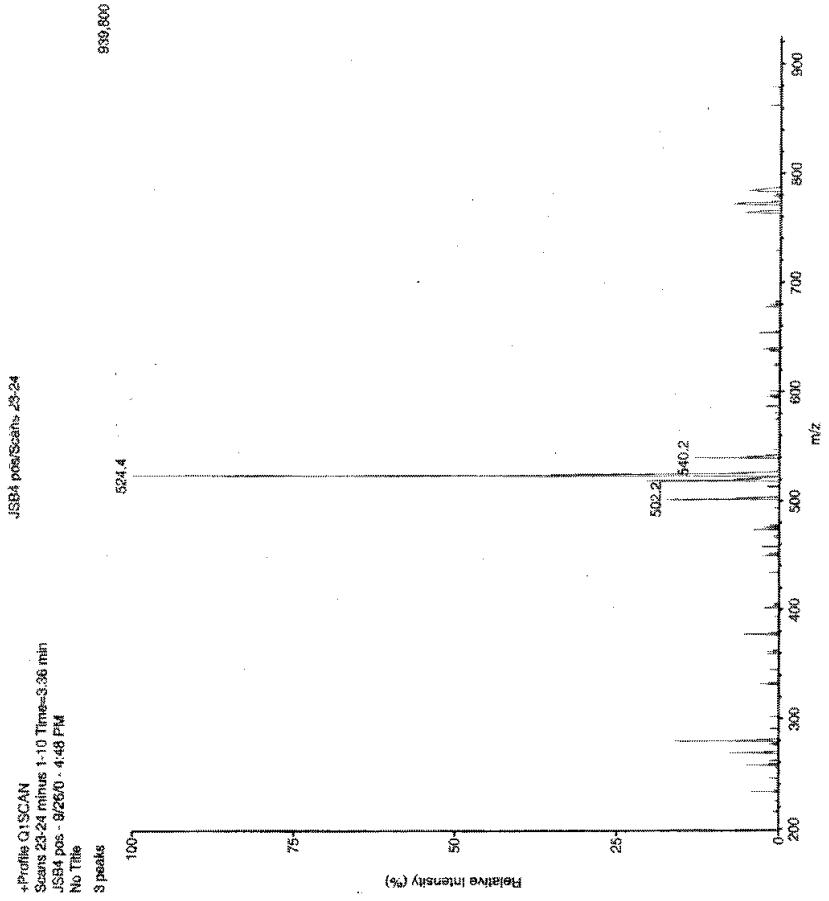

DI	50
ISV	5000
IN	650
OR	120
R0	30
M1	1000
RE1	121.6
DM1	0.040
R1	26.5
L7	-50
R2	-50
M3	1000
RE3	118
DM3	0.060
RX	-10
R3	-50
L9	50
FP	-50
MU	-4600
CC	10
DI µA	2.2
CGT	-1.3
IS v	5114.8
B-RAM	-10,004.9

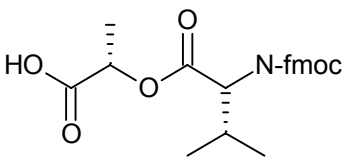

L-lac-D-val-N-fmoc (3)

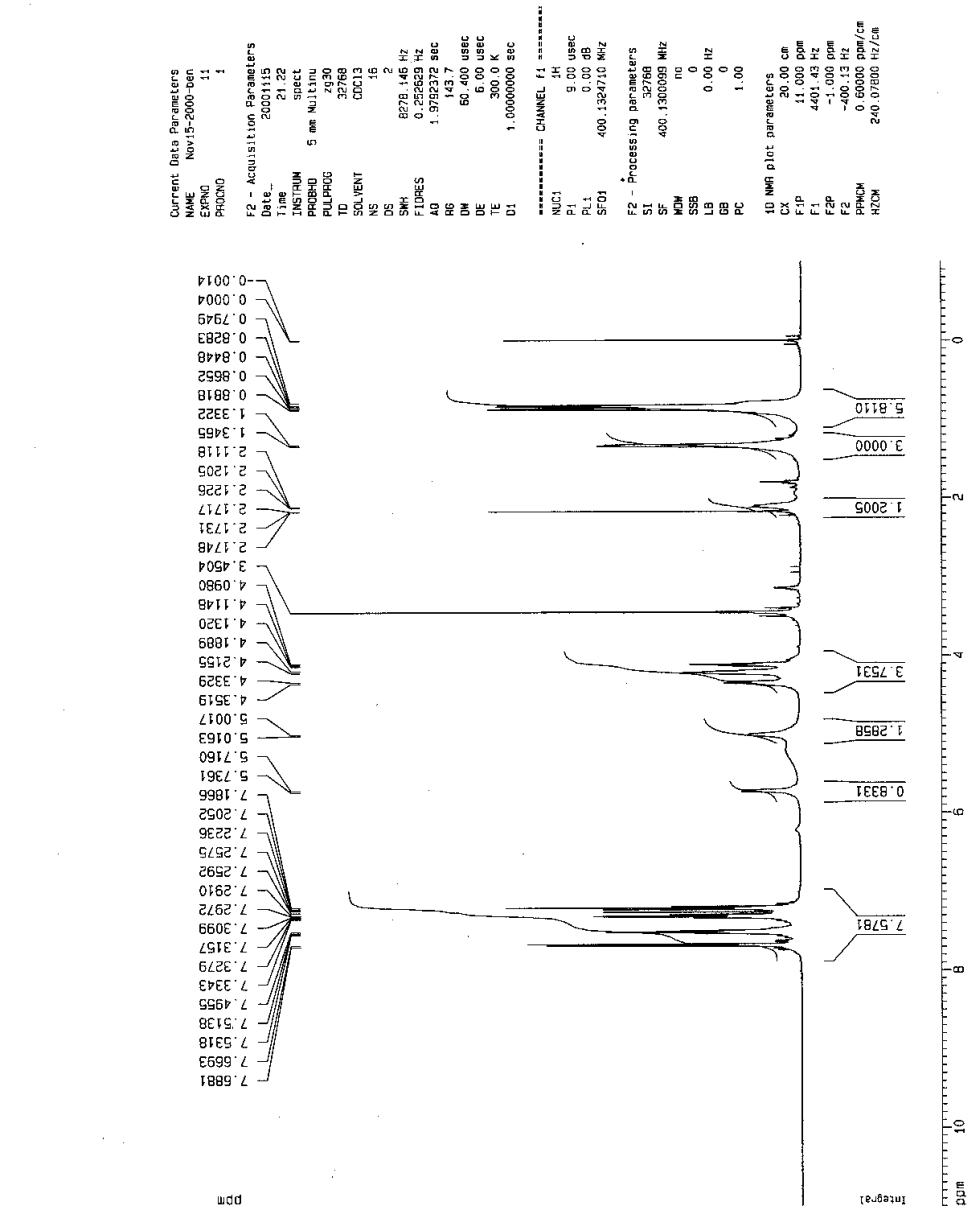

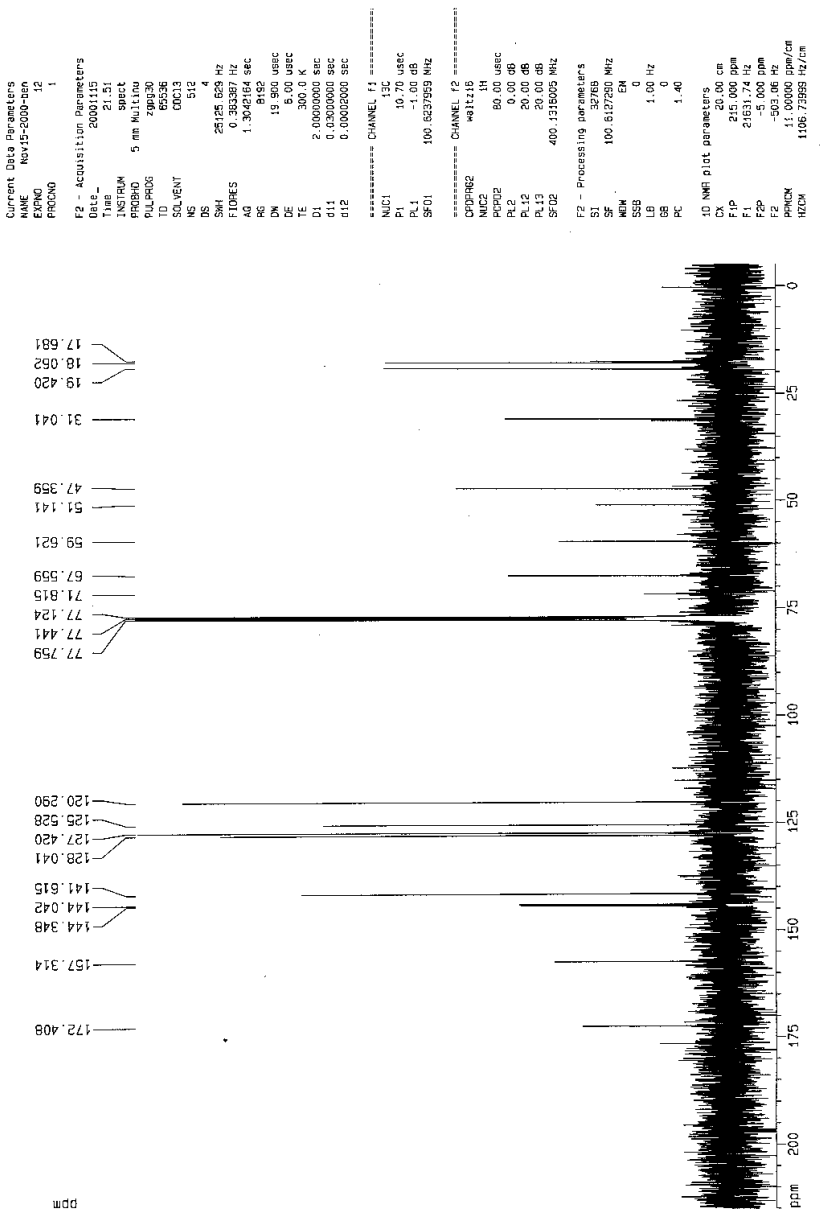
Current Data Parameters
NAME Nov15-2000-ben
EXPNO 12
PROCNO 1
F2 - Acquisition Parameters
Date_ 20001115
Time 21.51
INSTRUM spect
PROBHD 5 mm Multinu
PULPROG zgpg30
TD 65536
SOLVENT CDCl3
NS 512
DS 4
SWH 25125.629 Hz
FIDRES 0.383387 Hz
AQ 1.3042164 sec
RG 8192
DW 19.900 usec
DE 6.00 usec
TE 300.0 K
D1 2.00000000 sec
d11 0.03000000 sec
d12 0.00002000 sec
======== CHANNEL f1 ========
NUC1 13C
P1 10.70 usec
PL1 -1.00 dB
SFO1 100.6239959 MHz
======== CHANNEL f2 ========
CPDPRG2 waltz16
NUC2 1H
PCPD2 80.00 usec
PL2 0.00 dB
PL12 20.00 dB
PL13 20.00 dB
SFO2 400.1316005 MHz
F2 - Processing parameters
SI 32768
SF 100.6127290 MHz
WDW EM
SSB 0
LB 1.00 Hz
GB 0
PC 1.40
1D NMR plot parameters
CX 20.00 cm
F1P 215.000 ppm
F1 21631.74 Hz
F2P -5.000 ppm
F2 -503.06 Hz
PPMCM 11.00000 ppm/cm
HZCM 1106.73999 Hz/cm
17.681
18.062
19.420
31.041
47.359
51.141
59.621
67.559
71.815
77.124
77.441
77.759
120.290
125.528
127.420
128.041
141.615
144.042
144.348
157.314
172.408
ppm
0
25
50
75
100
125
150
175
200
ppm

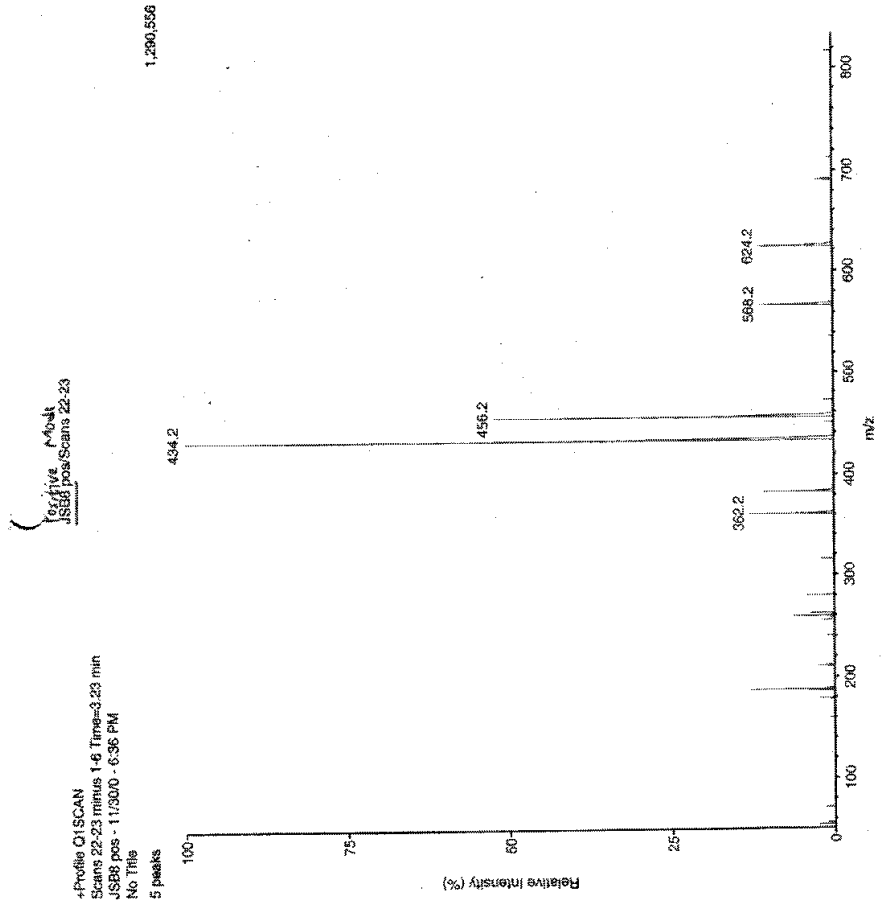

DI	50
ISV	5000
IN	650
OR	120
R0	30
M1	1000
RE1	122.10
DM1	0.040
R1	26.5
L7	-50
R2	-50
M3	1000
RE3	118
DM3	0.060
RX	-10
R3	-50
L9	50
FP	-50
MU	-4000
CC	10
DI µA	2.0
CGT	-1.3
IS v	5095.3
B-FAM	-10,004.9

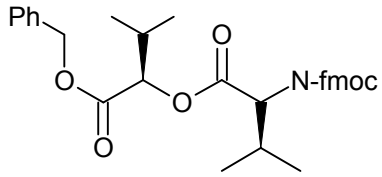

BzlO-D-hyval-L-val-N-fmoc (5)

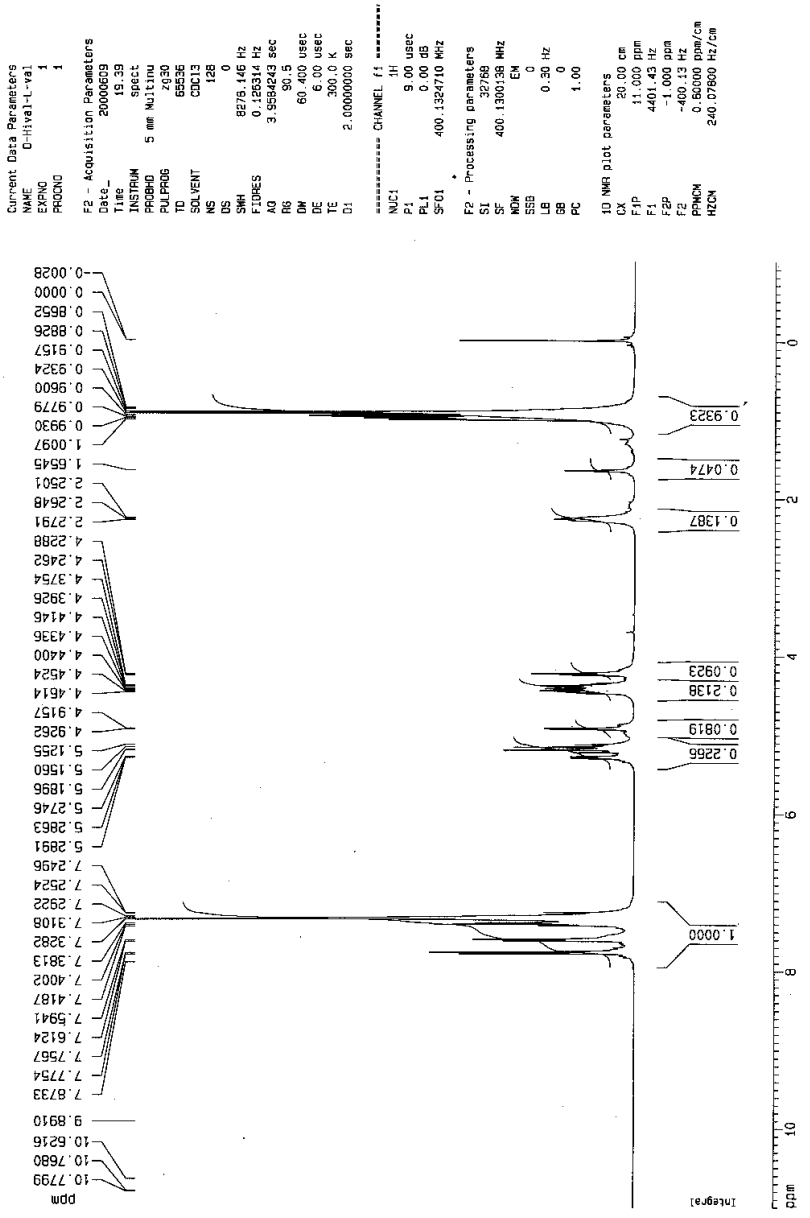

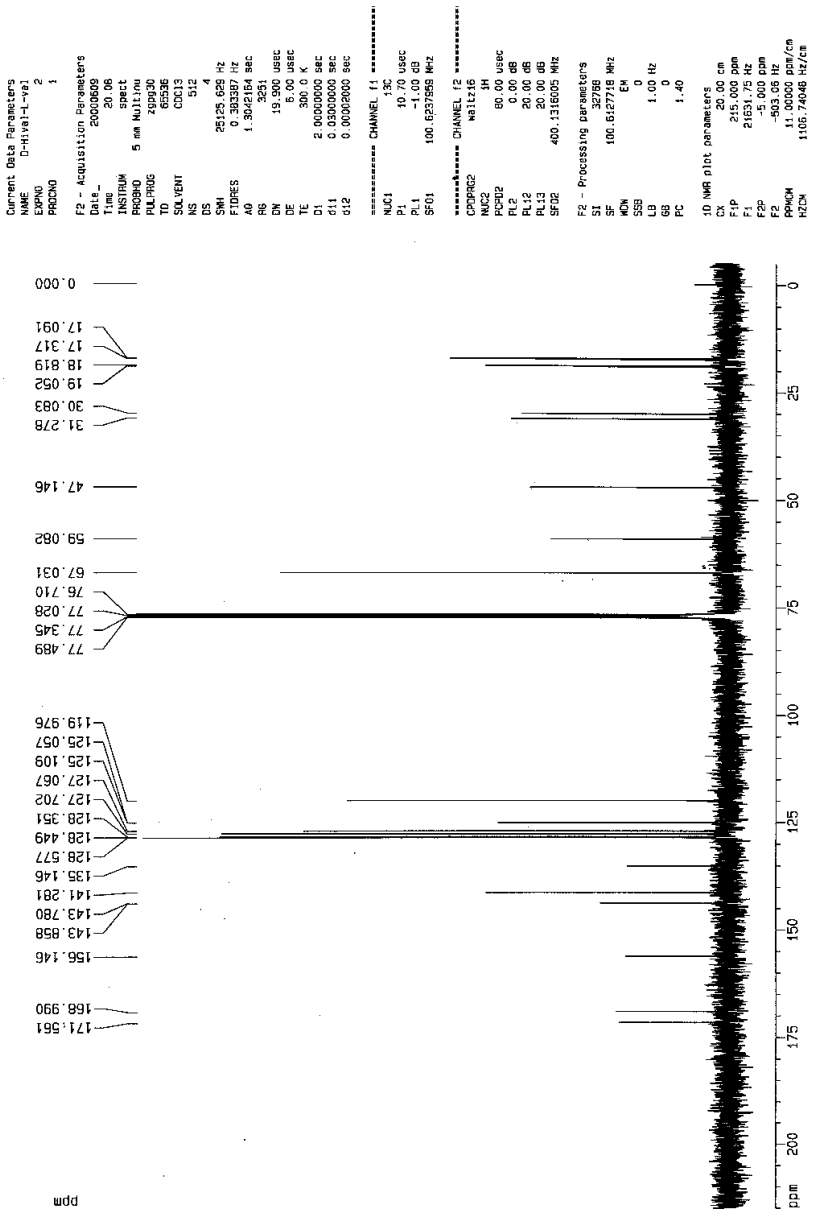
Current Data Parameters
NAME D-Hival-L-val
EXPNO 2
PROCNO 1
F2 - Acquisition Parameters
Date_ 20000609
Time 20.06
INSTRUM spect
PROBHD 5 mm Multinu
PULPROG zgpg30
TD 65536
SOLVENT CDCl3
NS 512
DS 4
SWH 25125.629 Hz
FIDRES 0.383387 Hz
AQ 1.3042164 sec
RG 3251
DW 19.900 usec
DE 6.00 usec
TE 300.0 K
D1 2.00000000 sec
d11 0.03000000 sec
d12 0.00002000 sec
CHANNEL f1
NUC1 13C
P1 10.70 usec
PL1 -1.00 dB
SFO1 100.6237956 MHz
CHANNEL f2
CPDPRG2 waltz16
NUC2 1H
PCPD2 80.00 usec
PL2 0.00 dB
PL12 20.00 dB
PL13 20.00 dB
SFO2 400.1316005 MHz
F2 - Processing parameters
SI 32768
SF 100.6127718 MHz
WDW EM
SSB 0
LB 1.00 Hz
GB 0
PC 1.40
1D NMR plot parameters
CX 20.00 cm
F1P 215.000 ppm
F1 21631.75 Hz
F2P -5.000 ppm
F2 -503.06 Hz
PPMCM 11.00000 ppm/cm
HZCM 1105.74048 Hz/cm
0.000
17.091
17.317
18.819
19.052
30.083
31.278
47.146
59.082
67.031
76.710
77.028
77.345
77.489
119.976
125.057
125.109
127.067
127.702
128.351
128.449
128.577
135.146
141.281
143.780
143.858
156.146
168.990
171.561
ppm
0
25
50
75
100
125
150
175
200

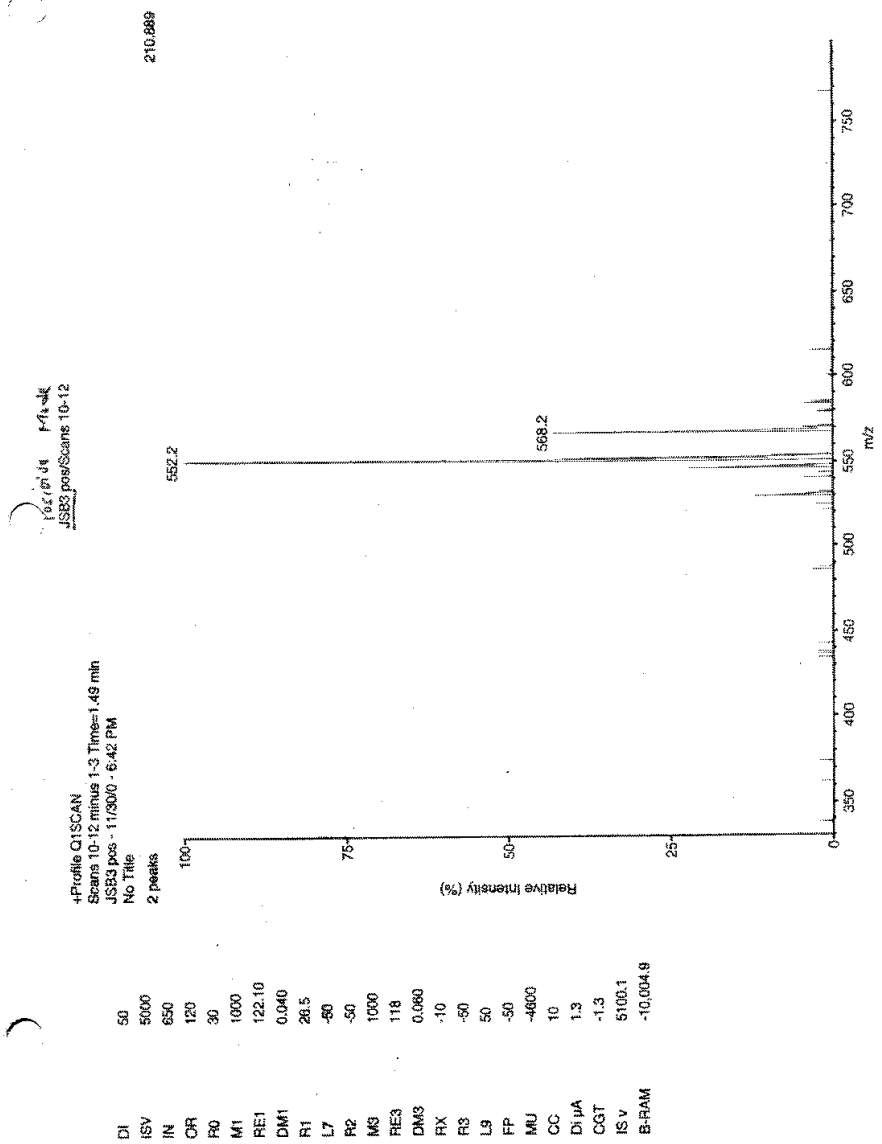
+Profile Q1SCAN
Scans 10-12 minus 1-3 Time=1.49 min
JSB3 pos - 11/30/0 - 6.42 PM
No Title
2 peaks
JSB3 pos/Scans 10-12
210.889
552.2
568.2
Relative Intensity (%)
m/z
100
75
50
25
0
350
400
450
500
550
600
650
700
750
DI 50
ISV 5000
IN 650
OR 120
R0 30
M1 1000
RE1 122.10
DM1 0.040
R1 26.5
L7 -60
R2 -50
M3 1000
RE3 118
DM3 0.060
RX -10
R3 -50
L9 50
FP -50
MU -4600
CC 10
Di µA 1.3
CGT -1.3
IS v 5100.1
B-RAM -10,004.9

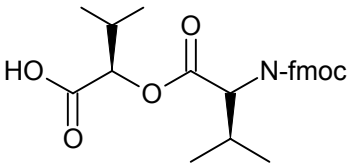

D-hyval-L-val-N-fmoc (6)

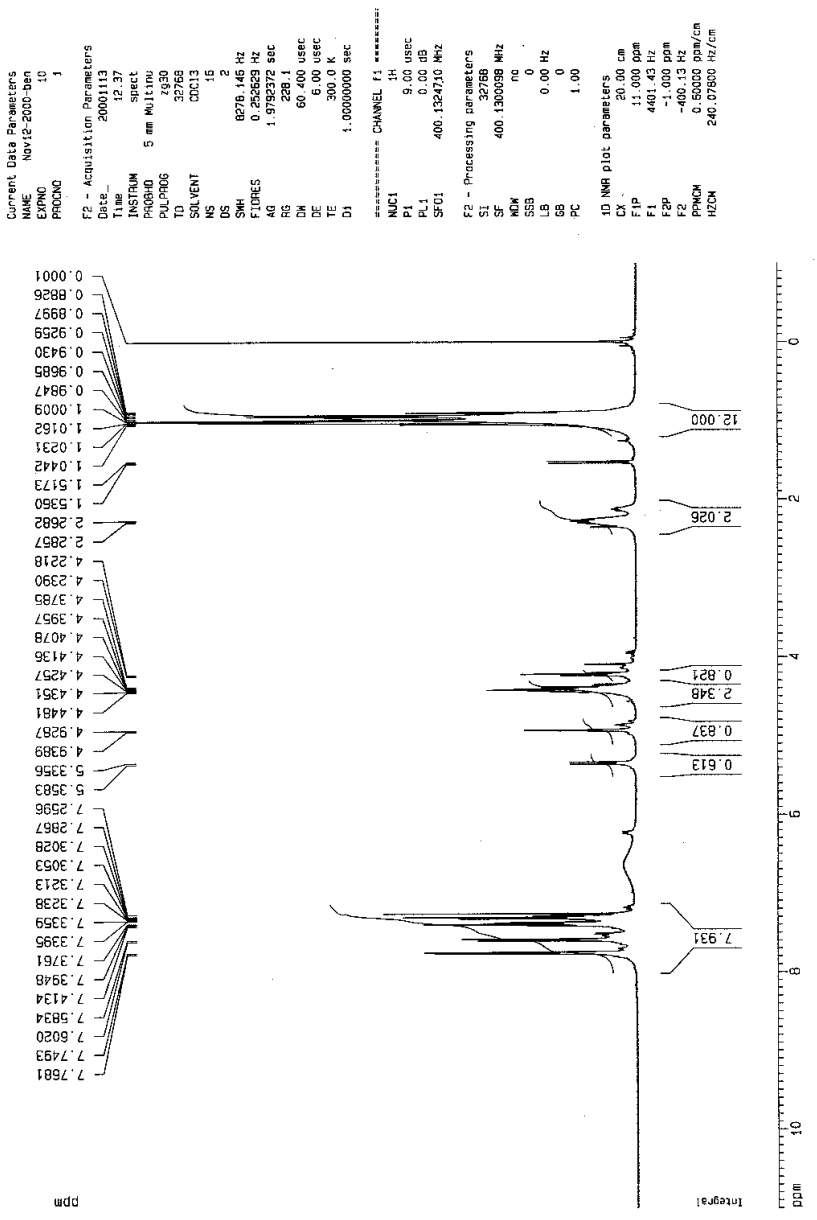

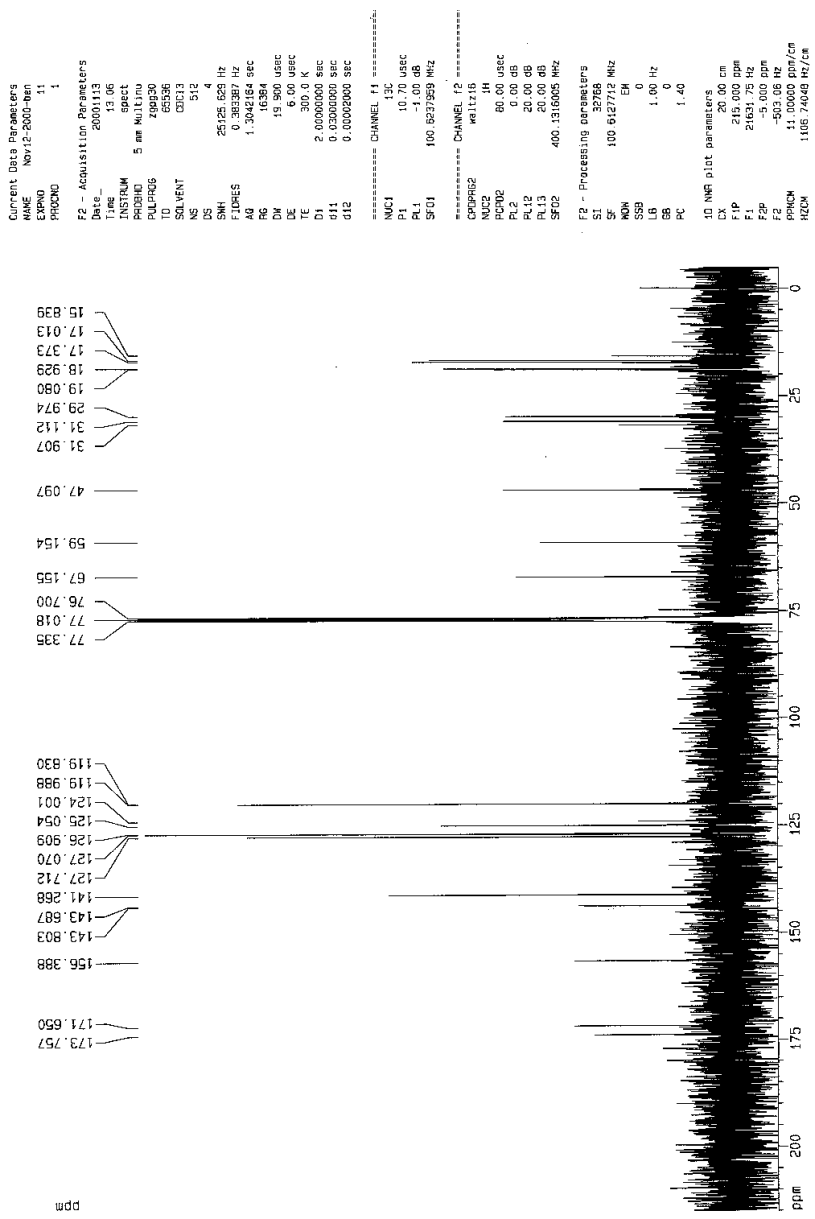
Current Data Parameters
NAME Nov12-2000-ben
EXPNO 11
PROCNO 1
F2 - Acquisition Parameters
Date_ 20001112
Time 13.06
INSTRUM spect
PROBHD 5 mm Multinu
PULPROG zgpg30
TD 65536
SOLVENT CDCl3
NS 512
DS 4
SWH 25125.628 Hz
FIDRES 0.383387 Hz
AQ 1.3042164 sec
RG 16384
DW 19.900 usec
DE 6.00 usec
TE 300.0 K
D1 2.00000000 sec
d11 0.03000000 sec
d12 0.00002000 sec
========== CHANNEL f1 ==========
NUC1 13C
P1 10.70 usec
PL1 -1.00 dB
SFO1 100.6237959 MHz
========== CHANNEL f2 ==========
CPDPRG2 waltz16
NUC2 1H
PCPD2 80.00 usec
PL2 0.00 dB
PL12 20.00 dB
PL13 20.00 dB
SFO2 400.1316005 MHz
F2 - Processing parameters
SI 32768
SF 100.6127712 MHz
WDW EM
SSB 0
LB 1.00 Hz
GB 0
PC 1.40
1D NMR plot parameters
CX 20.00 cm
F1P 215.000 ppm
F1 21631.75 Hz
F2P -5.000 ppm
F2 -503.06 Hz
PPMCM 11.00000 ppm/cm
HZCM 1106.74048 Hz/cm
15.839
17.013
17.373
18.929
19.080
29.974
31.112
31.907
47.097
59.154
67.155
76.700
77.018
77.335
119.830
119.988
124.001
125.054
126.909
127.070
127.742
141.268
143.687
143.803
156.388
173.650
173.757
ppm
0
25
50
75
100
125
150
175
200

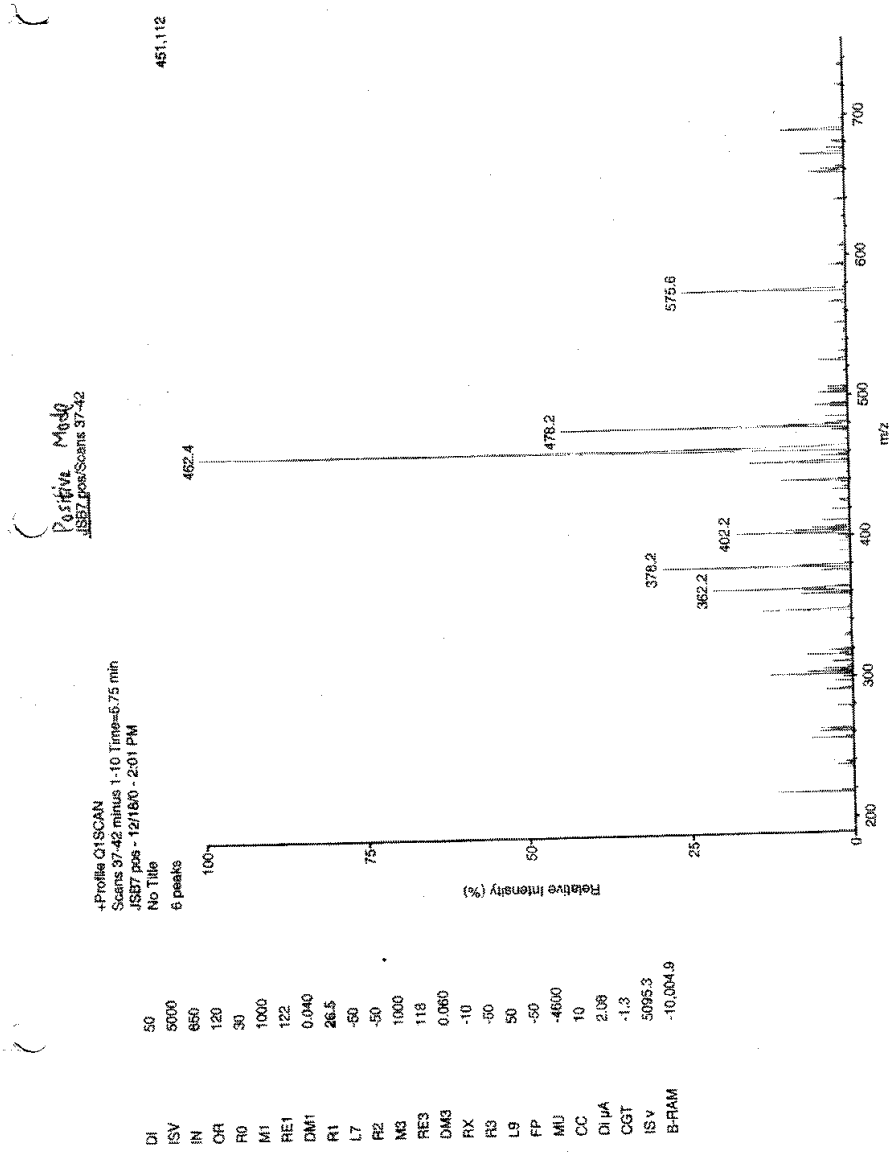
Positive Mode
JSB7 pos/Scans 37-42
+Profile Q1SCAN
Scans 37-42 minus 1-10 Time=5.75 min
JSB7 pos - 12/18/0 - 2:01 PM
No Title
6 peaks
451.112
462.4
478.2
575.6
378.2
362.2
402.2
Relative Intensity (%)
m/z
DI 50
ISV 5000
IN 650
OR 120
R0 30
M1 1000
RE1 122
DM1 0.040
R1 26.5
L7 -50
R2 -50
M3 1900
RE3 118
DM3 0.060
RX -10
R3 -50
L9 50
FP -50
MU -4600
CC 10
DI µA 2.06
CGT -1.3
IS v 5095.3
B-RAM -10,004.9

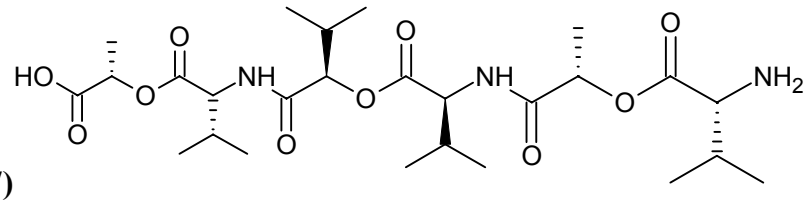

acyclic depsipeptide (7)

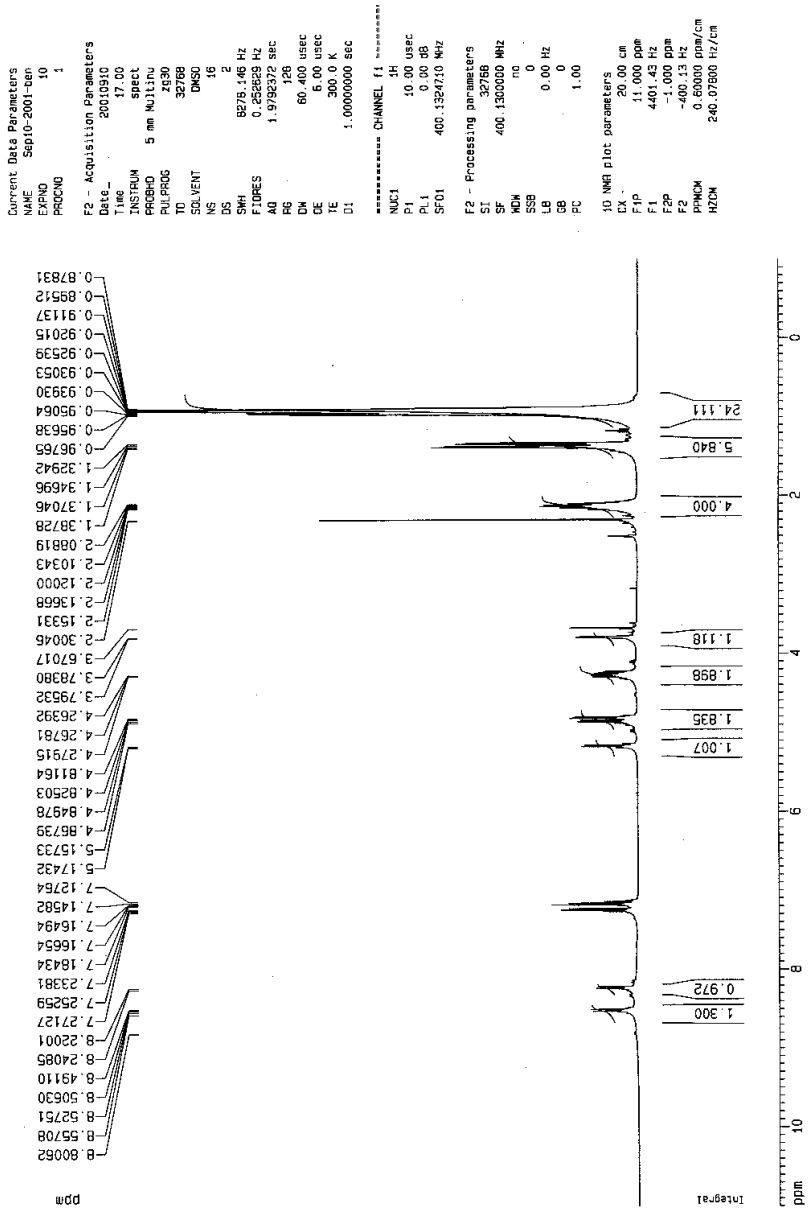

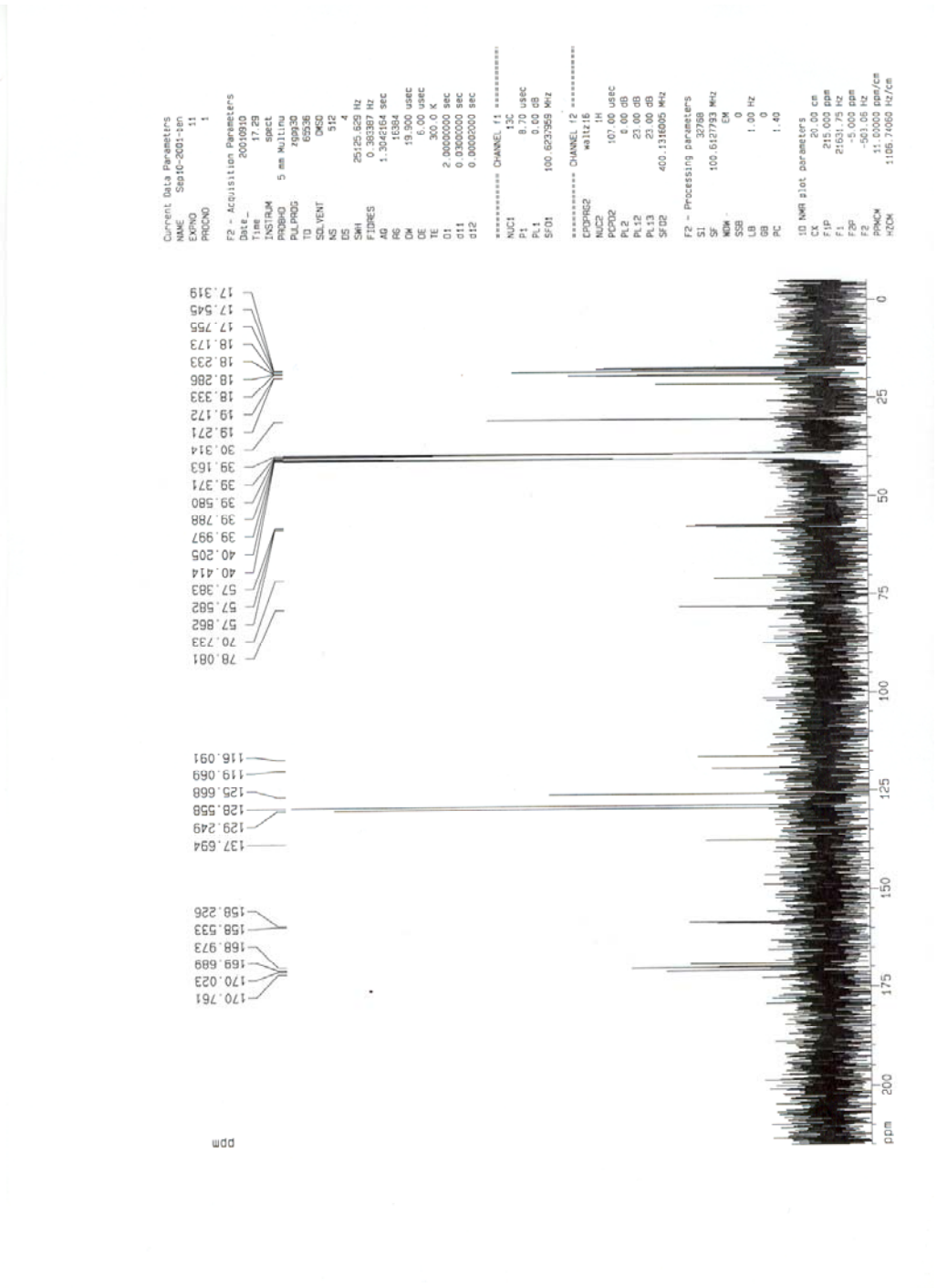
Current Data Parameters
NAME Sep10-2001-ten
EXPNO 11
PROCNO 1
F2 - Acquisition Parameters
Date_ 20010910
Time 17.29
INSTRUM spect
PROBHD 5 mm Multinu
PULPROG zgpg30
TD 65536
SOLVENT CMSO
NS 512
DS 4
SWH 25125.629 Hz
FIDRES 0.383387 Hz
AQ 1.3042164 sec
RG 16384
DW 19.900 usec
DE 6.00 usec
TE 300.0 K
D1 2.00000000 sec
D11 0.03000000 sec
D12 0.00002000 sec
======== CHANNEL f1 ========
NUC1 13C
P1 8.70 usec
PL1 0.00 dB
SFO1 100.6237959 MHz
======== CHANNEL f2 ========
EXPNAM2 waltz16
NUC2 1H
PCPD2 107.00 usec
PL2 6.00 dB
PL12 23.00 dB
PL13 23.00 dB
SFO2 400.1316005 MHz
F2 - Processing parameters
SI 32768
SF 100.6127793 MHz
WDW EM
SSB 0
LB 1.00 Hz
GB 0
PC 1.40
1D NMR plot parameters
CX 20.00 cm
F1P 215.000 ppm
F1 21631.75 Hz
F2P -5.000 ppm
F2 -563.06 Hz
PPMCM 11.60000 ppm/cm
HZCM 1166.74060 Hz/cm
ppm
0
25
50
75
100
125
150
175
200
17.319
17.545
17.755
18.173
18.233
18.286
18.333
19.172
19.271
30.314
39.163
39.371
39.580
39.788
39.997
40.205
40.414
57.383
57.582
57.862
70.733
78.081
116.091
119.069
125.668
128.558
129.249
137.694
158.226
158.533
168.973
169.689
170.023
170.761

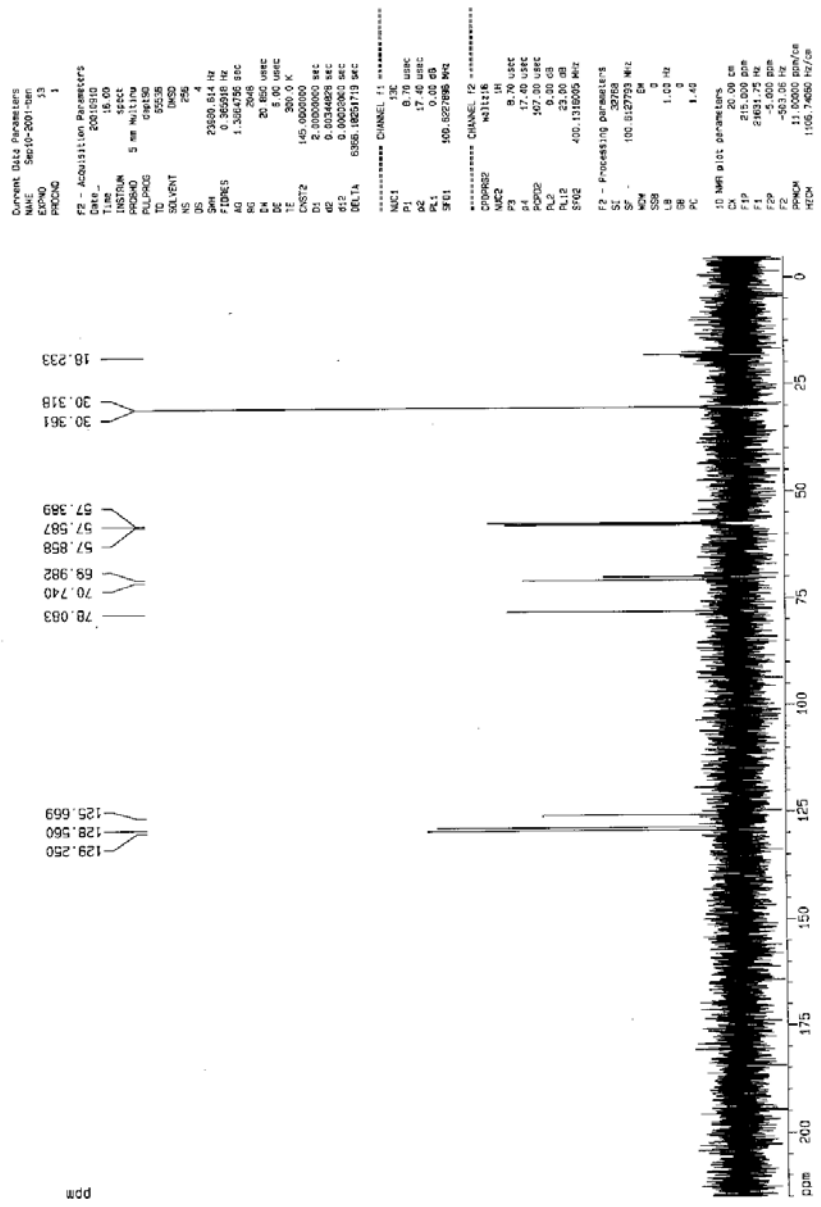
Current Data Parameters
NAME Sep10-2001-1H
EXPNO 13
PROCNO 1
F2 - Acquisition Parameters
Date_ 20010910
Time_ 16.09
INSTRUM spect
PROBHD 5 mm Multinu
PULPROG zgpg30
TD 65536
SOLVENT DMSO
NS 256
DS 4
SWH 29308.814 Hz
FIDRES 0.447158 Hz
AQ 1.1206736 sec
RG 2048
DW 25.650 usec
DE 6.00 usec
TE 300.0 K
CNST2 145.0000000
D1 2.00000000 sec
d2 0.00344829 sec
d12 0.00020000 sec
DELTA 6366.18251719 sec
======== CHANNEL f1 ========
NUC1 13C
P1 8.70 usec
PL1 17.40 dBm
SFO1 100.6227695 MHz
======== CHANNEL f2 ========
CPDPRG2 waltz16
NUC2 1H
P3 8.70 usec
P4 17.40 usec
PCPD2 107.00 usec
PL2 9.00 dB
PL12 23.00 dB
SFO2 400.1316005 MHz
F2 - Processing parameters
SI 32768
SF 100.6127793 MHz
WDW EM
SSB 0
LB 1.00 Hz
GB 0
PC 1.40
1D NMR plot parameters
CX 20.00 cm
F1P 215.600 ppm
F1 21631.75 Hz
F2P -0.400 ppm
F2 -40.26 Hz
PPMCM 11.00000 ppm/cm
HZCM 1106.74060 Hz/cm
18.233
30.318
30.361
57.389
57.587
57.858
69.982
70.740
78.083
125.669
128.560
129.250
ppm
0
25
50
75
100
125
150
175
200

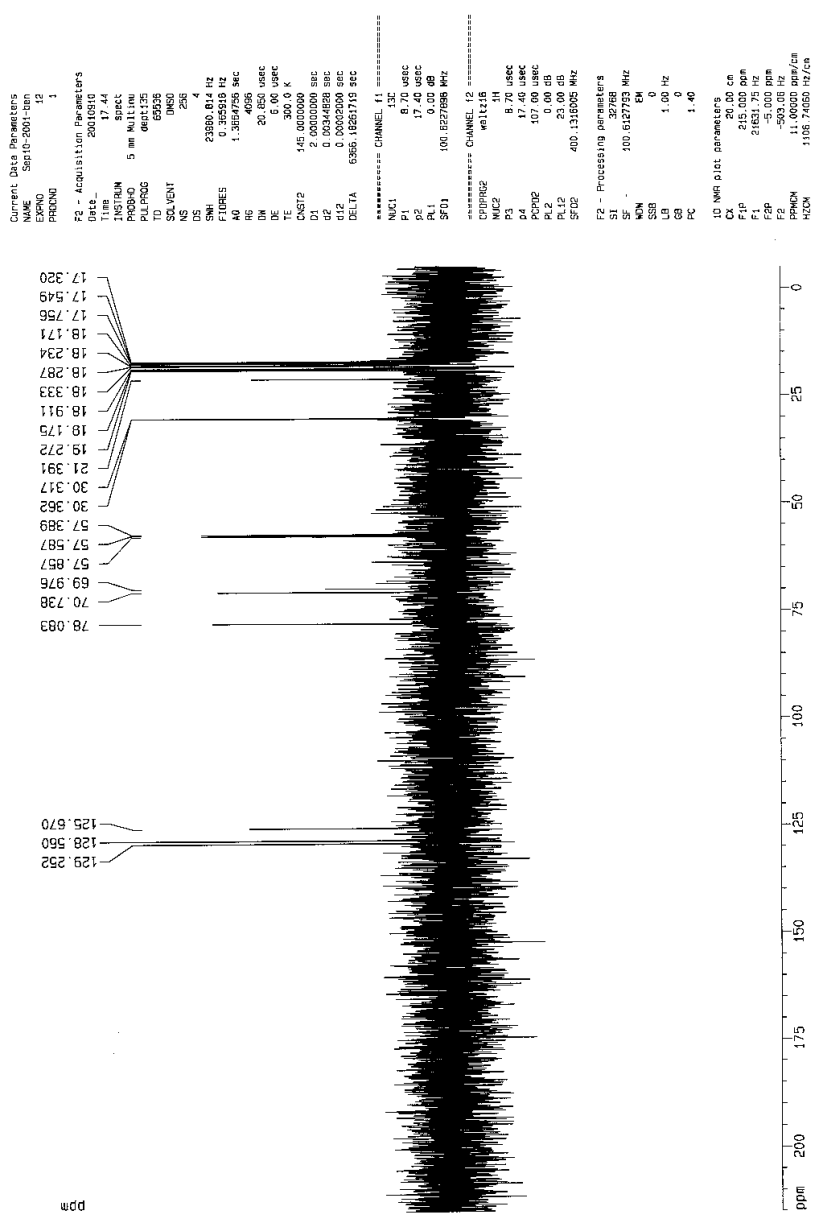
Current Data Parameters
NAME Sept0 2001 tan
EXPNO 12
PROCNO 1
F2 - Acquisition Parameters
Date_ 20010910
Time 17.44
INSTRUM spect
PROBHD 5 mm Multinu
PULPROG dept135
TD 65536
SOLVENT DMSO
NS 256
DS 4
SWH 23980.814 Hz
FIDRES 0.365516 Hz
AQ 1.3654755 sec
RG 4096
DW 20.850 usec
DE 6.00 usec
TE 300.0 K
CNST2 145.0000000
D1 2.00000000 sec
d2 0.00344828 sec
d12 0.00002000 sec
DELTA 6366.18261719 sec
======== CHANNEL f1 ========
NUC1 13C
P1 8.70 usec
P2 17.40 usec
PL1 0.00 dB
SFO1 100.8227898 MHz
======== CHANNEL f2 ========
CPDPRG2 waltz16
NUC2 1H
P3 8.70 usec
P4 17.40 usec
PCPD2 107.00 usec
PL2 0.00 dB
PL12 23.00 dB
SFO2 400.1316005 MHz
F2 - Processing parameters
SI 32768
SF 100.6127793 MHz
WDW EM
SSB 0
LB 1.00 Hz
GB 0
PC 1.40
1D NMR plot parameters
CX 20.00 cm
F1P 215.000 ppm
F1 21651.75 Hz
F2P -593.00 ppm
F2 -59701.01 Hz
PPMCM 11.00000 ppm/cm
HZCM 1106.74060 Hz/cm
17.320
17.549
17.756
18.171
18.234
18.287
18.333
18.911
18.975
19.272
21.391
30.317
30.362
57.389
57.587
57.857
69.976
70.738
78.083
125.670
128.560
129.252
ppm
0
25
50
75
100
125
150
175
200
ppm

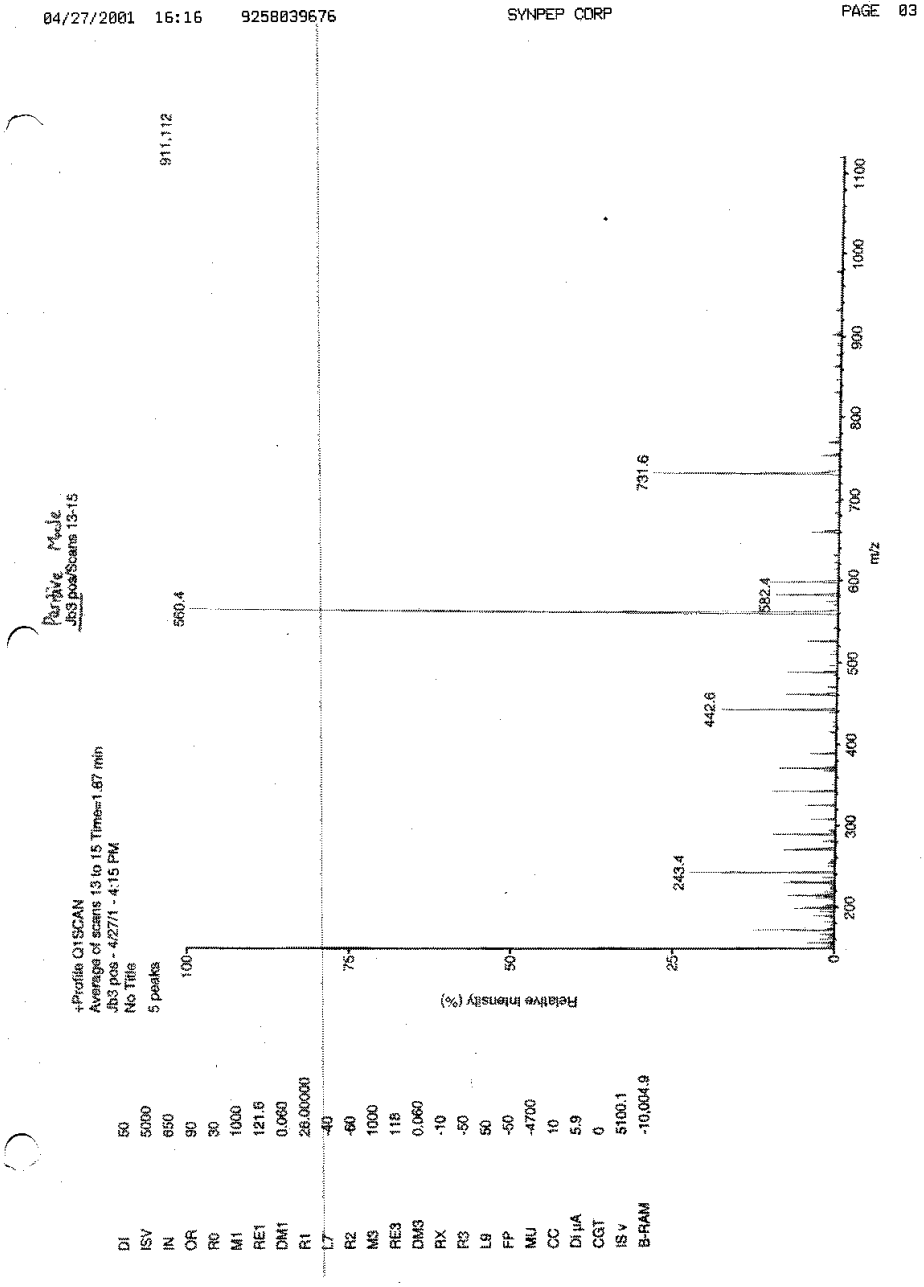
+Profile Q1SCAN
Average of scans 13 to 15 Time=1.67 min
Jb3 pos - 4/27/1 - 4:15 PM
No Title
5 peaks
Positive Mode
Jb3 pos#Scans 13-15
911.112
560.4
731.6
582.4
442.6
243.4
Relative Intensity (%)
m/z
DI 50
ISV 5000
IN 650
OR 90
R0 30
M1 1000
RE1 121.6
DM1 0.060
R1 26.00000
L7 40
R2 60
M3 1000
RE3 118
DM3 0.060
RX -10
R3 -50
L9 50
FP -50
MU -4700
CC 10
DI µA 5.9
CGT 0
IS v 5100.1
B-RAM -10,004.9

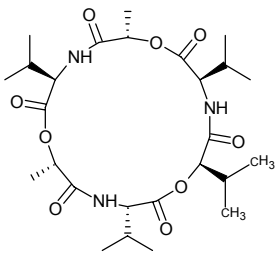

cyclo-depsipeptide (8)

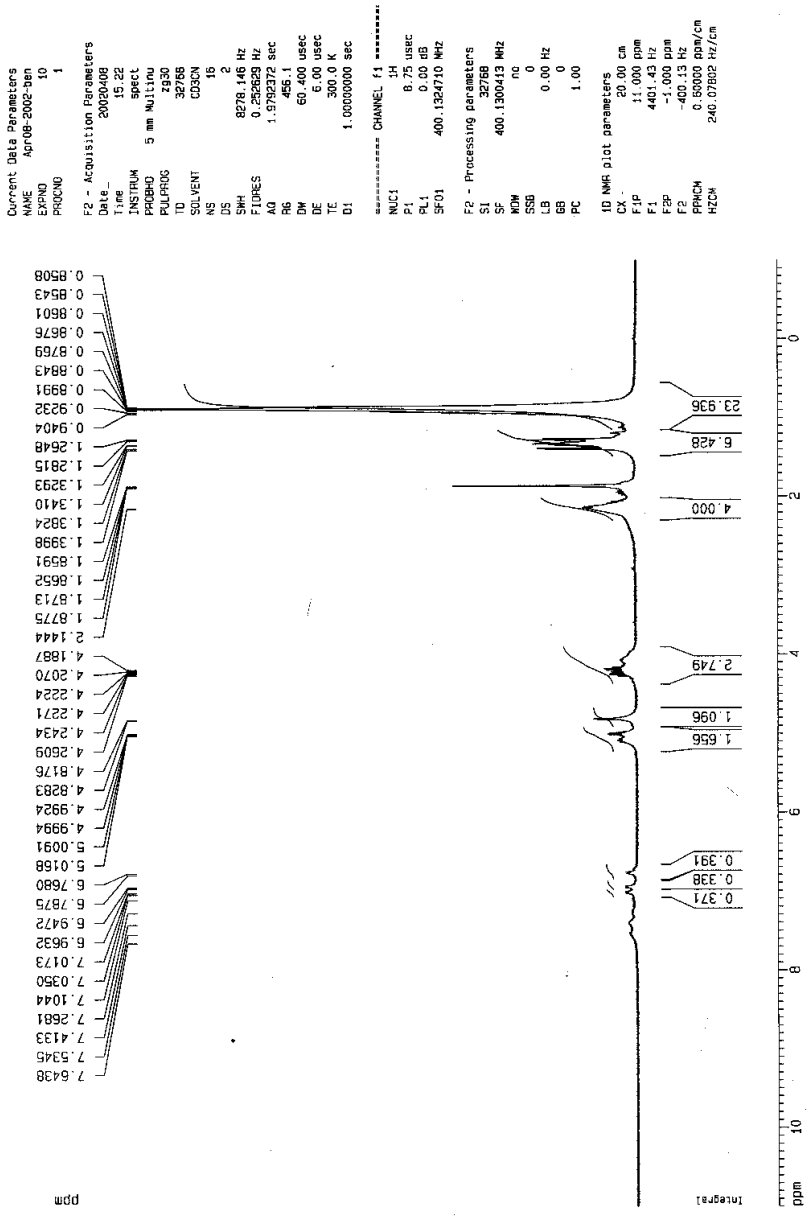

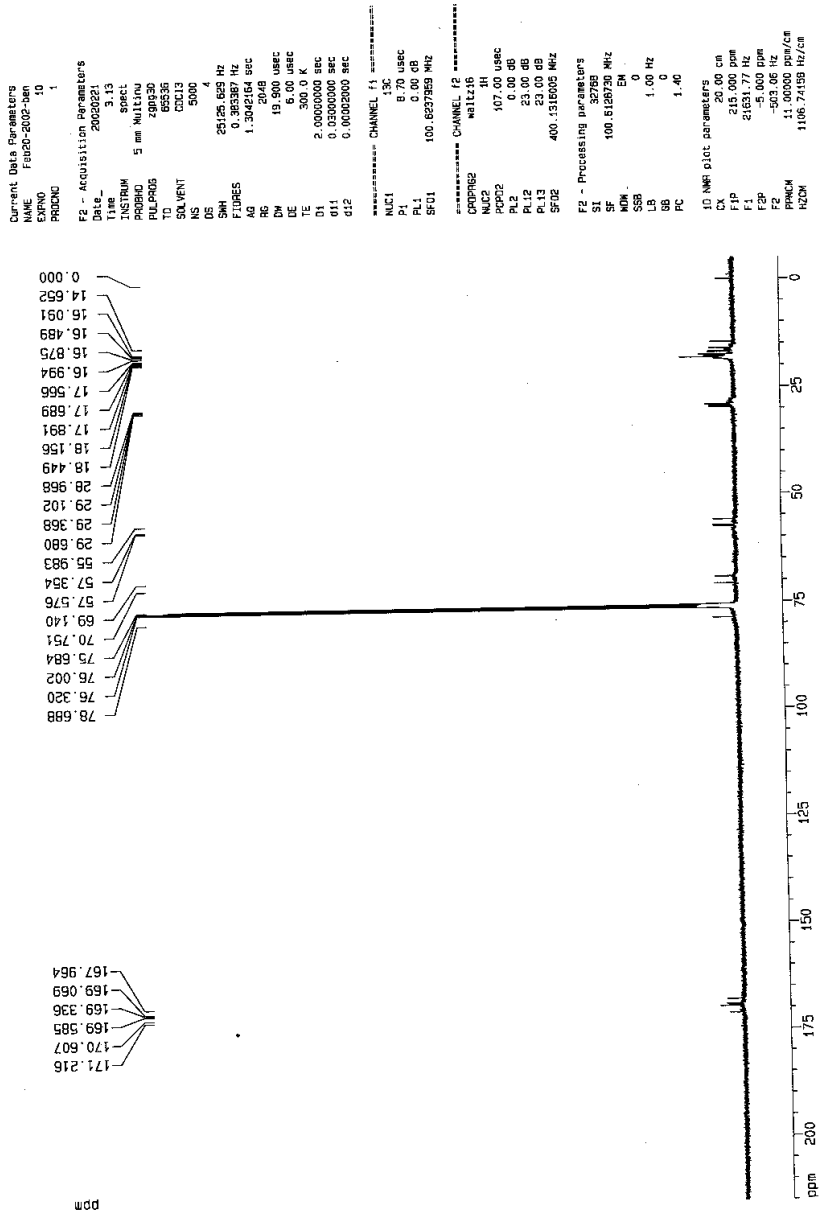
Current Data Parameters
NAME Feb20-2002-ben
EXPNO 10
PROCNO 1
F2 - Acquisition Parameters
Date_ 20020221
Time_ 3.13
INSTRUM spect
PROBHD 5 mm Multinu
PULPROG zgpg30
TD 65536
SOLVENT CDCl3
NS 5000
DS 4
SWH 25125.629 Hz
FIDRES 0.383387 Hz
AQ 1.3042164 sec
RG 2048
DW 19.900 usec
DE 6.00 usec
TE 300.0 K
D1 2.00000000 sec
d11 0.03000000 sec
d12 0.00002000 sec
CHANNEL f1
NUC1 13C
P1 8.70 usec
PL1 0.00 dB
SFO1 100.6237959 MHz
CHANNEL f2
CPDPRG2 waltz16
NUC2 1H
PCPD2 107.00 usec
PL2 0.00 dB
PL12 23.00 dB
PL13 23.00 dB
SFO2 400.1316005 MHz
F2 - Processing parameters
SI 32768
SF 100.6128730 MHz
WDW EM
SSB 0
LB 1.00 Hz
GB 0
PC 1.40
1D NMR plot parameters
CX 20.00 cm
F1P 215.000 ppm
F1 21631.77 Hz
F2P -5.000 ppm
F2 -503.06 Hz
PPMCM 11.00000 ppm/cm
HZCM 1106.74159 Hz/cm
0.000
14.652
16.091
16.489
16.875
16.994
17.566
17.689
17.891
18.156
18.449
28.968
29.102
29.368
29.680
55.983
57.354
57.576
69.140
70.751
75.684
76.002
76.320
78.688
167.964
169.069
169.336
169.585
170.607
171.216
ppm
0
25
50
75
100
125
150
175
200

Current Data Parameters
NAME Feb20-2002-ben
EXPNO 11
PROCNO 1
F2 - Acquisition Parameters
Date_ 20020221
Time 5.08
INSTRUM spect
PROBHD 5 mm Multinu
PULPROG dept135
TD 65536
SOLVENT CDCl3
NS 2000
DS 4
SWH 23980.814 Hz
FIDRES 0.365918 Hz
AQ 1.3664756 sec
RG 4096
DW 20.850 usec
DE 6.00 usec
TE 300.0 K
CNST2 145.0000000
D1 2.00000000 sec
d2 0.00344828 sec
d12 0.00002000 sec
DELTA 5365.182817719 sec
---------- CHANNEL f1 ----------
NUC1 13C
P1 8.70 usec
P2 17.40 usec
PL1 0.00 dB
SFO1 100.6227888 MHz
---------- CHANNEL f2 ----------
CPDPRG2 waltz16
NUC2 1H
P3 8.70 usec
P4 17.40 usec
PCPD2 107.00 usec
PL2 0.00 dB
PL12 23.00 dB
SFO2 400.1316005 MHz
F2 - Processing parameters
SI 32768
SF 100.6128772 MHz
WDW EM
SSB 0
LB 1.00 Hz
GB 0
PC 1.40
1D NMR plot parameters
CX 20.00 cm
F1P 215.000 ppm
F1 21631.77 Hz
F2P -50.000 ppm
F2 -5031.95 Hz
PPMCM 11.00000 ppm/cm
HZCM 1106.74158 Hz/cm
0.0000
14.6553
16.0924
16.4781
16.8788
16.9993
17.5690
17.6927
17.8953
18.1609
18.4633
28.9692
29.1046
29.3734
29.6853
55.9872
57.3613
57.5824
69.1440
70.7559
78.6924
ppm
0
25
50
75
100
125
150
175
200

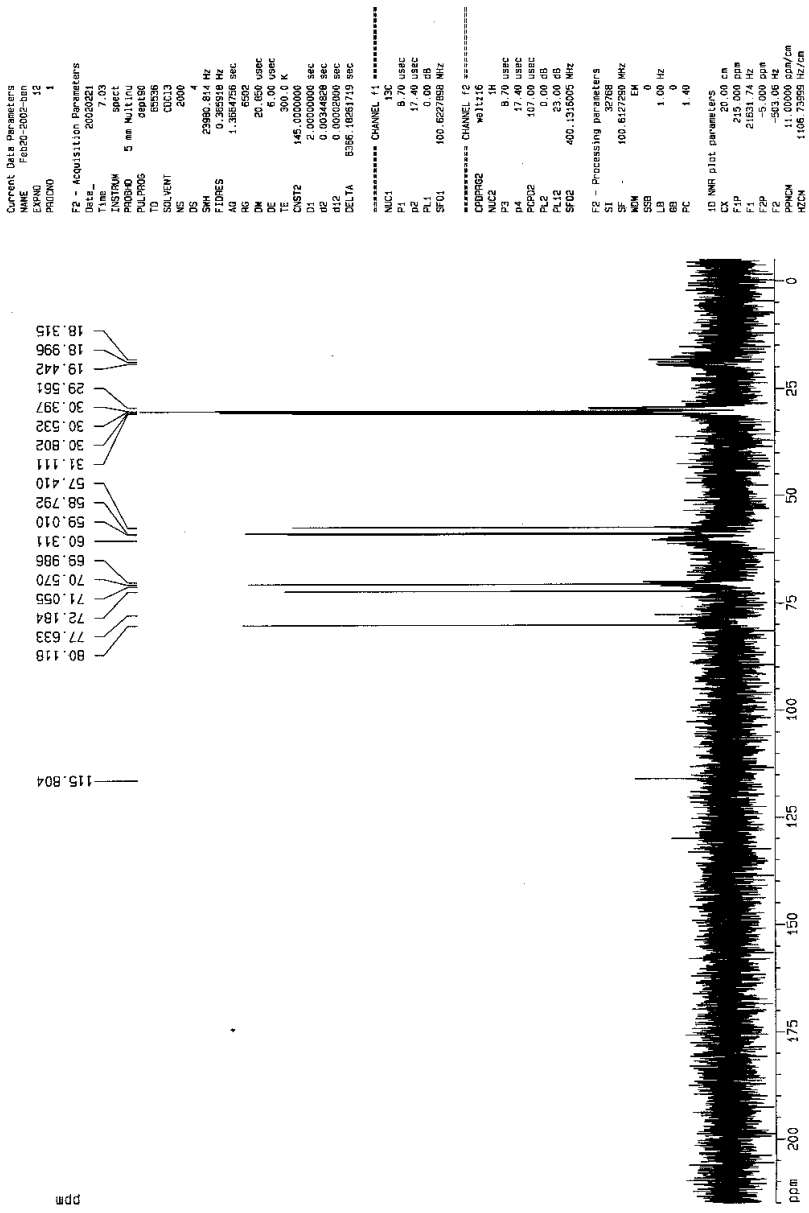
Current Data Parameters
NAME Feb20-2002-1bn
EXPNO 12
PROCNO 1
F2 - Acquisition Parameters
Date_ 20020221
Time 7.03
INSTRUM spect
PROBHD 5 mm Multinu
PULPROG deptq90
TD 65536
SOLVENT CDCl3
NS 2000
DS 4
SWH 29996.814 Hz
FIDRES 0.457516 Hz
AQ 1.3587755 sec
RG 8502
DW 20.850 usec
DE 6.00 usec
TE 300.0 K
CNST2 145.0000000
D1 2.00000000 sec
d2 0.00344828 sec
d12 0.00002000 sec
DELTA 8396.18361719 sec
======== CHANNEL f1 ========
NUC1 13C
P1 9.70 usec
p2 17.40 usec
PL1 0.00 dB
SF01 100.6227858 MHz
======== CHANNEL f2 ========
CPDPRG2 waltz16
NUC2 1H
P3 9.70 usec
p4 17.40 usec
PCPD2 107.00 usec
PL2 0.00 dB
PL12 23.00 dB
SFO2 400.1316005 MHz
F2 - Processing parameters
SI 32768
SF 100.6127250 MHz
WDW EM
SSB 0
LB 1.00 Hz
GB 0
PC 1.40
1D NMR plot parameters
CX 20.00 cm
F1P 215.000 ppm
F1 21631.70 Hz
F2P -5.000 ppm
F2 -503.06 Hz
PPMCM 11.00000 ppm/cm
HZCM 1106.73999 Hz/cm
18.315
18.996
19.442
29.561
30.397
30.532
30.802
31.111
57.410
58.792
59.010
60.311
69.986
70.570
71.055
72.184
77.633
80.118
115.804
ppm
0
25
50
75
100
125
150
175
200

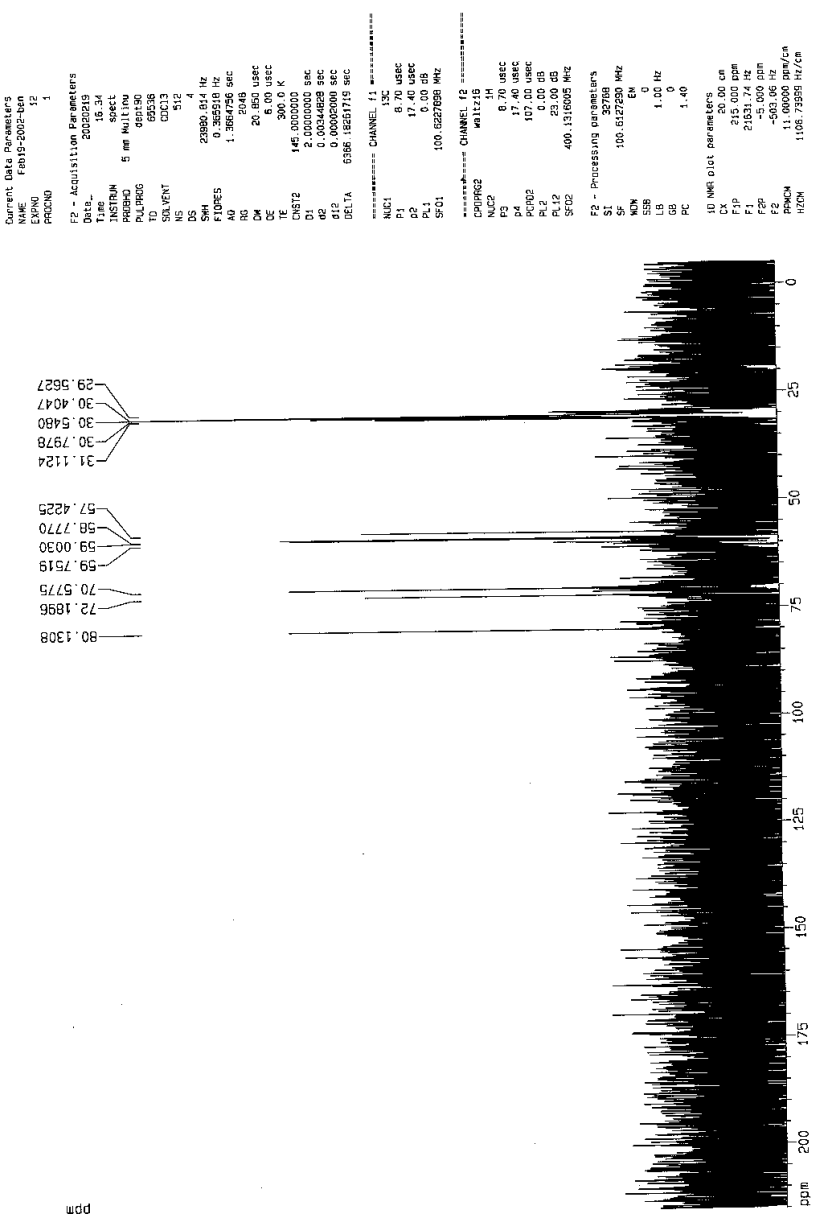
Current Data Parameters
NAME Feb19-2002-ben
EXPNO 12
PROCNO 1
F2 - Acquisition Parameters
Date_ 20020219
Time 16.34
INSTRUM spect
PROBHD 5 mm Multinu
PULPROG deptsp
TD 65536
SOLVENT CDCl3
NS 512
DS 4
SWH 23980.814 Hz
FIDRES 0.365918 Hz
AQ 1.3664796 sec
RG 2048
DW 20.850 usec
DE 6.00 usec
TE 300.0 K
CNST2 145.0000000
D1 2.0000000 sec
d2 0.0034483 sec
d12 0.0000200 sec
DELTA 6386.1626171 sec
======== CHANNEL f1 ========
NUC1 13C
P1 8.70 usec
p2 17.40 usec
PL1 0.00 dB
SFO1 100.6227698 MHz
======== CHANNEL f2 ========
CPDPRG2 waltz16
NUC2 1H
PCPD2 107.00 usec
PL2 0.00 dB
PL12 23.00 dB
SFO2 400.1316005 MHz
F2 - Processing parameters
SI 32768
SF 100.6127230 MHz
WDW EM
SSB 0
LB 1.00 Hz
GB 0
PC 1.40
1D NMR plot parameters
CX 20.00 cm
F1P 215.000 ppm
F1 21631.74 Hz
F2P -5.000 ppm
F2 -503.06 Hz
PPMCM 11.00000 ppm/cm
HZCM 1106.73999 Hz/cm
29.5627
30.4047
30.5480
30.7978
31.1124
57.4225
58.7770
59.0030
59.7519
70.5775
72.1896
80.1308
ppm
0
25
50
75
100
125
150
175
200

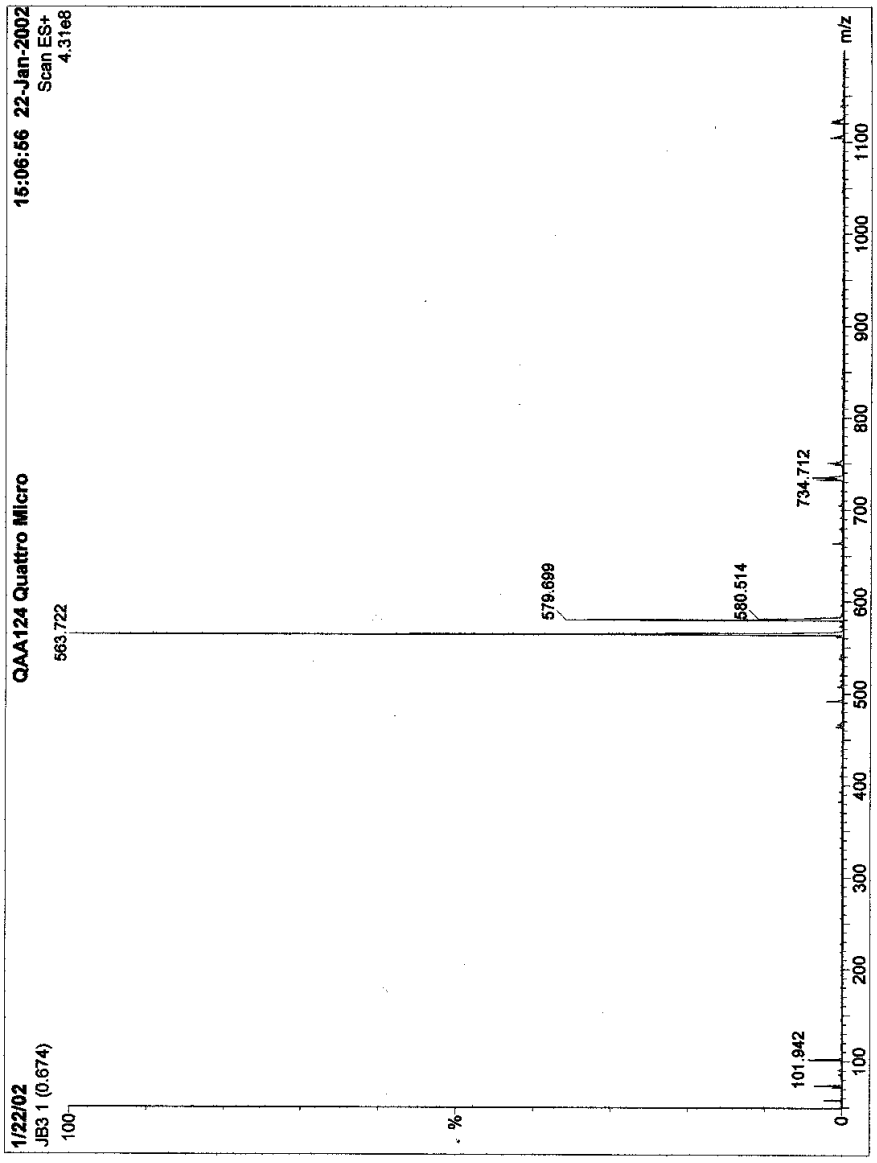
1/22/02
JB3 1 (0.674)
QAA124 Quattro Micro
15:06:56 22-Jan-2002
Scan ES+
4.31e8
100
%
0
563.722
579.699
580.514
734.712
101.942
100
200
300
400
500
600
700
800
900
1000
1100
m/z

Appendix A2:

NMR and Mass Spectroscopy data for N-(9-methyl-anthracene)-25,27-bis(1-propyloxy)calix[4]arene-azacrown-5**(10)**

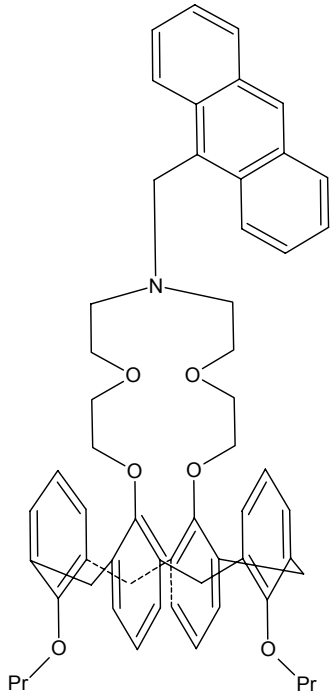

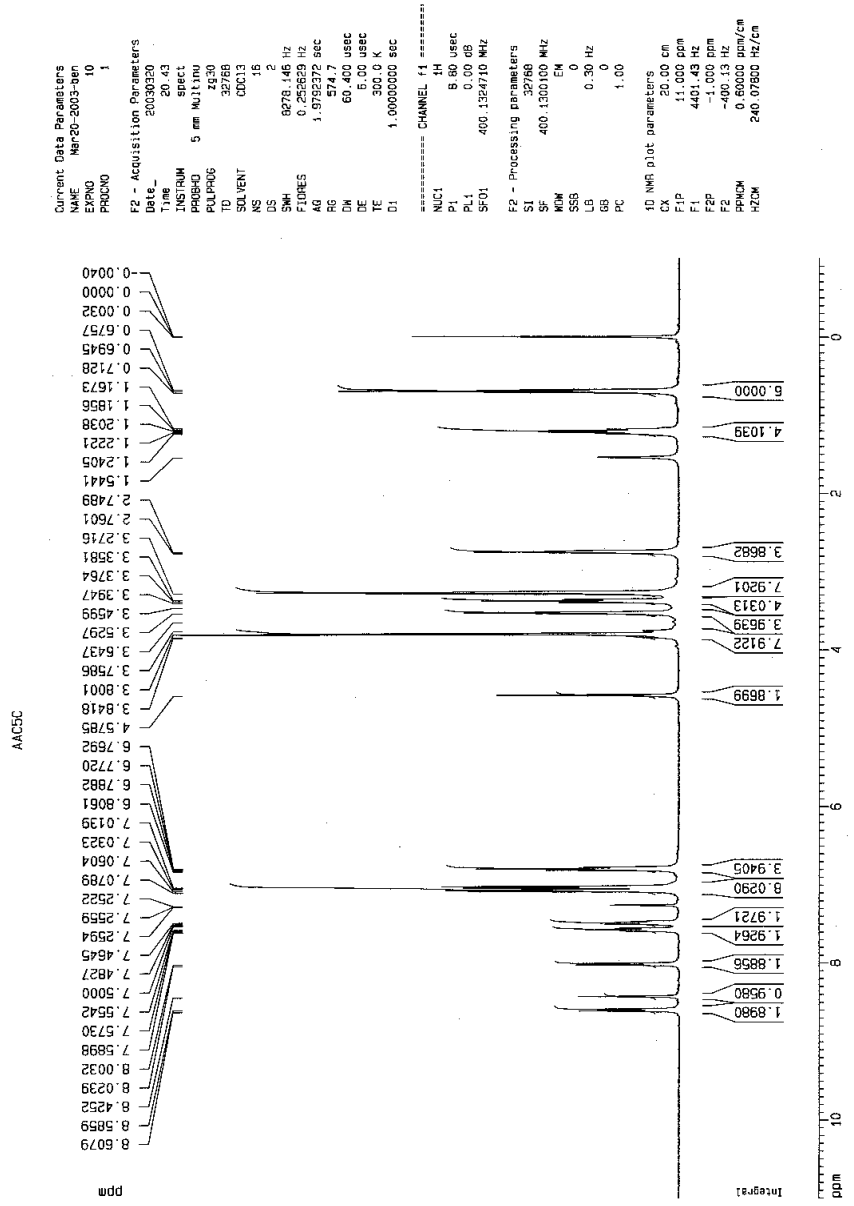
Current Data Parameters
NAME Nan20-2003-ben
EXPNO 10
PROCNO 1
F2 - Acquisition Parameters
Date_ 20030320
Time 20.43
INSTRUM spect
PROBHD 5 mm Multinu
PULPROG zg30
TD 32768
SOLVENT CDCl3
NS 16
DS 2
SWH 8278.146 Hz
FIDRES 0.252829 Hz
AQ 1.9799372 sec
RG 574.7
DW 60.400 usec
DE 6.00 usec
TE 300.0 K
D1 1.00000000 sec
======== CHANNEL f1 ========
NUC1 1H
P1 8.80 usec
PL1 0.00 dB
SFO1 400.1324710 MHz
F2 - Processing parameters
SI 32768
SF 400.1300100 MHz
WDW EM
SSB 0
LB 0.30 Hz
GB 0
PC 1.00
1D NMR plot parameters
CX 20.00 cm
F1P 11.000 ppm
F1 4401.43 Hz
F2P -1.000 ppm
F2 -400.13 Hz
PPMCM 0.66000 ppm/cm
HZCM 240.07800 Hz/cm
AAC5C
ppm
Integral
0.0040
0.0000
0.0032
0.6757
0.6945
0.7128
1.1673
1.1856
1.2038
1.2221
1.2405
1.5441
2.7489
2.7601
3.2716
3.3581
3.3764
3.3947
3.4599
3.5297
3.6437
3.7586
3.8001
3.8418
4.5785
6.7692
6.7720
6.7882
6.8061
7.0139
7.0323
7.0604
7.0789
7.2522
7.2559
7.2594
7.4645
7.4827
7.5000
7.5542
7.5730
7.5898
8.0032
8.0239
8.4252
8.5859
8.6079
6.0000
4.1039
3.8682
7.9201
4.0313
3.9639
7.9122
1.8699
3.9405
8.0290
1.9721
1.9264
1.8856
0.9580
1.8980
0
2
4
6
8
10

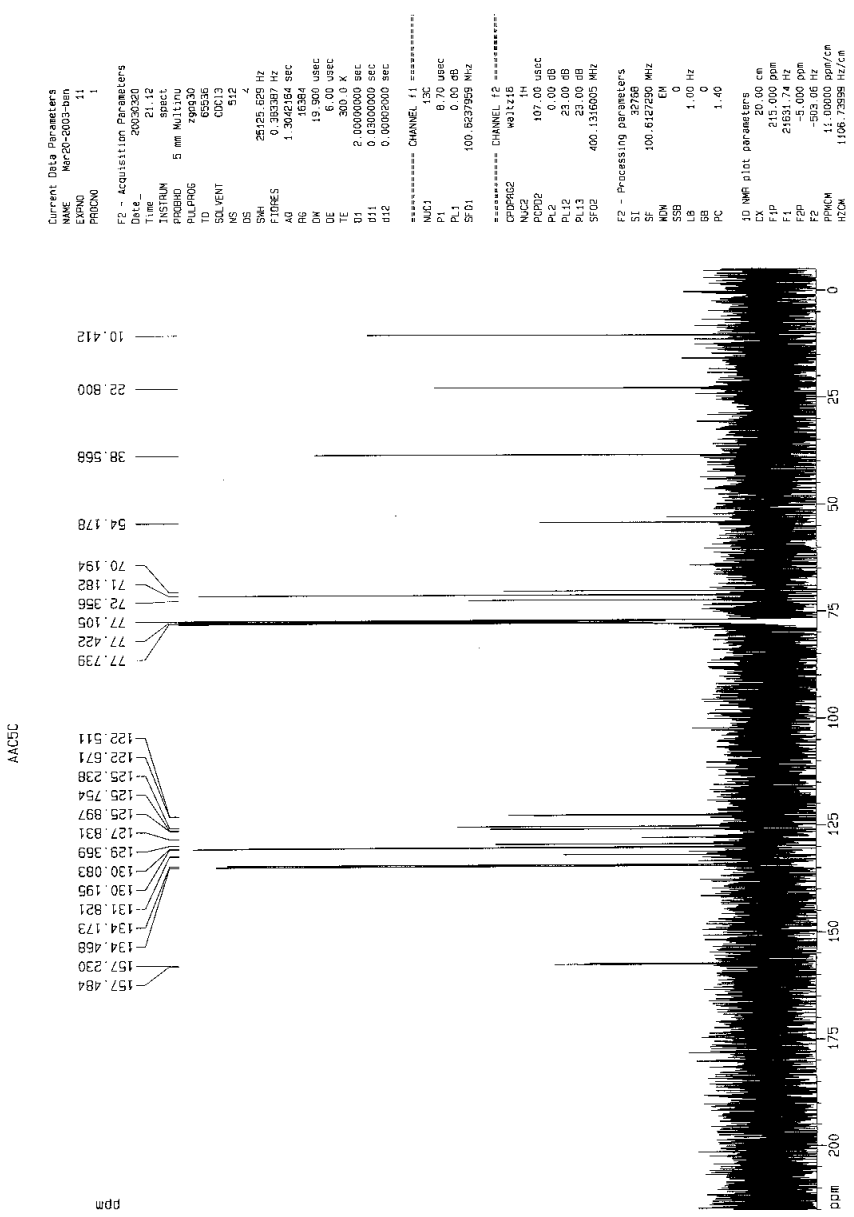
Current Data Parameters
NAME Mar20-2003-bern
EXPNO 11
PROCNO 1
F2 - Acquisition Parameters
Date_ 20030320
Time 21.12
INSTRUM spect
PROBHD 5 mm Multinu
PULPROG zgpg30
TD 65536
SOLVENT CDCl3
NS 512
DS 4
SWH 25125.628 Hz
FIDRES 0.383387 Hz
AQ 1.3042184 sec
RG 16384
DW 19.900 usec
DE 6.00 usec
TE 300.1 K
D1 2.00000000 sec
d11 0.03000000 sec
d12 0.00002000 sec
CHANNEL f1
NUC1 13C
P1 8.70 usec
PL1 0.00 dB
SFO1 100.6237959 MHz
CHANNEL f2
CPDPRG2 waltz16
NUC2 1H
PCPD2 107.00 usec
PL2 0.00 dB
PL12 23.00 dB
PL13 23.00 dB
SFO2 400.1316005 MHz
F2 - Processing parameters
SI 32768
SF 100.6127290 MHz
WDW EM
SSB 0
LB 1.00 Hz
GB 0
PC 1.40
1D NMR plot parameters
CX 20.00 cm
F1P 215.000 ppm
F1 21631.74 Hz
F2P -5.000 ppm
F2 -503.06 Hz
PPMCM 11.00000 ppm/cm
HZCM 1106.73999 Hz/cm
AACSC
10.412
22.800
38.568
54.178
70.194
71.182
72.356
77.105
77.422
77.739
122.511
122.671
125.238
125.754
125.897
127.831
129.369
130.083
130.195
131.821
134.173
134.468
157.230
157.484
ppm
0
25
50
75
100
125
150
175
200
ppm

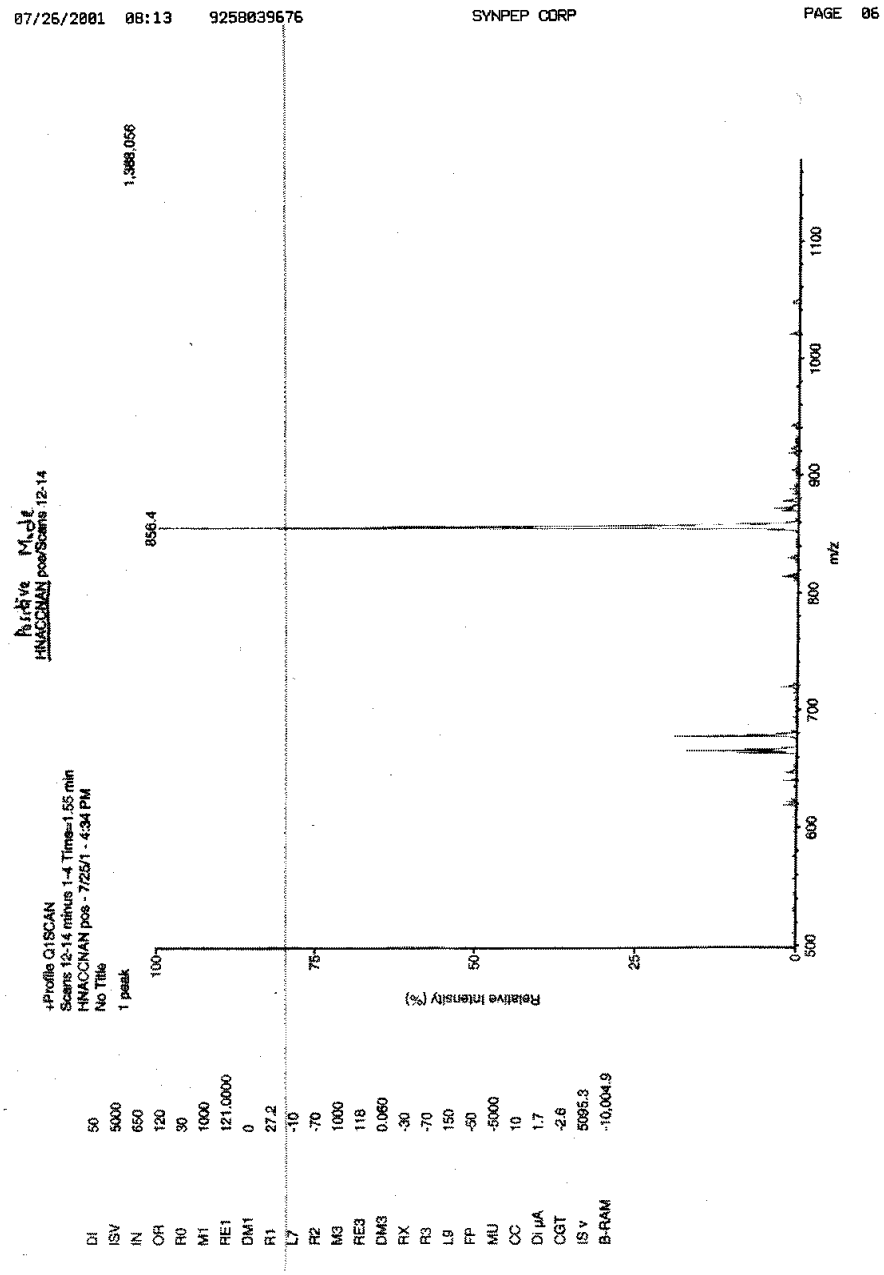
07/26/2001 08:13 9258039676 SYNPEP CORP PAGE 06
Native Model
HNAOCNAN pos/Scans 12-14
+Profile Q1SCAN
Scans 12-14 minus 1-4 Time=1.55 min
HNAOCNAN pos - 7/25/1 - 4:34 PM
No Title
1 peak
1,388.056
856.4
Relative Intensity (%)
m/z
DI 50
ISV 5000
IN 650
OR 120
R0 30
M1 1000
RE1 121.0000
DM1 0
R1 27.2
L7 -10
R2 -70
M3 1000
RE3 118
DM3 0.060
RX -30
R3 -70
L9 150
FP -50
MU -5000
CC 10
DI µA 1.7
CGT -2.6
IS v 5095.3
B-RAM -10,004.9

Appendix A3:

NMR and Mass Spectroscopy data for **11**

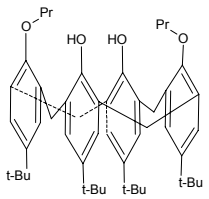

Dipropyl-4-tert-butylcalix[4]arene

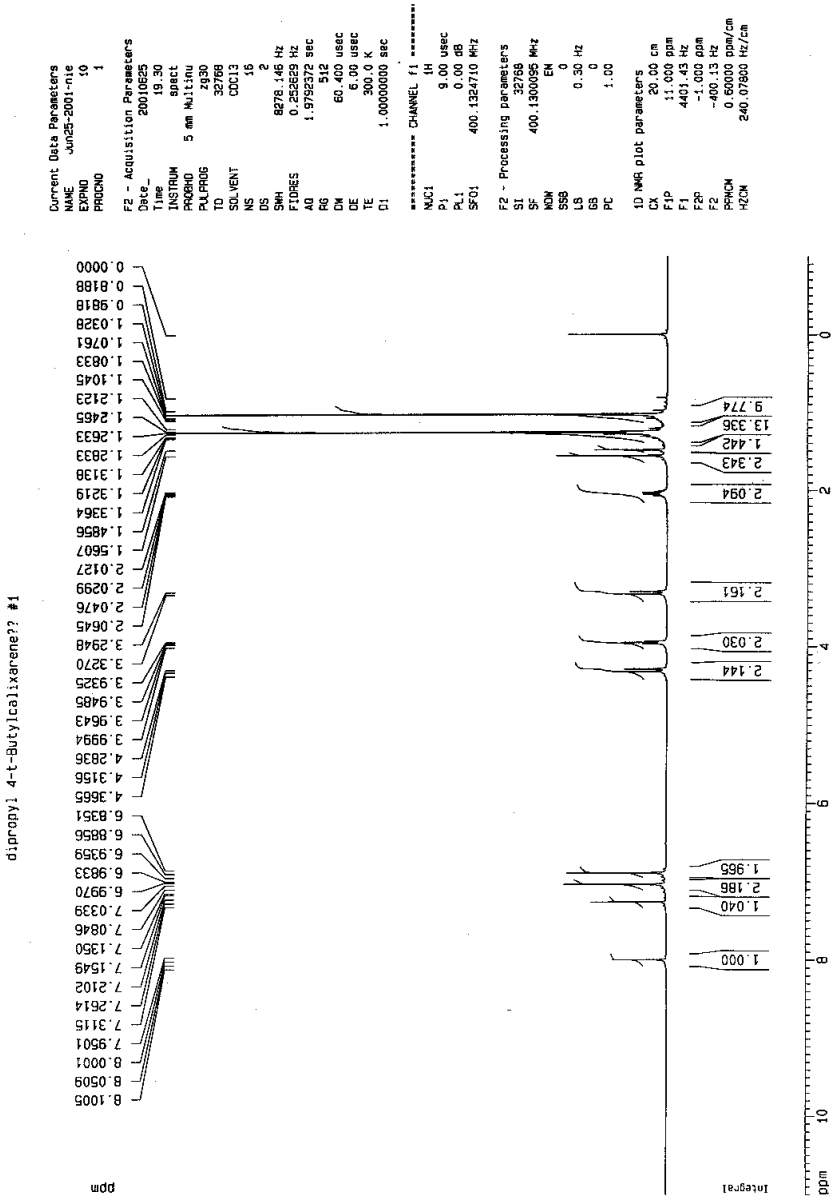

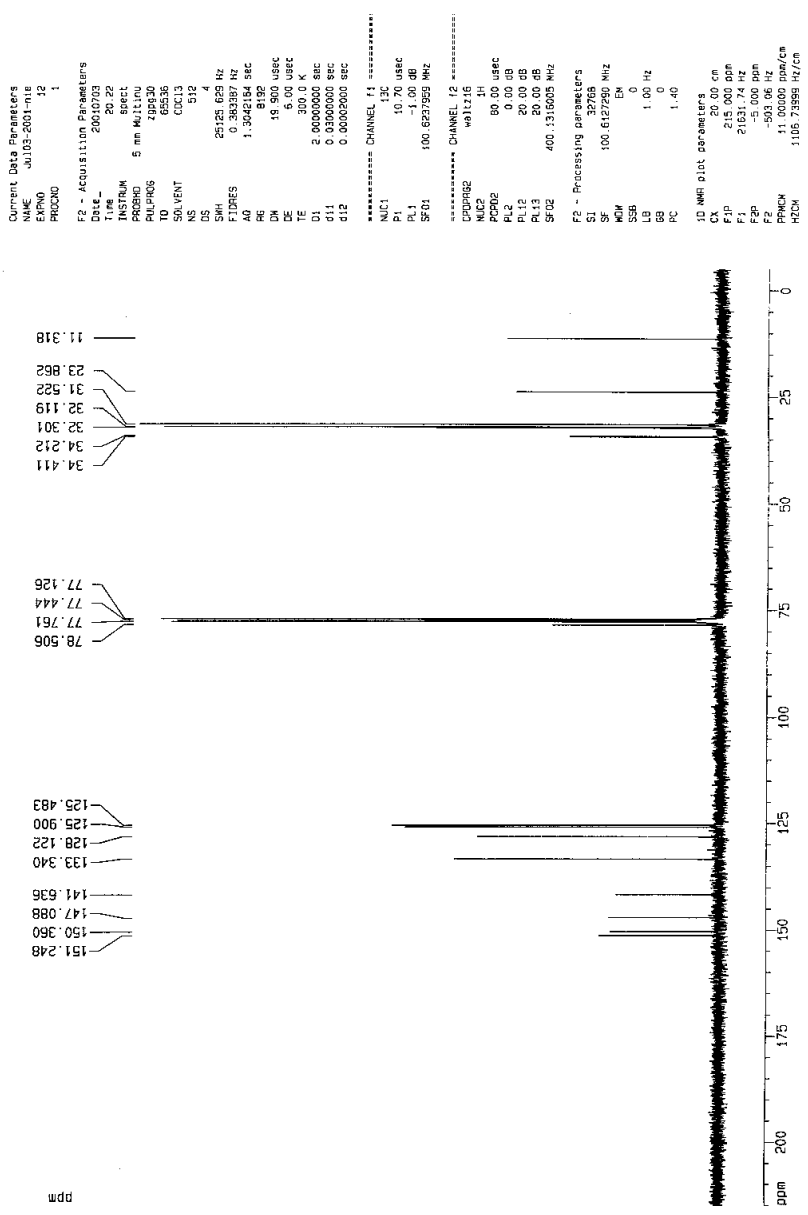
Current Data Parameters
NAME Ju103-2001-nie
EXPNO 12
PROCNO 1
F2 - Acquisition Parameters
Date_ 20010703
Time 20.22
INSTRUM spect
PROBHD 5 mm Multinu
PULPROG zgpg30
TD 65536
SOLVENT CDCl3
NS 512
DS 4
SWH 25125.629 Hz
FIDRES 0.383397 Hz
AQ 1.3042184 sec
RG 8192
DW 19.900 usec
DE 6.00 usec
TE 300.0 K
D1 2.00000000 sec
d11 0.03000000 sec
d12 0.00002000 sec
======== CHANNEL f1 ========
NUC1 13C
P1 10.70 usec
PL1 -1.00 dB
SFO1 100.6257959 MHz
======== CHANNEL f2 ========
CPDPRG2 waltz16
NUC2 1H
PCPD2 80.00 usec
PL2 0.00 dB
PL12 20.00 dB
PL13 20.00 dB
SFO2 400.1316005 MHz
F2 - Processing parameters
SI 32768
SF 100.6127290 MHz
WDW EM
SSB 0
LB 1.00 Hz
GB 0
PC 1.40
1D NMR plot parameters
CX 20.00 cm
F1P 215.000 ppm
F1 21631.74 Hz
F2P -5.000 ppm
F2 -503.06 Hz
PPMCM 11.00000 ppm/cm
HZCM 1106.73999 Hz/cm
11.318
23.862
31.522
32.119
32.301
34.212
34.411
77.126
77.444
77.761
78.506
125.483
125.900
128.122
133.340
141.636
147.088
150.360
151.248
ppm
0
25
50
75
100
125
150
175
200

Dipropyl-(di-2-chloroethoxy)-4-tert-butylcalix[4]arene

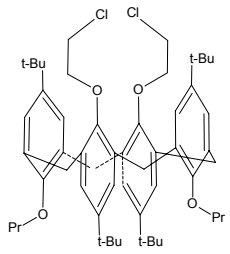

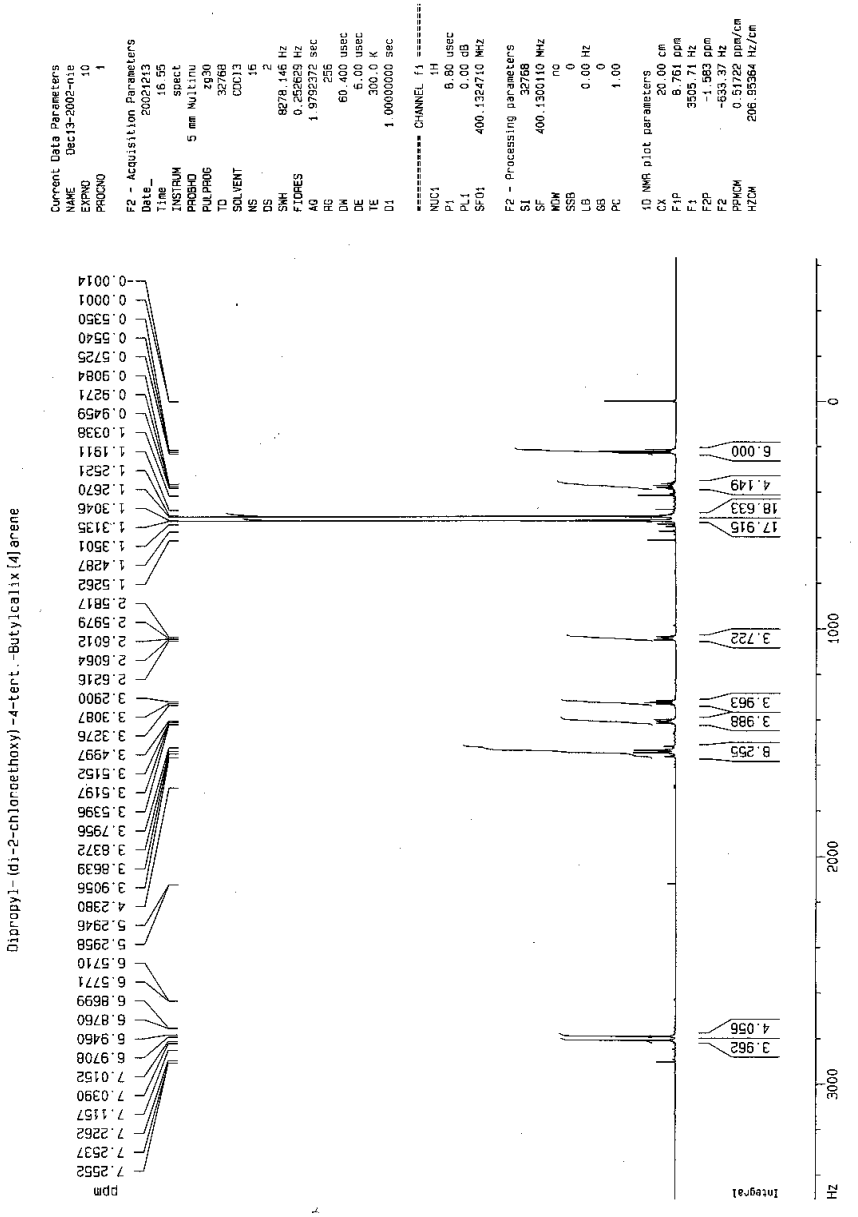

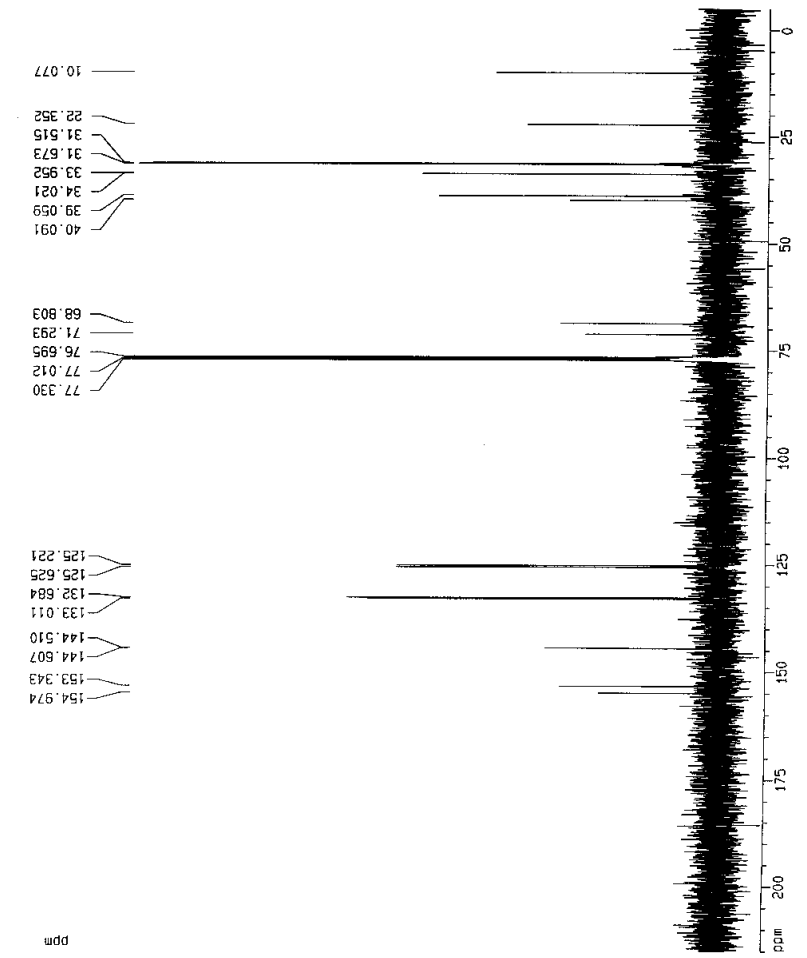
Current Data Parameters
NAME Dec13-2002-nie
EXPNO 11
PROCNO 1
F2 - Acquisition Parameters
Date_ 20021213
Time 17.24
INSTRUM spect
PROBHD 5 mm Multinu
PULPROG zgpg30
TD 65536
SOLVENT CDCl3
NS 512
DS 4
SWH 25125.629 Hz
FIDRES 0.383387 Hz
AQ 1.3042164 sec
RG 1024
DW 19.900 usec
DE 6.00 usec
TE 300.0 K
D1 2.00000000 sec
d11 0.03000000 sec
d12 0.00002000 sec
======== CHANNEL f1 ========
NUC1 13C
P1 8.70 usec
PL1 0.00 dB
SFO1 100.6237959 MHz
======== CHANNEL f2 ========
CPDPRG2 waltz16
NUC2 1H
PCPD2 107.00 usec
PL2 0.00 dB
PL12 23.00 dB
PL13 23.00 dB
SFO2 400.1316005 MHz
F2 - Processing parameters
SI 32768
SF 100.6127682 MHz
WDW EM
SSB 0
LB 1.00 Hz
GB 0
PC 1.40
1D NMR plot parameters
CX 20.00 cm
F1P 215.000 ppm
F1 21631.75 Hz
F2P -5.000 ppm
F2 -503.06 Hz
PPMCM 11.00000 ppm/cm
HZCM 1106.74048 Hz/cm
10.077
22.352
31.515
31.673
33.952
34.021
39.059
40.091
68.803
71.293
76.695
77.012
77.330
125.221
125.625
132.684
133.011
144.510
144.607
153.343
154.974
ppm
0
25
50
75
100
125
150
175
200

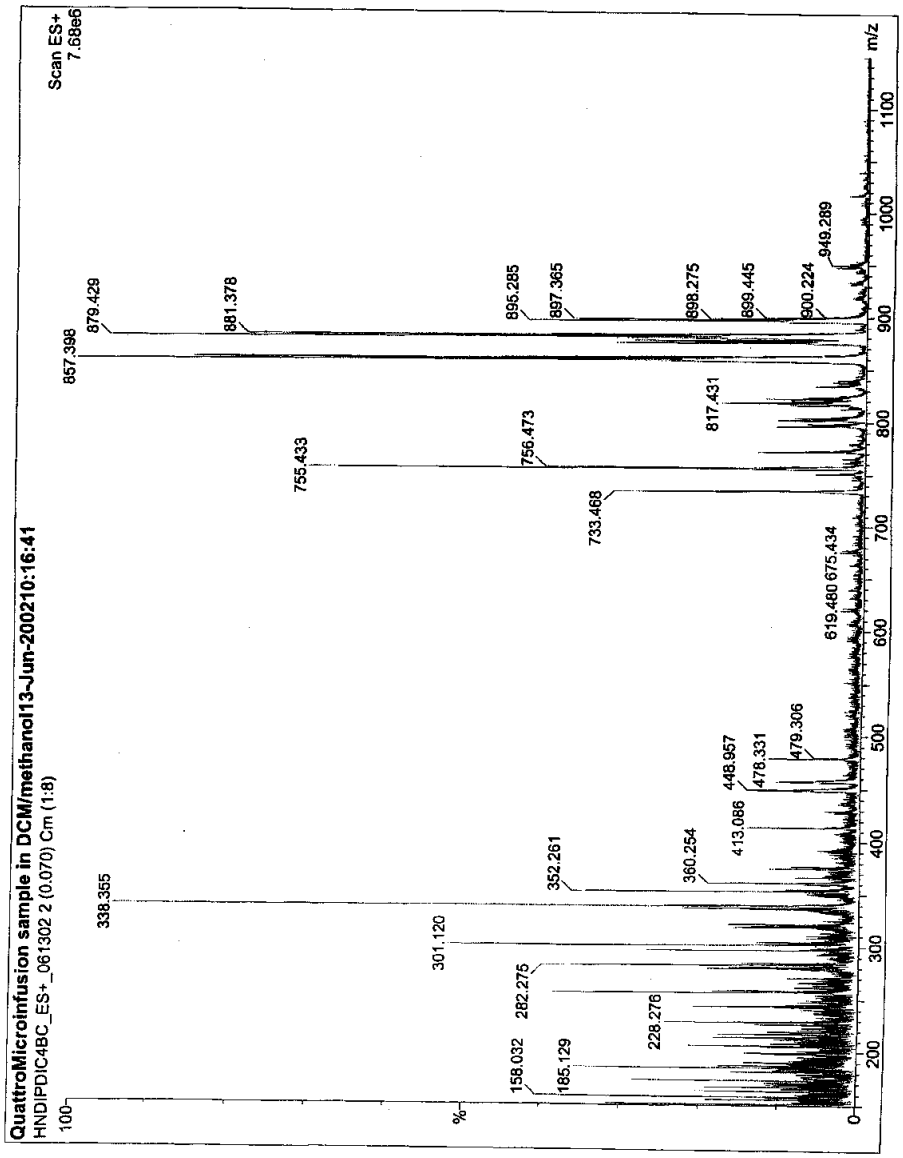

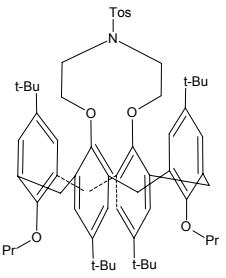

N-Tosyl 25,27-bis(1-propyloxy)-4-tert-butylcalix[4]arene-azacrown-3

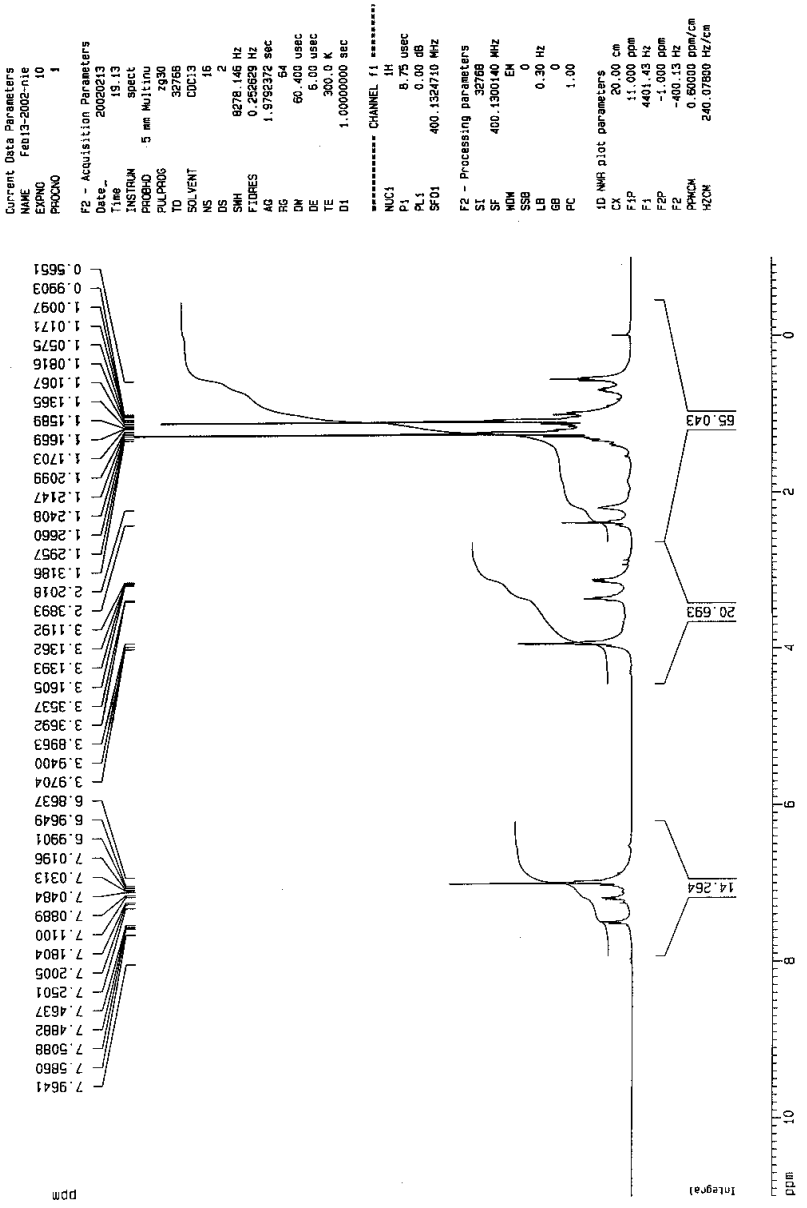

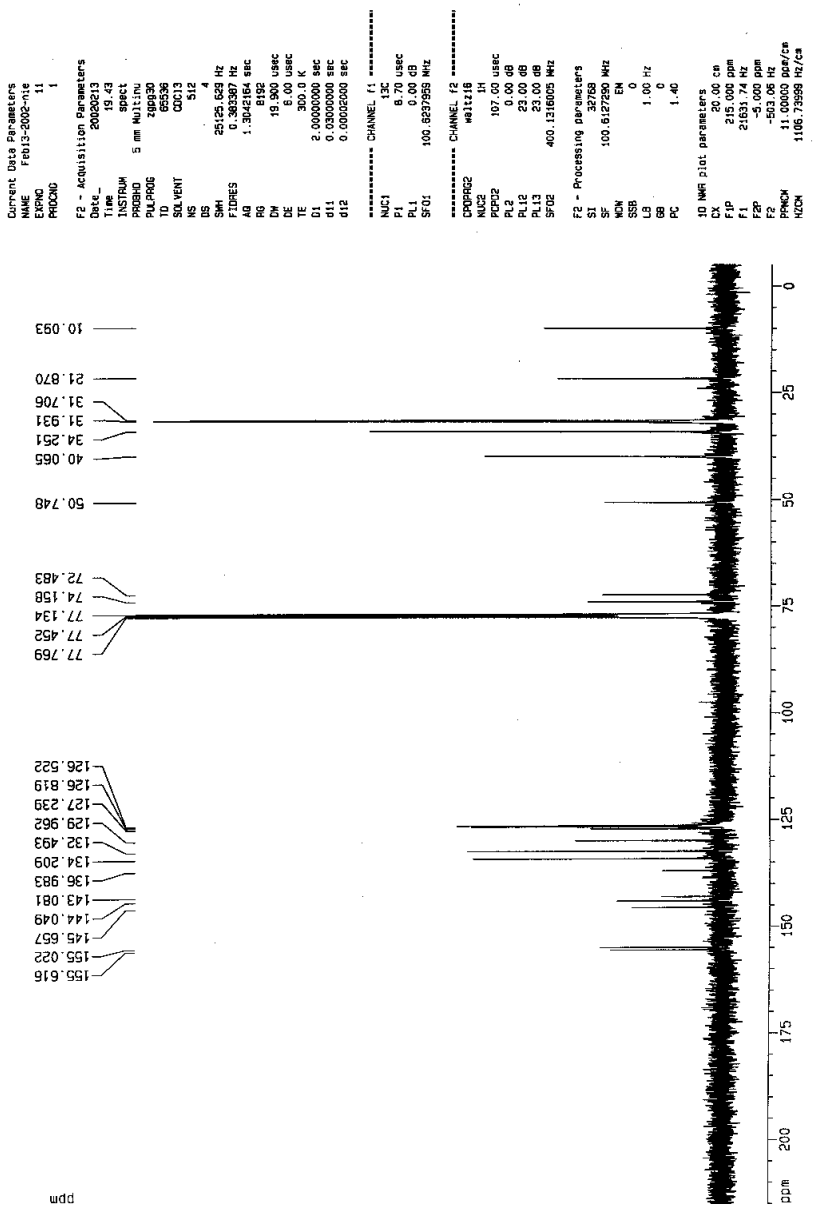
Current Data Parameters
NAME Feb13-2002-nie
EXPNO 11
PROCNO 1
F2 - Acquisition Parameters
Date_ 20020213
Time 19.43
INSTRUM spect
PROBHD 5 mm Multinu
PULPROG zgpg30
TD 65536
SOLVENT CDCl3
NS 512
DS 4
SWH 25125.629 Hz
FIDRES 0.383307 Hz
AQ 1.3042164 sec
RG 8192
DW 19.900 usec
DE 6.00 usec
TE 300.0 K
D1 2.00000000 sec
d11 0.03000000 sec
d12 0.00002000 sec
CHANNEL f1
NUC1 13C
P1 8.70 usec
PL1 0.00 dB
SFO1 100.6237959 MHz
CHANNEL f2
CPDPRG2 waltz16
NUC2 1H
PCPD2 107.00 usec
PL2 0.00 dB
PL12 23.00 dB
PL13 23.00 dB
SFO2 400.1316005 MHz
F2 - Processing parameters
SI 32768
SF 100.6127290 MHz
WDW EM
SSB 0
LB 1.00 Hz
GB 0
PC 1.40
1D NMR plot parameters
CX 20.00 cm
F1P 215.000 ppm
F1 21631.74 Hz
F2P -5.000 ppm
F2 -503.06 Hz
PPMCM 11.00000 ppm/cm
HZCM 1106.73959 Hz/cm
10.093
21.870
31.706
31.931
34.251
40.065
50.748
72.483
74.158
77.134
77.452
77.769
126.522
126.819
127.239
129.962
132.493
134.209
136.983
143.081
144.049
145.657
155.022
155.616
ppm
0
25
50
75
100
125
150
175
200
ppm

02/21/02 THU 10:08 FAX 011

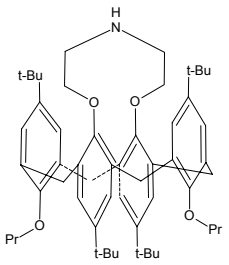

25,27-Bis(1-propyloxy)-4-tert-butylcalix[4]arene-azacrown-3

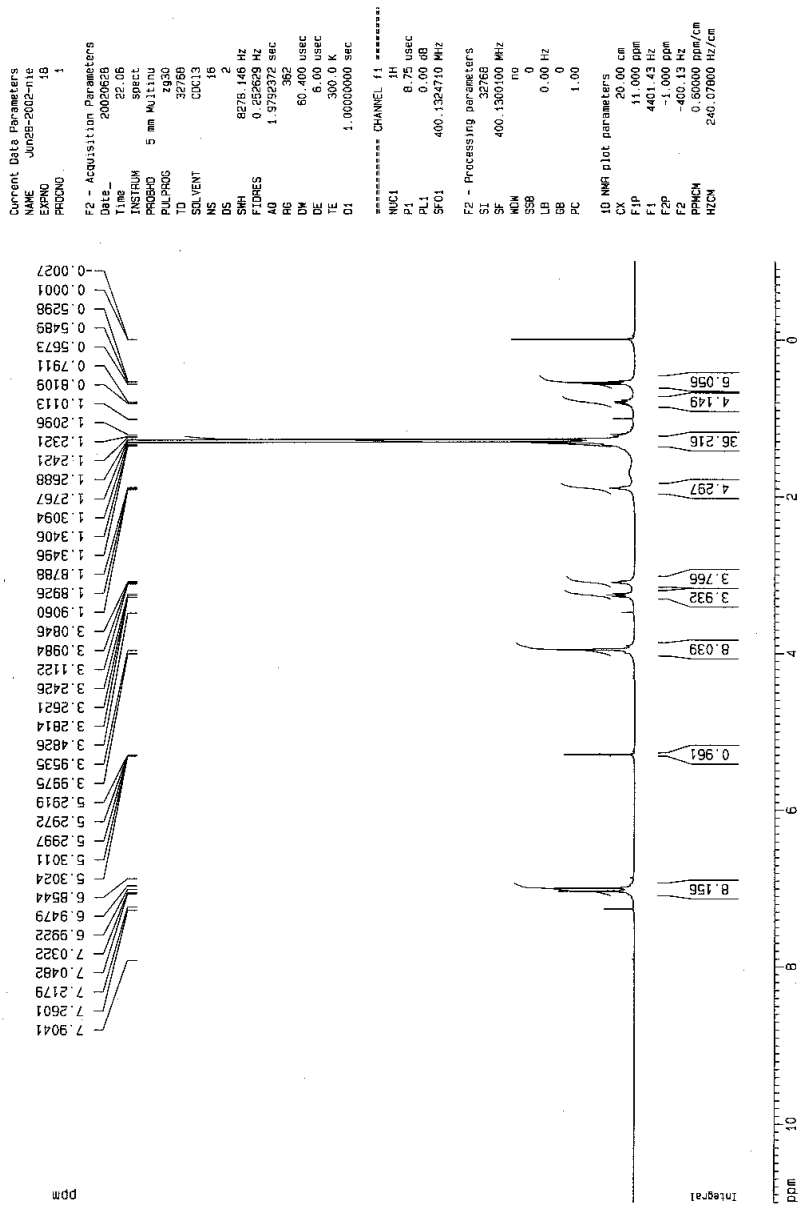

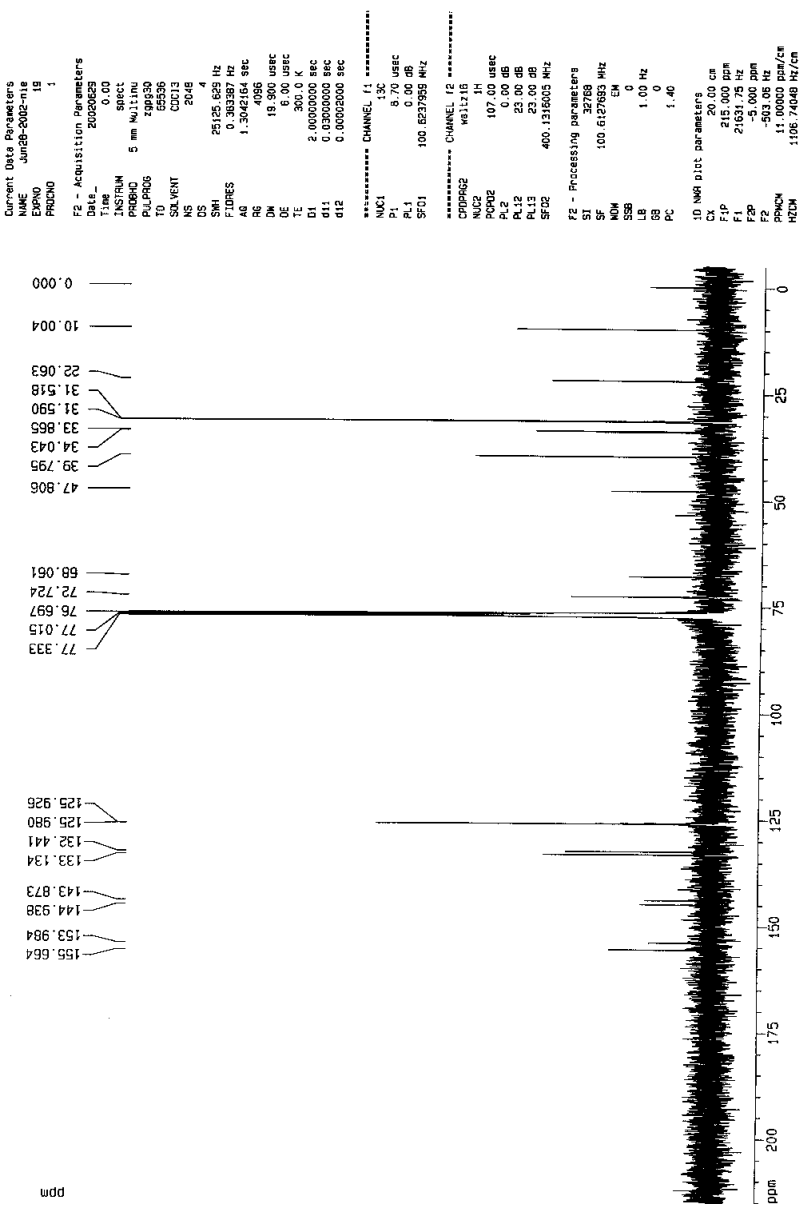
Current Data Parameters
NAME Jun28-2002-nie
EXPNO 19
PROCNO 1
F2 - Acquisition Parameters
Date_ 20020628
Time 0.00
INSTRUM spect
PROBHD 5 mm Multinu
PULPROG zgpg30
TD 65536
SOLVENT CDCl3
NS 4
DS 4
SWH 25125.629 Hz
FIDRES 0.383387 Hz
AQ 1.3042164 sec
RG 4096
DW 19.900 usec
DE 6.00 usec
TE 300.0 K
D1 2.00000000 sec
D11 0.03000000 sec
D12 0.00002000 sec
CHANNEL f1
NUC1 13C
P1 8.70 usec
PL1 0.00 dB
SFO1 100.6237959 MHz
CHANNEL f2
CPDPRG2 waltz16
NUC2 1H
PCPD2 107.60 usec
PL2 0.00 dB
PL12 23.00 dB
PL13 23.00 dB
SFO2 400.1316005 MHz
F2 - Processing parameters
SI 32768
SF 100.6127693 MHz
WDW EM
SSB 0
LB 1.00 Hz
GB 0
PC 1.40
1D NMR plot parameters
CX 20.00 cm
F1P 215.000 ppm
F1 21631.75 Hz
F2P -5.000 ppm
F2 -503.06 Hz
PPMCM 11.00000 ppm/cm
HZCM 1106.74048 Hz/cm
0.000
10.004
22.063
31.518
31.590
33.865
34.043
39.795
47.806
68.061
72.724
76.697
77.015
77.333
125.926
125.980
132.441
133.134
143.873
144.938
153.984
155.664
ppm
0
25
50
75
100
125
150
175
200

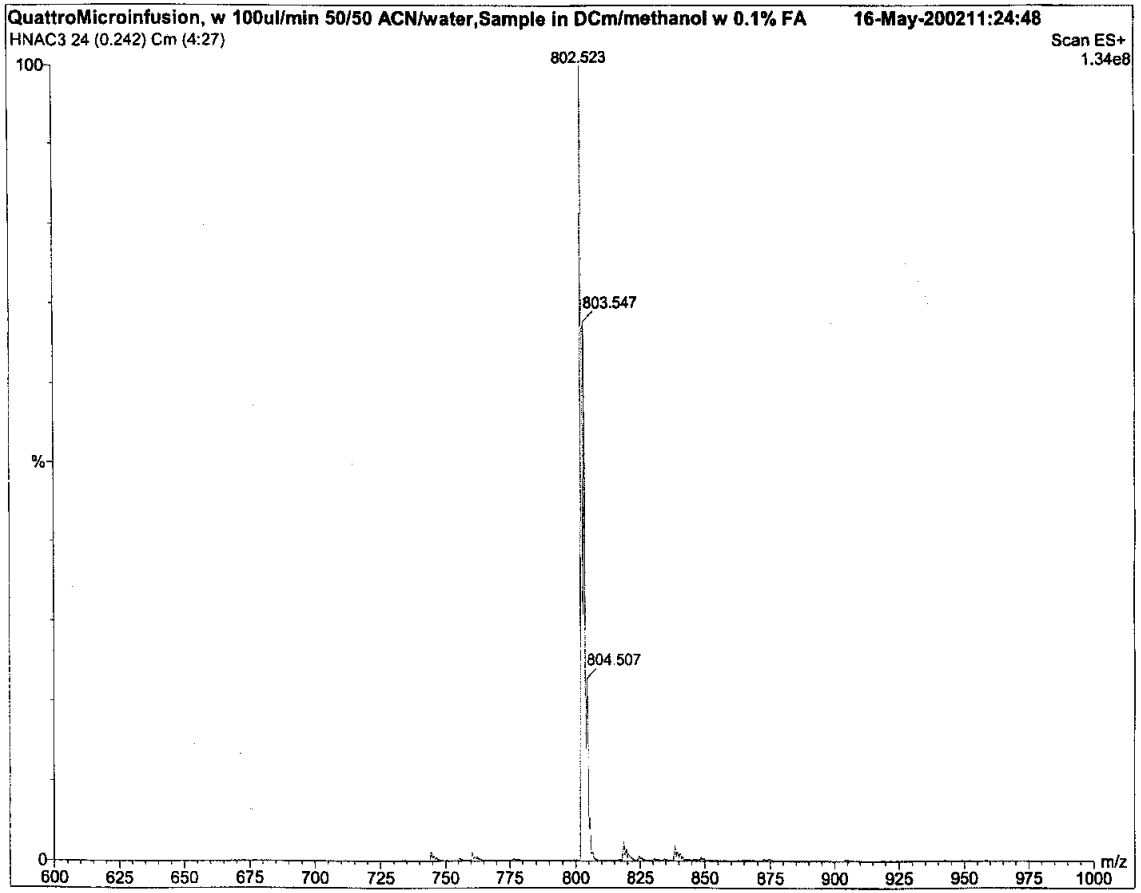
QuattroMicroinfusion, w 100ul/min 50/50 ACN/water,Sample in DCm/methanol w 0.1% FA
16-May-200211:24:48
HNAC3 24 (0.242) Cm (4:27)
Scan ES+
1.34e8
802.523
803.547
804.507
100
%
0
600
625
650
675
700
725
750
775
800
825
850
875
900
925
950
975
1000
m/z
05/16/02 THU 13:45 FAA

Compound (11)

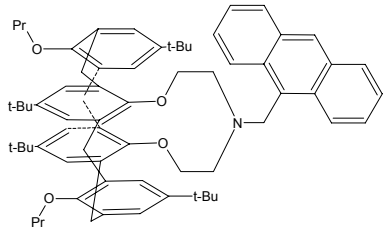
Pr
O
t-Bu
t-Bu
O
N
t-Bu
O
t-Bu
O
Pr

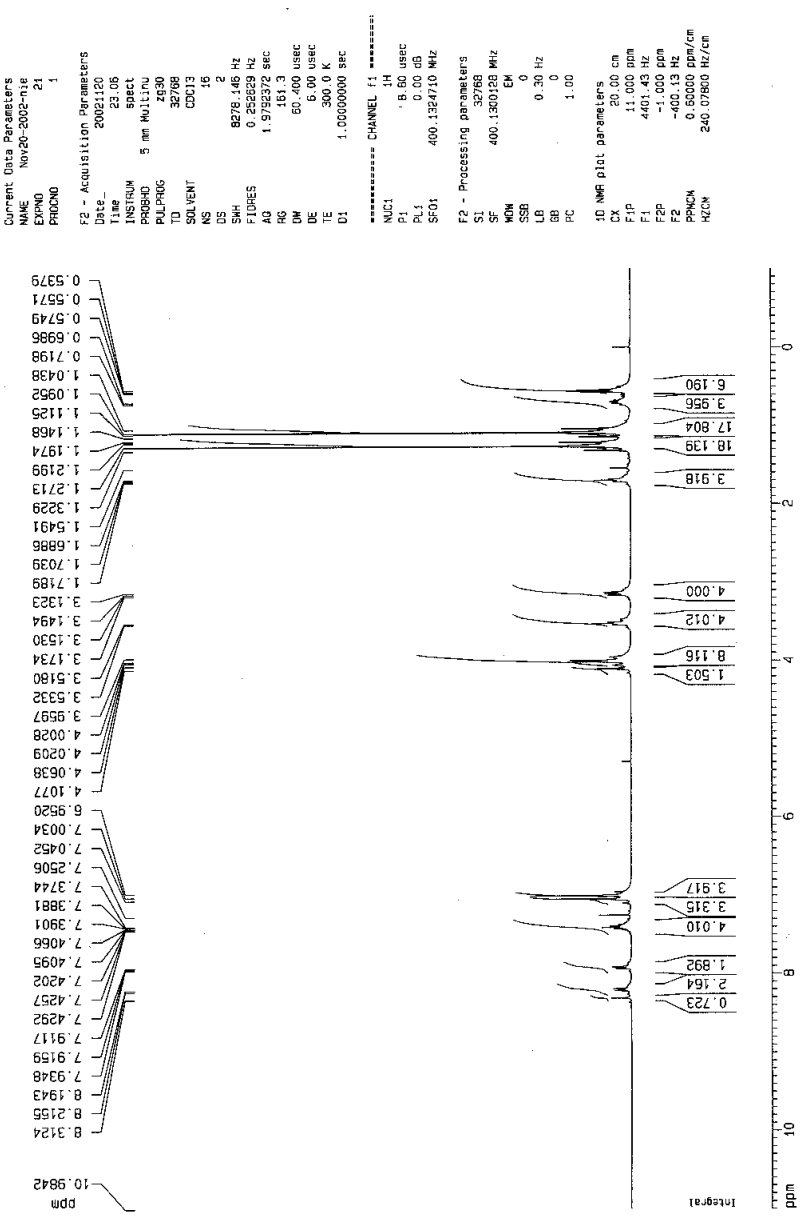
Current Data Parameters
NAME Nov20-2002-nie
EXPNO 21
PROCNO 1
F2 - Acquisition Parameters
Date_ 20021120
Time 23.06
INSTRUM spect
PROBHD 5 mm Multinu
PULPROG zg30
TD 32768
SOLVENT CDCl3
NS 16
DS 2
SWH 8278.146 Hz
FIDRES 0.252829 Hz
AQ 1.9792372 sec
RG 161.3
DW 60.400 usec
DE 6.00 usec
TE 300.0 K
D1 1.00000000 sec
======== CHANNEL f1 ========
NUC1 1H
P1 8.60 usec
PL1 0.00 dB
SFO1 400.1324710 MHz
F2 - Processing parameters
SI 32768
SF 400.1300128 MHz
WDW EM
SSB 0
LB 0.30 Hz
GB 0
PC 1.00
1D NMR plot parameters
CX 20.00 cm
F1P 11.000 ppm
F1 4401.43 Hz
F2P -1.000 ppm
F2 -400.13 Hz
PPMCM 0.50000 ppm/cm
HZCM 240.07800 Hz/cm
10.9842
8.3124
8.2155
8.1943
7.9348
7.9159
7.9117
7.4292
7.4257
7.4202
7.4095
7.4066
7.3901
7.3881
7.3744
7.2506
7.0452
7.0034
6.9520
4.1077
4.0638
4.0209
4.0028
3.9597
3.5332
3.5180
3.1734
3.1530
3.1494
3.1323
1.7189
1.7039
1.6886
1.5491
1.3229
1.2713
1.2199
1.1974
1.1468
1.1125
1.0952
1.0438
0.7198
0.6986
0.5749
0.5571
0.5379
6.190
3.956
17.804
18.139
3.918
4.000
4.012
8.116
1.503
3.917
3.315
4.010
1.892
2.164
0.723
Integral
ppm

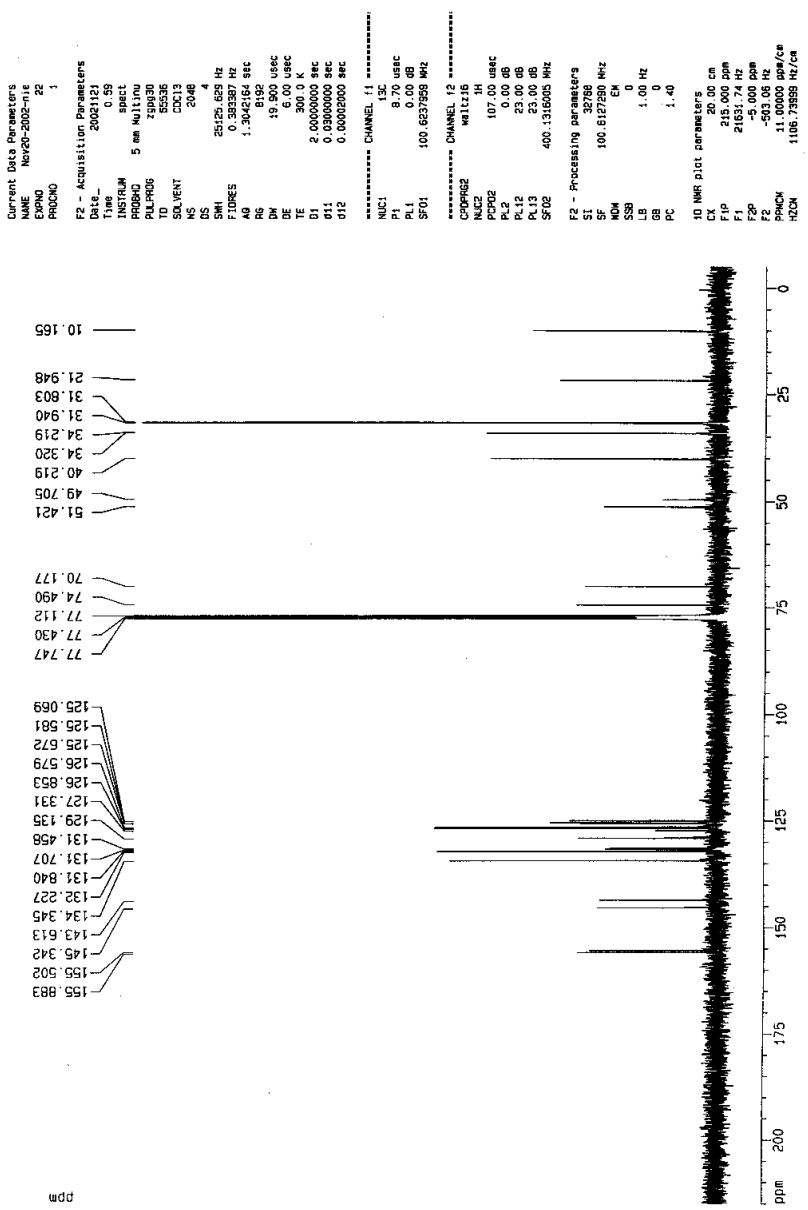
Current Data Parameters
NAME Nov20-2002-nie
EXPNO 22
PROCNO 1
F2 - Acquisition Parameters
Date_ 20021121
Time 0.59
INSTRUM spect
PROBHD 5 mm Multinu
PULPROG zgpg30
TD 65536
SOLVENT CDCl3
NS 2048
DS 4
SWH 25125.629 Hz
FIDRES 0.383387 Hz
AQ 1.3042164 sec
RG 8192
DW 19.900 usec
DE 6.00 usec
TE 300.0 K
D1 2.00000000 sec
D11 0.03000000 sec
D12 0.00002000 sec
CHANNEL f1
NUC1 13C
P1 8.70 usec
PL1 0.00 dB
SFO1 100.6237959 MHz
CHANNEL f2
CPDPRG2 waltz16
NUC2 1H
PCPD2 107.00 usec
PL2 0.00 dB
PL12 23.00 dB
PL13 23.00 dB
SFO2 400.1316005 MHz
F2 - Processing parameters
SI 32768
SF 100.6127690 MHz
WDW EM
SSB 0
LB 1.00 Hz
GB 0
PC 1.40
1D NMR plot parameters
CX 20.00 cm
F1P 215.000 ppm
F1 21631.74 Hz
F2P -5.000 ppm
F2 -503.05 Hz
PPMCM 11.00000 ppm/cm
HZCM 1106.73959 Hz/cm
10.165
21.948
31.803
31.940
34.219
34.320
40.219
49.705
51.421
70.177
74.490
77.112
77.430
77.747
125.069
125.581
125.672
126.579
126.853
127.331
129.135
131.458
131.707
131.840
132.227
134.345
143.613
145.342
155.502
155.883
ppm
0
25
50
75
100
125
150
175
200
ppm

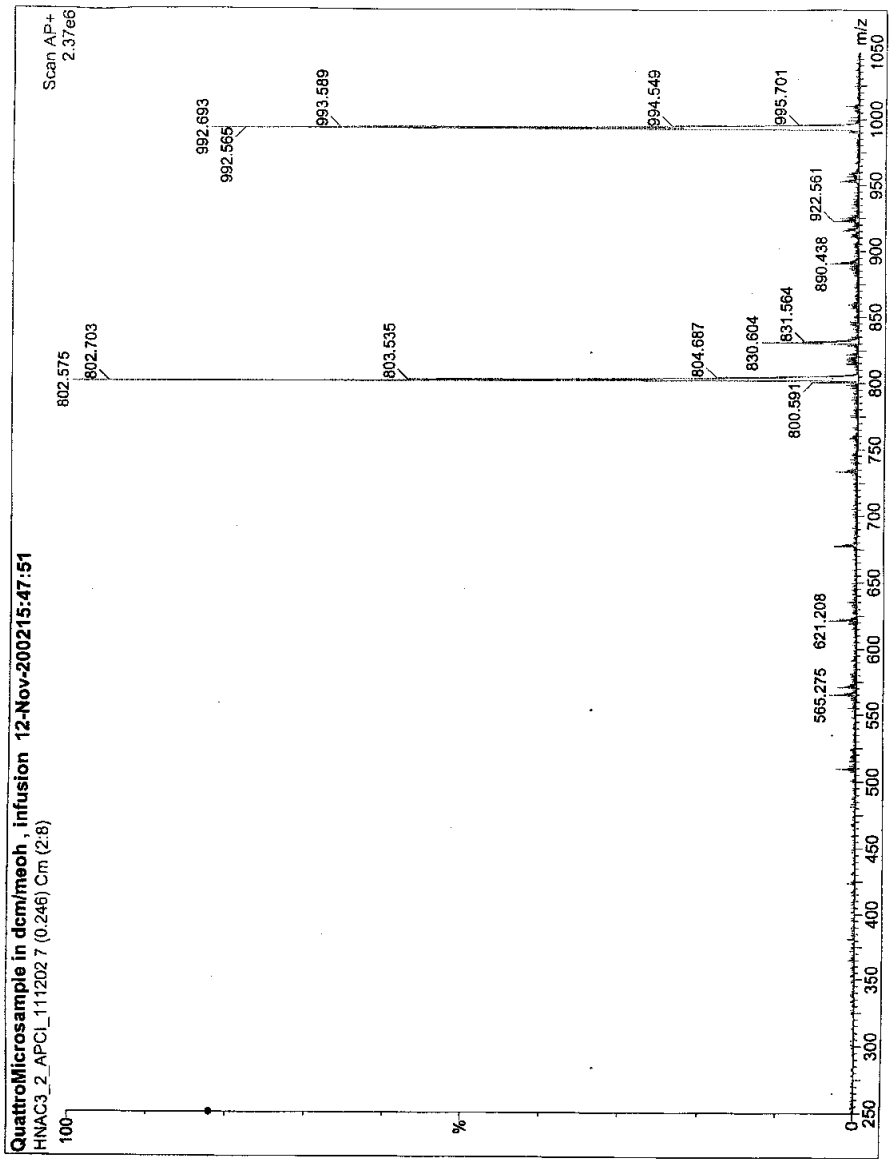
QuattroMicrosample in dcm/meoh , infusion 12-Nov-200215:47:51
HNAC3_2_APCI_111202 7 (0.246) Cm (2:8)
Scan AP+
2.37e6
100
%
0
m/z
250
300
350
400
450
500
550
600
650
700
750
800
850
900
950
1000
1050
565.275
621.208
800.591
802.575
802.703
803.535
804.687
830.604
831.564
890.438
922.561
992.565
992.693
993.589
994.549
995.701

Appendix A4:

Experimental, NMR and Mass Spectroscopy data for **21**, based on a modified procedure.[106]

4-carboxydihydrotetramethylrosamine (19)

To a 115 ml solution of 3:3 H_2SO_4/H_20 was added 12.5 g (9.1 mmol) of 3-dimehtylaminophenol and 6.84 g (4.6 mol) of 4-carboxybenzaldehyde. This was stirred under light reflux for 18 hr. The pink suspension was neutralized with 90% KOH to pH 7.0. The resulting purple suspension is obtained by filtration, washed with water and dried. The 4 g of the crude product was taken up in EtOAc and purified on silica gel (EtOAc). This gave 3.2 g of light pink product, yield 34%. No yield was given in original synthesis. Recrystallization from DCM/Hexane also proved to be effective. R_f =.74 (EtOAc). H^1 NMR (400 MHz, MeOD-d_4) δ 2.80 (s, 12 H), 4.98 (s, H), 6.32-6.35 (m, 4H), 6.74 (d, *J* = 8.1, 2H), 7.02 (d, *J* = 8.2, 2H), 7.70 (d, *J* = 8.2, 2H).

dihydro-4-(hydroxymethyl)tetramethylrosamine (20)

2.2 g of **19** (5.66 mmol) was dissolved into 100 ml dry THF to which .43 g (11.3 mmol) of $LiAlH_4$ was added. This was stirred under N_2 for 2.5 hr. at which point the excess $LiAlH_4$ was destroyed with stoichiometric amounts of water. The oxide was then filtered off and the solvent removed *in vacuo* to give 1.6 of a pink solid, yield 75.5%. This was used without further purification. R_f = .50 (1:1 hexane/EtOAc). H^1 NMR (400 MHz, $CDCl_3$) δ 2.93 (s, 12H), 4.62 (s, 2H), 5.05 (s, 1H), 6.38 (d, *J* = 8.4, 2H), 6.44 (s, 2H), 6.83 (d, *J* = 8.4, 2H), 7.18 (d, *J* = 6.3, 2H), 7.24 (d, *J* = 7.60, 2H).

4-bromomethyldihydrotetramethylrosamine (21)

100 mg (.27 mmol) of **20** was dissolved in benzene t which .6 eq of PBr_3 was added. This was stirred under reflux for 4 hr. at which point the solvent was removed *in vacuo*. The residue was taken up in EtOAc and purified by chromatography on silica gel (1:1 hexane/EtOAc) yielding 16 mg of product. R_f = .84 (1:1 hexane/EtOAc).). H^1 NMR (400 MHz, $CDCl_3$) δ 2.93 (s, 12 H), 4.44 (s, 2H), 5.07 (s, 1H), 6.38 (d, *J* = 8.5, 2H), 6.44 (s, 2H), 6.83 (d, *J* = 8.5, 2H), 7.15 (d, *J* = 8.0, 2H), 7.25 (d, *J* = 8.0, 2H). ESI MS m/z calcd. for $C_{24}H_{26}Br^{79}N_2O$ [$M+H^+$], 435.102, found 435.081(55), for $C_{24}H_{26}Br^{80}N_2O$ [$M+H^+$], 437.092, found 437.034(55).

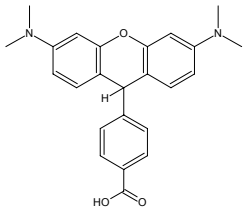

4-carboxydihydrotetramethylrosamine (19)

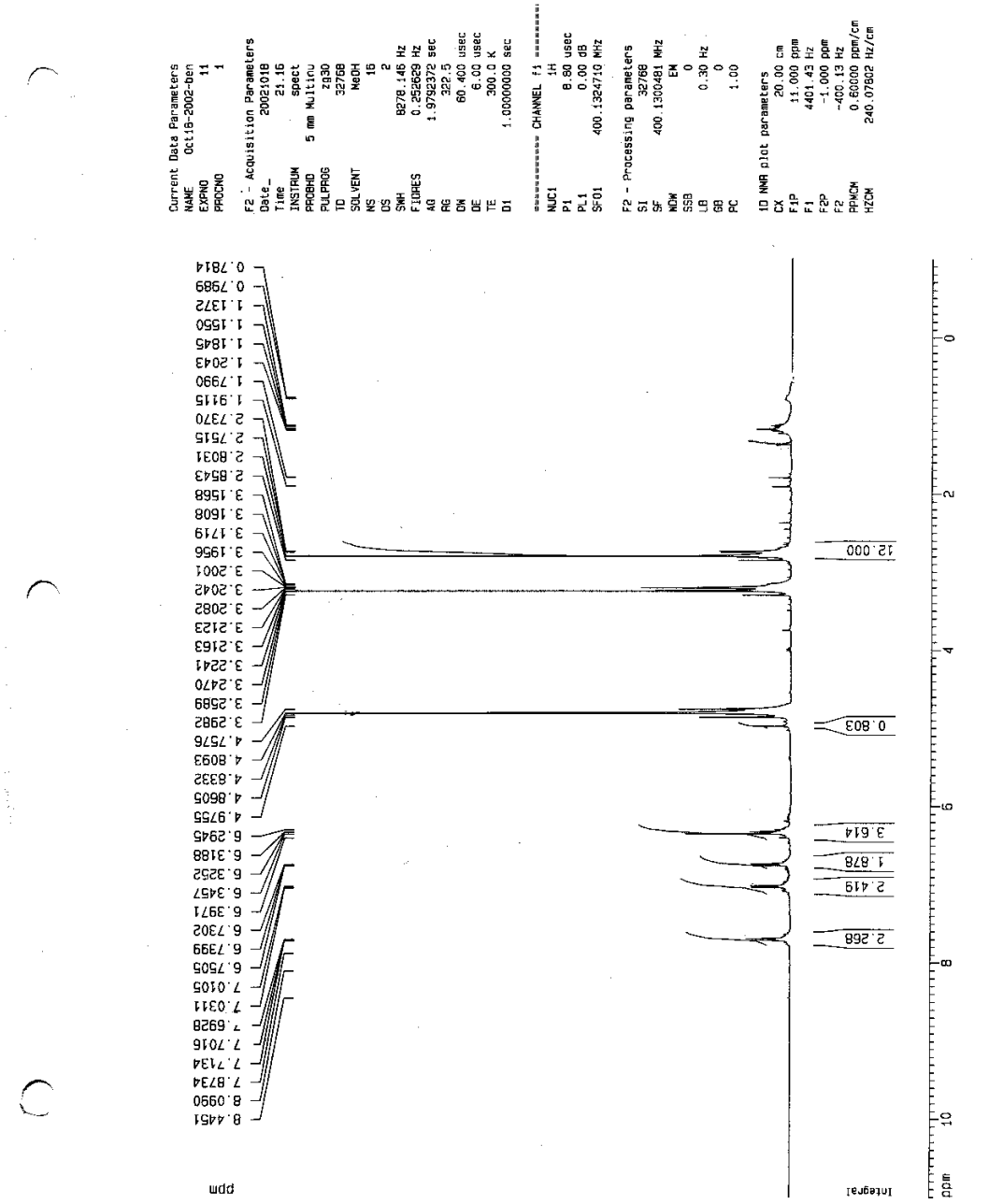

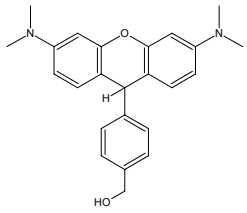

Dihydro-4-(hydroxymethyl)tetramethylrosamine (20)

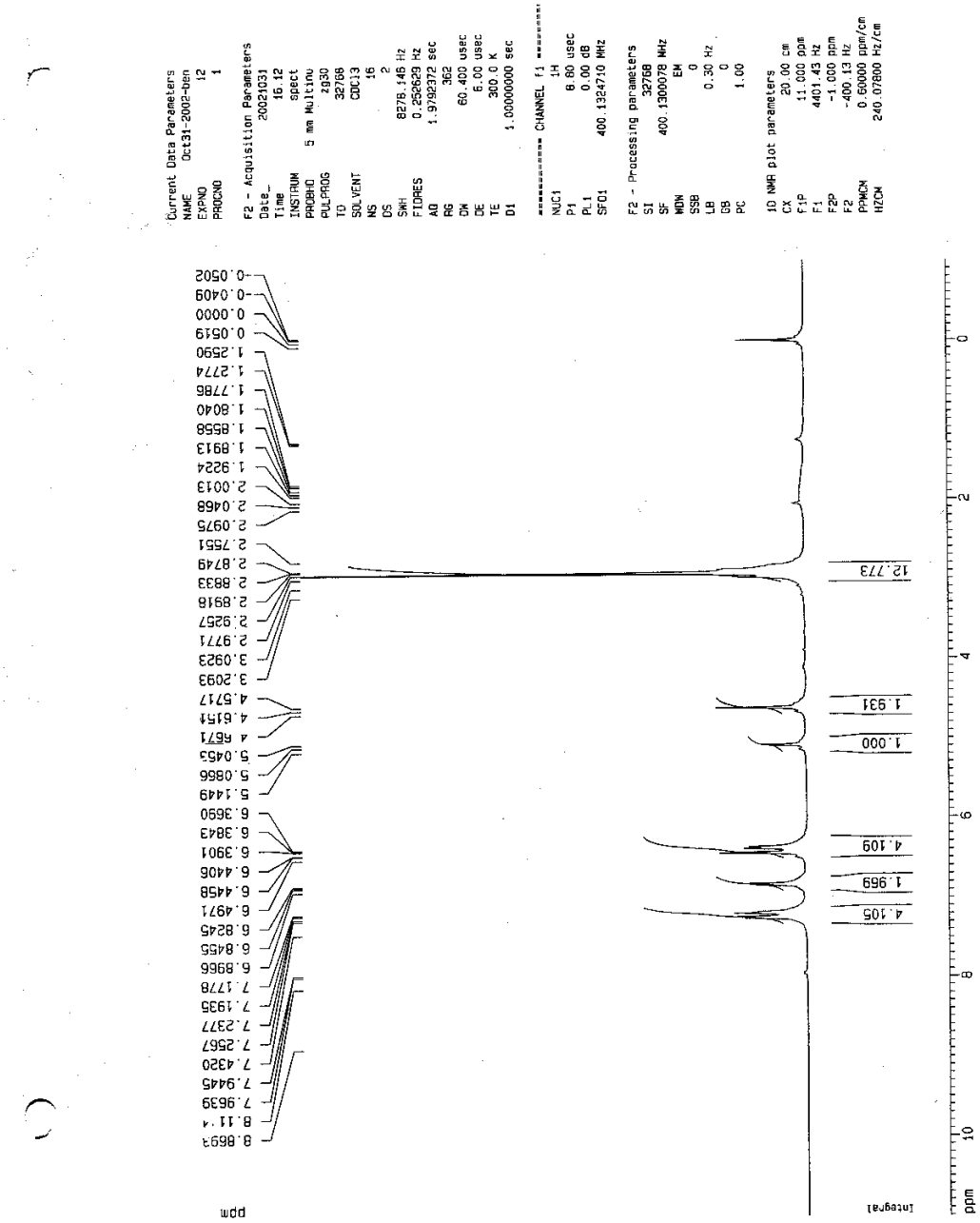

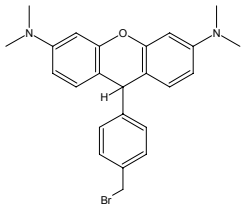

4-bromomethyldihydrotetramethylrosamine (21)

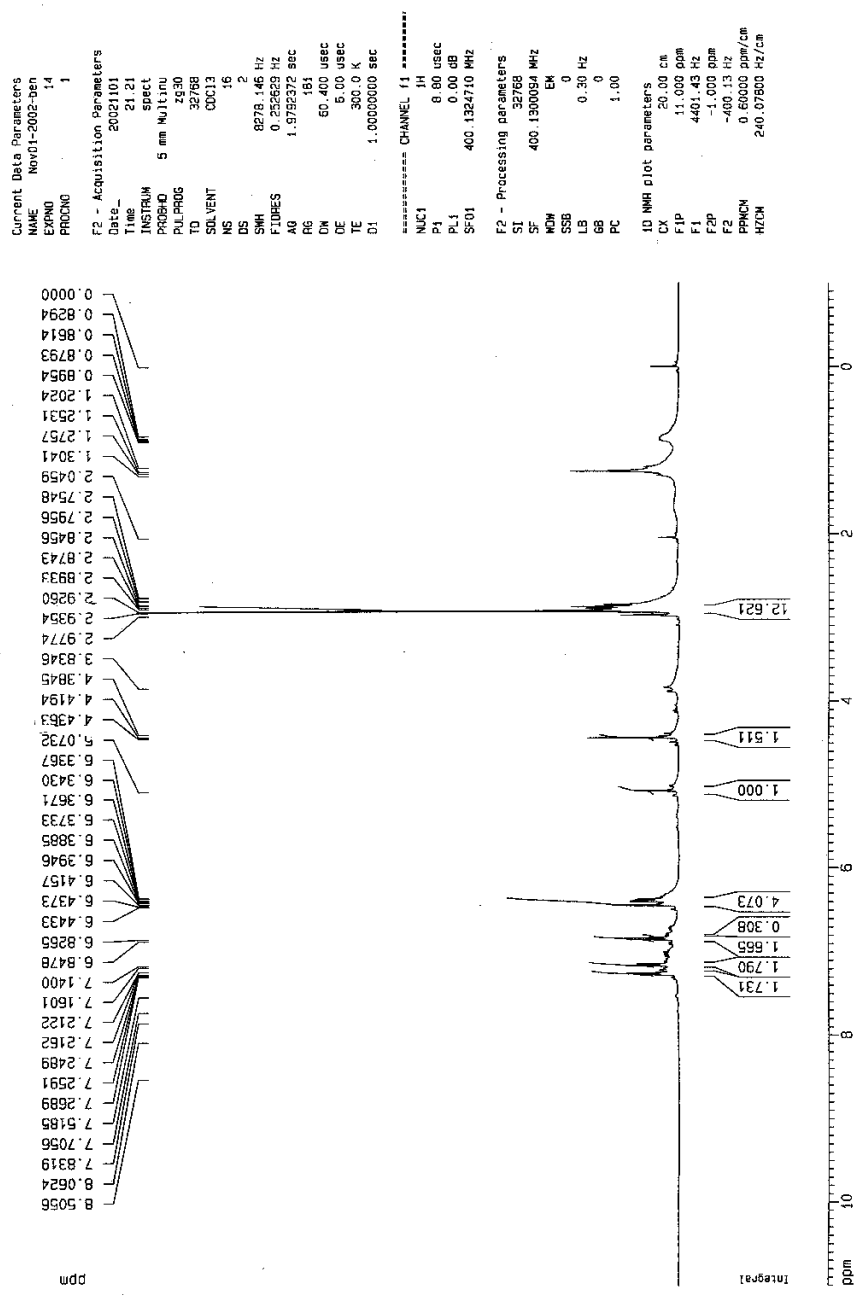

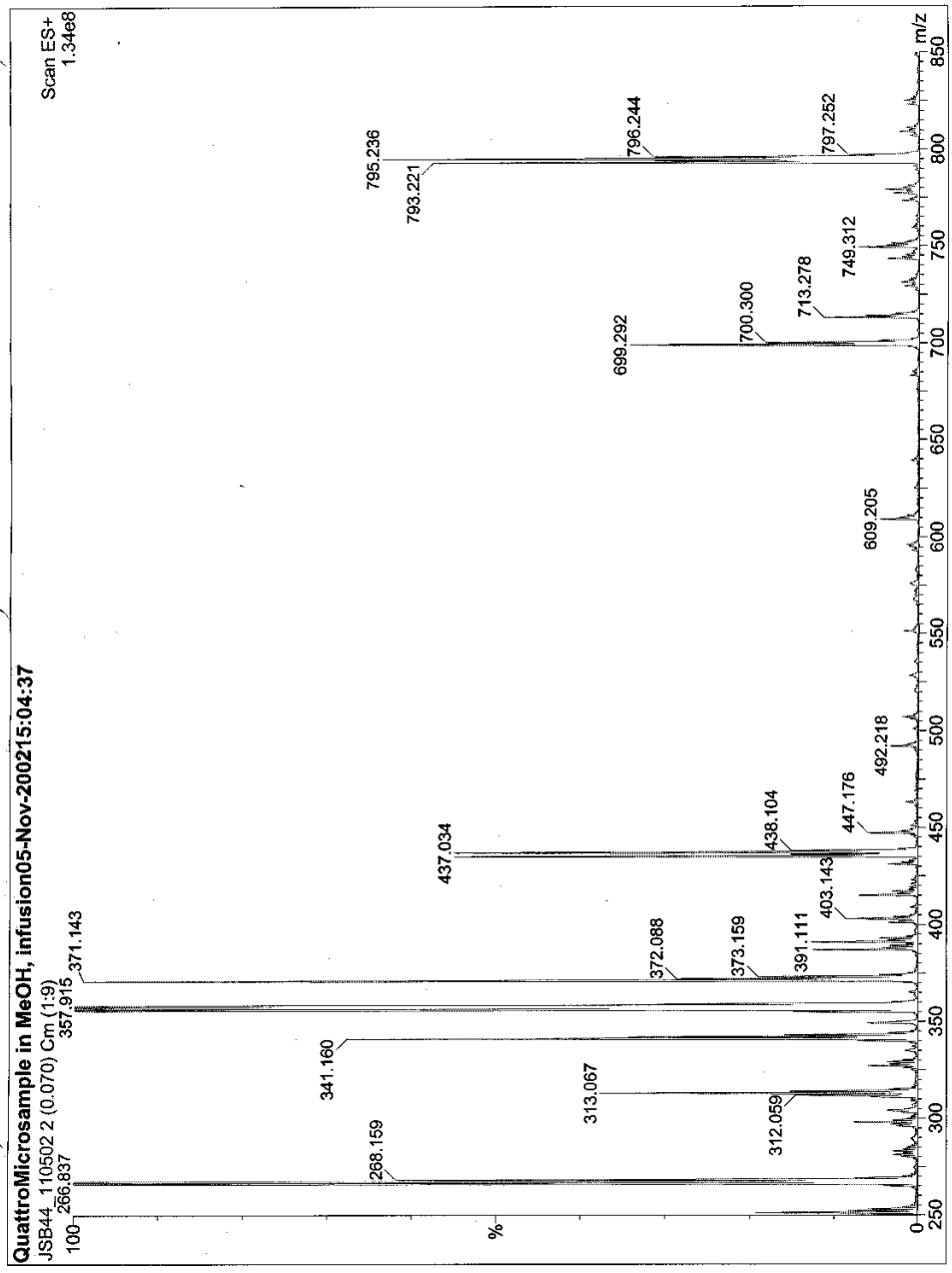
QuattroMicrosample in MeOH, infusion05-Nov-200215:04:37
JSB44_110502 2 (0.070) Cm (1:9)
Scan ES+
1.34e8
100
%
0
m/z
250
300
350
400
450
500
550
600
650
700
750
800
850
266.837
268.159
312.059
313.067
341.160
357.915
371.143
372.088
373.159
391.111
403.143
437.034
438.104
447.176
492.218
609.205
699.292
700.300
713.278
749.312
793.221
795.236
796.244
797.252

Appendix A5:
Experimental details, NMR and Mass Spectroscopy data for compound **28**

BzO-L-lac-D-val-N-tBoc (23): Based on a modified procedure.[42] On an ice bath, 20.6 g (.0948 mol) of HO-D-valine-N-tBoc was dissolved in 150 DCM to which 14.8 ml (1 eq.) of DIPCDI, 1.16 g DMAP (.1eq.) and 17.1 g (1eq.) of BzO-L-lactic acid (**1**, prepared as previously described) was added. The reaction mixture was then allowed to return to RT after 1 hr. and stirred for an additional 17 hr. The insoluble urea thus formed was filtered off and the organic phase washed thrice with 10% citric acid, thrice with saturated $NaHCO_3$, once with brine, dried over Na_2SO_4 and concentrated totally to give a colorless oil, 35.54 g, yield 96%. ^{1}H-NMR (400 MHz, $CDCl_3$), δ .90 (d, J = 6.9 Hz, 3 H), .97 (d, J = 6.8 Hz, 3H), 1.45 (s, 9H, t-Butyl), 1.51 (d, J = 7.0 Hz, 3H), 2.19 (m, 1H), 4.31 (m, 1H), 5.00 (d, J = 8.9 Hz, 1H), 5.17 (m, 3H), 7.33 (m, 5H). ^{13}C-NMR (100 MHz, $CDCl_3$) δ 16.9, 17.4 (CH_3), 28.3 (t-Butyl), 31.2 (CH_3), 58.5 (CH), 67.1 (CH_2), 69.2 (CH), 79.8 (C), 128.4, 128.5, 128.6 (CH, Ar), 135.1 (C, Ar), 155.5, 170.1, 171.5 (C=O).

BzO-L-asp(TCE)-N-tBoc. Based on a modified procedure.(Matthews, J. L., Gademann, K., Jaun, B., Seebach, D. *J. Chem. Soc.,Perkin Trans. 1* **1998,** 3331-3340.) On an ice bath, 20 g (.0618 mol) of BzO-L-asp(OH)-N-tBoc was dissolved in 150 mL DCM to which, 9.7 ml (1eq) of DIPCDI, .755 g (.1 eq) DMAP and 5.93 ml (1 eq.) 2,2,2-trichloro ethanol and was stirred for 1 hr. at which point it was allowed to return to RT and stirred for an additional 17 hr. The insoluble urea thus formed was filtered off and reaction mixture was washed thrice with 10% citric acid, thrice with saturated $NaHCO_3$, once with

brine, dried over Na_2SO_4 and concentrated totally to give 20.5 g of a white solid, yield 72.9%. R_f =.57 (3:1 Hexane/EtOAC), mp = 46-48 ºC, The NMR conforms to the literature values. ^{1}H-NMR (400 MHz, $CDCl_3$), δ 1.43 (s, 9H, t-Butyl), 3.02 (dd, *J* = 4.7, 17.2 Hz, 1H), 3.17 (dd, *J* = 4.6, 17.2 Hz, 1H), 4.66 (m, 3H), 5.19 (d, *J* = 7.1 Hz, 2H), 5.50 (d, *J* = 8.2 Hz, 1H), 7.37 (m, Ar, 5H). ^{13}C-NMR (100 MHz, $CDCl_3$) δ 28.7 (CH_3, t-butyl), 36.9 (CH), 50.3 (CH_2), 68.1 (CH_2), 74.5 (CH_2), 80.7 (C), 94.9 (C), 128.8, 128.9, 129.0 (CH, Ar), 135.4 (C, Ar), 155.7, 169.7, 170.9 (C=O).). ESI MS *m/z* calcd. for $C_{18}H_{22}Cl_3NO_6Na$ [M+Na^+], 476.04 found 476.2.

BzO-D-Hval-L-asp(TCE)-N-tBOC. 15.7g (.0346 mol) of BzO-L-asp(TCE)-N-tBoc was de-protected using 2g of Pd/C 10 wt% with atmospheric H_2 in DCM for 3 hr. The catalyst was filtered off, the organic phase concentrated totally and the intermediate thus formed in quantitative yield was used without further purification. The residue was taken up into 150 ml DCM and cooled on an ice bath. To the solution was added 5.42 ml (1eq.) DIPCDI and mixed for .5 hr. at which time 7.2 g (1 eq.) of BzO-D-Hval-OH (**4**, prepared as previously described) and .423g (1eq.) of DMAP was added. This was allowed to return to RT and mixed for an additional 17 hr. The insoluble urea was filter off from the brown solution and the organic was washed thrice with saturated $NaHCO_3$, thrice with 10% citric acid, once with brine, dried over Na_2SO_4 and concentrated totally. The product was fractionally recrystallized from hexane to give 12.0 g of a white solid, yield 62.5%. ^{1}H-NMR (400 MHz, $CDCl_3$), δ .91 (d, *J* = 6.8 Hz, 3H), .95 (d, *J* = 6.9 Hz, 3H), 1.45 (s, t-butyl, 9H), 2.28 (m, 1H), 3.09 (dd, *J* = 4.7, 9.0 Hz, 1H), 3.17 (dd, *J* = 4.4, 9.0 Hz, 1H), 4.75 (m, 3H), 4.94 (d, *J* = 4.2 Hz, 1H), 5.18 (q, 2H), 5.52 (d, *J* = 8.2 Hz,

1H), 7.37 (m, Ar, 5H). ^{13}C-NMR (100 MHz, $CDCl_3$) δ 17.4 (CH_3), 19.1 (CH_3), 28.7 (CH_3, t-butyl), 30.5 (CH), 36.7 (CH), 50.2 (CH_2), 67.5 (CH_2) 74.6 (CH_2), 78.2 (CH), 80.7 (C), 94.9 (C), 128.8, 128.9, 128.0 (CH, Ar), 135.6 (C, Ar), 155.6, 169.3, 169.7, 170.8 (C=O).

BzO-L-lac-D-val-D-Hval-L-asp(TCE)-N-tBoc (25). 2.54 g (6.7 mmol) of BzO-L-lac-D-val-N-tBoc (**23)** was dissolved in 40 ml 1:1 TFA/DCM and stirred for 1 hr. at which point the solvent was removed *in vacuo*. The residue was taken up into toluene twice and concentrated to remove excess TFA. The intermediate amine salt (BzO-L-lac-D-val-$NH_3^+TFA^-$, **24a**) was used immediately without further purification. 2.81 g (6.05 mmol) of the HO-D-Hval-L-asp(TCE)-N-tBoc acid was prepared in same manner as above and was added to a 0 ºC stirred solution of 3.15 g (1eq.) PyBop, .818 g (1 eq.) HOBT, and 2.21 ml (2 eq.) DIPEA. To this was added the intermediate amine salt (BzO-L-lac-D-val-$NH_3^+TFA^-$) and stirred for .5 hr. at which point it was allowed to return to RT and mixed for an additional 18 hr. The organic was then washed thrice with $NaHCO_3$, thrice with 10% citric acid, dried over Na_2SO_4 and concentrated totally. The product was purified by flash chromatography (Biotage), 3:1 hexane/EtOAC to afford 2.65 g of a colorless gum, yield 60%. R_f = .40 (3:1 hexane/EtOAC). ^{1}H-NMR (400 MHz, $CDCl_3$), δ .93 (m, 12H), 1.45 (s, t-butyl, 9H), 1.48 (d, J = 7.1 Hz, 3H), 2.30 (m, 2H), 3.05 (dd, J = 4.7, 9.0 Hz, 1H), 3.20 (dd, J = 4.4, 9.0 Hz, 1H), 4.60 (m, 1 H), 4.70-4.78 (m, 3H), 5.08-5.18 (m, 4H), 5.72 (d, J = 8.1 Hz, 1H), 6.85 (d, J = 8.2 Hz, 1H), 7.31-7.37 (m, Ar, 5H). ^{13}C-NMR (100 MHz, $CDCl_3$) δ 17.2, 17.3, 19.2, 19.4 (CH_3), 28.7 (CH_3, t-butyl), 30.8 (CH_3), 31.0, 31.1 (CH), 36.7 (CH_2), 50.3, 57.5 (CH), 67.4 (CH_2), 69.6 (CH), 72.4 (CH_2), 79.9 (CH), 80.8

(C), 94.8 (C), 128.6, 128.7, 128.8 (CH, Ar), 135.5 (C, Ar), 155.6, 169.4, 170.3, 170.4, 170.5, 170.6, 170.9 (C=O).

BzO-L-lac-D-val-D-Hval-L-asp(TCE)-L-lac-D-val-N-tBoc (26). 2.65 g (3.65 mmol) of BzO-L-lac-D-val-D-Hval-L-asp(TCE)-N-tBoc (**25**) was treated with 40 ml of 3:1 TFA/DCM for 1.5 hr. at which point the solvent was removed *in vacuo* and the residue taken up twice in toluene and concentrated to remove excess TFA to give the tetradepsipeptide amine-TFA salt, BzO-L-lac-D-val-D-Hval-L-asp(TCE)-$NH_3^+TFA^-$. This was used without further purification. 1.5 g (3.95 mmol) of BzO-L-lac-D-val-N-tBoc (**23**) was deprotected as above in 100 ml DCM with .5g Pd/C 10 wt% in atmospheric H_2 over 3 hr. The catalyst was filtered off and the organic concentrated totally. The HO-L-lac-D-val-N-tBoc acid was used without further purification and was dissolved into a 100 ml, 0 ºC DCM solution to which, 2.05 g (1eq.) PyBop, .535 g (1eq.) HOBT, 1.52 ml (2.2 eq) DIPEA and the amine-TFA salt, BzO-L-lac-D-val-D-Hval-L-asp(TCE)-$NH_3^+TFA^-$ was added. This was stirred for .5hr and allowed to return to RT and mixed for an additional 18 hr. The organic was then washed thrice with saturated $NaHCO_3$, thrice with 10% citric acid, dried over Na_2SO_4 and concentrated totally. The product was purified by flash chromatography (Biotage), 3:1 hexane/EtOAC to give 2.40 g of a colorless gum, yield 73.3%. R_f = .40 (3:1 hexane/EtOAC). ^{1}H-NMR (400 MHz, $CDCl_3$) δ .96-.99 (m, 18H), 1.43 (s, t-butyl, 9H), 1.48-1.50 (m, 6H), 2.05 (m, 1H), 2.30 (m, 2H), 3.05 (dd, *J* = 7.8, 11.6 Hz, 1H), 3.33 (dd, *J* = 8.0, 11.4 Hz) 3.98 (t, 1H), 4.50 (t, 1H), 4.74-4.82 (m, 3H), 5.04 (d, *J* = 3.5 Hz, 2H), 5.13-5.21 (m, 3H), 5.33 (d, *J* = 8.2 Hz, 1H), 7.07 (d, *J* = 8.5 Hz, 1H), 7.33-7.37 (m, Ar, 5H), 7.73 (d, *J* = 8.2 Hz, 1H). ^{13}C-NMR

(100 MHz, $CDCl_3$) δ 17.1, 17.2, 17.7, 18.7, 18.9, 19.3, 19.3, 19.5 (CH_3), 28.7 (CH_3, t-butyl), 30.7, 30.8, 30.9 (CH), 35.8 (CH_2), 49.8, 58.1, 60.1 (CH), 67.4 (CH_2), 69.6, 70.6 (CH), 74.6 (CH_2), 80.0 (CH), 81.0 (C), 94.9 (C), 128.6, 128.8, 129.0 (CH, Ar), 135.7 (C, Ar), 156.5,169.4, 169.6, 169.6, 170.6, 170.9, 171.3, 171.9 (C=O). ESI MS *m/z* calcd. for $C_{39}H_{56}Cl_3N_3O_{14}Na$ [$M+Na^+$] 918.3 found 918.4.

Cyclo (-L-lac-D-val-D-Hval-L-asp(TCE)-L-lac-D-val-) (27). 2.4 g (2.7 mmol) of BzO-L-lac-D-val-D-Hval-L-asp(TCE)-L-lac-D-val-N-tBoc (**26**) was dissolved in 100 DCM to which 1g of Pd/C 10wt% was added. This was stirred for 3 hr. with atmospheric H_2 at which point the catalyst was filtered off and the organic concentrated totally. The white residue was taken up into 40 ml, 3:1 TFA/DCM and stirred for 1 hr. The organic was concentrated totally and dissolved twice more with toluene to remove excess TFA. This was used without further purification. The white residue was taken up in 50 ml $SOCl_2$ and mixed for 1 hr. whereupon the acid chloride was concentrated. The acid chloride intermediate was then taken up in benzene and concentrated again to remove excess $SOCl_2$. The residue was dissolved into 250 ml benzene by stirring to which 1 ml of Et_3N was added. After 2 hr. the benzene was removed *in vacuo* and the residue taken up in DCM whereupon the organic was washed once with 10% citric acid and then once with saturated $NaHCO_3$. The aqueous phases were extracted twice more each with DCM, the organic phases were combined and concentrated totally to give .55 g of a white foam, yield 31.4%. ^{1}H-NMR (400 MHz, $CDCl_3$) δ 1.00-1.02 (m, 18H), 1.4-1.57 (m, 6H), 2.00 (m, 1H), 2.10-2.29 (m, 2H), 3.22 (m, 2H), 4.17 (t, 1H), 4.60 (t, 1H), 4.77 (m, 2H), 5.08 (d, J = 5.6 Hz, 1H), 5.20 (d, J = 7.0 Hz, 1H), 5.30 (m, 2H), 6.47, (d, J = 8.0 Hz, 1H), 6.79

(d, J = 7.3 Hz, 1H), 7.53 (d, J = 7.0 Hz, 1H). ^{13}C-NMR (100 MHz, $CDCl_3$) δ 15.7, 17.9,18.0, 18.3, 18.9, 19.4, 19.4, 19.7 (CH_3), 30.2, 30.5, 31.5 (CH), 35.2 (CH_2), 49.4, 57.2, 60.2, 70.1, 72.3 (CH), 74.6 (CH_2), 80.8 (CH), 95.0 (C), 169.0, 169.9, 170.0, 170.3, 171.0, 171.7, 172.4 (C=O). ESI MS *m/z* calcd. for $C_{27}H_{40}Cl_3N_3O_{11}$, [M+H$^+$] 688.17 found 688.2, for [M+Na$^+$] 710.6 found 710.2.

Cyclo (-L-lac-D-val-D-Hval-L-asp(OH)-L-lac-D-val-) (28). .55g (.85 mmol) of the cyclo-depsipeptide **27** was dissolved in 20 ml acetic acid to which 1 g of Zn powder was added. This was mixed vigorously for 24 hr. The Zn powder was filtered off and the solution was concentrated totally. The residue was taken up in benzene and concentrated again to remove excess acid to give in quantitative yield .445 g of the free acid as a white solid. R_f = .35 (9:1 DCM/MeOH), mp188-190 ºC, ^{1}H-NMR (400 MHz, CD_3CN) δ .67-.81 (m, 18H), .98-1.02 (m, 6H), 2.66-2.78 (m, 2H), 4.08 (m, 2H), 4.69 (m, 2H), 4.98 (m, 2H), 6.88 (b, 1N<u>H</u>), 7.35 (b, 1N<u>H</u>), 7.61 (b, 1N<u>H</u>). ^{13}C-NMR-DEPT135 (100 MHz, CD_3CN) δ 15.7, 16.4, 16.6, 17.1, 17.2, 17.3, 17.5, 21.8 (CH_3), 42.0 (CH_2). ^{13}C-NMR-DEPT90, δ 30.5, 30.7, 31.0, 49.6, 58.4, 59.2, 71.1, 71.8, 80.3 (CH). ^{13}C-NMR δ 157.2, 168.8, 169.4, 169.8, 170.2, 170.5, 170.7 (C=O). ESI MS *m/z* calcd. for $C_{25}H_{39}N_3O_{11}$ [M+H$^+$] 558.27 found 588.3.

Chromophore attachment (28a). Aminorhodamine B was prepared as previously reported. .11 g (.197 mmol) of cyclo-depsipeptide free acid, Cyclo (-L-lac-D-val-D-Hval-L-asp(OH)-L-lac-D-val-), **22**, was dissolved in 50 ml $SOCl_2$ and mixed for 1 hr. at which point it was concentrated totally. The residue was taken up in benzene and

concentrated to remove excess $SOCl_2$. The residue was dissolved again in benzene to which a 10 ml benzene solution of .12 g (.243 mmol) of the purified aminorhodamine B and .3 ml Et_3N was added. This was mixed for 48 hr. whereupon the solvent was removed *in vacuo* and the red residue taken up in DCM. The organic was washed four times with 100 ml 1N HCl and dried over Na_2SO_4 and concentrated totally. The crude mixture was chromatographed by preparative TLC, 9:1 DCM/MeOH. Fractions were isolated and Mass Spec. analysis was preformed. No product was found.

This was repeated using .1 g of the cyclo-depsipeptide free acid and DIPCDI (1 eq.), DMAP (.1eq.) with 1 eq. of the chromophore in benzene solvent system. This was reacted for 24 hr. and the organic phase was treated and washed as above. Again purification on TLC and Mass Spec. analysis showed no product formed.

This was repeated again using standard amino acid coupling techniques using 1 eq. of the cyclo-depsipeptide free acid, 1 eq. each of the chromophore, PyBop and HOBT and 2 eq. DIPEA in a DMF solvent system. This was reacted for 24 hr. and treated as above. Again no product was found in the crude mixture or from prep. TLC fractions.

Chromophore attachment II Cyclo (-L-lac-D-val-D-Hval-L-asp(MNBD)-L-lac-D-val-) (28b). .1 g of the cyclo-depsipeptide free acid was dissolved in 20 ml $SOCl_2$ and mixed for 1 hr. at which point it was concentrated totally. The residue was taken up in benzene and concentrated to remove excess $SOCl_2$. This was taken up in 10 ml anhydrous MeCN to which 1 eq of 4-(N-methylhydrazino)-7-nitro-2,1,3-benzooxadiazole (MNBD)

and 3 eq. Et_3N was added. This was stirred for 24 hr. at which point the solvent was removed *in vacuo* and the organic phase was washed thrice with saturated $NaHCO_3$, thrice with 10% citric acid, dried over Na_2SO_4. This was chromatographed on preparative TLC (9:1 DCM/MeOH) and 2 fractions were found, isolated and analyzed via Mass Spec. Fraction 2 with R_f = .50 contained a small amount of the desired product, calcd. [M+H$^+$] (%) 749.25 found 749.26 (12).

This was repeated using the general DIPCDI and PyBop methods as above. In both cases no product was found in the Mass Spec.

Cyclo (-L-lac-D-val-D-Hval-L-glu(MNBD)-L-lac-D-val-) (29a). The glutamic version was formed using the same general procedure used for Cyclo (-L-lac-D-val-D-Hval-L-asp(MNBD)-L-lac-D-val-) except that BzO-L-glu(OH)-N-tBoc replaced BzO-L-gasp(OH)-N-tBoc. 68.3 mg (.119 mmol) of the cyclo depsipeptide free acid was dissolved in 20 ml $SOCl_2$ and mixed for 1 hr. at which point it was concentrated totally. The residue was taken up in benzene and concentrated to remove excess $SOCl_2$. This was taken up in 10 ml anhydrous MeCN to which 25 mg (1 eq) of 4-(N-methylhydrazino)-7-nitro-2,1,3-benzooxadiazole (MNBD) and 3 eq. Et_3N was added. This was stirred for 24 hr. at which point the solvent was removed *in vacuo* and the organic phase was washed thrice with saturated $NaHCO_3$, thrice with 10% citric acid, dried over Na_2SO_4. This was chromatographed on preparative TLC (9:1 DCM/MeOH). The fraction with R_f = .55 was isolated and gave 2 mg of a brown solid. This was analyzed via Mass Spec. which

showed the product was formed but was impure, [M+Na^+] (%) calcd. 785.24 found 785.15 (80).

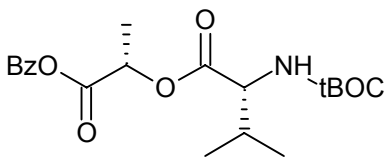

BzO-L-lac-D-val-N-tBoc

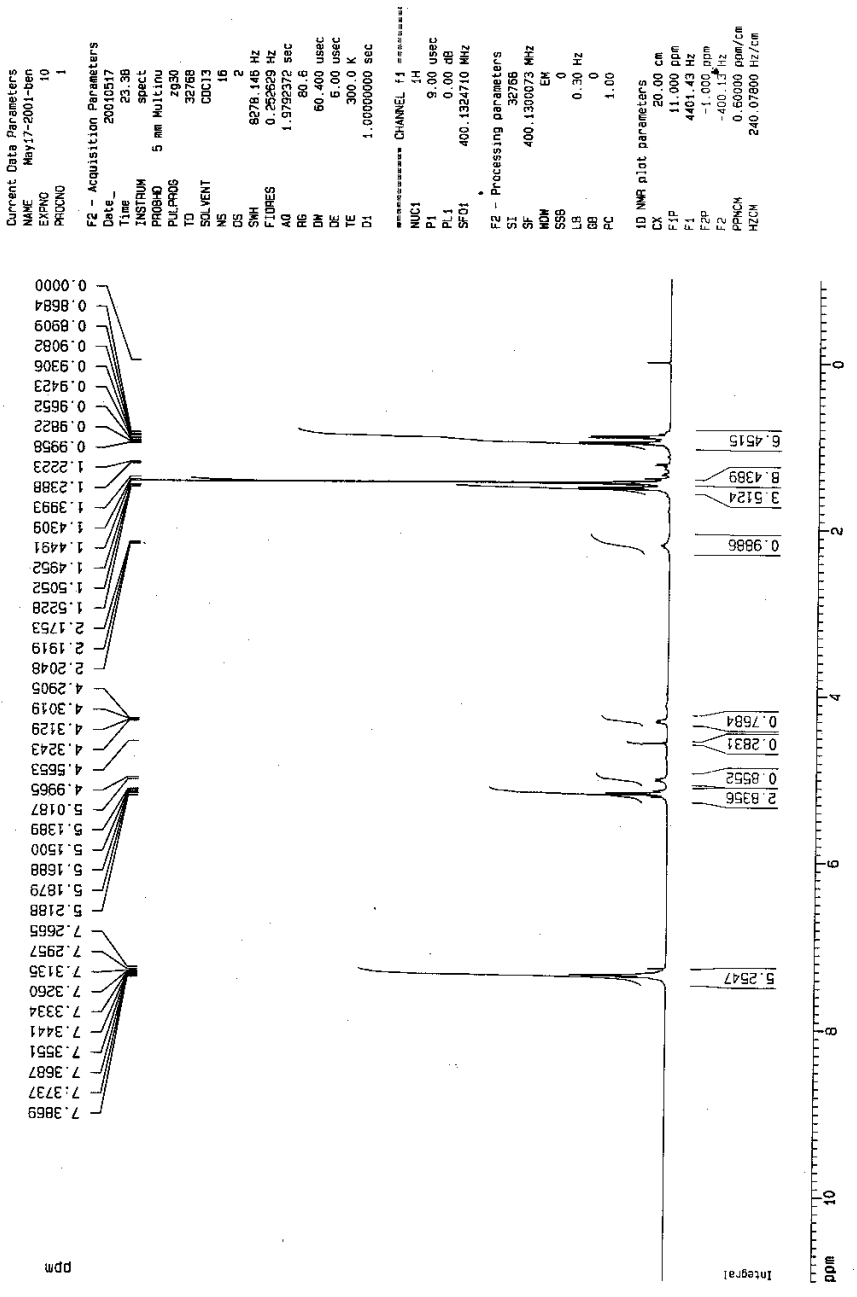

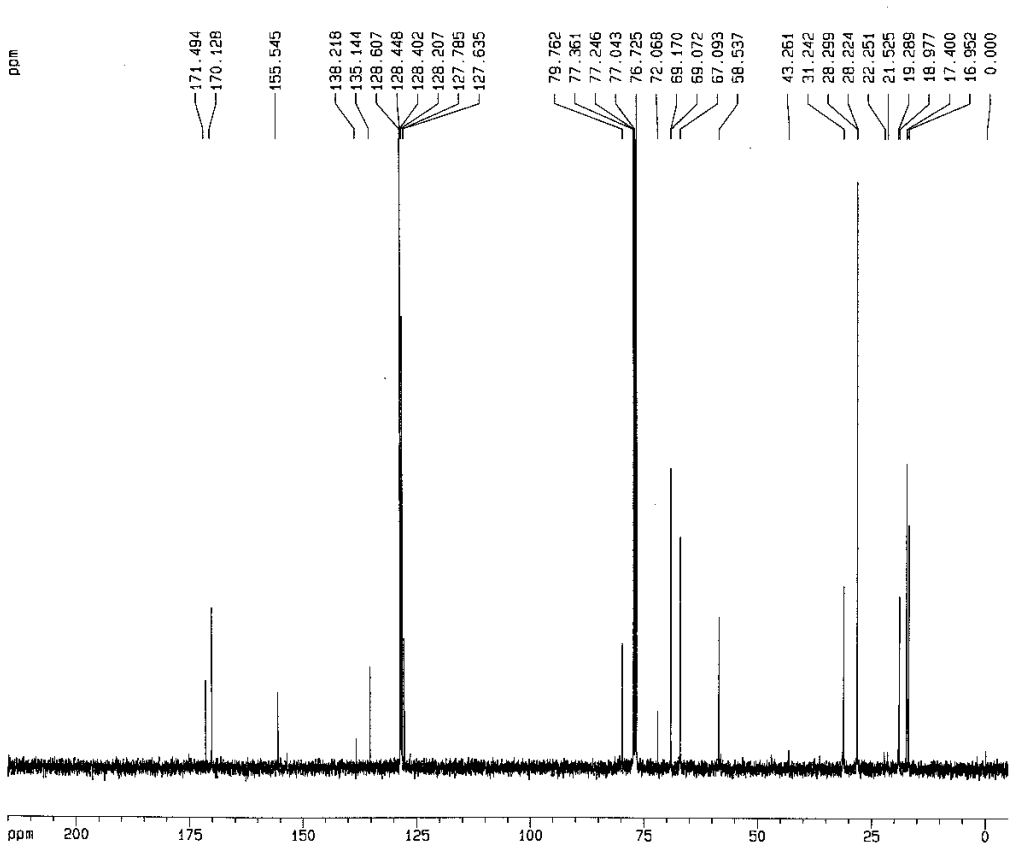


```
Current Data Parameters
NAME      May17-2001-ben
EXPNO              11
PROCNO              1

F2 - Acquisition Parameters
Date_          20010518
Time               0.07
INSTRUM           spect
PROBHD     5 mm Multinu
PULPROG         zgpg30
TD               65536
SOLVENT          CDCl3
NS                 512
DS                   4
SWH          25125.629 Hz
FIDRES        0.383387 Hz
AQ            1.3042164 sec
RG                4096
DW              19.900 usec
DE               6.00 usec
TE              300.0 K
D1           2.00000000 sec
d11          0.03000000 sec
d12          0.00002000 sec

========== CHANNEL f1 ==========
NUC1               13C
P1               10.70 usec
PL1              -1.00 dB
SFO1        100.6237959 MHz

========== CHANNEL f2 ==========
CPDPRG2         waltz16
NUC2               1H
PCPD2            80.00 usec
PL2               0.00 dB
PL12             20.00 dB
PL13             20.00 dB
SFO2        400.1316005 MHz

F2 - Processing parameters
SI                32768
SF          100.6127711 MHz
WDW                EM
SSB                 0
LB               1.00 Hz
GB                  0
PC               1.40

1D NMR plot parameters
CX              20.00 cm
F1P            215.000 ppm
F1           21631.75 Hz
F2P             -5.000 ppm
F2            -503.06 Hz
PPMCM         11.00000 ppm/cm
HZCM        1106.74048 Hz/cm
```

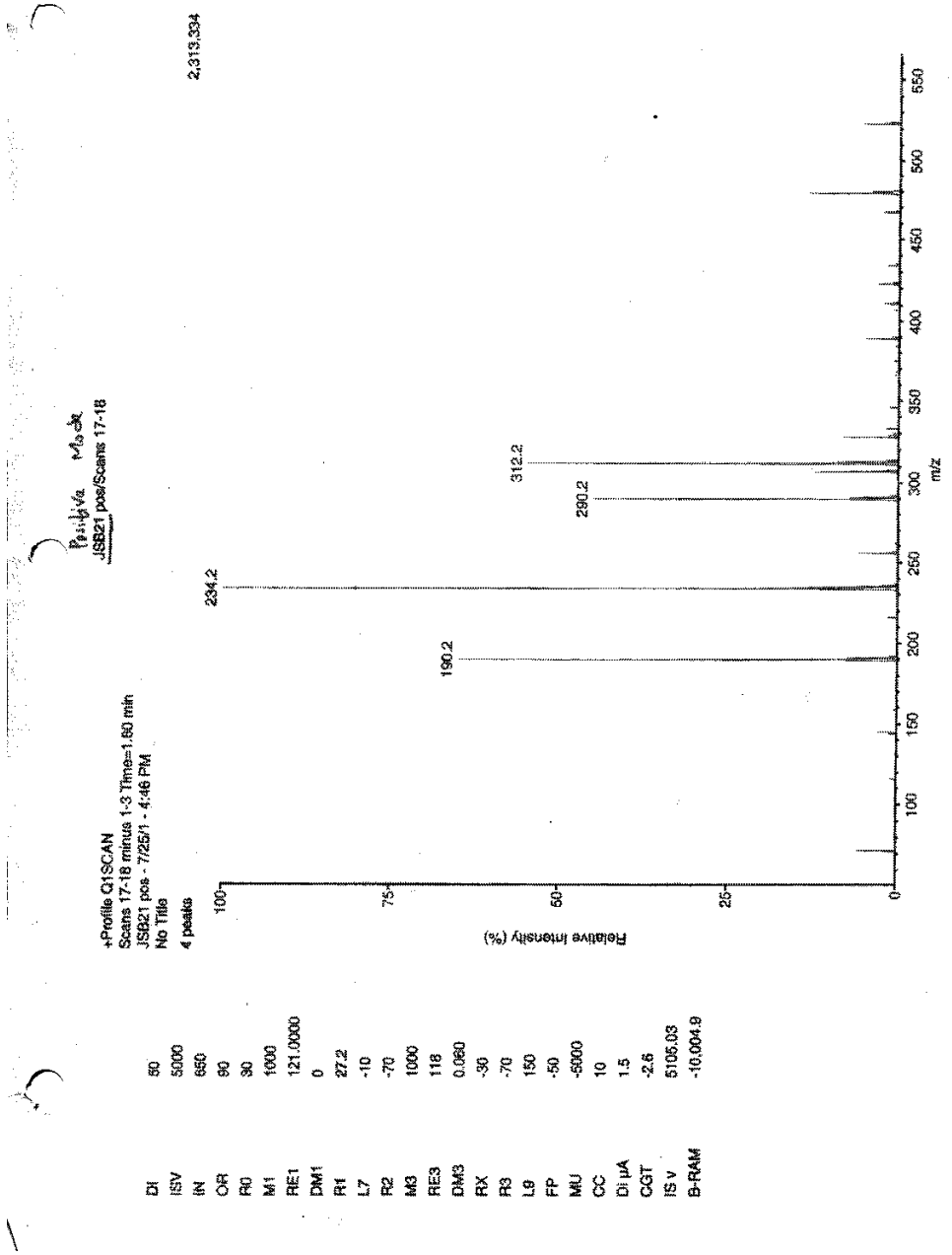
+Profile Q1SCAN
Scans 17-18 minus 1-3 Time=1.80 min
JSB21 pos - 7/25/1 - 4:46 PM
No Title
4 peaks
JSB21 pos/Scans 17-18
2,313.334
234.2
190.2
312.2
290.2
Relative Intensity (%)
m/z
DI 60
ISV 5000
IN 650
OR 90
R0 30
M1 1000
RE1 121.0000
DM1 0
R1 27.2
L7 -10
R2 -70
M3 1000
RE3 116
DM3 0.060
RX -30
R3 -70
L9 150
FP -50
MU -5000
CC 10
Di µA 1.5
CGT -2.6
IS v 5105.03
B-RAM -10,004.9

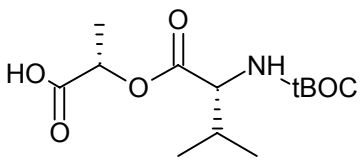

HO-L-lac-D-val-N-tBoc

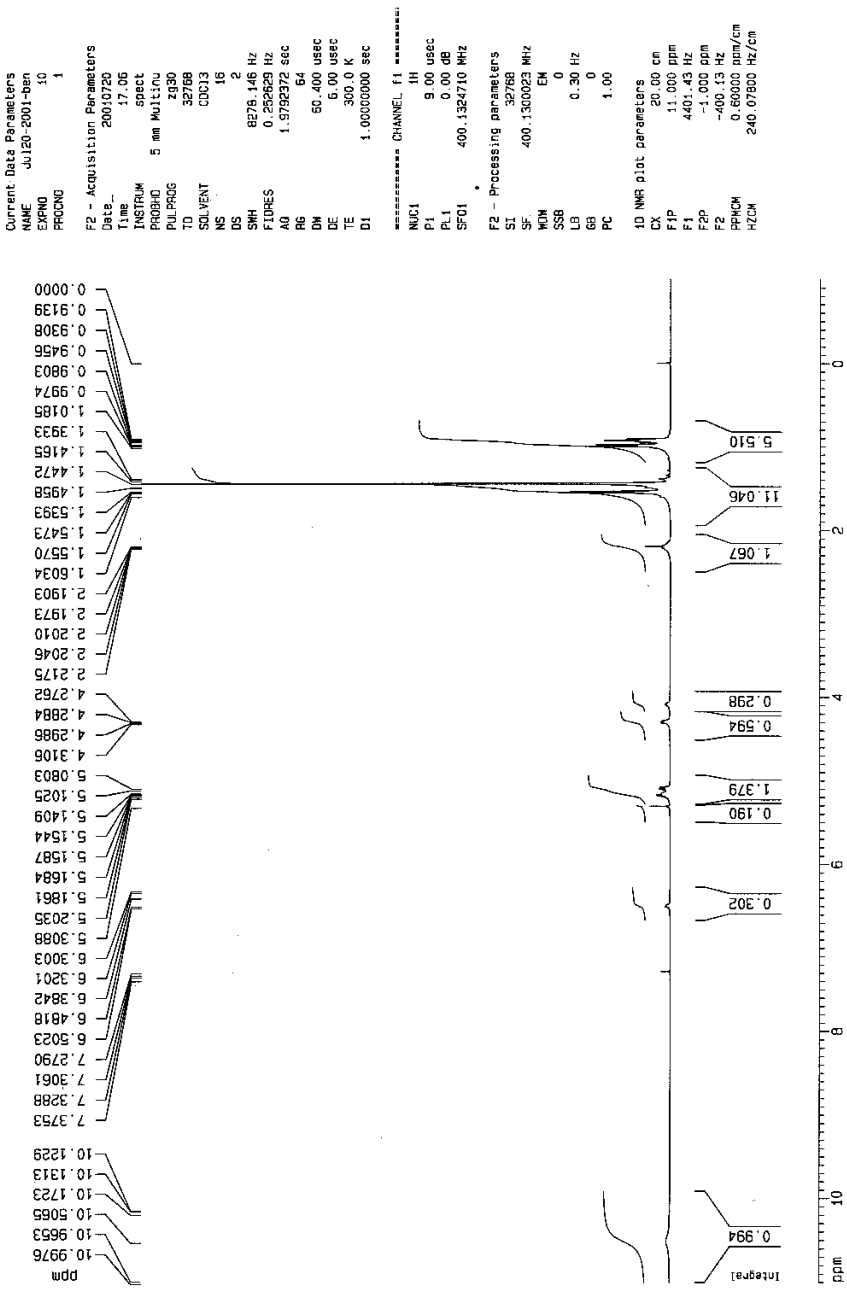

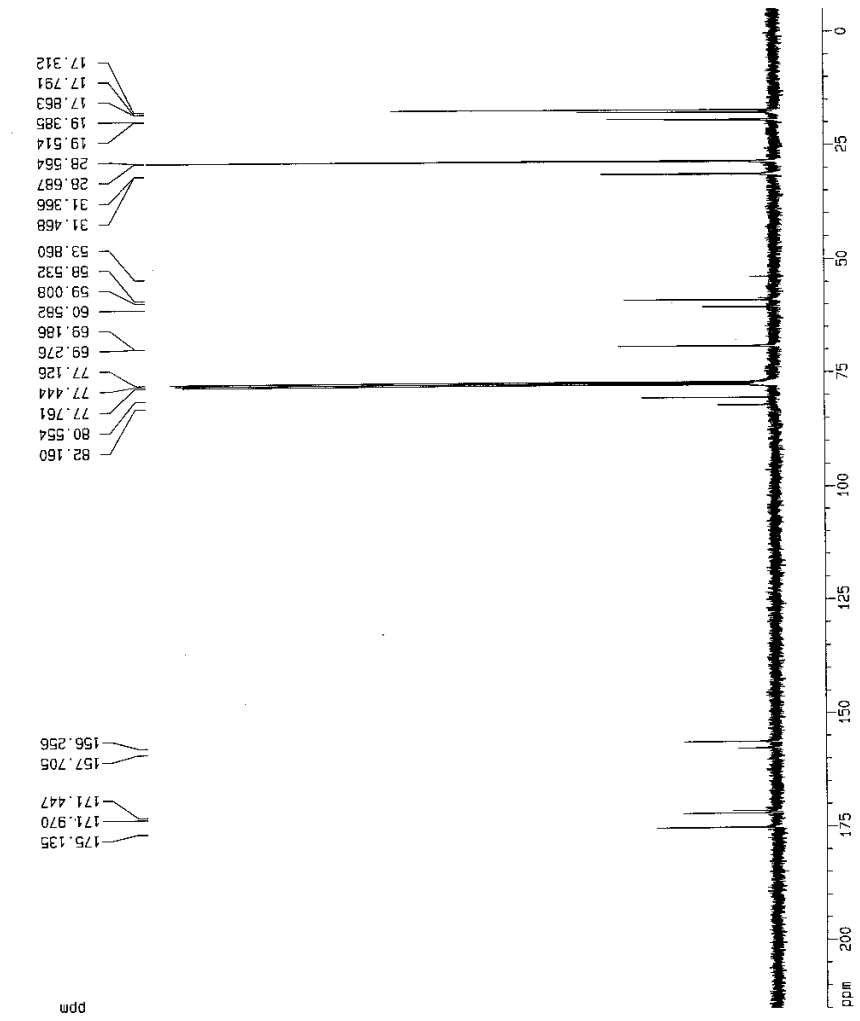
Current Data Parameters
NAME Ju120-2001-den
EXPNO 11
PROCNO 1
F2 - Acquisition Parameters
Date_ 20010720
Time 17.25
INSTRUM spect
PROBHD 5 mm Multinu
PULPROG zgpg30
TD 65536
SOLVENT CDCl3
NS 512
DS 4
SWH 25125.629 Hz
FIDRES 0.383387 Hz
AQ 1.3042164 sec
RG 4096
DW 19.900 usec
DE 6.00 usec
TE 300.0 K
D1 2.00000000 sec
d11 0.03000000 sec
d12 0.00002000 sec
CHANNEL f1
NUC1 13C
P1 10.70 usec
PL1 -1.00 dB
SFO1 100.6227959 MHz
CHANNEL f2
CPDPRG2 waltz16
NUC2 1H
PCPD2 80.00 usec
PL2 0.00 dB
PL12 20.00 dB
PL13 20.00 dB
SFO2 400.1316005 MHz
F2 - Processing parameters
SI 32768
SF 100.6127269 MHz
WDW EM
SSB 0
LB 1.00 Hz
GB 0
PC 1.40
1D NMR plot parameters
CX 20.00 cm
F1P 215.000 ppm
F1 21631.74 Hz
F2P -5.000 ppm
F2 -503.06 Hz
PPMCM 11.00000 ppm/cm
HZCM 1106.73998 Hz/cm
17.312
17.791
17.863
19.385
19.514
28.564
28.687
31.366
31.468
53.860
58.532
59.008
60.582
69.186
69.276
77.126
77.444
77.761
80.554
82.160
156.256
157.705
171.447
171.970
175.135
ppm
0
25
50
75
100
125
150
175
200

BzO-L-asp-(TCE)-N-tBoc

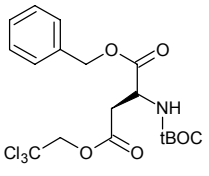

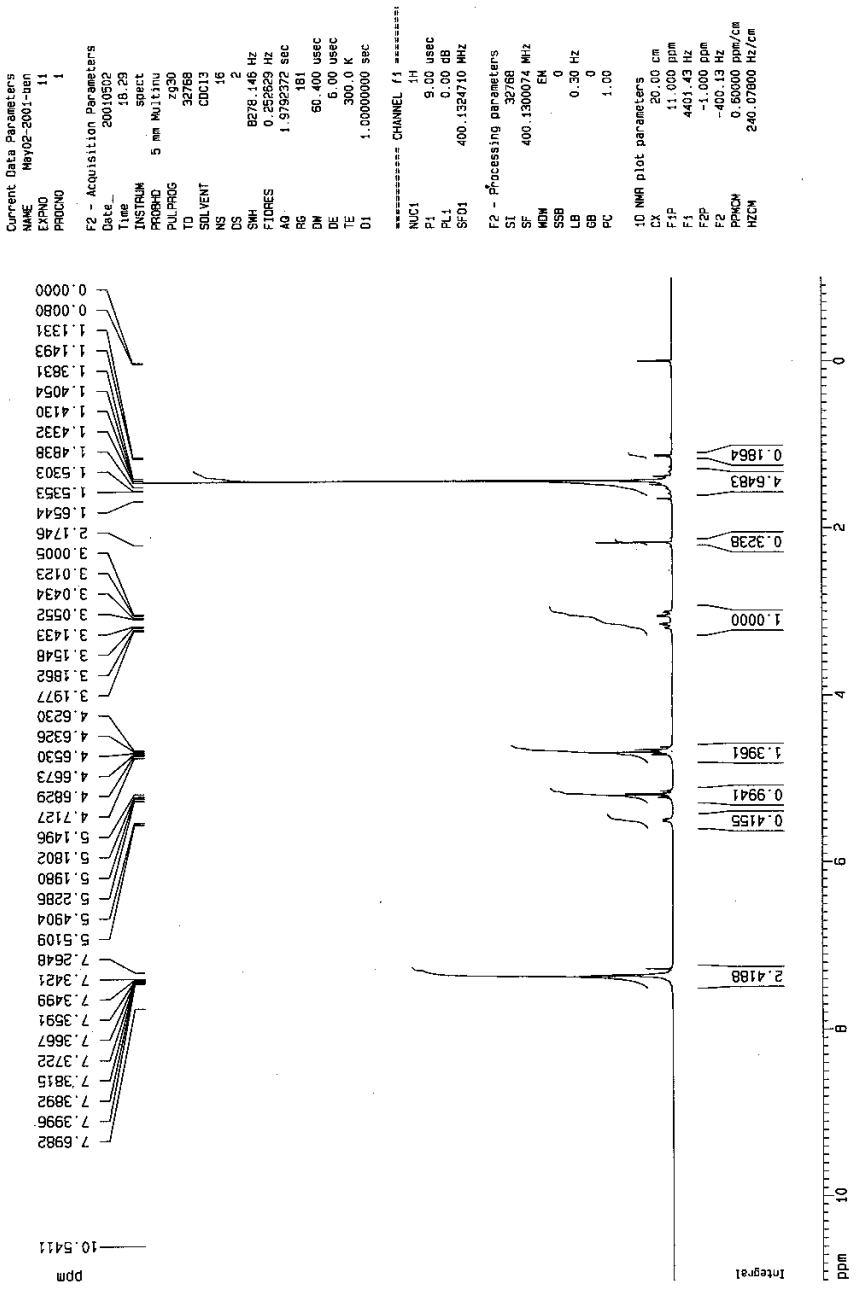

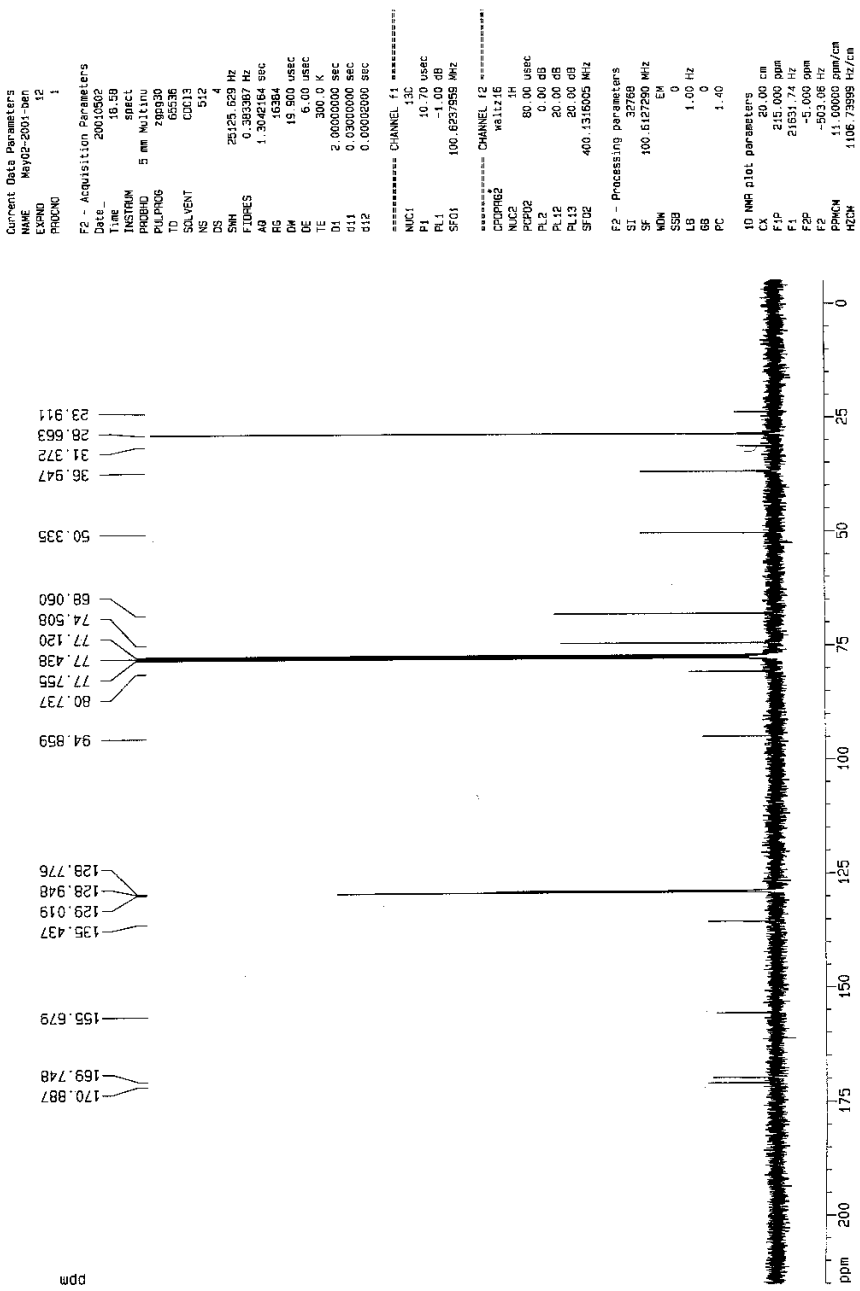
Current Data Parameters
NAME MayO2-2001-ben
EXPNO 12
PROCNO 1
F2 - Acquisition Parameters
Date_ 20010502
Time 10.39
INSTRUM spect
PROBHD 5 mm Multinu
PULPROG zgpg30
TD 65536
SOLVENT CDCl3
NS 512
DS 4
SWH 25125.629 Hz
FIDRES 0.383367 Hz
AQ 1.3042164 sec
RG 16384
DW 19.900 usec
DE 6.00 usec
TE 300.0 K
D1 2.00000000 sec
d11 0.03000000 sec
d12 0.00002000 sec
CHANNEL f1
NUC1 13C
P1 10.70 usec
PL1 -1.00 dB
SFO1 100.6237958 MHz
CHANNEL f2
CPDPRG2 waltz16
NUC2 1H
PCPD2 80.00 usec
PL2 0.00 dB
PL12 20.00 dB
PL13 20.00 dB
SFO2 400.1316005 MHz
F2 - Processing parameters
SI 32768
SF 100.6127690 MHz
WDW EM
SSB 0
LB 1.00 Hz
GB 0
PC 1.40
1D NMR plot parameters
CX 20.00 cm
F1P 215.000 ppm
F1 21631.74 Hz
F2P -5.000 ppm
F2 -503.06 Hz
PPMCM 11.00000 ppm/cm
HZCM 1106.73999 Hz/cm
23.911
28.663
31.372
36.947
50.335
68.060
74.508
77.120
77.438
77.755
80.737
94.859
128.776
128.948
129.019
135.437
155.679
169.748
170.887
ppm
0
25
50
75
100
125
150
175
200

Positive Mode
JSB-12 pos/Scans 10-11
+Profile Q1SCAN
Scans 10-11 minus 1-2 Time=1.35 min
JSB-12 pos - 5/23/1 - 4:58 PM
No Title
7 peaks
613,334
476.2
354.2
398.2
456.2
618.4
285.4
145.4
Relative Intensity (%)
m/z
DI 50
ISV 5000
IN 650
OR 80
R0 30
M1 1000
RE1 121.3
DM1 0.040
R1 26.00000
L7 40
R2 60
M3 1000
RE3 118
DM3 0.060
RX -10
R3 -50
L9 50
FP -50
MU -4700
CC 10
DI µA 2.08
CGT 0
IS v 5119.7
B-RAM -10,004.9

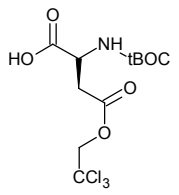

HO-L-asp-(TCE)-N-tBoc

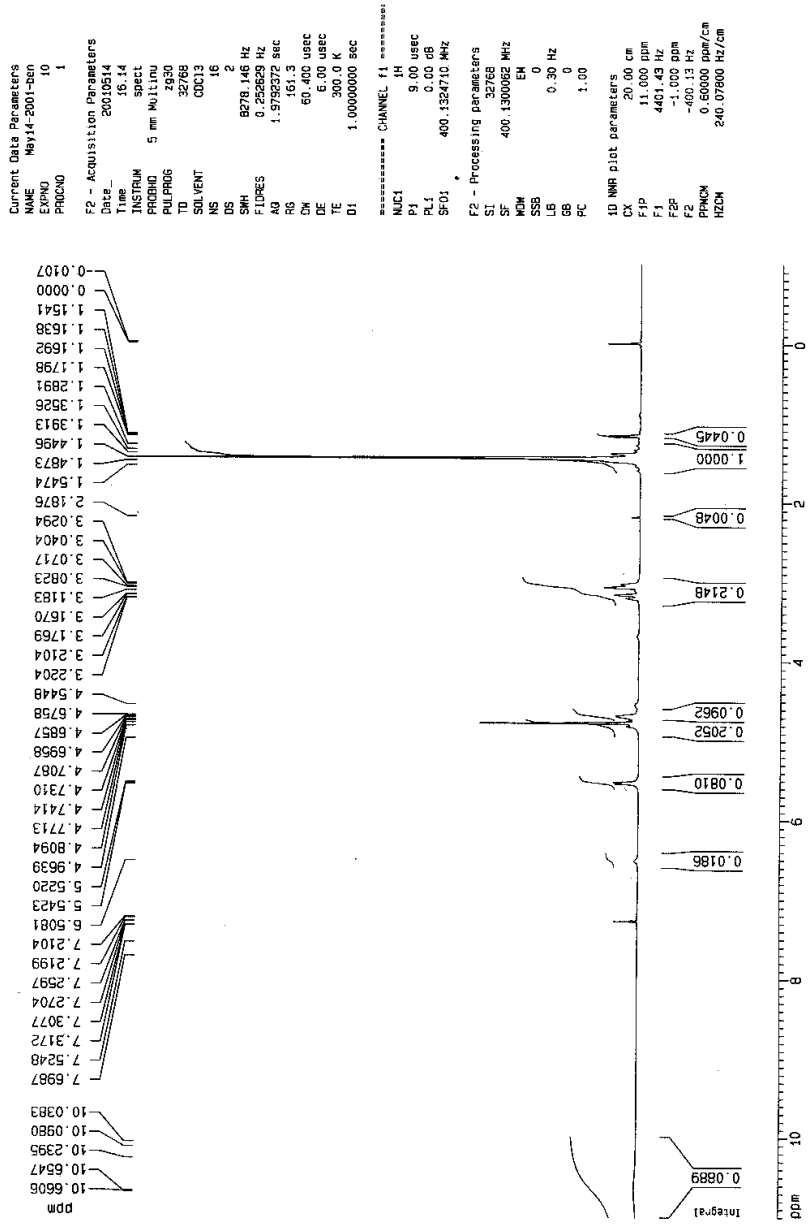

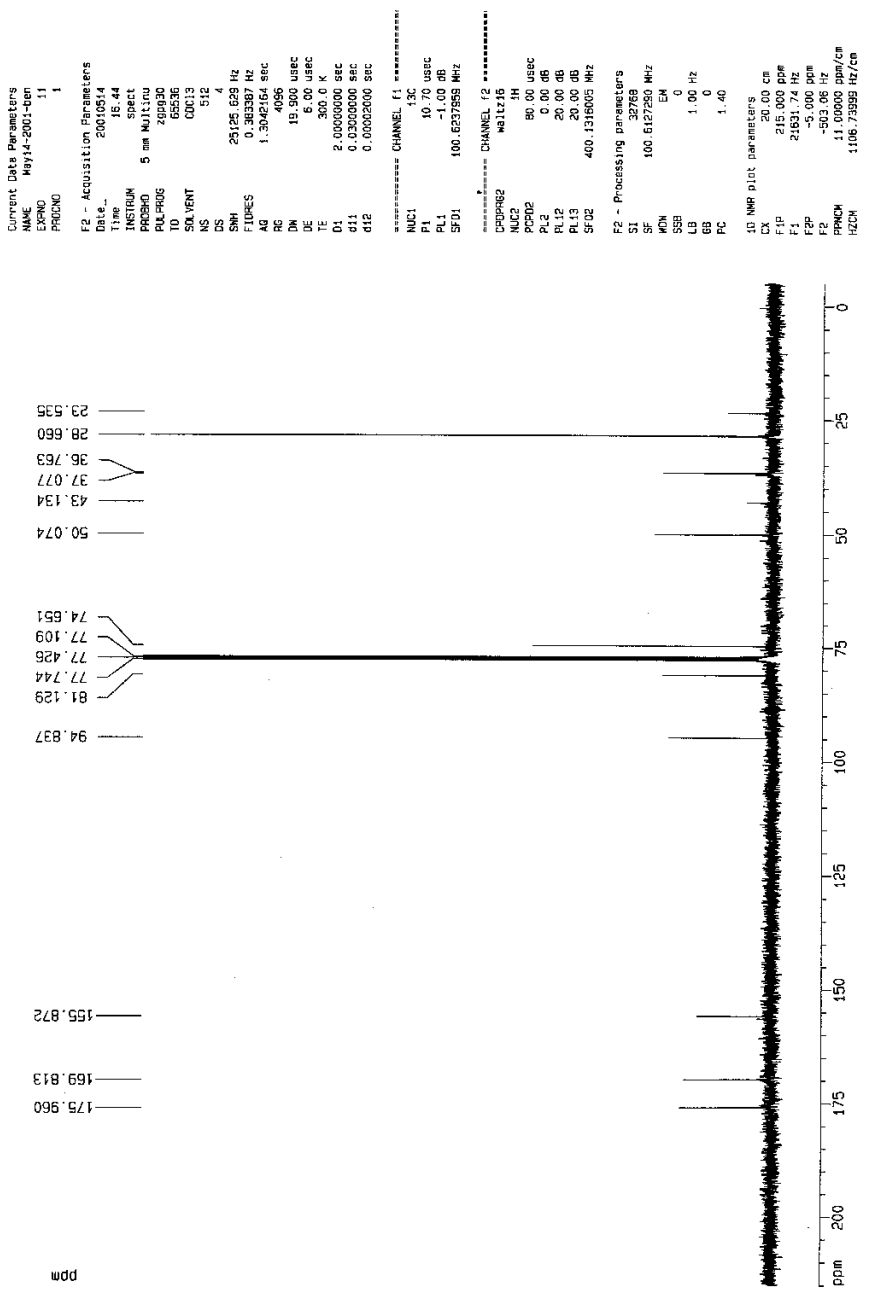
Current Data Parameters
NAME May14-2001-ben
EXPNO 11
PROCNO 1
F2 - Acquisition Parameters
Date_ 20010514
Time 16.44
INSTRUM spect
PROBHD 5 mm Multinu
PULPROG zgpg30
TD 65536
SOLVENT CDCl3
NS 512
DS 4
SWH 25125.629 Hz
FIDRES 0.383387 Hz
AQ 1.3042164 sec
RG 4096
DW 19.900 usec
DE 6.00 usec
TE 300.0 K
D1 2.00000000 sec
d11 0.03000000 sec
d12 0.00002000 sec
======== CHANNEL f1 ========
NUC1 13C
P1 10.70 usec
PL1 -1.00 dB
SFO1 100.6237958 MHz
======== CHANNEL f2 ========
CPDPRG2 waltz16
NUC2 1H
PCPD2 80.00 usec
PL2 0.00 dB
PL12 20.00 dB
PL13 20.00 dB
SFO2 400.1316005 MHz
F2 - Processing parameters
SI 32768
SF 100.6127260 MHz
WDW EM
SSB 0
LB 1.00 Hz
GB 0
PC 1.40
1D NMR plot parameters
CX 20.00 cm
F1P 215.000 ppm
F1 21631.74 Hz
F2P -5.000 ppm
F2 -503.06 Hz
PPMCM 11.00000 ppm/cm
HZCM 1106.73999 Hz/cm
23.535
28.660
36.763
37.077
43.134
50.074
74.651
77.109
77.426
77.744
81.129
94.837
155.872
169.813
175.960
wdd
ppm
0
25
50
75
100
125
150
175
200

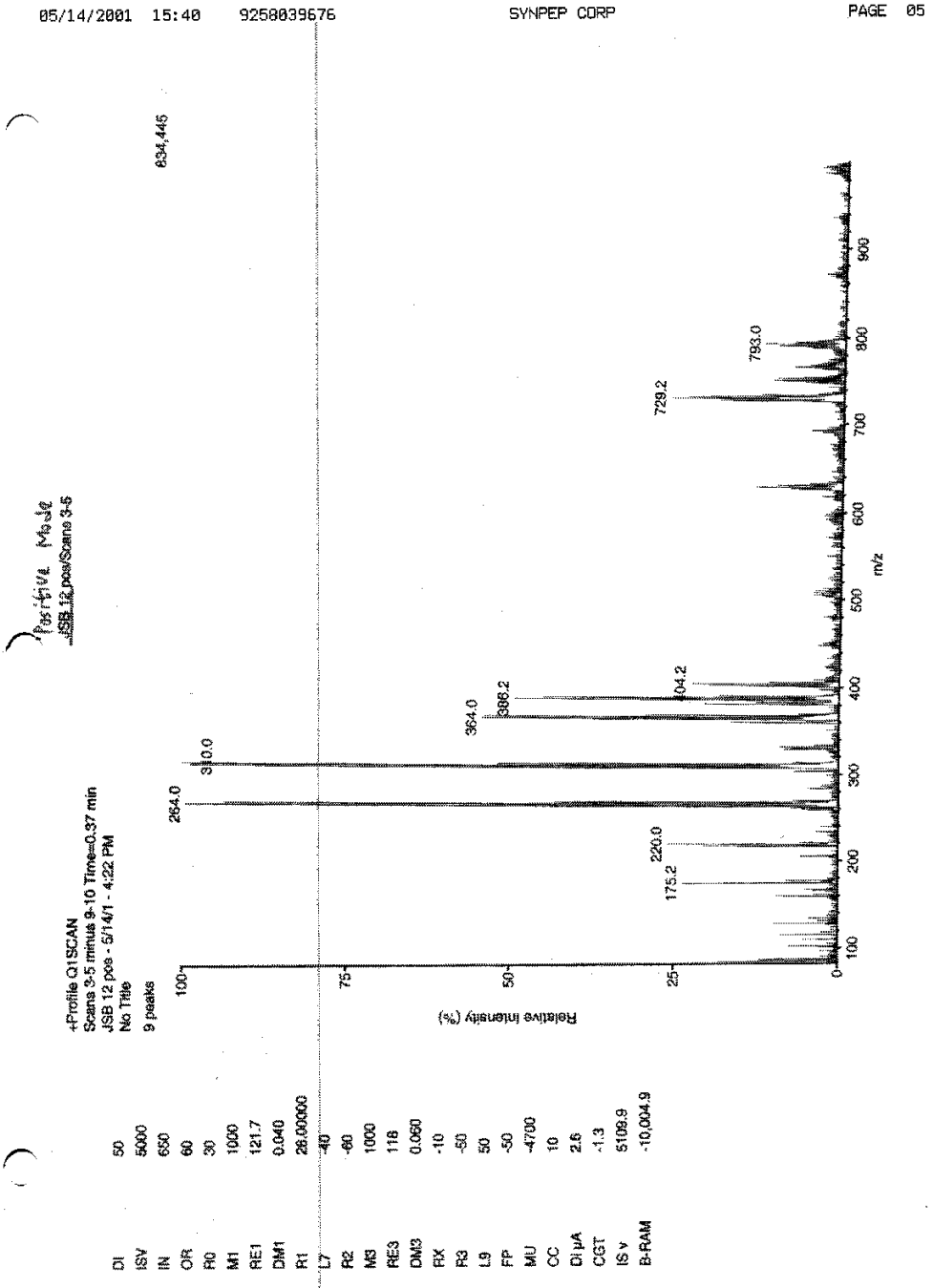
Positive Mode
JSB 12 pos/Scans 3-5
+Profile Q1SCAN
Scans 3-5 minus 9-10 Time=0.37 min
JSB 12 pos - 5/14/1 - 4:22 PM
No Title
9 peaks
834.445
DI 50
ISV 5000
IN 650
OR 60
R0 30
M1 1000
RE1 121.7
DM1 0.040
R1 26.00000
L7 40
R2 60
M3 1000
RE3 118
DM3 0.060
RX -10
R3 -50
L9 50
FP -50
MU -4700
CC 10
DI µA 2.6
CGT -1.3
IS v 5109.9
B-RAM -10,004.9
Relative Intensity (%)
m/z
264.0
310.0
364.0
386.2
404.2
175.2
220.0
729.2
793.0

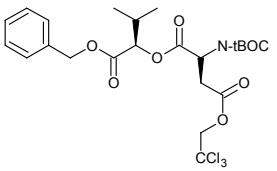

BzO-D-Hval-L-asp(TCE)-N-tBoc

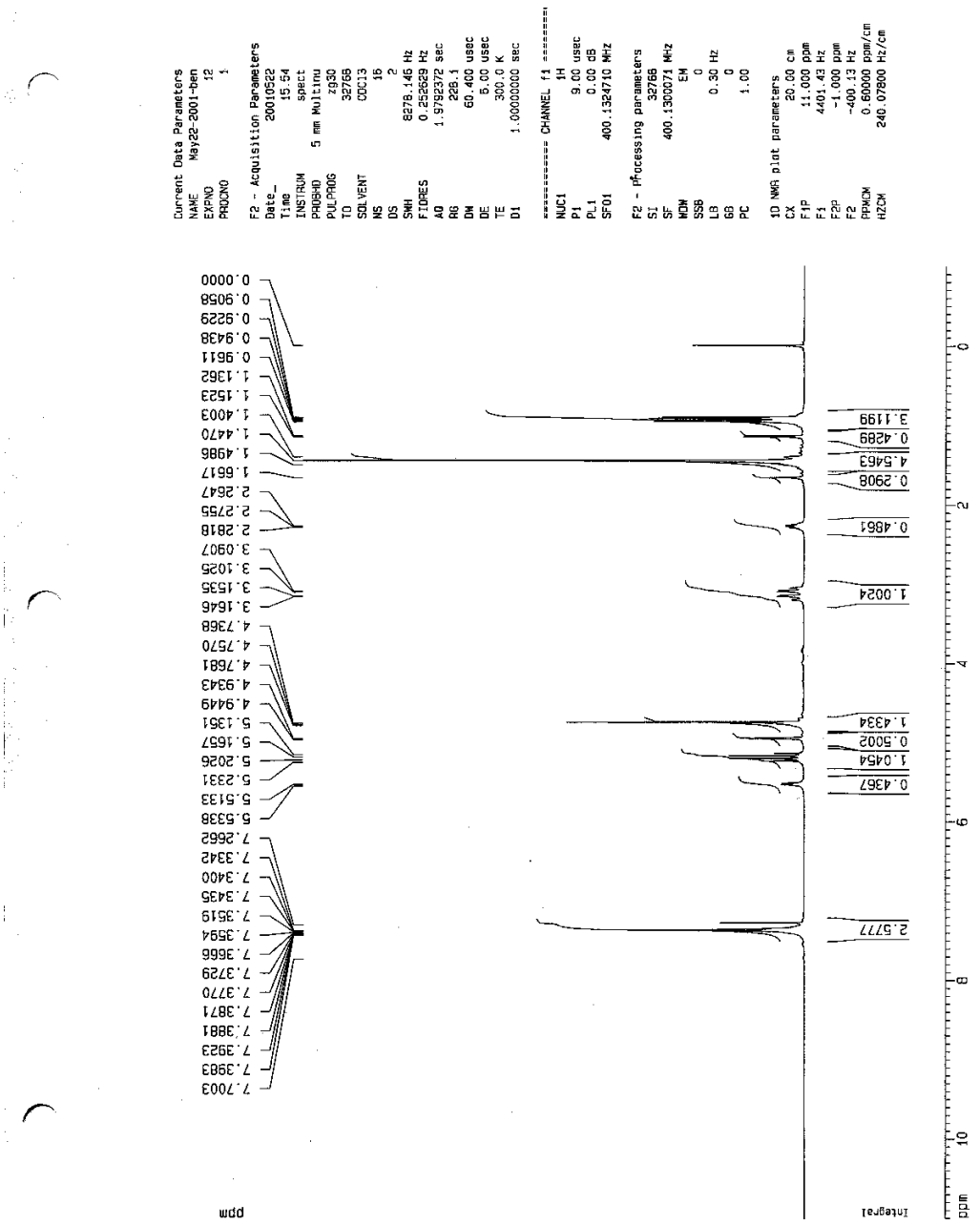

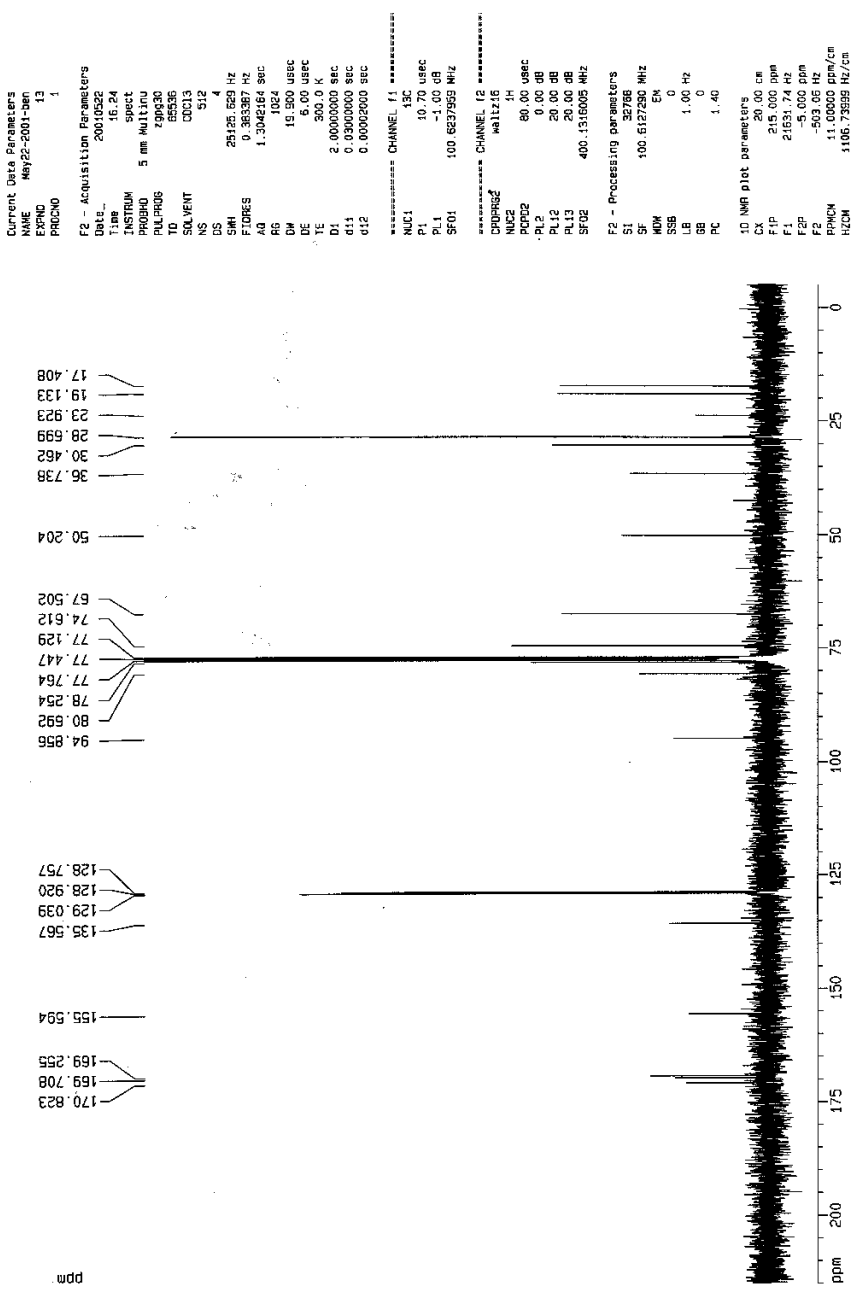
Current Data Parameters
NAME May22-2001-ben
EXPNO 13
PROCNO 1
F2 - Acquisition Parameters
Date_ 20010522
Time 16.24
INSTRUM spect
PROBHD 5 mm Multinu
PULPROG zgpg30
TD 65536
SOLVENT CDCl3
NS 512
DS 4
SWH 25125.629 Hz
FIDRES 0.383367 Hz
AQ 1.3042164 sec
RG 1024
DW 19.900 usec
DE 6.00 usec
TE 300.0 K
D1 2.00000000 sec
d11 0.03000000 sec
d12 0.00002000 sec
======== CHANNEL f1 ========
NUC1 13C
P1 10.70 usec
PL1 -1.00 dB
SFO1 100.6237959 MHz
======== CHANNEL f2 ========
CPDPRG2 waltz16
NUC2 1H
PCPD2 80.00 usec
PL2 0.00 dB
PL12 20.00 dB
PL13 20.00 dB
SFO2 400.1316005 MHz
F2 - Processing parameters
SI 32768
SF 100.6127290 MHz
WDW EM
SSB 0
LB 1.00 Hz
GB 0
PC 1.40
1D NMR plot parameters
CX 20.00 cm
F1P 215.000 ppm
F1 21631.74 Hz
F2P -5.000 ppm
F2 -503.06 Hz
PPMCM 11.00000 ppm/cm
HZCM 1106.73999 Hz/cm
17.408
19.133
23.923
28.699
30.462
36.738
50.204
67.502
74.612
77.129
77.447
77.764
78.254
80.692
94.856
128.757
128.920
129.039
135.567
155.594
169.255
169.708
170.823
ppm
0
25
50
75
100
125
150
175
200
ppm

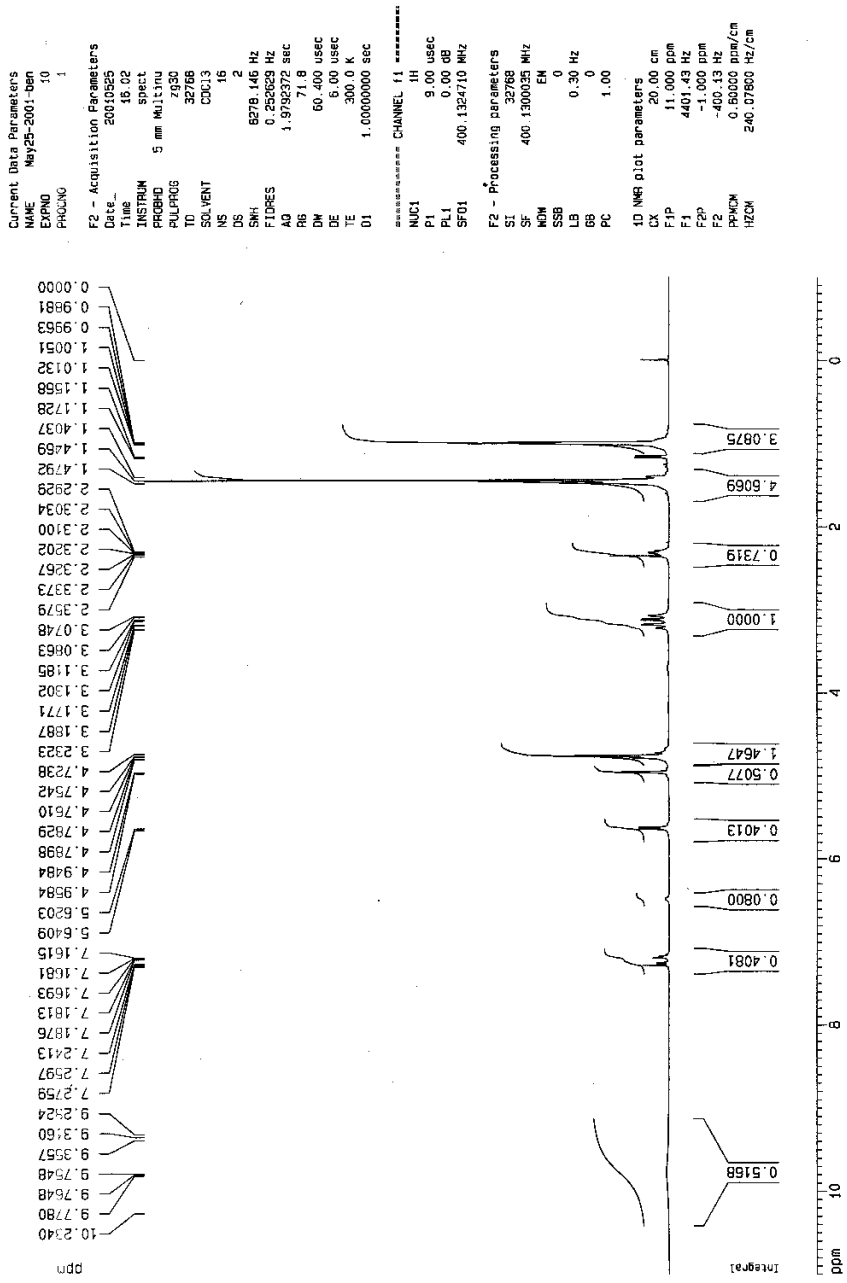
Current Data Parameters
NAME May25-2001-ben
EXPNO 10
PROCNO 1
F2 - Acquisition Parameters
Date_ 20010525
Time 16.02
INSTRUM spect
PROBHD 5 mm Multinu
PULPROG zg30
TD 32768
SOLVENT CDCl3
NS 16
DS 2
SWH 8278.146 Hz
FIDRES 0.252629 Hz
AQ 1.9792372 sec
RG 71.8
DW 60.400 usec
DE 6.00 usec
TE 300.0 K
D1 1.00000000 sec
CHANNEL f1
NUC1 1H
P1 9.00 usec
PL1 0.00 dB
SFO1 400.1324710 MHz
F2 - Processing parameters
SI 32768
SF 400.1300035 MHz
WDW EM
SSB 0
LB 0.30 Hz
GB 0
PC 1.00
1D NMR plot parameters
CX 20.00 cm
F1P 11.000 ppm
F1 4401.43 Hz
F2P -1.000 ppm
F2 -400.13 Hz
PPMCM 0.60000 ppm/cm
HZCM 240.07800 Hz/cm
0.5168
0.4081
0.0800
0.4013
0.5077
1.4647
1.0000
0.7319
4.6069
3.0875
Integral
ppm
0
2
4
6
8
10
ppm
10.2340
9.7780
9.7648
9.7548
9.3557
9.3160
9.2524
7.2759
7.2597
7.2413
7.1876
7.1813
7.1693
7.1681
7.1615
5.6409
5.6203
4.9584
4.9484
4.7898
4.7829
4.7610
4.7542
4.7238
3.2323
3.1887
3.1771
3.1302
3.1185
3.0863
3.0748
2.3579
2.3373
2.3267
2.3202
2.3100
2.3034
2.2929
1.4792
1.4469
1.4037
1.1728
1.1558
1.0132
1.0051
0.9963
0.9881
0.0000

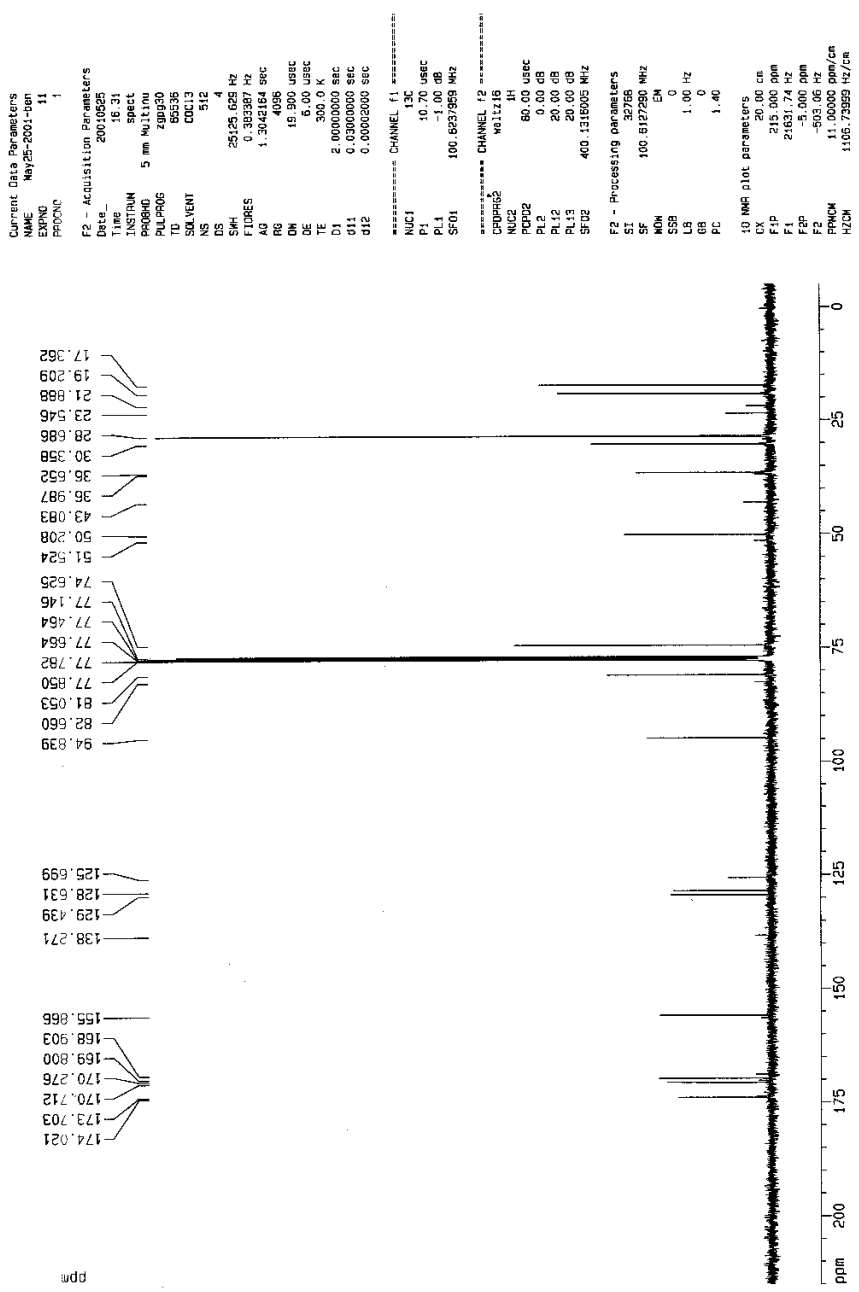
Current Data Parameters
NAME May25-2001-pen
EXPNO 11
PROCNO 1
F2 - Acquisition Parameters
Date_ 20010525
Time 16.31
INSTRUM spect
PROBHD 5 mm Multinu
PULPROG zgpg30
TD 65536
SOLVENT CDCl3
NS 512
DS 4
SWH 25125.628 Hz
FIDRES 0.383387 Hz
AQ 1.3042164 sec
RG 4096
DW 19.900 usec
DE 6.00 usec
TE 300.0 K
D1 2.00000000 sec
d11 0.03000000 sec
d12 0.00002000 sec
======== CHANNEL f1 ========
NUC1 13C
P1 10.70 usec
PL1 -1.00 dB
SFO1 100.6233959 MHz
======== CHANNEL f2 ========
CPDPRG2 waltz16
NUC2 1H
PCPD2 80.00 usec
PL2 0.00 dB
PL12 20.00 dB
PL13 20.00 dB
SFO2 400.1316005 MHz
F2 - Processing parameters
SI 32768
SF 100.6127280 MHz
WDW EM
SSB 0
LB 1.00 Hz
GB 0
PC 1.40
10 NMR plot parameters
CX 20.00 cm
F1P 215.000 ppm
F1 21631.74 Hz
F2P -5.000 ppm
F2 -503.06 Hz
PPMCM 11.00000 ppm/cm
HZCM 1106.73999 Hz/cm
17.362
19.209
21.888
23.546
28.686
30.358
36.652
36.987
43.083
50.208
51.524
74.625
77.146
77.464
77.664
77.782
77.850
81.053
82.660
94.839
125.699
128.631
129.439
138.271
155.866
168.903
169.800
170.276
170.712
173.703
174.021
ppm
0
25
50
75
100
125
150
175
200
ppm

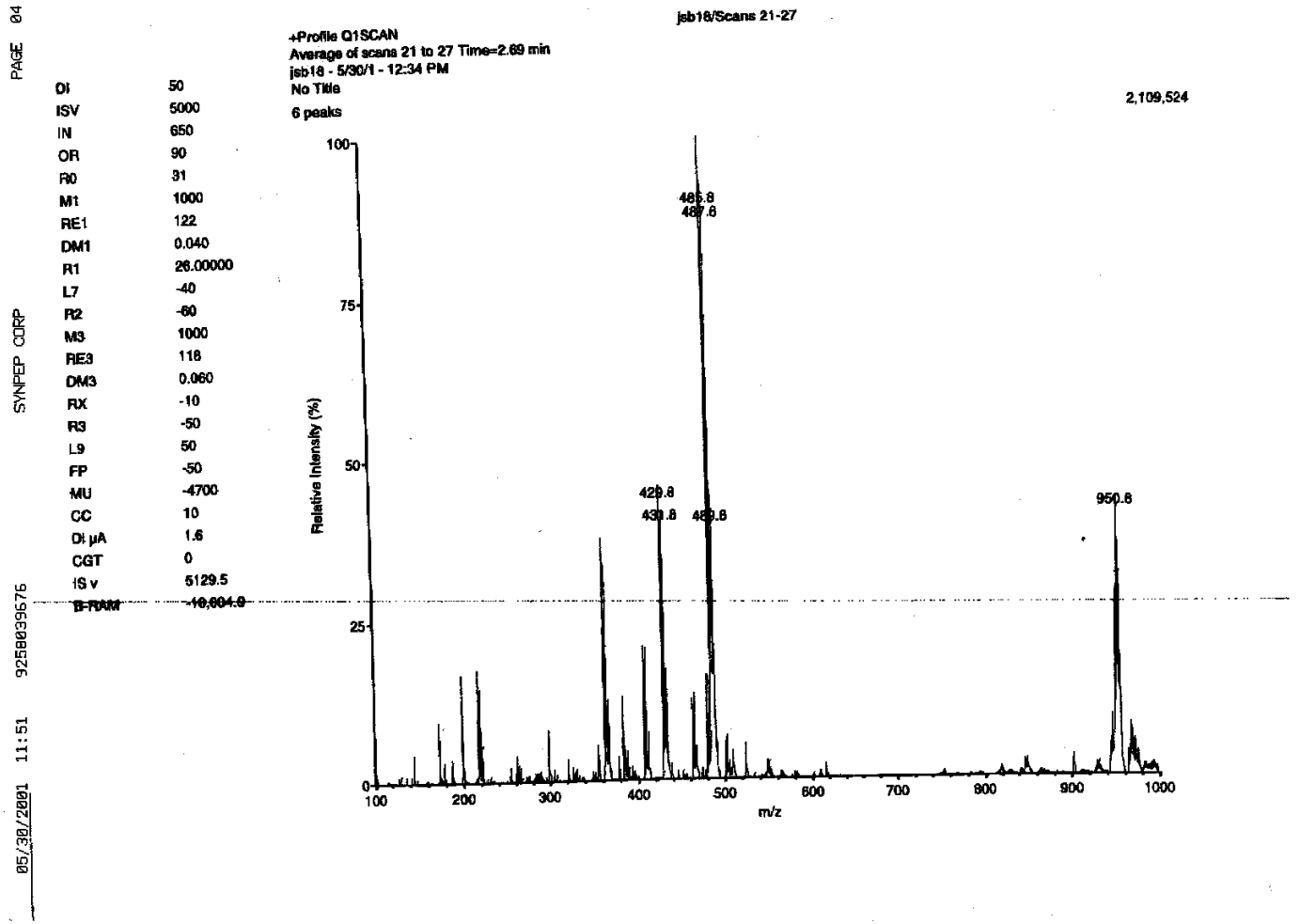
PAGE 04
SYNPEP CORP
9258039676
05/30/2001 11:51
DI 50
ISV 5000
IN 650
OR 90
R0 31
M1 1000
RE1 122
DM1 0.040
R1 26.00000
L7 -40
R2 -60
M3 1000
RE3 118
DM3 0.060
RX -10
R3 -50
L9 50
FP -50
MU -4700
CC 10
DI µA 1.6
CGT 0
IS v 5129.5
B-RAM -10,604.0
+Profile Q1SCAN
Average of scans 21 to 27 Time=2.69 min
jsb18 - 5/30/1 - 12:34 PM
No Title
6 peaks
jsb18/Scans 21-27
2,109,524
Relative Intensity (%)
m/z
429.8
430.8
485.8
487.8
950.8

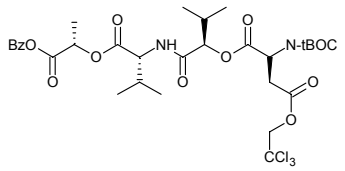

BzO-L-lac-D-val-D-Hval-L-asp(TCE)-N-tBoc

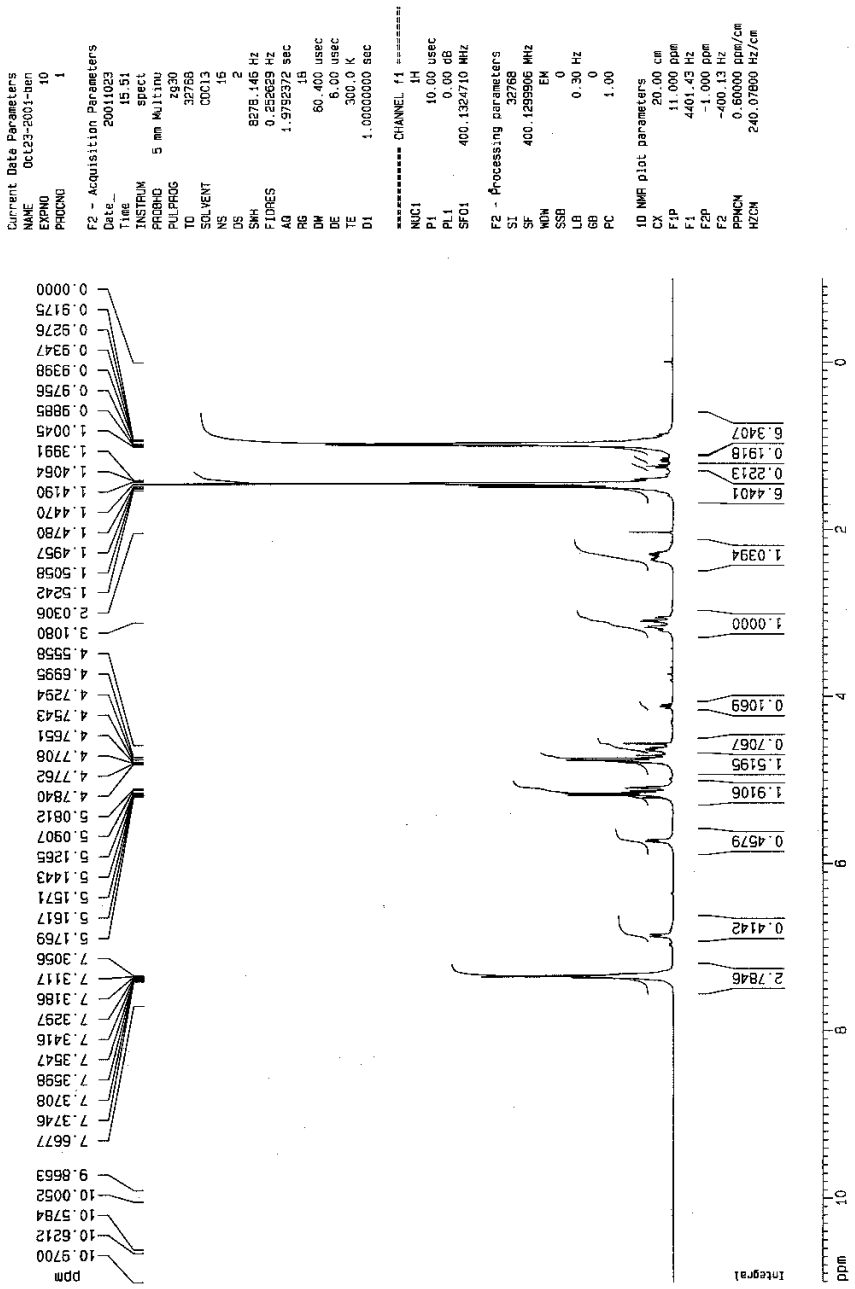

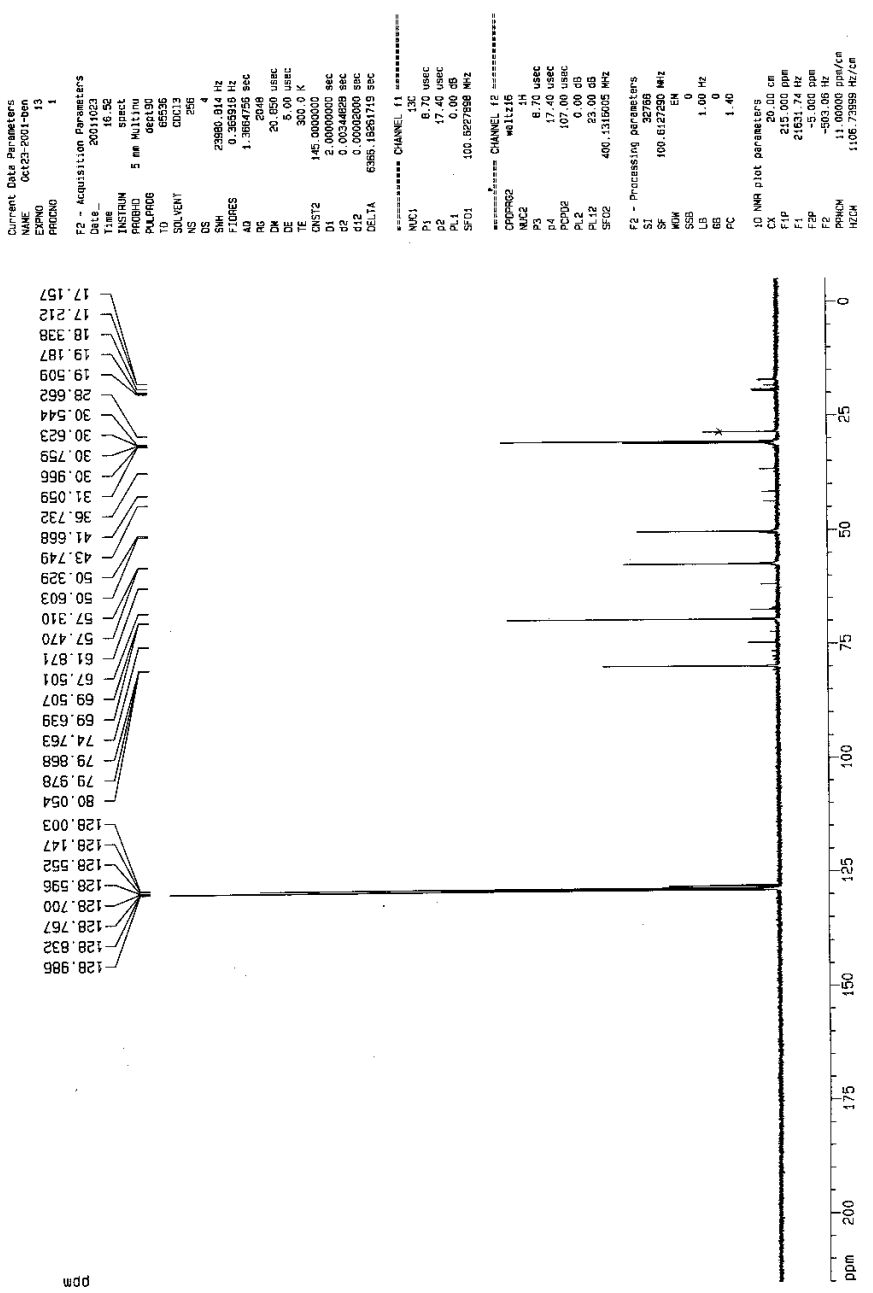
Current Data Parameters
NAME Oct23-2001-ben
EXPNO 13
PROCNO 1
F2 - Acquisition Parameters
Date_ 20011023
Time_ 16.52
INSTRUM spect
PROBHD 5 mm Multinu
PULPROG dept90
TD 65536
SOLVENT CDCl3
NS 256
DS 4
SWH 23980.814 Hz
FIDRES 0.365916 Hz
AQ 1.3664756 sec
RG 2048
DW 20.850 usec
DE 6.00 usec
TE 300.0 K
CNST2 145.0000000
D1 2.00000000 sec
D2 0.00344089 sec
D12 0.00002000 sec
DELTA 6366.18951719 sec
CHANNEL f1
NUC1 13C
P1 8.70 usec
P2 17.40 usec
PL1 0.00 dB
SFO1 100.6227898 MHz
CHANNEL f2
CPDPRG2 waltz16
NUC2 1H
P3 8.70 usec
P4 17.40 usec
PCPD2 107.00 usec
PL2 0.00 dB
PL12 23.00 dB
SFO2 400.1316005 MHz
F2 - Processing parameters
SI 32768
SF 100.6127280 MHz
WDW EM
SSB 0
LB 1.00 Hz
GB 0
PC 1.40
1D NMR plot parameters
CX 20.00 cm
F1P 215.000 ppm
F1 21651.74 Hz
F2P -1.001 ppm
F2 -503.06 Hz
PPMCM 11.00000 ppm/cm
HZCM 1106.73999 Hz/cm
17.157
17.212
18.338
19.187
19.509
28.682
30.544
30.623
30.759
30.966
31.059
36.732
41.668
43.749
50.329
50.603
57.310
57.470
61.871
67.501
69.507
69.639
74.763
79.868
79.978
80.054
128.003
128.147
128.552
128.596
128.700
128.767
128.832
128.986
ppm
200
175
150
125
100
75
50
25
0

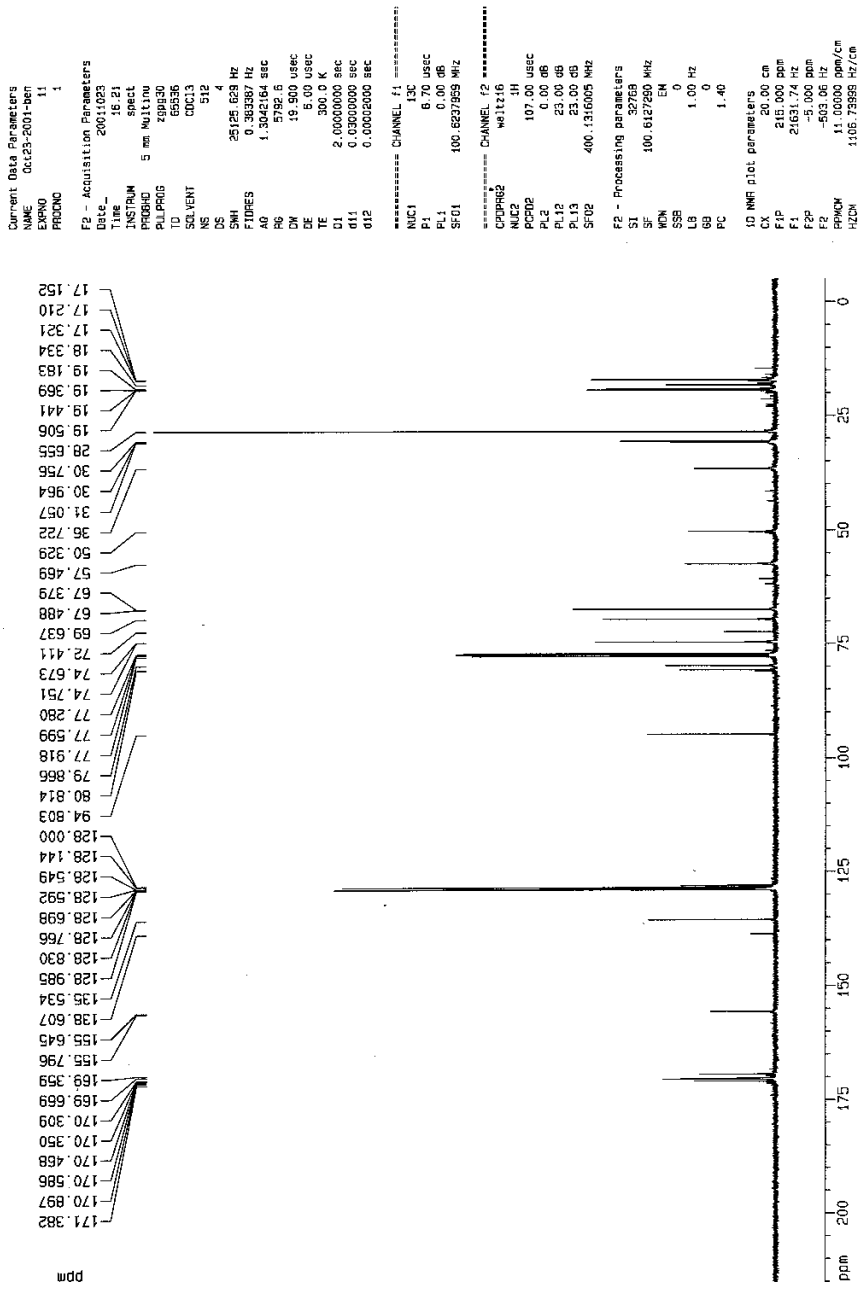
Current Data Parameters
NAME Occ23-2001-ben
EXPNO 11
PROCNO 1
F2 - Acquisition Parameters
Date_ 20011023
Time 16.21
INSTRUM spect
PROBHD 5 mm Multinu
PULPROG zgpg30
TD 65536
SOLVENT CDCl3
NS 512
DS 4
SWH 25125.629 Hz
FIDRES 0.383387 Hz
AQ 1.3042164 sec
RG 5792.6
DW 19.900 usec
DE 6.00 usec
TE 300.0 K
D1 2.00000000 sec
d11 0.03000000 sec
d12 0.00002000 sec
CHANNEL f1
NUC1 13C
P1 8.70 usec
PL1 0.00 dB
SFO1 100.6237899 MHz
CHANNEL f2
CPDPRG2 waltz16
NUC2 1H
PCPD2 107.00 usec
PL2 0.00 dB
PL12 23.00 dB
PL13 23.00 dB
SFO2 400.1316005 MHz
F2 - Processing parameters
SI 32768
SF 100.6127290 MHz
WDW EM
SSB 0
LB 1.00 Hz
GB 0
PC 1.40
1D NMR plot parameters
CX 20.00 cm
F1P 216.000 ppm
F1 21631.74 Hz
F2P -5.000 ppm
F2 -503.06 Hz
PPMCM 11.00000 ppm/cm
HZCM 1106.73895 Hz/cm
ppm
171.382
170.897
170.586
170.468
170.350
170.309
169.669
169.359
155.796
155.645
138.607
135.534
128.985
128.830
128.766
128.698
128.592
128.549
128.144
128.000
94.803
80.814
79.866
77.918
77.599
77.280
74.751
74.673
72.411
69.637
67.488
67.379
57.469
50.329
36.722
31.057
30.964
30.756
28.655
19.506
19.441
19.369
19.183
18.334
17.321
17.210
17.152
ppm
0
25
50
75
100
125
150
175
200

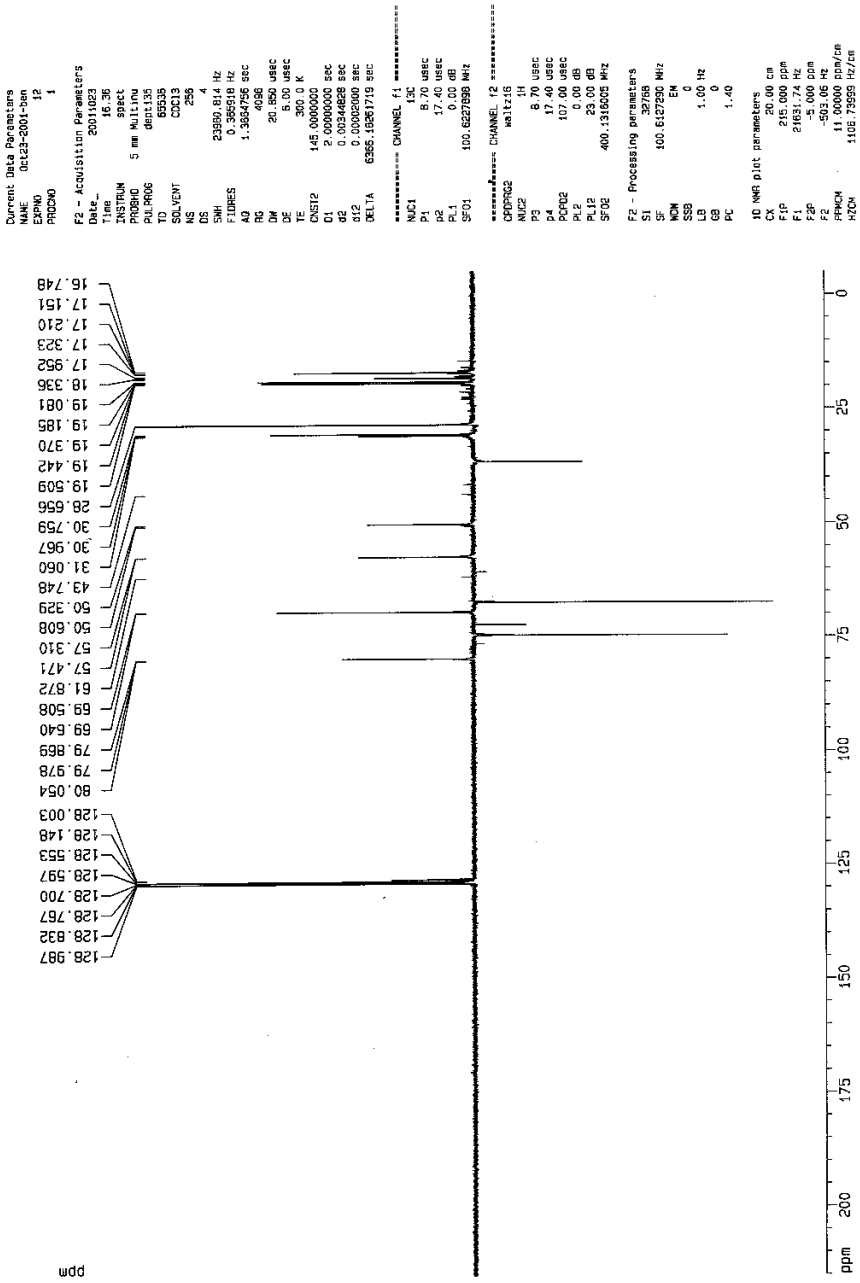
Current Data Parameters
NAME Oct23-2001-ban
EXPNO 12
PROCNO 1
F2 - Acquisition Parameters
Date_ 20011023
Time 16.36
INSTRUM spect
PROBHD 5 mm Multinu
PULPROG dept135
TD 65536
SOLVENT CDCl3
NS 256
DS 4
SWH 23980.814 Hz
FIDRES 0.365618 Hz
AQ 1.3934795 sec
RG 4096
DW 20.850 usec
DE 6.00 usec
TE 300.0 K
CNST2 145.0000000
D1 2.00000000 sec
d2 0.00344828 sec
d12 0.00002000 sec
DELTA 6365.19361719 sec
CHANNEL f1
NUC1 13C
P1 8.70 usec
p2 17.40 usec
PL1 0.00 dB
SF01 100.6227898 MHz
CHANNEL f2
CPDPRG2 waltz16
NUC2 1H
PP 8.70 usec
P4 17.40 usec
PCPD2 107.00 usec
PL2 0.00 dB
PL12 23.00 dB
SF02 400.1316005 MHz
F2 - Processing parameters
SI 32768
SF 100.6127250 MHz
WDW EM
SSB 0
LB 1.00 Hz
GB 0
PC 1.40
1D NMR plot parameters
CX 20.00 cm
F1P 245.000 ppm
F1 24631.74 Hz
F2P -5.000 ppm
F2 -503.06 Hz
PPMCM 11.00000 ppm/cm
HZCM 1106.73999 Hz/cm
16.748
17.151
17.210
17.323
17.952
18.336
19.081
19.185
19.370
19.442
19.509
28.656
30.759
30.967
31.060
43.748
50.329
50.608
57.310
57.471
61.872
69.508
69.640
79.869
79.978
80.054
128.003
128.148
128.553
128.597
128.700
128.767
128.832
128.987
ppm
0
25
50
75
100
125
150
175
200
ppm

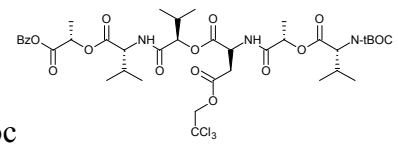

BzO-L-lac-D-val-D-Hval-L-asp(TCE)-L-lac-D-val-N-tBoc

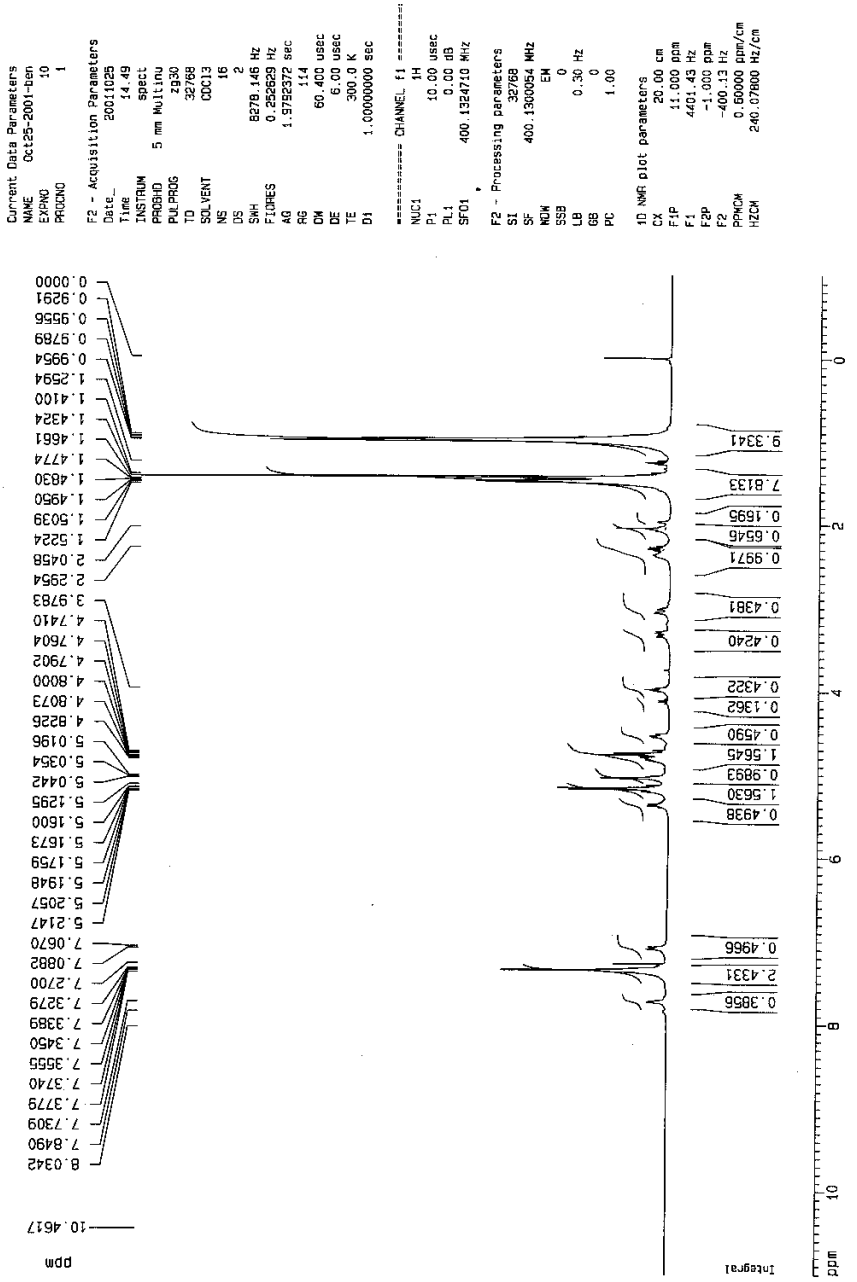

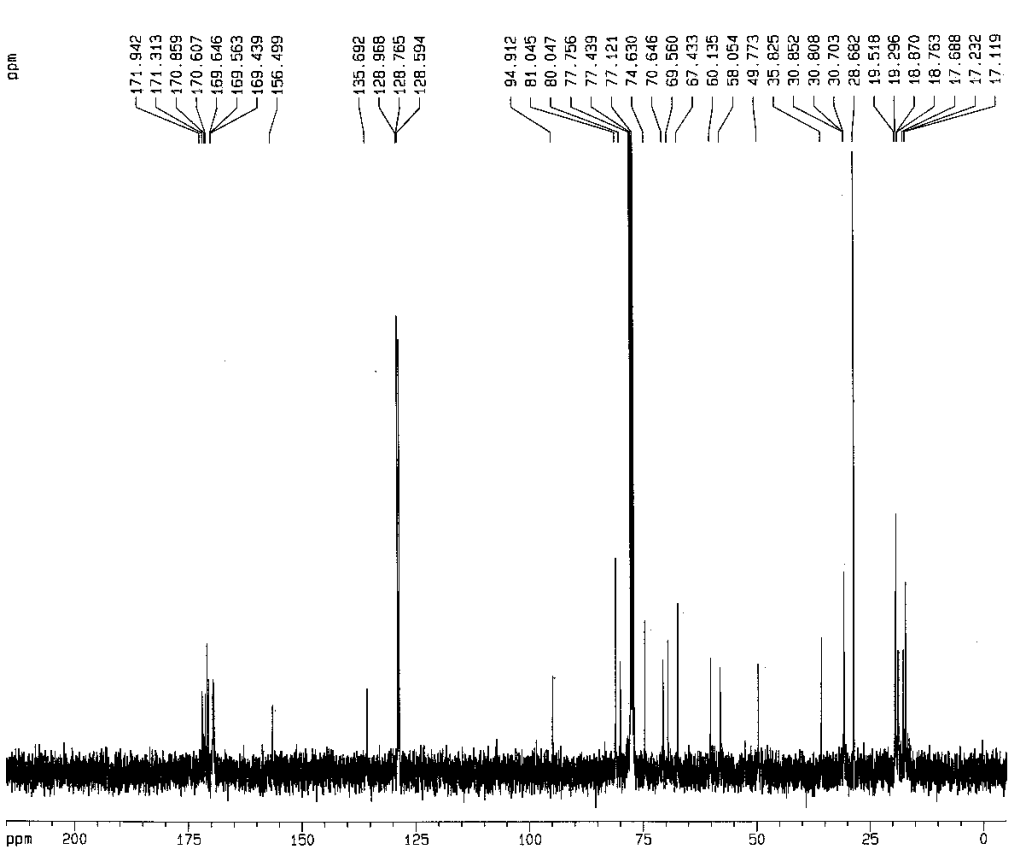


```
Current Data Parameters
NAME      Oct25-2001-ben
EXPNO                 11
PROCNO                 1

F2 - Acquisition Parameters
Date_           20011025
Time               15.18
INSTRUM             spect
PROBHD     5 mm Multinu
PULPROG          zgpg30
TD                65536
SOLVENT           CDCl3
NS                  512
DS                    4
SWH           25125.629 Hz
FIDRES            0.383387 Hz
AQ             1.3042164 sec
RG                 8192
DW                19.900 usec
DE                 6.00 usec
TE                300.0 K
D1             2.00000000 sec
d11            0.03000000 sec
d12            0.00002000 sec

============ CHANNEL f1 ============
NUC1                 13C
P1                  8.70 usec
PL1                 0.00 dB
SF01          100.6237959 MHz

============ CHANNEL f2 ============
CPDPRG2          waltz16
NUC2                  1H
PCPD2              107.00 usec
PL2                 0.00 dB
PL12               23.00 dB
PL13               23.00 dB
SF02          400.1316005 MHz

F2 - Processing parameters
SI                 32768
SF            100.6127290 MHz
WDW                   EM
SSB                    0
LB                  1.00 Hz
GB                     0
PC                  1.40

1D NMR plot parameters
CX                 20.00 cm
F1P               215.000 ppm
F1              21631.74 Hz
F2P                -5.000 ppm
F2               -503.06 Hz
PPMCM             11.00000 ppm/cm
HZCM           1106.73999 Hz/cm
```

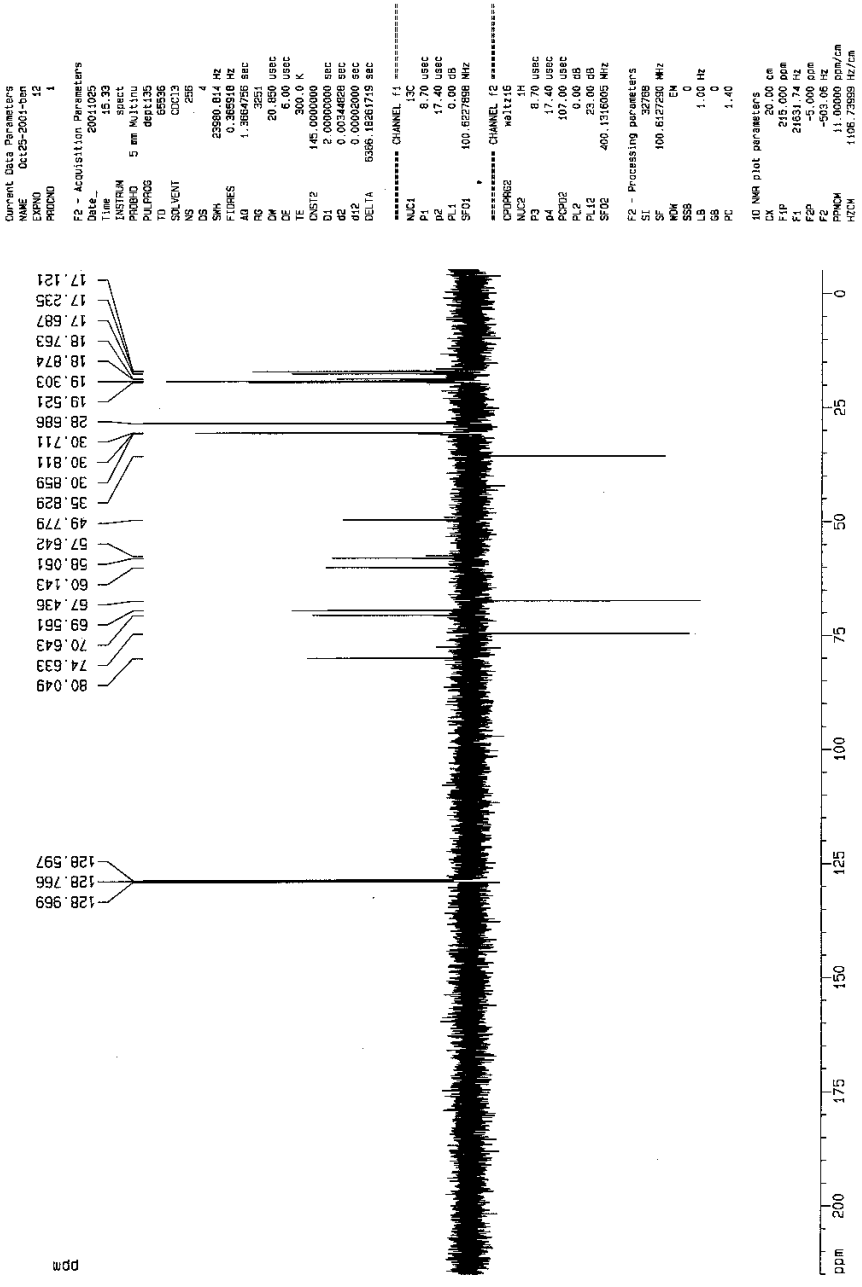
Current Data Parameters
NAME Oct25-2001-ben
EXPNO 12
PROCNO 1
F2 - Acquisition Parameters
Date_ 20011025
Time 15.33
INSTRUM spect
PROBHD 5 mm Multinu
PULPROG dept135
TD 65536
SOLVENT CDCl3
NS 256
DS 4
SWH 23980.814 Hz
FIDRES 0.365918 Hz
AQ 1.36847586 sec
RG 2521
DW 20.850 usec
DE 6.00 usec
TE 300.0 K
CNST2 145.0000000
D1 2.00000000 sec
d2 0.00344828 sec
d12 0.00002000 sec
DELTA 5386.18261719 sec
========== CHANNEL f1 ==========
NUC1 13C
P1 8.70 usec
P2 17.40 usec
PL1 0.00 dB
SFO1 100.6227898 MHz
========== CHANNEL f2 ==========
CPDPRG2 waltz16
NUC2 1H
P3 8.70 usec
P4 17.40 usec
PCPD2 107.00 usec
PL2 0.00 dB
PL12 23.00 dB
SFO2 400.1316005 MHz
F2 - Processing parameters
SI 32768
SF 100.6127250 MHz
WDW EM
SSB 0
LB 1.00 Hz
GB 0
PC 1.40
1D NMR plot parameters
CX 20.00 cm
F1P 215.000 ppm
F1 21631.74 Hz
F2P -5.000 ppm
F2 -503.06 Hz
PPMCM 11.00000 ppm/cm
HZCM 1106.73999 Hz/cm
17.121
17.235
17.687
18.763
18.874
19.303
19.521
28.686
30.711
30.811
30.859
35.829
49.779
57.642
58.061
60.143
67.436
69.561
70.643
74.633
80.049
128.597
128.766
128.969
ppm
0
25
50
75
100
125
150
175
200
ppm

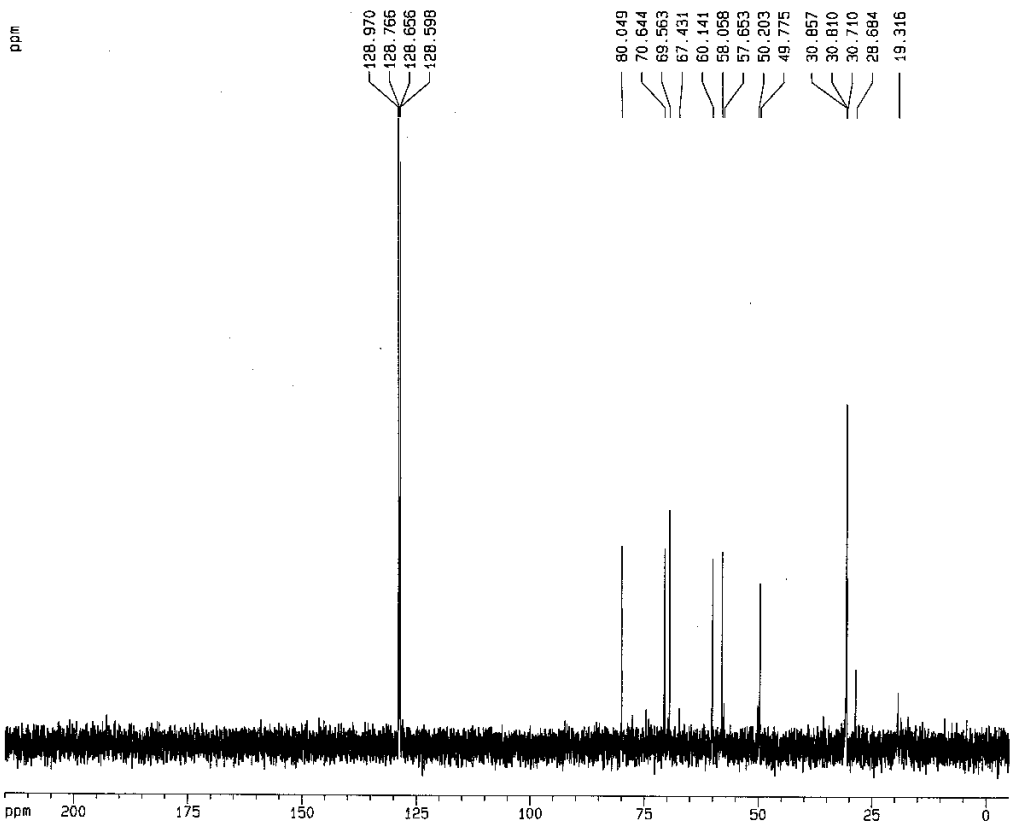


```
Current Data Parameters
NAME      Oct25-2001-ben
EXPNO              13
PROCNO             1

F2 - Acquisition Parameters
Date_          20011025
Time              15.49
INSTRUM           spect
PROBHD     5 mm Multinu
PULPROG          dept90
TD                65536
SOLVENT           CDCl3
NS                  256
DS                    4
SWH           23980.814 Hz
FIDRES        0.365918 Hz
AQ            1.3664756 sec
RG                 4096
DW               20.850 usec
DE                6.00 usec
TE              300.0 K
CNST2         145.0000000
D1            2.00000000 sec
d2            0.00344828 sec
d12           0.00002000 sec
DELTA      6866.18261719 sec

========== CHANNEL f1 ============
NUC1               13C
P1                8.70 usec
p2               17.40 usec
PL1               0.00 dB
SFO1        100.6227698 MHz

========== CHANNEL f2 ============
CPDPRG2         waltz16
NUC2               1H
P3                8.70 usec
p4               17.40 usec
PCPD2           107.00 usec
PL2               0.00 dB
PL12             23.00 dB
SFO2        400.1316005 MHz

F2 - Processing parameters
SI                32768
SF          100.6127290 MHz
WDW                EM
SSB                0
LB              1.00 Hz
GB                 0
PC              1.40

1D NMR plot parameters
CX              20.00 cm
F1P           215.000 ppm
F1            21631.74 Hz
F2P            -5.000 ppm
F2             -503.06 Hz
PPMCM         11.00000 ppm/cm
HZCM        1106.73999 Hz/cm
```

jsb25 pos/Scans 5-8
+Profile Q1SCAN
Scans 5-8 minus 1-2 Time=0.71 min
jsb25 pos - 10/31/1 - 2:02 PM
No Title
1 peak
50,000
918.4
Relative Intensity (%)
m/z
DI 50
ISV 5000
IN 650
OR 120
R0 30
M1 1000
RE1 118.3
DM1 0.040
R1 25.5
L9 -100
FP 50
MU -5000
CC 1
DI µA 2.8
IS v 5109.9
UV -1167.6
SYNPEP CORP
PAGE 03
10/31/2001 13:12 9258039676

Cyclo(-L-lac-D-val-D-Hval-L-asp(TCE)-L-lac-D-val-)

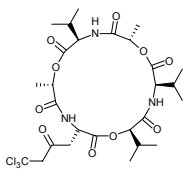

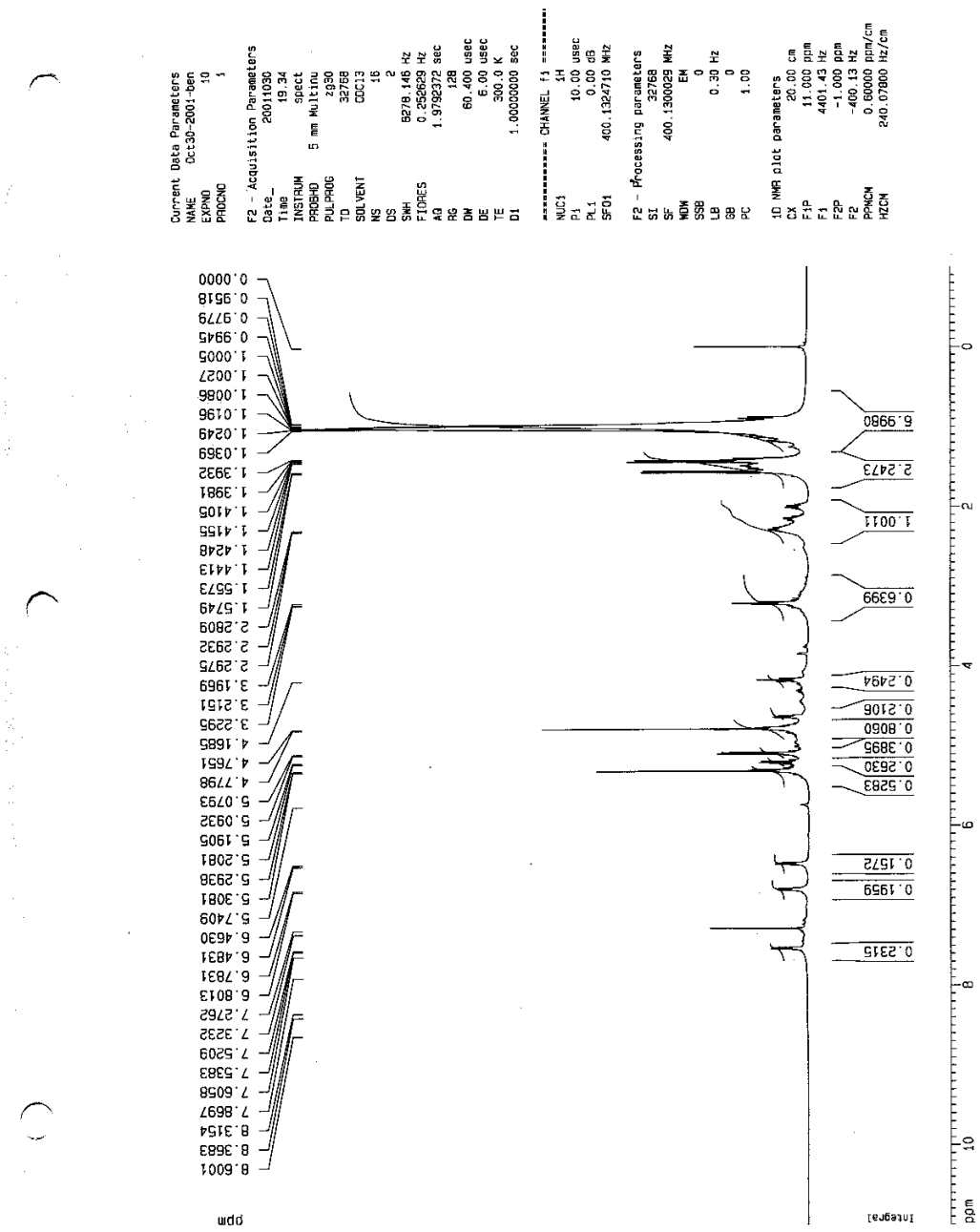

Current Data Parameters
NAME Oct30-2001-ben
EXPNO 11
PROCNO 1
F2 - Acquisition Parameters
Date_ 20011030
Time 20.03
INSTRUM spect
PROBHD 5 mm Multinu
PULPROG zgpg30
TD 65536
SOLVENT CDCl3
NS 512
DS 4
SWH 25125.629 Hz
FIDRES 0.383387 Hz
AQ 1.3042164 sec
RG 8192
DW 19.900 usec
DE 6.00 usec
TE 300.0 K
D1 2.00000000 sec
d11 0.03000000 sec
d12 0.00002000 sec
CHANNEL f1
NUC1 13C
P1 8.70 usec
PL1 0.00 dB
SFO1 100.6237959 MHz
CHANNEL f2
CPDPRG2 waltz16
NUC2 1H
PCPD2 107.00 usec
PL2 0.00 dB
PL12 23.00 dB
PL13 23.00 dB
SFO2 400.1315605 MHz
F2 - Processing parameters
SI 32768
SF 100.6127690 MHz
WDW EM
SSB 0
LB 1.00 Hz
GB 0
PC 1.40
1D NMR plot parameters
CX 20.00 cm
F1P 215.000 ppm
F1 21631.74 Hz
F2P -5.000 ppm
F2 -503.06 Hz
PPMCM 11.00000 ppm/cm
HZCM 1106.73999 Hz/cm
95.005
80.833
77.759
77.440
77.123
74.588
72.298
70.147
60.194
57.180
53.854
49.440
35.219
31.455
30.517
30.237
19.658
19.375
18.874
18.321
18.033
17.891
15.978
15.720
172.416
171.704
171.009
170.257
169.990
169.870
168.999
ppm

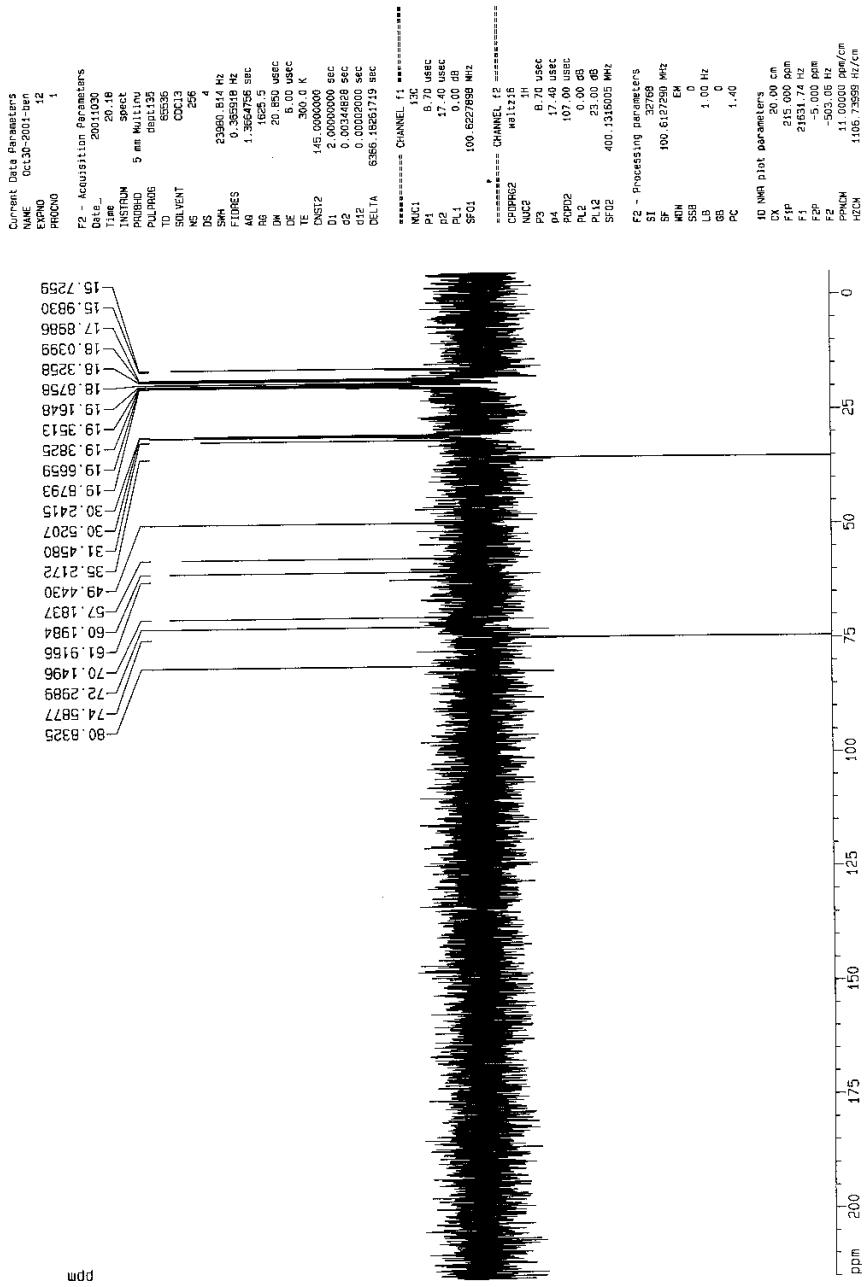
Current Data Parameters
NAME Oct30-2001-ben
EXPNO 12
PROCNO 1
F2 - Acquisition Parameters
Date_ 20011030
Time_ 20.18
INSTRUM spect
PROBHD 5 mm Multinu
PULPROG deptl35
TD 65536
SOLVENT CDCl3
NS 256
DS 4
SWH 23980.814 Hz
FIDRES 0.365318 Hz
AQ 1.3664756 sec
RG 1625.5
DW 20.850 usec
DE 6.00 usec
TE 300.0 K
CNST12 145.00000000
D1 2.00000000 sec
d2 0.00344828 sec
d12 0.00002000 sec
DELTA 6366.18261719 sec
======== CHANNEL f1 ========
NUC1 13C
P1 8.70 usec
p2 17.40 usec
PL1 0.00 dB
SFO1 100.6227898 MHz
======== CHANNEL f2 ========
CPDPRG2 waltz16
NUC2 1H
P3 8.70 usec
p4 17.40 usec
PCPD2 107.00 usec
PL2 0.00 dB
PL12 23.00 dB
SFO2 400.1316005 MHz
F2 - Processing parameters
SI 32768
SF 100.6127290 MHz
WDW EM
SSB 0
LB 1.00 Hz
GB 0
PC 1.40
1D NMR plot parameters
CX 20.00 cm
F1P 215.000 ppm
F1 21631.74 Hz
F2P -5.000 ppm
F2 -503.06 Hz
PPMCM 11.00000 ppm/cm
HZCM 1106.73999 Hz/cm
15.7259
15.9830
17.8986
18.0399
18.3258
18.8758
19.1648
19.3513
19.3825
19.6659
19.8793
30.2415
30.5207
31.4580
35.2172
49.4430
57.1837
60.1984
61.9166
70.1496
72.2989
74.5877
80.8325
ppm
0
25
50
75
100
125
150
175
200
ppm

Current Data Parameters
NAME Oct30-2001-ben
EXPNO 13
PROCNO 1
F2 - Acquisition Parameters
Date_ 20011030
Time 20.34
INSTRUM spect
PROBHD 5 mm Multinu
PULPROG dept90
TD 65536
SOLVENT CDCl3
NS 256
DS 4
SWH 23980.814 Hz
FIDRES 0.365918 Hz
AQ 1.3664756 sec
RG 2048
DW 20.850 usec
DE 6.00 usec
TE 300.0 K
CNST2 145.0000000
D1 2.00000000 sec
D2 0.00344828 sec
D12 0.00002000 sec
DELTA 5366.18291719 sec
CHANNEL f1
NUC1 13C
P1 8.70 usec
P2 17.40 usec
PL1 0.00 dB
SFO1 100.6227898 MHz
CHANNEL f2
CPDPRG2 waltz16
NUC2 1H
P3 8.70 usec
P4 17.40 usec
PCPD2 107.00 usec
PL2 0.00 dB
PL12 23.00 dB
SFO2 400.1316005 MHz
F2 - Processing parameters
SI 32768
SF 100.6127290 MHz
WDW EM
SSB 0
LB 1.00 Hz
GB 0
PC 1.40
1D NMR plot parameters
CX 20.00 cm
F1P 215.000 ppm
F1 21631.74 Hz
F2P -5.000 ppm
F2 -503.06 Hz
PPMCM 11.00000 ppm/cm
HZCM 1106.73999 Hz/cm
19.6650
30.2428
30.5221
30.6351
31.4594
43.9341
49.4444
57.1836
60.1986
61.9143
70.1513
71.8474
72.2989
80.8327
ppm
0
25
50
75
100
125
150
175
200

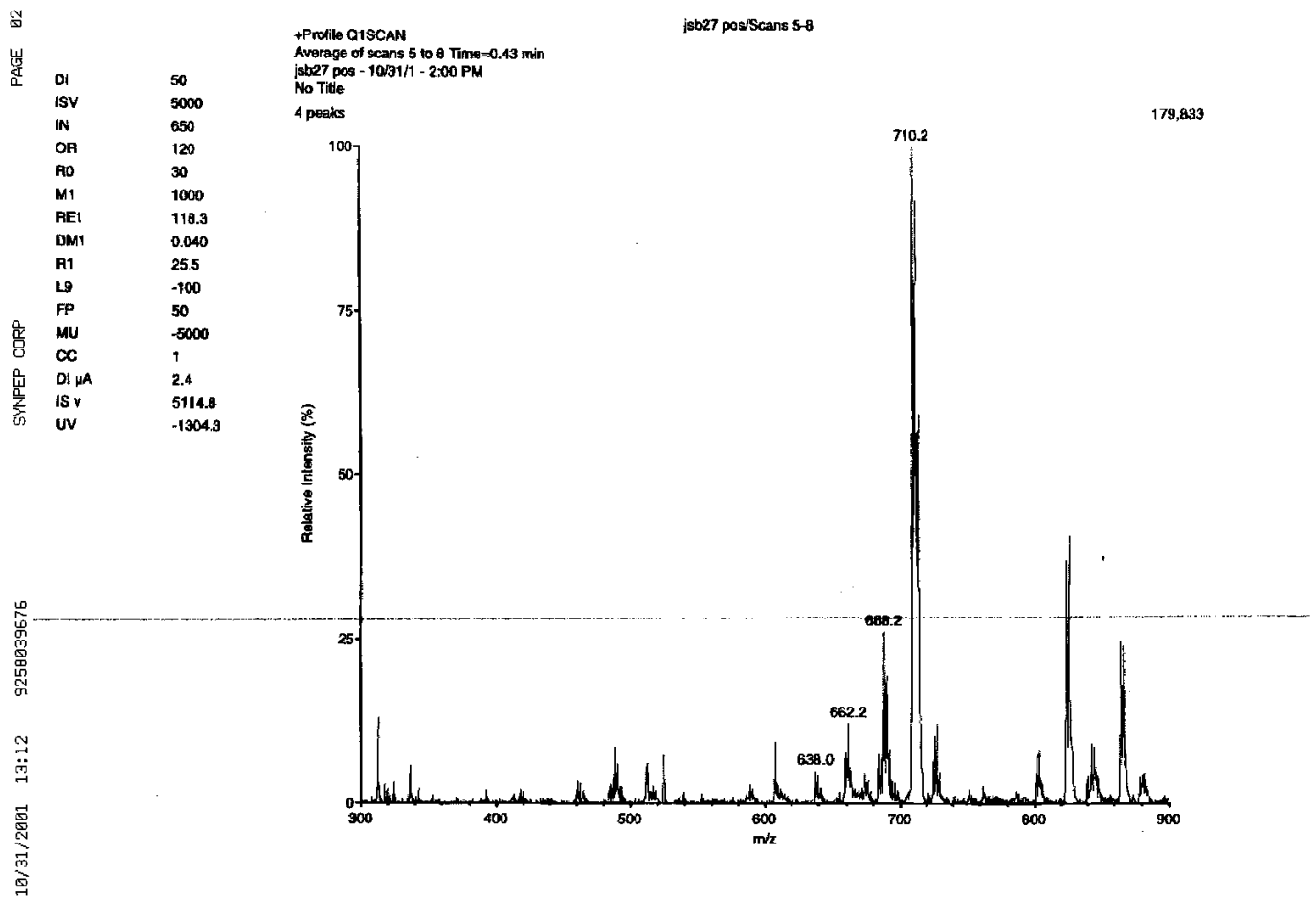
PAGE 02
SYNPEP CORP
10/31/2001 13:12 9258039576
DI 50
ISV 5000
IN 650
OR 120
R0 30
M1 1000
RE1 118.3
DM1 0.040
R1 25.5
L9 -100
FP 50
MU -5000
CC 1
DI µA 2.4
IS v 5114.8
UV -1304.3
+Profile Q1SCAN
Average of scans 5 to 8 Time=0.43 min
jsb27 pos - 10/31/1 - 2:00 PM
No Title
4 peaks
jsb27 pos/Scans 5-8
179,833
710.2
688.2
662.2
638.0
Relative Intensity (%)
100
75
50
25
0
300
400
500
600
700
800
900
m/z

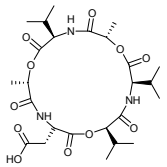

cyclo(-L-lac-D-val-D-Hval-L-asp(OH)-L-lac-D-val-)

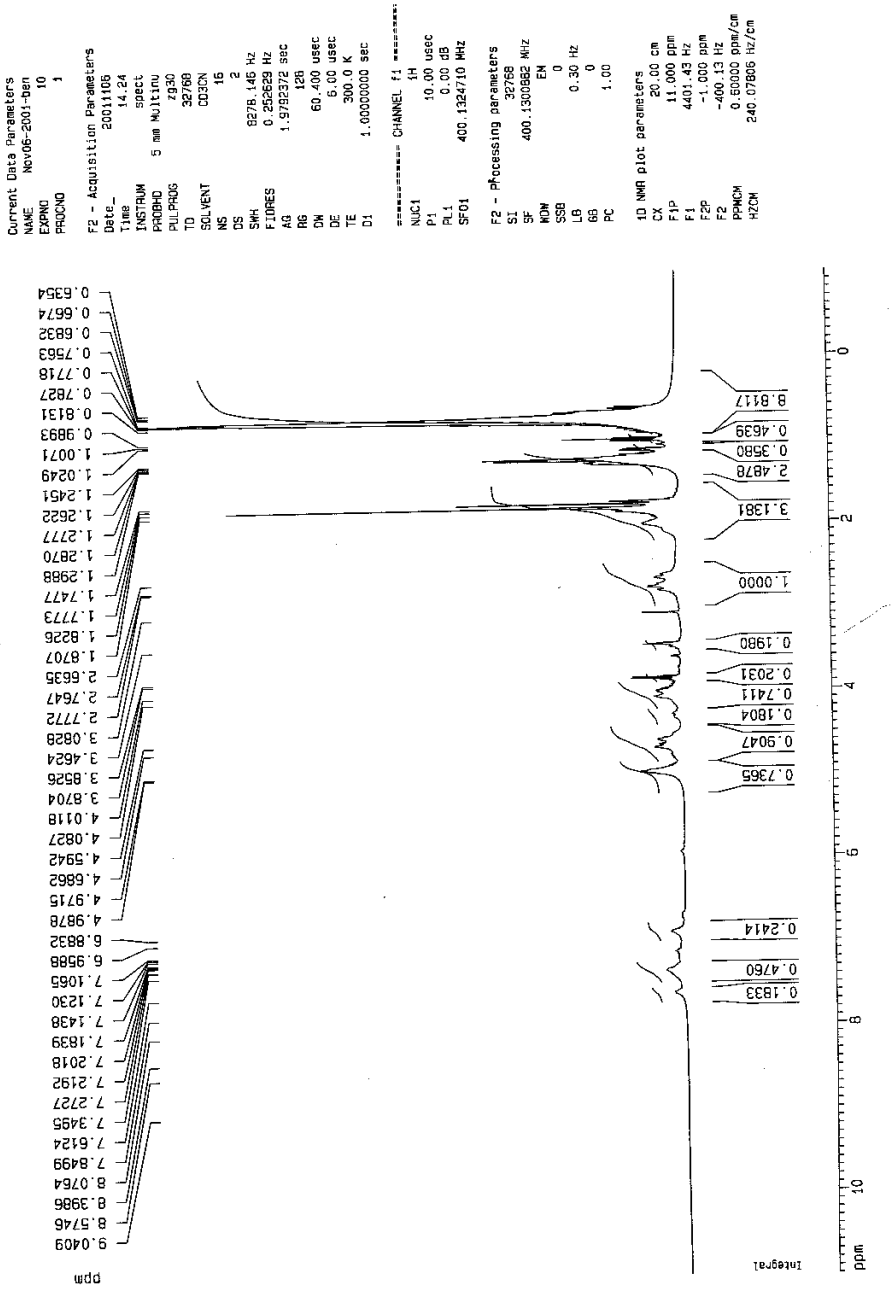

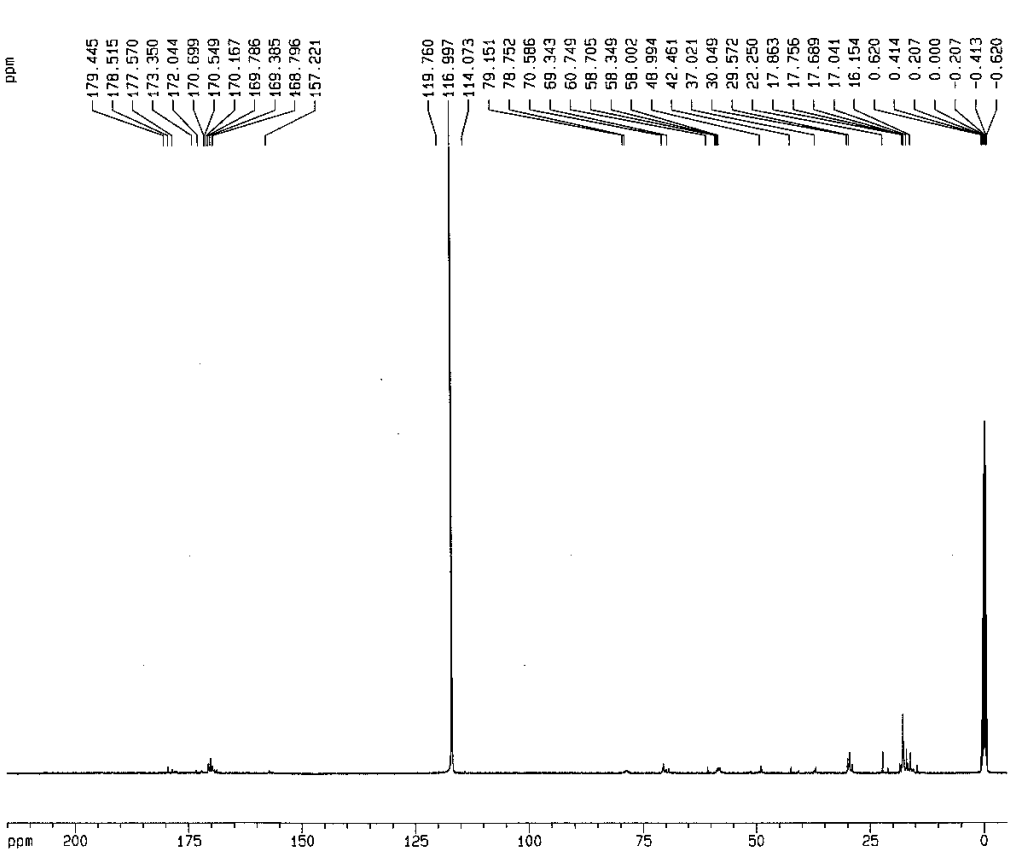


```
Current Data Parameters
NAME      Mar01-2002-ben
EXPNO                 17
PROCNO                 1

F2 - Acquisition Parameters
Date_           20020302
Time               13.35
INSTRUM            spect
PROBHD     5 mm Multinu
PULPROG          zgpg30
TD                65536
SOLVENT           CD3CN
NS                 6000
DS                    4
SWH           25125.629 Hz
FIDRES        0.383387 Hz
AQ            1.3042164 sec
RG                 8192
DW               19.900 usec
DE                6.00 usec
TE              300.0 K
D1            2.00000000 sec
d11           0.03000000 sec
d12           0.00002000 sec

============ CHANNEL f1 ============
NUC1                13C
P1                 8.70 usec
PL1                0.00 dB
SFO1        100.6237958 MHz

============ CHANNEL f2 ============
CPDPRG2         waltz16
NUC2                1H
PCPD2            107.00 usec
PL2                0.00 dB
PL12              23.00 dB
PL13              23.00 dB
SFO2        400.1316005 MHz

F2 - Processing parameters
SI                 32768
SF          100.6128100 MHz
WDW                   EM
SSB                    0
LB                  1.00 Hz
GB                     0
PC                  1.40

1D NMR plot parameters
CX                20.00 cm
F1P              215.000 ppm
F1             21631.76 Hz
F2P               -5.000 ppm
F2              -503.06 Hz
PPMCM           11.00000 ppm/cm
HZCM          1108.74084 Hz/cm
```

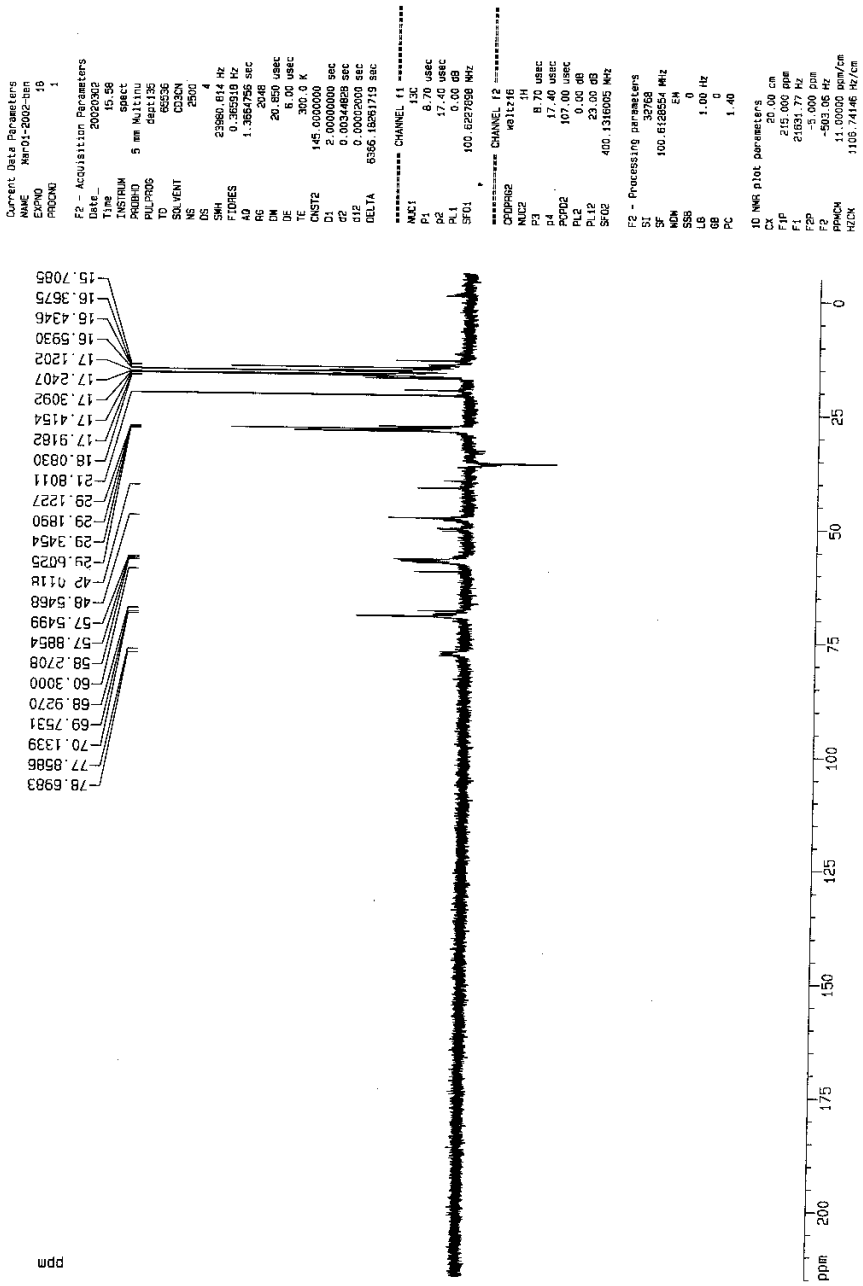
Current Data Parameters
NAME Mar01-2002-ben
EXPNO 16
PROCNO 1
F2 - Acquisition Parameters
Date_ 20020302
Time 15.56
INSTRUM spect
PROBHD 5 mm Multinu
PULPROG dept135
TD 65536
SOLVENT CD3CN
NS 2500
DS 4
SWH 23980.814 Hz
FIDRES 0.365910 Hz
AQ 1.36647756 sec
RG 2048
DW 20.850 usec
DE 6.00 usec
TE 300.0 K
CNST2 145.0000000
D1 2.00000000 sec
d2 0.00344828 sec
d12 0.00002000 sec
DELTA 6366.18261719 sec
CHANNEL f1
NUC1 13C
P1 8.70 usec
P2 17.40 usec
PL1 0.00 dB
SFO1 100.6227698 MHz
CHANNEL f2
CPDPRG2 waltz16
NUC2 1H
P3 8.70 usec
P4 17.40 usec
PCPD2 107.00 usec
PL2 0.00 dB
PL12 23.00 dB
SFO2 400.1316005 MHz
F2 - Processing parameters
SI 32768
SF 100.6128554 MHz
WDW EM
SSB 0
LB 1.00 Hz
GB 0
PC 1.40
1D NMR plot parameters
CX 20.00 cm
F1P 215.000 ppm
F1 21631.77 Hz
F2P -5.000 ppm
F2 -503.06 Hz
PPMCM 11.00000 ppm/cm
HZCM 1106.74146 Hz/cm
15.7085
16.3675
16.4346
16.5930
17.1202
17.2407
17.3092
17.4154
17.9182
18.0830
21.8011
29.1227
29.1890
29.3454
29.6025
42.0118
48.5468
57.5499
57.8854
58.2708
60.3000
68.9270
69.7531
70.1339
77.8586
78.6983
wdd
ppm
200
175
150
125
100
75
50
25
0

Current Data Parameters
NAME Nov02-2001-ben
EXPNO 13
PROCNO 1
F2 - Acquisition Parameters
Date_ 20011102
Time 20.48
INSTRUM spect
PROBHD 5 mm Multinu
PULPROG dept90
TD 65536
SOLVENT Acetic
NS 256
DS 4
SWH 23980.814 Hz
FIDRES 0.365918 Hz
AQ 1.3664756 sec
RG 2048
DW 20.850 usec
DE 6.00 usec
TE 300.0 K
CNST2 145.0000000
D1 2.000000000 sec
d2 0.00344828 sec
d12 0.000020000 sec
DELTA 6366.18261719 sec
========== CHANNEL f1 ==========
NUC1 13C
P1 8.70 usec
p2 17.40 usec
PL1 0.00 dB
SFO1 100.5627895 MHz
========== CHANNEL f2 ==========
CPDPRG2 waltz16
NUC2 1H
P3 8.70 usec
p4 17.40 usec
PCPD2 107.00 usec
PL2 0.00 dB
PL12 23.00 dB
SFO2 400.1316005 MHz
F2 - Processing parameters
SI 32768
SF 100.5612780 MHz
WDW EM
SSB 0
LB 1.00 Hz
GB 0
PC 1.40
1D NMR plot parameters
CX 20.00 cm
F1P 215.000 ppm
F1 21631.74 Hz
F2P -5.000 ppm
F2 -503.06 Hz
PPMCM 11.00000 ppm/cm
HZCM 1106.73999 Hz/cm
128.512
80.309
71.100
71.835
59.238
58.420
49.556
30.975
30.740
30.505
ppm
0
25
50
75
100
125
150
175
200
ppm

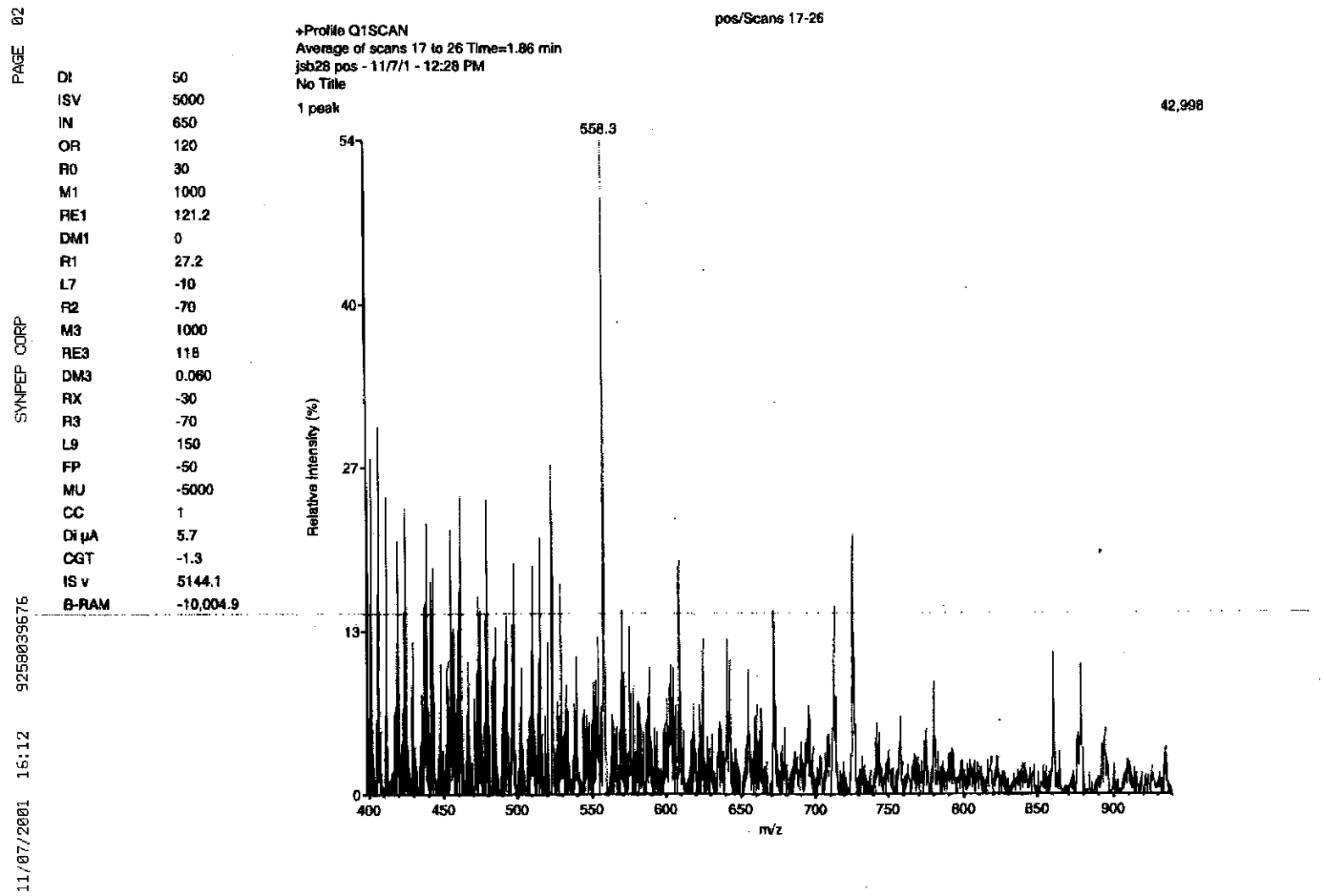
PAGE 02
SYNPEP CORP
9258039676
11/07/2001 16:12
DI 50
ISV 5000
IN 650
OR 120
R0 30
M1 1000
RE1 121.2
DM1 0
R1 27.2
L7 -10
R2 -70
M3 1000
RE3 118
DM3 0.060
RX -30
R3 -70
L9 150
FP -50
MU -5000
CC 1
DI µA 5.7
CGT -1.3
IS v 5144.1
B-RAM -10,004.9
+Profile Q1SCAN
Average of scans 17 to 26 Time=1.86 min
jsb28 pos - 11/7/1 - 12:28 PM
No Title
1 peak
pos/Scans 17-26
42,998
558.3
Relative Intensity (%)
m/z

Appendix A6: Curriculum Vitae

John S. Benco
139 Rolling Meadow Dr.
Holliston, MA 01746
508-429-4655
john.benco.b@bayer.com

Education

2003 Worcester Polytechnic Institute, Worcester MA.
Ph.D., Chemistry
Dissertation; The Rational Design and Synthesis of Ionophores and Fluoroionophores for the Selective Detection of Monovalent Cations.

2000 Worcester Polytechnic Institute, Worcester MA.
MS.; Chemistry
Thesis; Singlet-Singlet and Triplet-Triplet Energy Transfer in Polychromophoric Peptides.

1993 Framingham State College, Framingham MA.
BS.; Chemistry
Thesis; Photo-degradation of organic acids by semiconductor systems.

1989 Franklin Institute, Boston, MA.
Assoc., Automotive Technology

Professional Experience

Bayer Corporation; Medfield, MA

Research Scientist (2000-present)

- Designed, synthesized and developed optical based sensors for the detection of whole blood electrolytes to be used in clinical diagnostic systems.
- Designed, synthesized and developed novel ammonium cation ionophores for ion selective electrodes and optically based systems.

Senior Associate Research Scientist (1998-2000)

- Assisted in the successful commercial launch of a new Point of Care blood gas and electrolyte clinical diagnostic system.
- Member of lead multidisciplinary scientific team for product development.
- Provided expert scientific consultation on various electrochemical sensors.
- Determined root cause and corrective action of sensor and instrumentation technologies.

Chiron Diagnostics; Medfield, MA

Assistant Scientist (1995-1998)

- Collaborated with lead mechanical electrical and software engineers in the integration of sensor technologies into clinical diagnostic instrumentation.
- Developed ion selective electrodes for differential partial carbon dioxide measurements.
- Collaborated with peer scientists on the development of amperometric glucose and oxygen electrodes.
- Developed a new conductivity based hematocrit sensor.
- Worked intimately with manufacturing personal in the technology transfer of electrochemical sensors.
- Developed, in conjunction with formulation chemists, instrumentation calibration and quality control materials.

Ciba Corning Diagnostics; Medfield, MA

Associate Scientist (1993-1995)

- Developed metal-metal oxide pH electrodes for whole blood partial carbon dioxide determinations
- Collaborated with peer scientists on the development of pH, sodium, potassium, and calcium ion selective electrodes.

Technologist (1992-1993)

- Assisted senior level Ph.D. chemists in the development of thick film planar electrochemical sensors for the clinical analysis of blood gases.
- Prepared aqueous and whole blood test solutions for sensor development.
- Designed and executed test protocols.

Instrumentation Laboratories; Lexington, MA

Research Assistant (1990-1992)

- Assisted senior chemists in the development of ion selective electrodes for calcium and blood urea nitrogen.

Publications

Benco, J.S., Nienaber, H.A., McGimpsey, W.G.; Synthesis of an Ammonium Ionophore and its Application in a Planar Ion-Selective Electrode; *Anal. Chem.* **2003,** *75,* 152-156.

Benco, J.S., Nienaber, H.A., Dennen, K., McGimpsey, W.G.; A fluoroionophore for the detection of potassium ions: 9-anthryl-substituted azacrown ether covalently linked to a 1,3-alternate calix[4]arene; *J. Photochem. Photobio. A* **2002,** *152,* 33-40.

Benco, J.S., Nienaber, H.A., McGimpsey, W.G.; A sodium ion sensor based on a covalently-linked aminorhodamine B-calix[4]arene chromoionophore; *Sens. Actuators B* **2002,** *85,* 126-130.

Benco, J.S., Nienaber, H.A., McGimpsey, W.G.; Optical Sensors for Blood Analytes; *The Spectrum* **2001,** *14*, 1,5-11.

D'Orazio, P.A., Maley, T. C., McCaffrey, R.R., Chan, A. C., Orvedahl, D., Foos, J., Blake, D., Degnan, S., Benco, J.S., Murphy, C., Edelman, P.G., Ludi, H. *Clin. Chem.* **1997,** *43,* 1804.

U.S. Patents

Benco, J.S., Krouwer J.S.; *Method of Measuring pH;* U.S. Patent 6355158, **2002.**

Foos, J., Benco, J.S.; *Electrochemical planar metal/metal oxide electrode;* U.S. Patent 5785830*,* **1998.**

Foos, J., Benco, J. S.; *Method of preparing an electrochemical planar metal/metal oxide electrode;* U.S. Patent 5702575*,* **1997.**

Chan, A.D.C., Boden, M.W., Benco, J.S., Bergquist, R.A., Orvedahl, D.S.; *Fluoroelastomer gasket for blood sensors;* U.S. Patent 5700360*,* **1997.**

Benco, J.S., Foos, J.; *Planar bicarbonate sensor;* U.S. Patent 554272*,* **1996**.

European Patents

Benco, J.S., Krouwer J.S.; *Correcting protein induced error in pH-sensitive ISE comprising a polymeric membrane;* EP1141692, **2000.**

Chan, A.D.C., Boden, M.W., Benco, J.S., Bergquist, R.A., Orvedahl, D.S.; *Fluoroelastomer gasket for blood analyte sensors;* EP0772043, **1997.**

Foos, J., Benco, J.S.; *Electrochemical planar metal/metal oxide electrode;* EP0805976, **1996.**

Benco, J.S., Foos, J.; *Planar bicarbonate sensor;* EP0759551, **1996.**

Awards

Ciba Corning: R&D Quality Award, **1994.**

Chiron Diagnostics: Critical Care Quality Recognition Award, **1998.**

Chiron Diagnostics: Recognition Award; Outstanding Contributions, **1998.**

Bayer: Individual Science Award, **2001.**

WPI: Sigma Xi Ph.D. Research Award, **2003.**